THE ROLE OF DESORPTION KINETICS AND PHYSICAL HETEROGENEITY IN COLLOID-FACILITATED TRANSPORT OF CESIUM AND STRONTIUM IN AN UNSATURATED QUARTZ POROUS MEDIUM

by

TIMOTHY MARK DITTRICH

B.S., University of Wisconsin-Madison, 2001

M.S., Cornell University, 2004

A thesis submitted to the

Faculty of the Graduate School of the

University of Colorado in partial fulfillment

of the requirement for the degree of

Doctor of Philosophy

Department of Civil, Environmental, and Architectural Engineering

2012

This thesis entitled:
The Role of Desorption Kinetics and Physical Heterogeneity
in Colloid-Facilitated Transport of Cesium and Strontium in an
Unsaturated Quartz Porous Medium
written by Timothy Mark Dittrich
has been approved for the Department of Civil, Environmental, and Architectural Engineering

_____
Joseph Ryan

_____
Scott Summers

Date_____

The final copy of this thesis has been examined by the signatories, and we
Find that both the content and the form meet acceptable presentation standards
Of scholarly work in the above mentioned discipline.

Dittrich, Timothy Mark (Ph.D., Civil Engineering)

The Role of Desorption Kinetics and Physical Heterogeneity in Colloid-Facilitated Transport of Cesium and Strontium in an Unsaturated Quartz Porous Medium

Thesis directed by Professor Joseph N. Ryan

The sorption of contaminants to mobile colloids has been shown to increase the transport of the strongly sorbing contaminants. Our research goals were to (1) determine the effect of colloid type and desorption kinetics on the breakthrough of cesium and strontium in a saturated quartz column, (2) determine the effect of unsaturated conditions and desorption kinetics on the transport of cesium and strontium with illite clay, and (3) determine the effect of a macropore on the transport of cesium with illite clay.

Breakthrough experiments used a column packed with cleaned and well-sorted quartz sand (d_{50} = 0.325 mm). For macropore experiments, a 2.5 cm diameter vertical cylinder of sand (d_{50} = 1.6mm) was added to the center of the column. A rainfall simulator was suspended over the column and relative saturation values (S_{eff}) of 1.0, 0.80, or 0.21 were established. Moisture sensors and tensiometers monitored the flow conditions. A peristaltic pump transferred effluent to a fraction collector and was measured for total and dissolved cations, pH, and colloid concentration. A previously developed model for saturated colloid-facilitated transport of cesium and strontium was extended to accommodate unsaturated conditions.

The presence of all colloid types increased the transport of both cesium and strontium (illite > Oak Ridge colloids > silica). For illite, the transport of cesium was increased more than strontium, likely due to cesium binding more strongly to the frayed edges of the illite. The addition of colloids also reduced the cation binding capacity of the sand, presumably due to the attached colloids blocking sand binding sites. Unsaturated conditions increased the transport of

cesium and strontium relative to saturated conditions due to decreased residence time. The addition of a macropore increased the transport of cesium at high matrix sand moisture contents (S_{eff} = 1.0 and 0.80) when the macropore conducted pore water; however, the transport was not increased when the macropore was nearly dry (matrix S_{eff} = 0.21). This increased transport of total cesium occurred due to reduced residence time and because the macropore quartz had less sorptive surface area than the matrix quartz.

This work is dedicated to my family, especially to my parents and gramps,

Carolyn and Bob “Squirrel” Dittrich and Walter Henriksen,

who have supported me throughout my life and

have always reminded me of what is important- love and dignity

ACKNOWLEDGEMENTS

I am grateful for the opportunity to have worked in the Joe Ryan research group under the direction of Joe. His mentorship has taught me not only how to be a better scientist and teacher, but a better man. I have watched him balance his family life with being a father figure to many graduate students over the past 8 years, and will never forget how patient he has been with me in growing into the person I wanted to become. He helped me develop my research, design my experiments, fund my education, and interpret my results. His combination of humbleness, brilliance, versatility, and skill at presenting complicated material in a simple fashion is special.

I have also been lucky to have a diverse group of committee members help me develop my thoughts and research. Dr. Hari Rajaram has been one of the most inspirational teachers I have ever had. Through the 5 courses I took with him, I learned the beauty of numerical methods for solving problems and how to connect the power of equations with a practical conceptual model. I also learned from him the importance of patience when methodically teaching complicated concepts. Dr. Diane McKnight has taught me the importance of connecting with your students to ensure they value how fascinating the details of a problem and solution can be. Dr. Scott Summers has been a valuable friend and mentor with a unique perspective and watching how he runs his research program has taught me many lessons in team-building and the interconnectedness of all science and engineering research. Dr. Eric Small-Tilton reminded me to always remember the point of research is to solve actual problems, even when complicated details were blinding me from the connections to the "real" world. Thanks to Profs. Templeton, Crimaldi, and Hernandez for their passion and wisdom. I also have to thank faculty from my past, including Drs. Dave Bohnoff, Gary Bubenzer, Jim Converse, Sam Kung

and Ron Shuler from UW-Madison and Larry Geohring, Brian Richards, Steve Lyons, Drs. Mike and Todd Walters, Dr. Murray McBride, and Tammo from Cornell University.

The Joe Ryan Group has been a second family to me for the last 8 years and an incomplete list of the many people who have helped me find my place in Boulder have been: Ned Turner, Susan Bautts, Alice Wood, Audrey Norvell, Sanjay Mohanty, Chase Gerbig, Jeff Writer, Allison Craven, Jack Webster, and Brett Poulin. Others I am grateful for having met are Tesfa Yacob, Aditya Kausik, Arvind Mohanram, Dave Metge (USGS), Soo Kim, Sukyung Kung. I thank all of the students I have had the privilege to teach over the 6+ semesters I taught water chemistry lab sections for Joe and Diane- they have taught me as much as I hope I taught them. A special thanks to Mark Eaton of the ITLL for allowing me to build my experimental set-up and having the patience to help me and teach me how to use new tools in the shop.

Thanks to Big City Burritos and the crew at Harpo's, especially Harpo, Charlie, Max, Ashley, Ben and, of course, Alex- your friendship, service, and nourishing food kept me working hard, especially during the 3.5 years I was living on the streets in a trailer and needed a place to relax and feel at home.

I would also like to acknowledge the support of my family, Wally Dittrich & Co. (Sami, Brennan, Kailey, Justin, and Lily), Mike Dittrich & Co. (Angela, Joey, Johnny, and TBA), Uncle Ron and Auntie Carol & Co. (Kristy, Jill, Amy, and their families), and all my friends back in Schaumburg including the Aufmanns, Chris "Oten" Ohlsen, Coach Calamino, the Barrucas, and Linda. Thanks to Dan Morales for always letting me borrow his Jeep and Dave Blecker for giving me his, and helping me keep it on the road. Finally, I would like to acknowledge Tim Dittrich, who never gave up on me through this difficult and sometimes lonely journey.

This research was supported by the Department of Energy through grant number DOE-FG02-08ER64639.

CONTENTS

TABLES

FIGURES

CHAPTER 1

INTRODUCTION

PURPOSE OF STUDY

The sorption of contaminants to mobile colloids has been shown to increase the transport of the contaminants in a process known as colloid-facilitated transport. Laboratory experiments and model simulations have shown that enhanced transport can occur when a contaminant strongly associates with mobile colloids and release kinetics are slow relative to the rate of flow.

The colloid-facilitated transport of contaminants must be accounted for to accurately predict transport rates of strongly-sorbing contaminants in the environment. Some examples of contaminants that have the potential for colloid-facilitated transport are hydrophobic pesticides, polycyclic aromatic hydrocarbons (PAHs), actinide cations (e.g., Th, U, Pu, Am), and many metals (e.g, Pb, Cu, Hg). Many low solubility contaminants that have the potential for colloid-facilitated transport are also harmful or toxic to humans, underscoring the importance of accurate modeling techniques to protect water sources from contamination.

The main objective of this research was to investigate the effect of desorption rate kinetics on colloid-facilitated transport for (1) different colloid types, (2) unsaturated conditions, and (3) physically heterogeneous porous media.

SCOPE OF RESEARCH

A series of breakthrough experiments were conducted through well-characterized quartz sand systems to determine the potential for colloids to enhance contaminant transport. Cesium and strontium were chosen to represent contaminants due to their prevalence in the environment

and contrasting sorption properties due to their monovalent and divalent nature. Four types of colloids (two types of illite, silica, and natural colloids) were used to test the effect of colloid type on enhanced transport. Unsaturated conditions were tested using illite colloids with effective saturation (S_{eff}) values of 1.0, 0.80, and 0.21. The effect of physical heterogeneity was tested by adding a macropore to the center of the experimental column, represented by a cylinder of sand with diameter five times larger than the matrix sand. The results of colloid type and unsaturated conditions were evaluated with a mathematical model to analyze the effect of desorption kinetics from the colloids on transport and the model results were used to help interpret the macropore experiments.

ORGANIZATION OF THESIS

The thesis is divided into four chapters that address important aspects of our research. After the Introduction (Chapter 1), Chapter 2 reviews the relevant scientific literature regarding colloid transport, pore water transport, colloid-facilitated transport, surface chemistry, and mathematical model development. Chapter 3 details the experimental and model results that address the effect of colloid type on colloid-facilitated transport of cesium and strontium. Chapter 4 addresses the effect of unsaturated conditions on colloids-facilitated transport of cesium and strontium with illite. Chapter 5 addresses the effect of adding a macropore on colloid facilitated transport of cesium with illite. Chapter 6 provides conclusions from the previous chapters and Chapter 7 provides references from the previous chapters.

CHAPTER 2

COLLOID-FACILITATED TRANSPORT OF CESIUM AND STRONTIUM: PAST RESEARCH AND MODEL DEVELOPMENT

ABSTRACT

The process of colloid-facilitated transport has been observed and studied in both field and lab settings. Contaminants that adsorb strongly to mobile colloids and are harmful in very small concentrations are of the most concern. Cesium and strontium, both linked to increased cancer rates, are common contaminants on U.S. Department of Energy sites and the main sources of persistent radioactive contamination from nuclear weapons testing fallout and nuclear reactor accidents. Part 1 introduced the importance of colloid-facilitated transport of cesium and strontium, organizes past research, and introduces the needs of future research. Part 2 introduces a conceptual model that describes the fundamental mechanisms that play a role in colloid-facilitated transport and incorporates the governing equations into a framework for a mathematical model developed by Turner et al. (2006). This model will be used in later chapters to elucidate details regarding the processes that lead to differences in transport between cesium and strontium, different colloids, unsaturated conditions, and the addition of a macropore.

COLLOID-FACILITATED TRANSPORT OF CESIUM AND STRONTIUM: PART 1- PAST RESEARCH

INTRODUCTION

The transport of dissolved contaminants in saturated and unsaturated porous media is governed by the rate of contaminant movement within the pore water flow (advection), dispersion through available pore space, and the balance of sorption and desorption rates of the solid phases (sand, soil, etc.) . The addition of a second solid phase (mobile particles) has the potential to increase transport, or in some cases retard transport, depending on the conditions present.

The presence of mobile colloids in natural soil and groundwater systems has been well established (McCarthy and Degueldre, 1993; Ryan and Elimelech, 1996; Kretzschmar et al., 1999; Bradford et al., 2002; Shevenell and McCarthy, 2002; 2004). Colloids generally have a high sorptive capacity resulting from their small surface area to mass ratio, which makes them effective sorbents of low solubility, strongly sorbing contaminants. Mobile colloids that sorb contaminants can increase the apparent solubility and transport rate of the contaminants when contaminant desorption from the colloids is slow relative to the rate of flow. This process is known as colloid-facilitated transport (CFT) (McCarthy and Zachara, 1989; Kretzschmar et al., 1999) (Figure 2.1).

Accounting for the additional transport of contaminants associated with mobile colloids allows for more accurate prediction of transport rates of strongly-sorbing contaminants in the environment. Some examples of contaminants that have the potential for enhanced transport are

hydrophobic pesticides, polycyclic aromatic hydrocarbons (PAHs), actinide cations (e.g., Th, U, Pu, Am), and many metals (e.g, Pb, Cu, Hg).

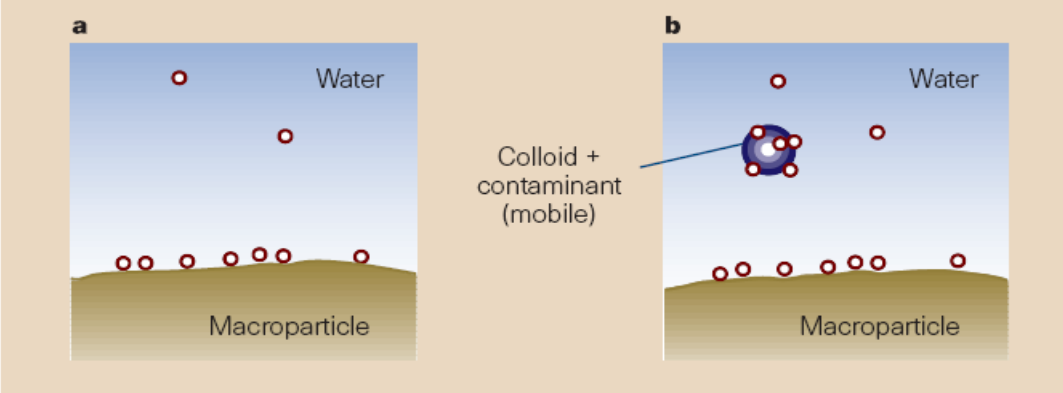

Figure 2.1. Schematic diagram showing (a) transport of contaminants in dissolved phases and (b) increased apparent solubility from contaminant sorption to a mobile colloid. From Honeyman, (1999.

Many low solubility contaminants that have the potential for CFT are also harmful or toxic to humans, underscoring the importance of accurate modeling techniques to protect water sources from contamination. "Model results are used to assess whether nuclear facilities are operated in compliance with regulatory requirements, to determine the need for remediation of contaminated sites, to estimate the effects on human health of past releases, and to predict the potential effects of accidental releases or new facilities," (Thiessen et al., 1999). As modeling techniques improve, the need for better understanding of the mechanisms driving transport in the vadose zone has become more important (NRC, 2000). The radionuclides ^{137}Cs and ^{90}Sr will be the focus of this review due to their prevalence in the environment, cancer risk in humans, and their different sorption characteristics with mineral surfaces. Due to the complexities of ion

exchange and surface complexation models, there is a need for multidisciplinary study by using high-purity materials with controlled structure and morphology (Fedoroff et al., 2004).

There are sites contaminated with nuclear material all over the world, many of which are near urban areas. Western Europe, Scandinavia, and areas affected by the Chernobyl nuclear release from 1986 maintain interest in accurate understanding of cesium and strontium transport in the environment. Recent events such as the April 2011 Fukushima Daiichi Nuclear Power Station disaster have also increased interest in the risk of radionuclide transport. Table 2.1 summarizes the results of studies that have characterized cesium and strontium transport from environments around the world. One important application of cesium and strontium transport is in the modeling of waste disposal and dose reconstruction from environmental contamination.

Contaminated U.S. Department of Energy (DOE) sites have been particularly valuable research opportunities for studying the transport of radionuclides in the natural environment. The DOE has conducted energy and weapons research and development in thirty-one states and Puerto Rico and has introduced many toxic and radioactive chemicals into surface waters, soils, and groundwater (Kowall, 2001). Field experiments on DOE sites, including the Nevada Test Site (Kersting et al., 1999), the Hanford 200 Area tank farm (Czigany et al., 2005), Rocky Flats (Ryan et al., 1998), and Oak Ridge National Laboratory (Shevenell and McCarthy, 2002), have confirmed that metals and radionuclides have moved further than expected due to colloid-facilitated transport.

Table 2.1. Environmental Field Assessments of Potential for Cesium and Strontium Transport.

Reference	Location	Goal of Study	Observations/Conclusions
Jackson and Inch (1989)	Chalk River Nuclear Lab (Ottawa, Canada)	Understand fate and reactive transport of surface disposed liquid radioactive waste (natural conditions)	-Sr^{2+} traveling at 3% of the groundwater velocity -Adsorption capacity of sediments effects transport more than competing cations -Sorption dominated by Fe/Al/Mn oxide coatings on sand rather than electrostatic adsorption (kinetically controlled)
Krosshavn et al. (1996)	Oslo Fjord, Norway	Determine colloidal distribution of Cs and Sr from wood pulp mill wastewater after discharge into seawater	-Sr in wastewater was 6% particulate (>0.45 µm), 33% colloidal (0.45 µm - 10 kDa), and 62% low molecular weight (<10 kDa) -In seawater, almost all Sr was < 10 kDa -Cs in wastewater was 5% colloidal and 95% low molecular weight.
Tegen and Dorr (1996)	Upper Rhine Valley, Germany	Understand mobilization of Cs (Chernobyl fallout) from organic-rich soil	-Studied downward movement of Cs in forest soils -Cs fluxes were order of magnitude higher in summer than winter -Cs bound to soil OM
Tipping (1996)	Cumbria, UK	Simulate reactive transport with Uplands model (CHUM) for Co, Cs, Sr, U, Th, and Am transport for 2 yrs after hypothetical release	-Highly selective sites important for Cs -DOM binding important for actinides (Th transport increased by >100% by complexing with fulvic acid) -Co, Sr, Cs lost from catchment in decades, actinides much more persistent
Dawson and Pohl (1997)	Sandia National Lab, New Mexico	Determine fate of Cs from 6 million gallons of radioactive cooling water disposed in unsaturated drainfield from 1963-1967	-30 year old radioactive liquid drain field assessed for Cs transport (concluded there was no risk of groundwater contamination) -No Cs >4.6 m from bottom of drainfield (no saturated flow for 20 years) -Equilibrium sorption coefficient was most important factor
Comans et al. (1998)	UK	Determine mobility of Cs from soil and sediment cores	-More transport in organic soils (organic exchange sites) -Ion exchange model worked well predicting all Cs on frayed edge sites of clay minerals in organic soil
Egeberg (2000)	Sweden	Investigate potential remediation applications for Cs from Chernobyl fallout	-River liming reduces levels of dissolved Cs in lake water -Acid insoluble particles and iron content of lime was important
Johansen et al. (2003)	Los Alamos, NM	Investigate potential for increased Cs transport after a forest fire	-Increased Cs transport immediately after forest fire
Robinson et al. (2003)	Coral Islands, N. Marshall Islands	Evaluate transport potential of contamination from weapons testing	-Evidence that Cs was transported to the groundwater from the soil column and root zone during heavy rains from perched water table recharge
van der Perk and Slavik (2003)	western Slovakia	Model redistribution of Chernobyl-derived Cs in sediments	-Dissolved Cs transport was reduced by 26 times since 1986, but was still measureable with most transport due to suspended sediments
Bea et al. (2004)	NA	Investigate remediation of contaminated soils	- Need to limit preferential flow with high periodic flushing of KCl^{+}seawater
Duran et al. (2004)	Asia-Pacific Ocean	Establish benchmarks for Cs and Pu in Asia-Pacific regional seas	-Cs concentrations are declining over time -Pu concentrations were lower than Cs
Hakanson (2004)	Northern Europe	Model radionuclide transport on land and in lakes	-Developed catchment area model for land and water transport of Cs with R^2>0.99 fit
Matsunaga et al. (2004)	Sahan River near Chernobyl, Ukraine	Determine distribution of dissolved Am, Cs, and Sr (< 0.20 µm) with natural colloids in waters within 30 km of Chernobyl	-Sr was found predominantly in the smallest size fraction (< 1kDa) -Pu and Am were mostly adsorbed to >10 kDa humic substances

Reference	Location	Goal of Study	Observations/Conclusions
Ito et al. (2007)	Japan Sea	Investigate potential for accumulation of radionuclides	-No accumulation of Cs or Sr in Japan Sea, but 40% increase in Pu over fallout concentration, suggesting accumulation
Kobayashi et al. (2007)	Irish Sea, UK	Develop model to assess dissolved, particle sorbed, and sediment sorbed Cs transport	-Possible to relate ocean transport model mechanisms to surface transport
Sims et al. (2007)	Alberta, Canada	Investigate potential for transport of Cs, Sr, and U from 1951 storage tank leak	-Leak poses no risk of groundwater contamination
Hull and Schafer (2008)	Snake River, Idaho National Lab	Understand transport of 70.4 m^3 dose of acidic, high I water with Sr^{2+} (15,700 Ci over 5 days in Nov. 1972) through 33 m of unsaturated gravel with reactive transport modeling	-Used multiphase reactive transport model (TOUGHREACT) -Partition coefficients couldn't explain both perched water table and soil concentrations -Exchange capacity, selectivity coefficients, and wetted pore space were most important model parameters
Jeong et al. (2009)	Korea	Predict potential for cesium contamination from a terrorist attack in Korea	- May be possible to relate ocean transport modeling to surface transport
Stepanets et al. (2009)	Ob River Basin near Mayak, Ukraine	Determine distribution of radionuclide (U, Cs, and Sr) contamination based on size fractionation	-Complex relationships between particle sizes and radionuclide distribution -Most Cs and Sr in Ob estuary was transported sorbed to sediment -Cs sorption kinetics played a role in downstream transport
Utsunomiya et al. (2009)	Nevada Test Site	Study potential Co-transport of U, Cs, Th, Co from groundwater samples 1.3 km from Benham underground nuclear test	Evidence of co-transport of U, Cs, Th, and Co in 100 nm colloids originating 1.3 km away
Laverov et al. (2010)	Lake Karachai, Ukraine	Understand subsurface transport of ^{60}Co, ^{40}K, U, and transuranic compounds	-Most U above 20 m was associated with colloids larger than 100 nm -Below 20 m, most U associated with humic complexes

CRITERIA FOR COLLOID-FACILITATED TRANPORT

Colloids have been shown to increase the transport rate of contaminants in saturated porous media (McCarthy and Zachara, 1989; Honeyman, 1999; Kretzschmar et al., 1999; McGechan, 2002; McGechan and Lewis, 2002; de Jonge et al., 2004a), unsaturated porous media (de Jonge et al., 2004b; DeNovio, 2004), and fractured rock (Vilks and Baik, 2001). Three conditions are necessary for colloid-facilitated transport to occur: (1) there must be a source of colloids, (2) contaminants must associate with the colloids and desorb slowly relative to the rate of transport, and (3) the colloids must be transported.

Sources of Colloids. The International Union of Pure and Applied Chemistry (IUPAC) defines a colloid as any particle that is between 1 nm and 1 μm in at least one dimension (IUPAC, 2002). Previous studies and review papers have documented the origin, size distribution, abundance, and chemical make-up of colloids in natural and perturbed subsurface systems (Ryan and Elimelech, 1996; McGechan and Lewis, 2002; de Jonge et al., 2004a; DeNovio et al., 2004). Typical colloids found in the environment consist of minerals (e.g., clay minerals, oxides), microbes (e.g., viruses, bacteria, protozoa), and decayed plant material classified as particulate organic matter (Figure 2.2a). An inverse logarithmic relationship between colloid size and colloid concentration shows that small colloids are much more abundant (Figure 2.2b). Mineral fragments and weathered silicates and phyllosilicates will be the focus of this review.

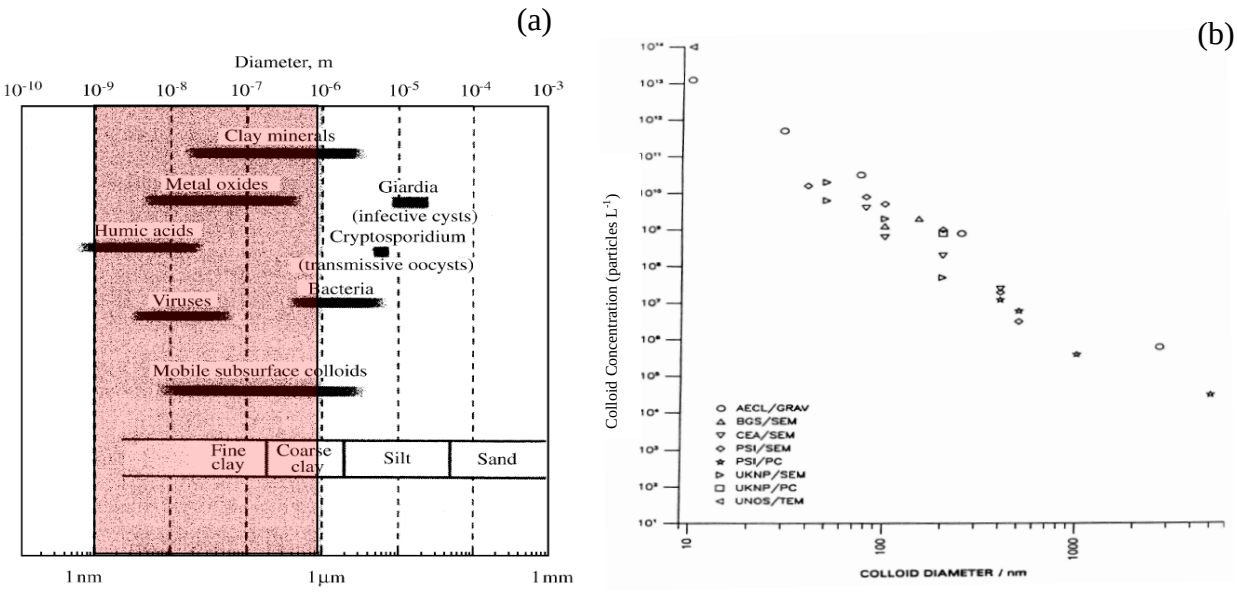

Figure 2.2. Types of colloids include clay minerals, metal oxides, humic acids, and viruses (a). A comparison of the relative sizes of common environmental colloids (b) exhibits an inverse log relationship between colloid diameter and colloid concentration measured using different spectrographic techniques. (a) adapted from Kretzschmar et al. (1999) and (b) adapted from McCarthy and Degueldre (1993).

The lowest concentrations of mobile colloids are near 1 µg L^{-1} and the highest are in excess of 1 g L^{-1}, which have been reported for both simulated and natural rainfall events (Allen, 1988; Ryan et al., 1998; DeNovio et al., 2004). Higher colloid concentrations are measured in surface and near-surface water and lower concentrations are measured in groundwater. Chemical and physical perturbations drive colloid mobilization.

Chemical Mechanisms of Colloid Mobilization. Chemical perturbations that can lead to colloid mobilization in saturated porous media include decreases in ionic strength (McDowell-Boyer, 1992; Ryan and Gschwend, 1994b, a; Swartz and Gschwend, 1998), increases in pH (Swartz and Gschwend, 1998; Bunn et al., 2002), or changes in dominant cation composition (Grolimund et al., 1996). A stepwise decrease in ionic strength can increase the repulsive forces between mineral surfaces resulting in large releases of silica colloids into solution (Figure 2.3).

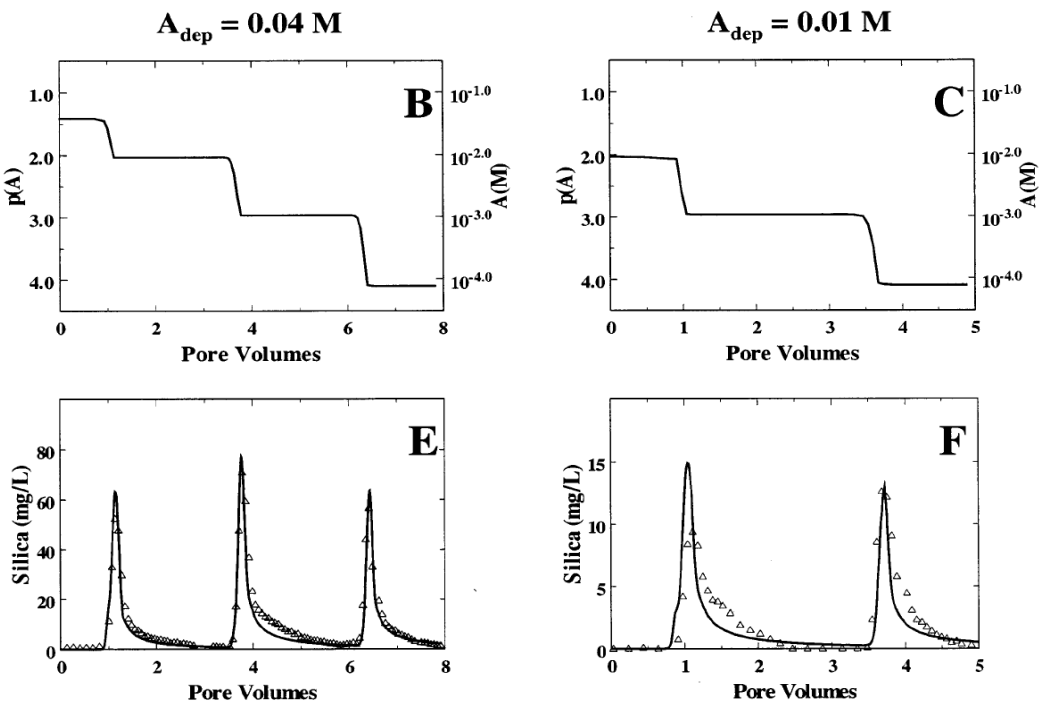

Figure 2.3. Column experiment results showing how a stepwise decrease in ionic strength results in large peak increases in silica release which approach steady, uniform release rates within 2 pore volumes after the solution chemistry change. The top graphs (a and b) show the ionic strength change and the bottom graphs (c and d) show the resulting colloid release with silica concentration on the x-axis in mg L^{-1} and pore volumes on the y-axis. (Lenhart and Saiers, 2003).

Similarly, a stepwise increase in pH can increase the negative surface charge and also release colloids to solution by (Figure 2.4).

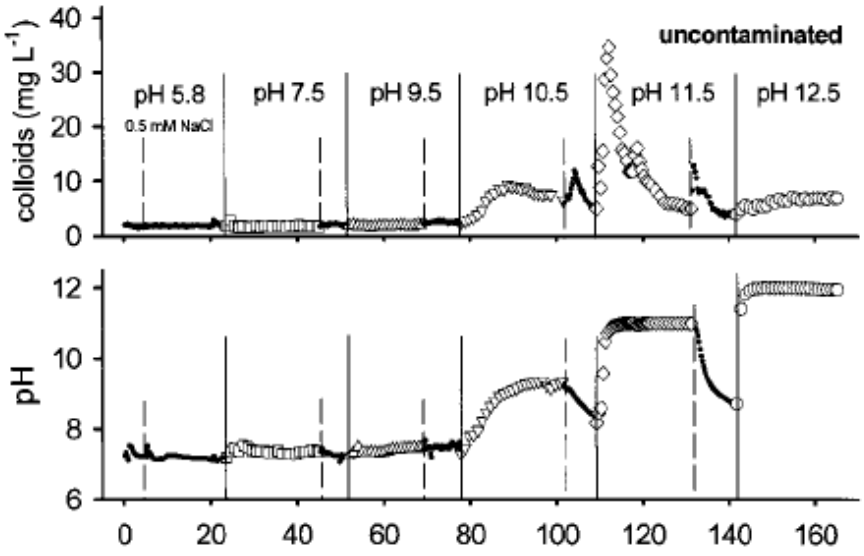

Figure 2.4. Column experiments that showing an increase in solution pH (bottom graph) resulting in releases in colloids from columns packed with soil material. Note that the colloid concentration remains constant until the pH of the influent solution is raised from 9.5 to 10.5. From Bunn et al. (2002).

The same chemical perturbations in ionic strength, pH, and dominant cation composition cause similar responses in unsaturated porous media colloid mobilization (Saiers and Lenhart, 2003b; Gao et al., 2004). One difference, however, is that pore water chemistry can change much more rapidly in unsaturated porous media due to flow transients transporting portions of the pore water much faster than the mean flow velocities found in a comparable saturated system (El-Farhan et al., 2000; Saiers and Lenhart, 2003a).

Physical Mechanisms of Colloid Mobilization. Field studies have shown that natural mineral and clay colloids are mobilized from saturated soils, even under steady flow conditions (Ryan et al., 1998; El-Farhan et al., 2000). This mobilization can result from colloids diffusing from the solid surface, through a boundary layer, and into a mobile water conduit (Ryan and Gschwend, 1994b; Jacobsen et al., 1997; Shevenell and McCarthy, 2002), or through shear forces physically removing colloids from the solid surface and entraining them into the pore

water (Laegdsmand et al., 1999; Weisbrod et al., 2002). Experiments have confirmed that colloid mobilization due to shear is minimal and the small amounts of mobile colloids produced during steady flow conditions are generally due to colloidal dispersion (Jacobsen et al., 1997; Ryan et al., 1998; Abadzic and Ryan, 2001). A linear relationship between cumulative mass of colloids released and the square root of time demonstrates diffusion-limited colloids release (Figure 2.5).

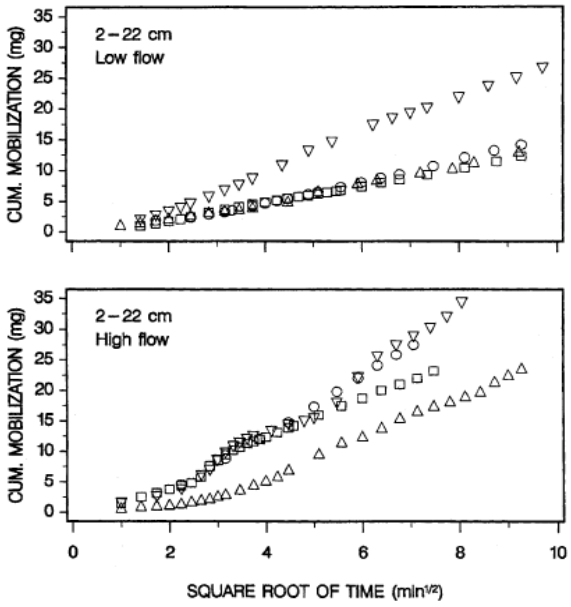

Figure 2.5. A linear relationship between cumulative mass of colloids and the square root of time ($t^{1/2}$) demonstrates diffusion-limited colloid release. From Jacobsen et al. (1997).

Unsaturated conditions introduce air to the porous media system, which enables two additional colloid mobilization mechanisms: (i) film expansion release and (ii) air-water interface scouring (DeNovio et al., 2004) (Figure 2.6).

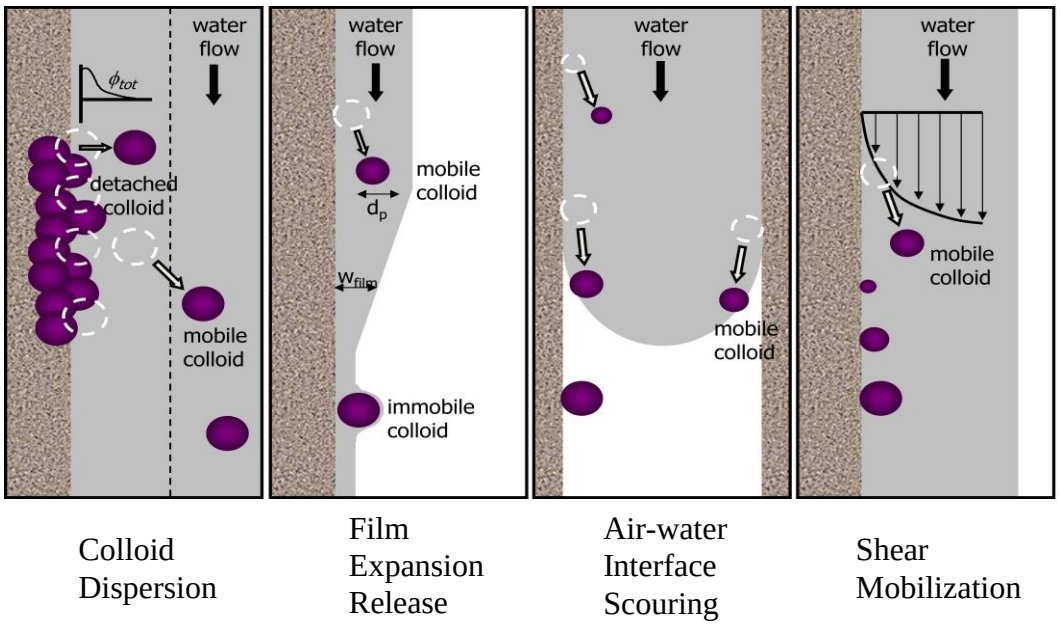

Figure 2.6. Conceptual diagram of physical release mechanism of colloids including (a) colloid dispersion, (b) film expansion release during imbibition, (c) air-water interface scouring, and (d) shear mobilization. From DeNovio (2004).

Colloid mobilization experiments with intact soil cores have shown a deviation from the colloid release relationship with the square root of time during imbibition and high flow, suggesting that other mobilization mechanisms such as air-water interface scouring or increased shear stress play a large role in colloid mobilization of unsaturated porous media (Jacobsen et al., 1997; Laegdsmand et al., 1999; El-Farhan et al., 2000). Laboratory studies have shown a close link between the amount of increase in the moisture content and the fraction of colloids made eligible for mobilization in column experiments (Wan and Wilson, 1994a; Wan and Tokunaga, 1997; Lenhart and Saiers, 2002; Saiers and Lenhart, 2003a). In laboratory columns, Wan and Tokunaga (1997) observed colloid release from sand surfaces when the water film thickness became greater than colloid diameter. The increased mobilization of silica colloids from quartz

during imbibition has been shown to be mostly due to the expansion of films (Lenhart and Saiers, 2002; Saiers and Lenhart, 2003a).

Colloids in unsaturated porous media may also be mobilized by moving air-water interfaces and air bubbles scavenging colloids from solid grain surfaces with passing wetting and drying fronts. Colloids have been shown to associate with air-water interfaces in lab experiments (Wan and Wilson, 1994a) (Figure 2.7).

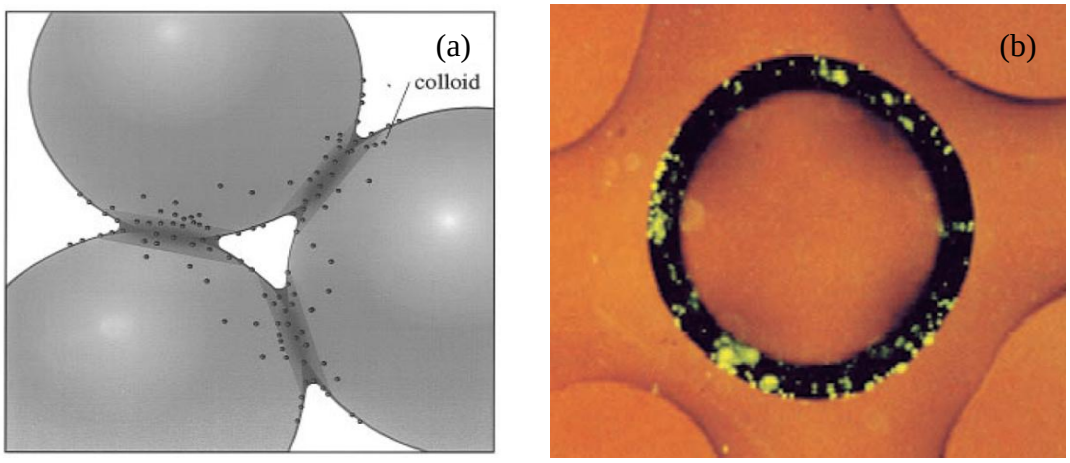

Figure 2.7. A conceptual drawing of colloids trapped at air-water interface of water trapped in an unsaturated porous media as an interpendular ring (a) and photograph showing evidence that a trapped air bubble (black circle) can accumulate colloids (yellow material) at the air-water interface (b). From Wan and Wilson (1994b).

Lab experiments have also shown that moving air bubbles increase the transport of colloids (Gomez-Suarez et al., 2000; Gomez-Suarez et al., 2001; Saiers et al., 2003). The intensity, duration, and frequency of infiltration events has been shown to affect the rate of colloid release in field experiments involving natural soils (El-Farhan et al., 2000). The passing of wetting and drying fronts can release large amounts of colloids into the mobile pore water solution (Figure 2.8).

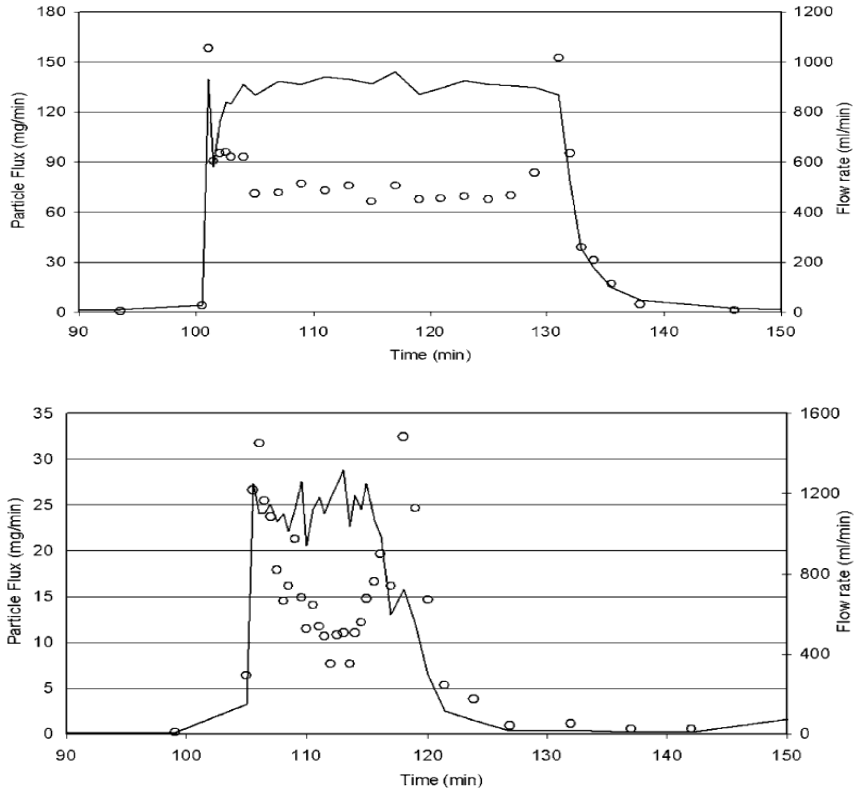

Figure 2.8. Column experiments showing a large increase in colloid mobilization with the passing of both the wetting front and drying front. From El-Farhan et al. (2000).

Contaminant Association with Colloids. Mobilization of colloids through porous media will have no effect on contaminant transport rates if (1) the contaminant doesn't associate with the colloids, (2) the aqueous contaminant travels faster than the colloids, or (3) the contaminant desorbs quickly from the colloids. Transport rates of contaminants that do not significantly sorb to colloids are unaffected by the presence of colloids (Spurlock and Biggar, 1990; Lafrance et al., 1994). Colloids (especially clays, metal oxides, and carbonates) can readily adsorb a variety of contaminants through ion exchange and surface complexation reactions (Ryan and Elimelech, 1996).

For colloid-facilitated transport to be significant, the contaminant must desorb slow relative to the rate of aqueous transport. Slow desorption kinetics allow for a contaminant to remain associated with a colloid even when there is very little contaminant remaining in the aqueous phase. Kersting et al. (1999) found greater than 99% of Eu and Pu, 91% of the Co, and 95% of the Cs in groundwater at the Nevada Test Site was associated with the colloidal and particulate fractions. Laboratory experiments have found Pu sorption to montmorillonite to be irreversible a 1 year timescale (Triay et al., 1997; Kersting et al., 1999). Even though Pu can have solubility as low as 10^{-17} M, it has been found 1.3 km from the Nevada Test Site (Honeyman, 1999; Kersting et al., 1999), presumably due to CFT. Vilks et al. (1993) estimated that colloids from a Canadian uranium deposit can retain U for as long as 8,000 y. Laboratory experiments by Roy and Dzombak (1997) demonstrated the importance of desorption rates on contaminant transport. Table 2.2 summarizes the major results regarding cesium and strontium sorption to colloids and porous media.

Table 2.2. Colloid and Soil Sediment Sorption Isotherm Experiments for Cesium and Strontium.

Reference	Cation	Colloids (Size& make)	Porous Media	Solution Chemistry	Major Results/Conclusions
Fujikawa and Fukui (1991)	Cs^+ & Co^{2+}	none	Rock powder and pieces	Saline water	-Two site kinetic model worked well for Cs adsorption to rock pieces (kinetics important for field-scale transport) -Adsorption rate was dependent on rock sizes
Comans and Hockley (1992)	Cs^+	illite	none	Varied	-Cs sorption to K- and Ca- saturated illite is kinetically controlled -Freundlich isotherms show reversible sorption with timescales greater than a few days and irreversible if less
Adeleye et al., (1994)	Cs^+, Sr^{2+}, & Eu^{3+}	kaolinite monmori-llonite	none	pH 2, 4, 7, 10 10^{-6} - 10^{-2} M nuclide concentrations	-Uptake increases in order of Cs < Sr < Eu -Sorption agrees with ion exchange equilibrium
Hsu and Chang (1994)	Cs^+	bentonite	sand	Groundwater	-Cs sorbed irreversibly to interlayer of bentonite -Cs sorbed to sand and humic acids was reversible -Humic acid blocked bentonite sorption sites (over 6% humic acid)
Zygmunt et al. (1998)	Cs^+	none	Two silt/loam soils	Natural pore water conditions	-Marl fraction of silty loam soil had more Cs sorption than weathered loam (58% vs. 14%) -Calculated only 0.045 to 0.3 cm yr^{-1} transport of Cs
Flury et al. (2004)	Cs^+	none	Hanford sediments and silica sand	I 0.001 to 1.0 M pH = 10	-Ionic strength had order of magnitude larger effect with sediments than silica
Missana et al. (2004)	Cs^+	bentonite	Grimsel Test Site groundwater system	Varied	-Bentonite showed two-site sorption behavior for Cs (not U) at low concentrations (< 1 x 10^{-9} M) -Fast planar sites took hours, slower sites took days-weeks
Kumar et al., (2006)	Cs^+	Silica and humic acid	none	-pH 3-10 -I = 0.05 M	-Below pH 7, humic acid enhanced Cs sorption to silica -Above pH 7, humic acid had no effect on Cs sorption
Sverjensky (2002, 2006)	Cs^+ & Sr^{2+}	Pure mineral surfaces	Pure mineral surfaces	Varied	-Binding dependent on dialectric constant of sobent -Strength of salvation energy linked to inner sphere or outer sphere binding
Turner et al. (2006)	Cs^+ & Sr^{2+}	Illite	none	pH 7.3 10^{-9} to 10^{-2} M	-Cesium exhibited two-site sorption -Strontium exhibited one-site linear adsorption
Bucur et al. (2007)	Cs^+	Clay colloids	Mineral soils	Natural pore water	-Clay can retard Cs transport in natural systems
Galambos et al. (2010)	Cs^+ & Sr^{2+}	bentonite	none	Varied	-Langmuir binding of Cs and Sr to Na-saturated clays -pH decreased with Sr sorption from H^+ exchange -Complete sorption occurred within minutes
Iijima et al., (2010)	Cs^+	monmori-llonite (< 0.8 μm)	none	-10^{-4} to 10^{-9} M Cs -0.92 mg L^{-1} colloids -pH 7.8	-Adsorption dominated by ion exchange at concentration below10^{-4} M and was reversible -Slight colloid size dependence suggests contribution of surface complexation - >10^{-3} M Cs concentration led to decrease in basal spacing and interlayer Cs fixation

Transport of Colloids. In order for CFT to occur, a colloid and the associated contaminant must move through the soil profile. Once mobilized, colloids travel through porous media by advection and dispersion until they are removed from flow by a variety of deposition mechanisms. In saturated soils, colloids can be removed from flow by (1) straining and (2) attachment to mineral grain surfaces. Straining is a physical mechanism and takes place when the size of a colloid moving through flow is larger than the size of the pore opening, resulting in the colloid getting "stuck" (McDowell-Boyer et al., 1986). Bradford et al. (2002, 2003) experimented with polystyrene microspheres in uniform and poorly sorted porous media and found that pore straining can be modeled as first-order removal with a rate coefficient dependent on the depth and mean grain diameter of the porous media.

Attachment to the mineral grain surface is a physicochemical mechanism that depends on the rate of colloid transport from the bulk fluid to the grain surface and the probability that a colloid-grain collision will result in attachment (Ryan and Elimelech, 1996; DeNovio et al., 2004). Colloids are transported from the bulk fluid to the grain surface by Brownian diffusion, interception, and sedimentation (Yao et al., 1971). The rates of these mechanisms for saturated porous media can be calculated as a function of colloid diameter and density, porous media grain size, and flow velocity (Yao et al., 1971; Tufenkji and Elimelech, 2004). The probability that a colloid-grain surface collision will result in attachment is related primarily to the electrostatic forces between the colloid and grain surfaces. The electrostatic forces as described by DLVO theory (Derjaguin and Landau, 1941; Verwey and Overbeek, 1948) are the sum of the double layer, van der Waals, and short-range solvation or steric forces (Ryan and Elimelech, 1996).

In unsaturated porous media, colloids can be removed from flow by (1) pore straining, (2) attachment to mineral grain surfaces, (3) air-water interface capture, and (4) film straining (DeNovio, 2004) (Figure 2.9)

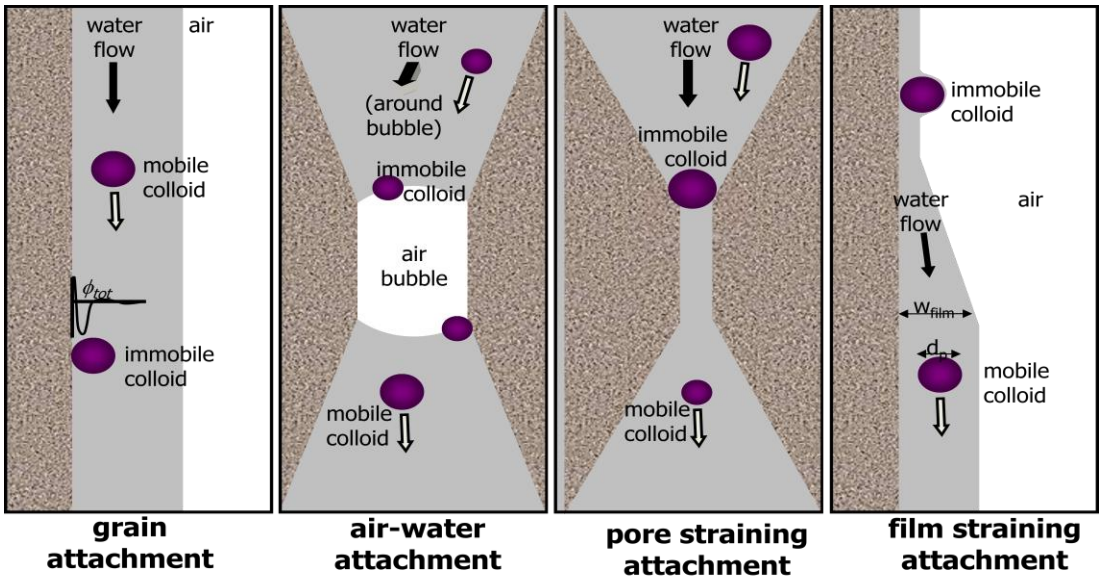

Figure 2.9. Processes affecting colloid movement in unsaturated porous media. Colloid deposition mechanisms attachment to grains by physicochemical filtration, attachment to immobile air-water interfaces, attachment by straining in water-filled pores, and entrapment in thinning water films during draining. From DeNovio (2004).

Pore straining in unsaturated soils takes place in the smaller pores that can remain filled with pore water after the larger pores begin to drain and fill with air. Attachment to mineral grain surfaces in unsaturated porous media is similar to that occurring in saturated porous media except that smaller flow paths increase the rate of colloid-grain surface collisions. The probability of attachment from each collision, however, should remain largely unchanged between saturated and unsaturated conditions when the pore water chemistry, porous media, and colloidal properties are the same.

Air-water interfaces also act as colloid collectors in unsaturated porous media. Colloids are retained at air-water interfaces by capillary or electrostatic forces which depend on pH, ionic strength, and colloid surface properties (Wan and Wilson, 1994a). The affinity of hydrophilic clay mineral colloids for the negative air-water interface; however, is minimal depends on colloid shape, surface charge distribution, and colloid- cation exchange capacity (Wan and Tokunaga, 2002).

Film straining attachment takes place in unsaturated soils at low moisture contents when most of the flow occurs through thin films that surround the porous media grains. When the film thickness reduces to around the thickness of the colloid diameter, surface tension can retain colloids against the porous media surfaces (Wan and Tokunaga, 1997; DeNovio et al., 2004). Smaller grain size and larger colloids increase the film straining efficiency (Wan and Wilson, 1994a, b).

Colloid-Facilitated Transport of Cesium and Strontium. If all three of the above criteria for colloid-facilitated transport are met, colloid-facilitated transport is likely to occur.

Quartz sand colloid-facilitated transport experiments have been conducted under saturated conditions for cesium with kaolinite (Saiers and Hornberger, 1996b, 1999) goethite (Satmark et al., 1996), and illite (Turner et al., 2006a). Noell et al. (1998) observed that silica colloids increased cesium transport through glass beads. Columns packed with sandy soils from the Hanford tank farm in WA have also shown that natural colloids increased cesium transport (Flury et al., 2002, 2004; Steefal et al., 2003; Zhuang et al., 2003; Lichtner et al., 2004). Colloid-facilitated transport of cesium has been observed with montmorillinite colloids in groundwater at the Grimsel Test Site in Switzerland (Bouby et al., 2011). Colloid-facilitated transport of cesium has been observed in unsaturated columns packed with sandy Hanford

sediments (Chen et al., 2005; Cheng and Saiers, 2010). Unsaturated colloid-facilitated cesium transport has been observed in sand from the Chernobyl area (Szenknecht et al., 2003).

Strontium colloid-facilitated transport has been observed in quartz sand columns with silica colloids (Solovitch-Vella et al., 2006) and illite colloids (Turner et al., 2006). Strontium retardation has been observed with silica colloids in quartz sand (Bekhit et al., 2006), bentonite colloids in a fractured granite core (Albarran et al., 2011), and with natural colloids and Hanford sediments (Pace et al., 2007). Colloid-facilitated transport of strontium in unsaturated sand from the Chernobyl area was observed with native colloids (Szenknect et al., 2003).

Rod et al. (2010) used high pH (pH >10) and high ionic strength simulated Hanford wastes with cesium and strontium under saturated and unsaturated conditions and found that cesium and strontium transport was retarded by co-precipitation of cesium with strontium eigencolloids, however cesium was less retarded than strontium. Table 2.3 summarizes the important results from column experiments studying CFT of Cs and Sr.

Table 2.3. Column Experiments for Colloid-Facilitated Transport of Cesium and Strontium.

Reference	Satur-ation	Cation	Colloids (Size&make)	Porous Media	Solution Chemistry/Flow	Major Results/Conclusions
Saiers and Horberger (1996b)	Sat	Cs^+	kaolinite	Sand	I 0.002 to 0.1 M 2.6×10^{-6} M Cs	-Cs sorption rate independent of I but desorption varies directly with I -Cs sorption capacity and fraction of kinetic sites decreased directly with increased ionic strength -Cs desorption was controlled by rate-limited reactions (long desorption tails)
Satmark et al. (1996)	Sat	Cs^+	Goethite (0.12 µm)	Quartz sand (200 µm)	pH 4.5 and 10 3×10^{-10} M Cs I = 0.001 M	-Flow rate, colloid concentration and pH controlled transport -Very little goethite transport at low pH -Facilitated transport observed at both pH 4.5 (no result for pH 10)
Noell et al. (1998)	Sat	Cs^+	Silica (100 nm)	Glass beads (150 and 420 µm)		-Silica colloids enhanced Cs+ transport through glass beads -Modeled with retardation coefficient with constant colloid loading
Saiers and Hornberger (1999)	Sat	Cs^+	kaolinite	Sand	I 0.002 to 0.1 M	-Ionic strength (I) had effect on partition coefficient, 1st order kaolin deposition rate, quartz desorption coefficient -I had no effect on adsorption rate coefficient or sorption capacity -Very little enhanced transport above I = 0.01 M (decreases above 0.002 M)
Flury et al. (2002)	Sat	Cs^+	Natural soil colloids (quartz, illite, kaolinite)	In situ and repacked column with Hanford, WA sediments	1 mM to 1 M $NaNO_3$ 0.02-0.2 mM Cs 0.1 mM Cs pulse in column experiments (pH 10)	-More cesium transport at high I -Cs sorbed to colloids was transported unretarded -Cs transport attributed to sorption to high affinity sites on mica and illite
Alonso et al. (2003)	Sat	Cs^+, Sr^{2+}, & Eu^{3+}	Bentonite (93% smectite) < 0.63 µm	Granite sheets from Grimsel, Switzerland	5.7-8.7 x10-3 M radionuclide conc. (pH 8.3)	-Bentonite colloid diffusion into the granite micropores promoted transport of radionuclides into granite in less than 8 days
Steefel et al. (2003)	Sat	Cs^+	Natural soil colloids	Uncontaminated SX tank farm Hanford sediment	Hanford waste	-3 site model predicted Cs transport w/ 2 sites being high selectivity frayed edge sites (0.02 and 0.22% CEC) and >99% planar sites -Cs sorption reversible -Self-sharpening Cs breakthrough curves
Szenknect et al. (2003)	Unsat	^{85}Sr & ^{134}Cs	Natural soil colloids	Natural sand f/ Chernobyl area	Simulated groundwater	-Decrease in moisture content led to a decrease in K_d value
Zhuang et al. (2003)	Sat	Cs^+	Colloids from reacting Hanford sed. with tank waste	-Hanford sediment -Silica sand	Simulated tank waste (10 cm column) -7.5 x 10^{-5} to 1.4 x 10^{-8} M Cs^+	-Highly nonlinear sorption of Cs -CFT more pronounced at low Cs concentration -Slow Cs breakthrough w/o colloids (except for sand) -Cs stripping from colloids is controlled by Cs concentration and matrix sorption capacity

Reference	Satur-ation	Cation	Colloids (Size&make)	Porous Media	Solution Chemistry/Flow	Major Results/Conclusions
Chen et al. (2005)	Unsat S_{eff}= 0.2-1	Cs^+	Hanford Tank Farm soil colloids	Hanford sediments	20 cm columns Simulated groundwater	-Higher flow rates = less Cs^+ stripped from colloids -Less Cs+ was stripped from colloids at lower saturation -Up to 70% of Cs^+ was desorbed from colloids
Bekhit et al. (2006)	Sat	Sr^{2+}	Silica (0.97 µm)	Quartz sand (0.125-0.250 mm)	5^{-5} M Sr^{2+} 1.0×10^{-4} to 3.0×10^{-2} I 4-7 pH	-Silica colloids slightly retarded strontium transport, especially at low pH
Solovitch-Vella et al. (2006)	Sat	Sr^{2+} & Co	various	Silica	Simulated groundwater	-A wide range of colloids can enhance transport
Turner et al. (2006)	Sat	Cs^+ & Sr^{2+}	Illite clay	Ottawa, well-rounded sand	I = 2.0 and 0.1 mM pH = 7.3 $NaHCO_3$, Cl^-	-Increased transport of Cs^+ and Sr^{2+} with illite present -Two-site kinetic model matched results for Cs better than Sr
Pace et al. (2007)	Sat and Unsat	Sr^{2+}	Natural colloids (none added)	Hanford sediments, repacked columns, and undisturbed core	pH 8 0.228 mM Sr^{2+} or $SrEDTA^{2-}$ I = 0.1 M with NaBr, NaCl, & NaOH	-$SrEDTA^{2-}$ complexes were unstable and dissociated (possibly replaced with Ca, Pb, Mg, and Mn) -less retardation and more irreversible sorption under unsaturated conditions (retardation resulted from more immobile water) -Fraction of Sr sorption in core (49 % carbonates, 37% ion exchange sites, and 14% oxide fraction)
Chang and Saiers (2010)	Unsat	Cs^+	Mobilized colloids	Hanford course sand (equilibrated with artificial Cs solution)	I = 0.16, 2 and 50 mM	-Transient conditions mobilized colloids -CFT of Cs in vadose zone increased with transient conditions Low ionic strength promoted CFT from increased colloid mobility and increased Cs sorption to colloids
Tang and Weisbrod (2010)	Sat	Cs^+	Montmori-llonite and humic acid	Fractured chalk core (Negev desert, Israel)	-pH 7.5 - I = 2.7 mM -0.2-0.4 mM Cs	-17% of cesium was transported as colloid-associated Cs -Humic acid didn't adsorb cesium; however, promoted Cs transport due to increasing colloid transport
Albarran et al. (2011)	Sat	Sr^{2+}	Ca-Mg-Bentonite (smectite) colloids	Granite core with 0.6 mm fracture	I = 5×10^{-4} M I 9.4 pH 1×10^{-6} m s^{-1}	-colloids retarded strontium transport -% recovery, however, was higher for colloids and strontium versus strontium w/o colloids
Bouby et al. (2011)	Sat	Cs^+, Eu^{3+}, Th^{4+}, U^{4+}	Montmoril-linite colloids	Grimsel Test Site, Switzerland	I = 10^{-3} M 9.6 pH	- Eu and Th mostly bound to colloids, U mostly in hydroxide complexes and Cs mostly dissolved - Humic acid addition led to humic complexes dominating speciation; however, Th remained mostly irreversibly bound to colloids

Effect of Physical Porous Medium Heterogeneity. Porous media heterogeneity can be both physical (e.g., macropores, fractures, soil structure, grain size variations) and geochemical (e.g., grain surface chemistry). In this proposal, we will focus on physical heterogeneity. Physical heterogeneity is the result of stratification during soil genesis, wetting and drying cycles, freezing and thawing cycles, plant root channels, worm holes, erosion, and eluviation (Li and Ghodrati, 1997).

Many experiments have observed increased water and solute transport rates due to the presence of macropores (Bouma and Anderson, 1977; Parker, 1984; Kluitenberg and Horton, 1989; Phillips et al., 1989; Czapar et al., 1992; Saiers et al., 1994a; Li and Ghodrati, 1997). Pore continuity and connectivity plays a large role in solute transport velocity (Li and Ghodrati, 1997). Pore continuity can be determined by analyzing solute breakthrough curves (Kissel et al., 1973; Cassel et al., 1974; Anderson and Bouma, 1977a, b).

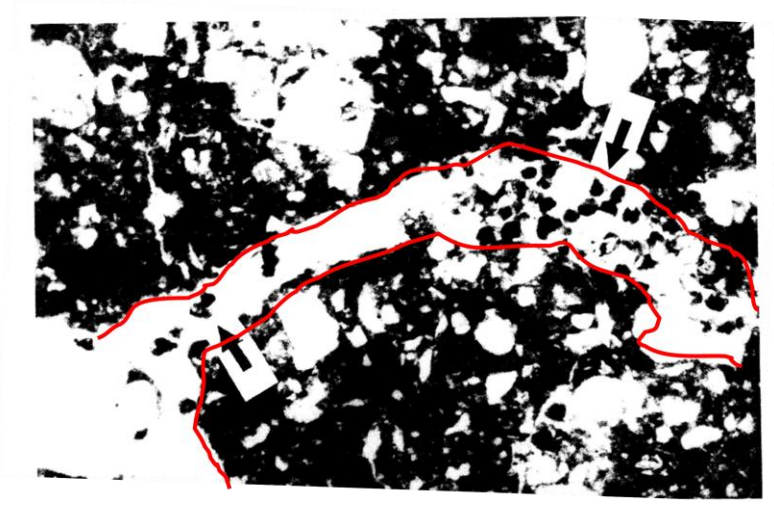

Figure 2.10. Image of a physical heterogeneity. The red denotes a worm burrow that has resulted in a macropore with a different soil texture than the matrix soil due to the small balls of worm castings partially filling the empty channel. From Litaor et al. (1994).

Fewer studies have focused on the role of macropores in colloid and contaminant transport. Pilgrim and Huff (1983) conducted *in situ* field experiments with loam and clay loam soils with macropores and found macropores allowed for transport of larger colloids. Ryan et al. (1998) found that macropore flow dominated water movement and transport at Rocky Flats and increased CFT of Pu. The accelerated flow velocities found in macropores may also be responsible for increased colloid generation; however, this has not been fully investigated. Knowing the origin of the colloids responsible for transporting contaminants is crucial in being able to model CFT in the presence of a macropore.

RESEARCH NEEDS

Recent studies suggest that colloid-facilitated transport also occurs under unsaturated conditions; however, the evidence linking this transport to physical mechanisms (colloid and porous media properties and solution chemistry) is scarce.

Previous work on unsaturated porous media has focused on aqueous transport and colloidal transport. The main objective of this research was to investigate the effect of desorption rate kinetics on colloid-facilitated transport under unsaturated conditions and in the presence of a physical heterogeneity. Specifically, to extend the work that has been done on saturated colloid-facilitated transport and unsaturated colloid transport. To evaluate this, we used cesium and strontium as our model.

The role of desorption kinetics in CFT must be investigated in further detail. Experiments must expand on the saturated porous media work of Vilks and Baik (2001), Turner et al. (2006b), and others to investigate the role of contaminant desorption rates in unsaturated soils and in the presence of macropores. A quantitative analysis of the effects of unsaturated flow and macropores on contaminant and colloid transport rates will provide better tools for

constructing contaminant transport models, especially for strongly sorbing contaminants such as cesium and strontium.

COLLOID-FACILITATED TRANSPORT OF CESIUM AND STRONTIUM: PART 2- MODEL DEVELOPMENT

INTRODUCTION

In order to model the effects that colloids and unsaturated conditions play in enhancing colloid-facilitated transport of cesium and strontium, an understanding of the mechanisms that drive saturated aqueous and colloid transport must first be established. A conceptual model has been developed to help visualize interactions between the contaminants, pore water, colloids, porous media grains, and air-water interfaces present in an unsaturated porous media system (Figure 2.11 and Table 2.4). Numbers in parenthesis for the following explanation are for mechanisms shown in Figure 2.11 and summarized in Table 1 below. The adsorption (1) and desorption (2) of dissolved cations to and from the surfaces of the porous media grains controls the removal of cations from the pore water. When colloids are present, cations adsorb to and desorb from deposited colloids (3 and 4, respectively). Cations adsorb to and desorb from mobile colloids in the pore water (5 and 6, respectively). Cations also move with colloids as they are transported and deposited through a porous medium. Cations adsorbed to a colloid can be removed from the pore water if the colloid is deposited onto the porous medium surface (7) or if the colloid is released from the colloid surface (8). Cations sorbed to a mobile colloid can be removed from the pore water if the colloid is strained from the pore water by being stuck in a pore that is too small to move through (9). The air-water interfaces (AWI) present in unsaturated porous media add additional mechanisms for transport and removal by cations being sorbed and

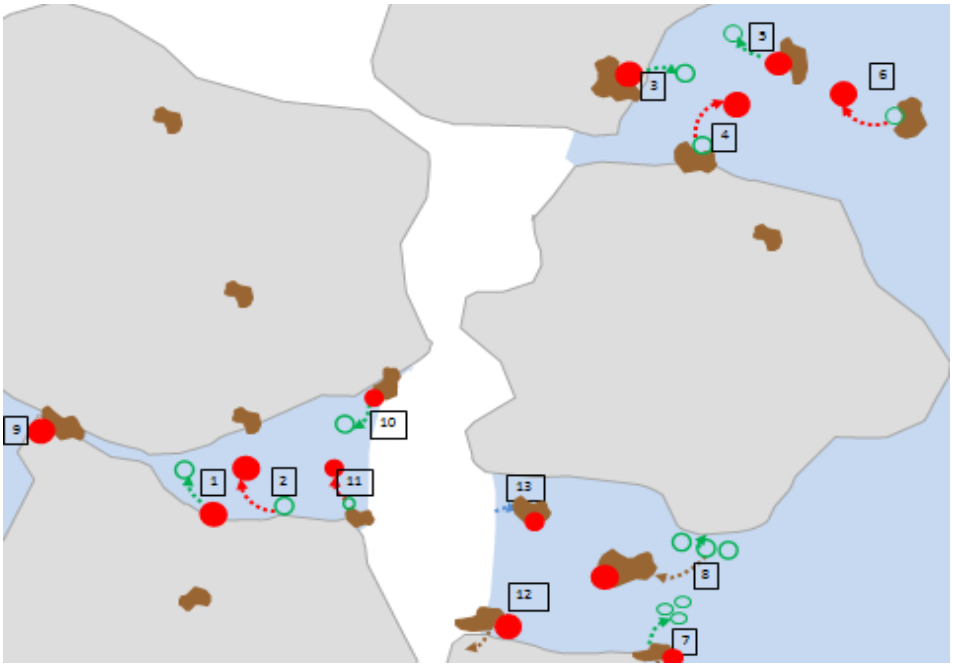

Figure 2.11. Conceptual model for unsaturated colloid-facilitated transport mechanisms (1-13) accounting for pore water, colloid, contaminant, and air-water interface reactions. Pore water is represented by blue, grain surfaces are grey, contaminant cations are red circles, competing cations (Na^+) are green open circles, and colloids are asymmetrical brown shapes. Interaction between contaminant cations and competing cations are represented by dashed arrows (green arrows for adsorption and red for desorption).

Table 2.4 Colloid-facilitated transport mechanisms. Numbers correspond to the visual depiction of each mechanism in Figure 2.11.

Rate Description	#
Aqueous Species	
Contaminant sorption to solid phase	1
Contaminant desorption from solid phase	2
Contaminant sorption to immobile colloids	3
Contaminant desorption from immobile colloids	4
Contaminant sorption to mobile colloids	5
Contaminant desorption from mobile colloids	6
Contaminant sorption to AWI-captured colloid	10
Contaminant desorption from AWI-captured colloid	11
Sorbed Species	
Colloid attachment to solid phase	7
Colloid detachment from solid phase	8
Colloid straining	9
Colloid attachment to AWI	12
Colloid detachment from AWI	13

released from a colloid attached to an AWI (10 and 11, respectively) or by a colloid with sorbed cations attaching to or being released from an AWI (12 and 13, respectively).

Water Flow. The flow of water drives the transport of both contaminants and colloids in porous media systems and will be discussed first. In all porous media, the pore size distribution dictates where water will go. For saturated flow, Darcy's law gives describes water flow:

$$q = K_S \frac{\Delta(P+z)}{L} = -K_S \frac{dH}{dz} \tag{2.1}$$

where q is the Darcy velocity (cm h^{-1}), K_s is the saturated hydraulic conductivity (cm h^{-1}), P is matric head (cm), z is gravitational head (cm), L is the flow length (cm), and dH (cm) is the change in pressure head over an infinitesimally thin slice with thickness dz (cm). For unsaturated flow, Eqn. 2.1. can be modified by using a function for hydraulic conductivity that relates conductivity to the matric potential (h) of the sand to become the following:

$$q = K(h) \frac{\Delta(h+z)}{L} = -K(h) \frac{dH}{dz} \tag{2.2}$$

where $K(h)$ is the unsaturated hydraulic conductivity.

The governing equation for one-dimensional Darcy flow in a variably- saturated porous media is Richards' equation and has the form:

$$\frac{\partial \theta(h)}{\partial t} = -\frac{\partial q}{\partial z} = \frac{\partial}{\partial z}\left(K(h)\frac{\partial h}{\partial z} + K(h)\right) \tag{2.3}$$

where θ is the volumetric water content (m^3 m^{-3}), t is time (h) h is pressure head (cm), z is the vertical coordinate positive upward (cm), and $K(h)$ is the unsaturated hydraulic conductivity function (cm h^{-1}). The retention curve can be determined analytically (van Genuchten, 1980) or by using software such as RETC can be used with numerical optimization. The Richards equation presented here takes advantage of many simplification and assumptions such as there are no temperature effects, no root uptake or evaporation of water, the air phase is neglected,

osmotic gradients in the soil potential are negligible, fluid density is uniform and independent of solute concentration, and the fluid and matrix are incompressible. Hysteresis can cause additional complications but will not be addressed in this summary.

Mineral Surface Chemistry. The first set of mechanisms (1-6) from Figure 2.10 and Table 2.5 involve sorption processes of Cs^+ and Sr^{2+} with the surface of either sand grains or mineral colloids. The solution pH determines the surface charge of the amphoteric binding sites at the mineral surface. The terminal oxygen atoms of the silica (SiO_2) quartz surface exhibit pH-dependent "edge" charge when the hydroxyl is deprotinated. As shown in Figure 2.12, the point of zero charge for quartz is near 2, meaning the surface charge is positive and protinated at pH < 2, near zero at pH 2, and negative at pH above 2 according to the following reactions:

$$\equiv Si\text{-}OH_2^+ \leftrightarrow H^+ + \equiv Si\text{-}OH \quad (2.4a)$$

$$\equiv Si\text{-}OH \leftrightarrow H^+ + \equiv Si\text{-}O^- \quad (2.4b)$$

where $\leftrightarrow$ represents a two-way reversible reaction and $\equiv$ represents the surface silicon bond to the solid quartz structure. This same relationship exists for silica colloids.

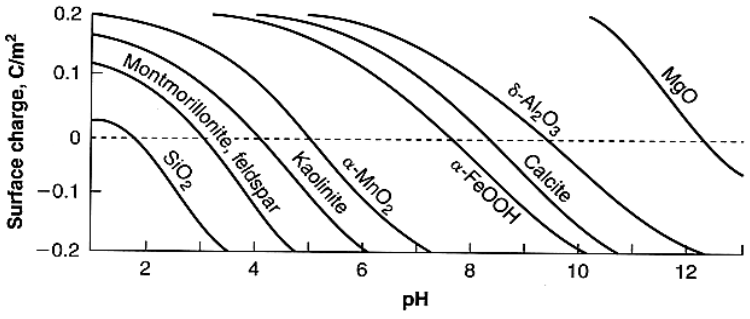

Figure 2.12. Surface charge at various pH for different mineral surfaces. From Stumm and Morgan (1996).

For phyllosilicate minerals such as kaolinite and illite, Al^{3+} substitution for Si^{4+} within the crystalline structure (known as isomorphic substitution) leaves the faces of these minerals with a permanent negative charge (Figure 2.13).

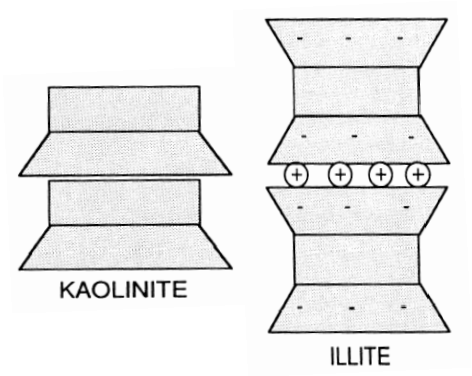

Figure 2.13. Kaolinite and illite clay particles. From McBride (1994).

1:1 clays such as kaolinite are made up of alternating sheets of SiO_4 tetrahedra and Al_4O_3 octahedral and only have permanent face charge. 1:2 clays such as illite consist of an alumina octahedral layer between two silica tetrahedral and have permanent face charge from isomorphic substitution as well as amphoteric charge with a pH_{pzc} between 7-8 according to the following reactions:

$$\equiv Al\text{-}OH_2^+ \leftrightarrow H^+ + \equiv Al\text{-}OH \quad (2.5a)$$

$$\equiv Al\text{-}OH \leftrightarrow H^+ + \equiv Al\text{-}O^- \quad (2.5b)$$

where $\leftrightarrow$ represents a two-way reversible reaction and $\equiv$ represents the aluminum bond to the bulk illite structure. Table 2.5 shows common mineral adsorption sites for clays and silica.

Table 2.5. Classification of mineral adsorption sites where M^{3+} represents Fe and Al and M^{2+} represents Fe and Mg. From McBride (1994).

Structure	Type	Affinity for H^+	Metal Bonding	Examples
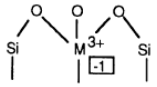	Tetrahedral, permanent	Low	Medium-range, electrostatic, fairly nonspecific	Some smectites, all vermiculites
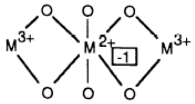	Octahedral, permanent	Low	Long-range, electrostatic, nonspecific	Some smectites
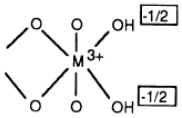	"Edge," pH-dependent (terminal OH)	High	Partially covalent, very specific	Fe oxides, Al oxides, layer silicate edges
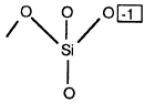	"Edge," pH-dependent (terminal O)	Moderate	Largely electrostatic, fairly specific	Silica, allophane, layer silicate edges

Since cesium and strontium ions have a positive charge and the quartz and colloidal surfaces have a negative charge at pH 7 (range for experiments), adsorption of ions to the quartz and colloidal surfaces is favored through electrostatic interactions. These interactions are dependent not only on pH, but the ionic strength of the solution as well. There are many electrostatic models that have been proposed with varying degrees of complexity (constant capacitance model, diffuse double layer model, triple layer model, etc.); however, the diffuse double layer model has been shown to be the most applicable for low ionic strength solutions (Davis and Kent, 1990; Stumm and Morgan, 1996).

The diffuse double layer model represents the mineral as a surface with a negative charge density and the liquid as a cloud of ions. The total net charge of the surface and the solution must equal zero, however, the charge of the negative mineral surface must be locally satisfied by attracting more cations in the solution than anions. If the solution has a high ionic strength

(concentration of ions), then the negative mineral surface charge can be satisfied within a close distance to the mineral surface by attracting positive cations. At lower ionic strength, the distance from the mineral surface that ions must be attracted to satisfy the surface charge becomes much larger. The double layer thickness (*d*) represents the distance from the surface where half of the electrical potential is satisfied. This distance is the inverse of the Debye-Hückel parameter, κ, in the following equation:

$$\kappa = \frac{1}{d} = \left(\frac{2F^2 I\left(10^3\right)}{\varepsilon\varepsilon_o RT} \right)^{1/2} \tag{2.6}$$

where *d* is the thickness of the "double layer", *F* is Faraday's constant (96485 C mol^{-1}), *I* is the ionic strength of the solution (M), ε is the relative permittivity (dielectric constant) of the electrolyte, ε_o is the permittivity of a vacuum, *R* is the gas constant (8.314 V C mol^{-1} $°K^{-1}$), and *T* is the temperature of the solution (298 °K).

The potential of the mineral surface to sorb ions is largely determined by the surface charge potential. The charge potential within the diffuse double layer can be predicted as a function of the surface charge potential (ψ_0) and distance from the surface (*x*) using the Gouy-Chapman equation:

$$\Psi(x) = \Psi_o e^{-\kappa x} \tag{2.7}$$

where $\psi(x)$ is the charge potential within the diffuse double layer as a function of distance from the surface (*x*), and κ is the Debye-Hückel parameter. The surface charge potential (ψ_0) can be estimated by measuring the zeta potential of the mineral surface.

Cesium and Strontium Sorption to Mineral Surfaces. The cations of interest in this review, Cs^+ and Sr^{2+}, exhibit different affinities for sand and mineral surfaces. Similar to the diffuse double layer of a mineral surface, the charge of the cation in solution must be satisfied by tightly

arranging water molecules around the atom with the oxygen atoms facing toward the cation and the hydrogen ions facing away. The ease with which these water molecules can be exchanged and replaced dictates to what extent the cation can be adsorbed to the mineral surface (Stumm, 1992). The presence of this sorbed water may also prevent the cation from approaching the mineral surface due to steric hindrance. The larger the radius of the cation, the larger the diameter of the outer electron shell will be. This large outer shell allows for a thinner layer of less strongly associated water molecules than a smaller radius cation. A smaller cation has a smaller outer electron shell allowing for more water molecules to associate tightly with the positively charged nucleus. This results in a distinct difference between Cs^{+} and Sr^{2+}. The hydrated radii of Cs^{+} and Sr^{2+} are 0.228 nm and 0.274 nm, respectively. The monovalent charge of the cesium ion allows it to lose the bound water and bind more strongly to the mineral surface.

There are two main types of binding for dissolved cations to sorb to mineral surfaces: inner sphere complexation and outer sphere ion exchange. Inner sphere complexes occur with larger ions that have relatively small hydration shells. This small hydration shell allows for the ion to closely approach the mineral surface and shed the sorbed water molecules to form a covalent bond with a deprotinated surface oxygen molecule. Cs^{+} has been shown to bind to the frayed edge sites of illite in an inner sphere manner (Comans and Hockley, 1992).

A bond that is electrostatic in nature is known as outer sphere binding. In this case, the sorbed surface water prevents the cation from forming a covalent bond with the surface oxygen of mineral surface. The electrostatic bond that is formed is not a specific point of surface of the mineral, but is a balance of the charge on the surface. Outer sphere bonds can be viewed as a probability function or as an average surface coating that satisfies the surface charge of a

mineral. It has been shown that both Cs^{+} and Sr^{2+} form outer sphere complexes with a quartz surface (Sverjensky, 2002).

Clays such as illite have the ability to form both inner and outer sphere complexes due to their two types of surface sites: permanent face charges and amphoteric edge charges. It has been shown that Cs^{+} can form outer sphere complexes with the face charge of illite and inner sphere complexes with the stronger edge charges (Cygan et al., 1996; Bostick et al., 2002).

Sorption can be one of two mechanisms: ion exchange or proton exchange. In the case of proton exchange, the cation exchanges with a proton that is bound to a surface oxygen (deprotinated hydroxyl group). If the pH of a solution is near the point of zero charge, this mechanism can be significant. When solution pH is far away from the point of zero charge of the surface, however, cation exchange becomes the dominant transfer mechanism. In most case, cations such as Na^{+} are present in much higher concentrations than the contaminant and cation competition and exchange reactions with Na^{+} must be accounted for. In a similar manner, other cations in solution (e.g., Mg^{2+}) will compete with Cs^{+} and Sr^{2+} for clay and quartz binding sites and must be accounted for. The higher the ionic strength, the more competition for binding sites and the less sorption will be observed for both Cs^{+} and Sr^{2+}. Due to the similarities between Na^{+} and Cs^{+}, more competition is observed between Na^{+} and Cs^{+}, that Sr^{2+} and Na^{+} (Turner et al., 2006).

Dissolved Contaminant Sorption Modeling. The dissolved transport of cesium and strontium is dominated by the cation/mineral surface sorption properties. Surface sorption is generally dictated by cation speciation (Sr vs SrOH vs Sr-IMt) and the affinity and capacity of the porous media for sorption of the species present. Due to the metallic behavior of cesium and strontium, speciation is very important and dependent on solution chemistry. Cesium and strontium are

present in water in the form of a metal-ligand complex, where the charge of the metal is satisfied by water molecules or other ligands present in solution. In general, the smaller and more highly charged the metal ion, the larger the complex. Metal ions attract the unshared electron pair from the O-H orbitals of the water molecules, making the dissociation of water to OH^- and H^+ easier than in the bulk solution and allowing metal ions to act as acids (Benjamin, 2002). In addition to H_2O, other ligands of interest in natural systems are OH^-, Cl^-, CO_3^{2-} and SO_4^-, however, the solution chemistry of interest in the research chapters that accompany this review paper ensured that the presence of these complexes was not significant.

Cesium and Strontium Speciation. Cesium ions usually have a coordination number greater than 6, meaning that under natural pore water chemistry ranges, cesium is relatively soluble and complexation with carbonate or hydroxide is insignificant. At extreme pH, ionic strength, and cation concentrations, cesium and strontium can form intrinsic particles or coprecipitate with other complexes. At high pH (above ~9), strontium can form strontium hydroxide particles that complicate aqueous strontium transport modeling. The initial pH of many of the waste streams on contaminated DOE sites is greater than pH 10. This has stimulated a number of breakthrough experiments, with strontium in particular, in high pH ranges that promote strontium hydroxide and eigencolloid production. The experiments conducted in the accompanying chapters focused on the eventual transport of cesium and strontium away from contaminated sites once the pH of cesium and strontium plumes are neutralized, either at the extreme edges of the plume or after significant time has passed and the pH has dropped to values closer to pH 7.3.

Cs^+ and Sr^{2+} Surface Sorption (Equilibrium vs. Kinetics). The binding of Cs^+ and Sr^{2+} to quartz and clay surfaces can be viewed in two parts: (1) the amount that can be sorbed at

equilibrium and (2) the amount that is sorbed over the timescale of the system being investigated. The equilibrium amount that can be sorbed is based on the surface potential and the rate that sorption occurs is based on kinetics. For equilibrium sorption, three major mass transfer relationships for isotherms can be used: linear, Freundlich, and Langmuir. These relationships relate the amount of contaminant bound to the surface to the amount that remains in solution at equilibrium. Linear mass transfer works well at low ranges when sorption is linear, however, the assumption that there is no maximum sorption makes this relationship less useful at high cation concentrations. Freundlich mass transfer allows for a decrease in sorption as the concentration of sorbed contaminant increases and Langmuir mass transfer produces a maximum sorbed concentration above which all the remaining contaminant stays in the aqueous phase. It has been shown that the Langmuir mass transfer mechanism is the most applicable to Cs^{+} and Sr^{2+} sorption to both clay and sand surfaces (Saiers and Hornberger, 1996a). In many cases, a combined Langmuir mass transfer equation that accounts for equilibrium sorption to one site and a time-dependent kinetic term to a second binding site represents the data best. The modeling technique investigated in this review and applied to the experiments in the following chapters will utilize a two-site Langmuir mass transfer mechanism, where both sites are kinetically controlled (Turner et al., 2006b). The equations for this model that represent the first and second mechanism from the conceptual model are as follows:

Two-site, second-order Langmuir quartz sorption:

$$\frac{\partial S(x,t)}{\partial t} = \frac{\partial S_1(x,t)}{\partial t} + \frac{\partial S_2(x,t)}{\partial t} \tag{2.8}$$

$$X_a = X_{a1} + X_{a2} \tag{2.9}$$

Site 1 (Slow Site) on Quartz:

$$\frac{\rho_b}{n}\frac{\partial S_1(x,t)}{\partial t} = k_{as1}{}'\left(X_{a1} - S_1(x,t)\right)\frac{\rho_b}{n}C(x,t) - \frac{\rho_b}{n}k_{sa1}{}'C_{Na}S_1(x,t) \tag{2.10}$$

Site 2 (Fast Site) on Quartz:

$$\frac{\rho_b}{n}\frac{\partial S_2(x,t)}{\partial t} = k_{as2}{}'\left(X_{a2} - S_2(x,t)\right)\frac{\rho_b}{n}C(x,t) - \frac{\rho_b}{n}k_{sa2}{}'C_{Na}S_2(x,t) \tag{2.11}$$

where $S_1(x,t)$ is the contaminant concentration adsorbed to site 1 of the quartz (μmol g^{-1}), $S_2(x,t)$ is the contaminant concentration adsorbed to site 2 of the quartz (μmol g^{-1}), $C(x,t)$ is the contaminant of the pore water (μM), C_{Na} is the sodium concentration in the pore water (μM), n is the porous medium porosity, ρ_b is the bulk density of the porous medium (g L^{-1}), X_a is the contaminant sorption capacity of the quartz (μmol g^{-1}), $k_{as1}{}'$ is the second-order rate coefficient for adsorption to site 1 on the quartz (μM^{-1} h^{-1}), $k_{as2}{}'$ is the rate coefficient for adsorption to site 2 on the quartz (μM^{-1} h^{-1}), $k_{sa1}{}'$ is the second-order rate coefficient for desorption from site 1 of the quartz (μM^{-1} h^{-1}), $k_{sa2}{}'$ is the second-order rate coefficient for desorption from site 2 of the quartz (μM^{-1} h^{-1}), t is time (h), and x is the distance (m).

In the case of quartz sand, surface impurities such as metal oxide coatings may require two binding sites to adequately represent the sorption processes; however, rigorous cleaning can ensure only slow binding sites remain, in which case, a single site can represent the binding relationship and the adsorption and desorption rate coefficients for the second binding site ($k_{as2}{}'$ and $k_{sa2}{}'$) can be set to zero.

Dissolved Solute and Contaminant Transport. This review and the following chapters will use a one-dimensional transport model. By applying the law of conservation of mass to a small

slice between x and $x+\Delta x$ of a vertical column (Figure 2.14), a partial differential equation that describes the solute transport as a function of space and time can be developed as:

$$\frac{\partial M(x,t)}{\partial t} = \frac{\partial C(x,t)}{\partial t} A\Delta x + \frac{\rho_b}{n}\frac{\partial S(x,t)}{\partial t} A\Delta x \\ = q(x,t)A - q(x+\Delta x,t)A - kC(x,t)A\Delta x \tag{2.12}$$

where q is the flow rate ($cm^3\ h^{-1}$), A is the cross-sectional area of a slice (cm^3), $C(x,t)$ is the solute concentration in the dissolved phase, $S(x,t)$ is the concentration of solute sorbed to the sand in the slice, $M(x,t)$ is the mass concentration in the soil, and $kCA\Delta x$ represents the decay of solute in the slice. This equation describes the change in mass of solute in the slice as a function of space and time.

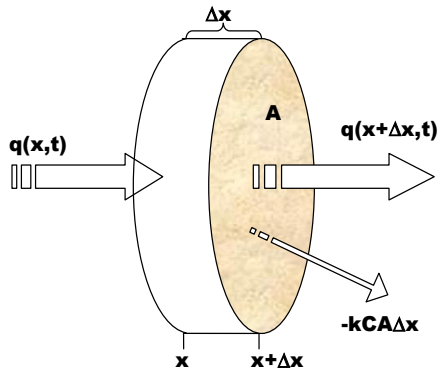

Figure 2.14. Drawing of a thin slice used for applying the law of mass conservation. From Turner (2005).

By decomposing the mass flux into advection and diffusion terms ($q_{adv}(x,t)$ and $q_{diff}(x,t)$, respectively), Equation 2.12 can be modified to:

$$\frac{\partial C(x,t)}{\partial t} + \frac{\rho_b}{n}\frac{\partial S(x,t)}{\partial t} = \frac{q_{adv}(x,t) - q_{adv}(x+\Delta x,t)}{\Delta x} \\ + \frac{q_{diff}(x,t) - q_{diff}(x+\Delta x,t)}{\Delta x} - kC(x,t) \tag{2.13}$$

Equation 2.13 can then be converted into a partial differential equation with respect to space and time as follows:

$$\frac{\partial C(x,t)}{\partial t} + \frac{\rho_b}{n}\frac{\partial S(x,t)}{\partial t} = -\frac{\partial q_{adv}(x,t)}{\partial x} - \frac{\partial q_{diff}(x,t)}{\partial x} - kC(x,t) \tag{2.14}$$

The mass flux per unit time can be associated to the contaminant concentration in the fluid by using an advection term linking concentration to the flow velocity and Fick's first law of diffusion as follows:

$$q_{adv}(x,t) = UC(x,t) \tag{2.15}$$

$$q_{diff}(x,t) = -D\frac{\partial C(x,t)}{\partial x} \tag{2.16}$$

where U is the constant fluid velocity (m h^{-1}) and D is the dispersion coefficient of the contaminant in the fluid (m^2 s^{-1}).

Equations 2.15 and 2.16 can then be incorporated into Equation 2.14 to yield the following one-dimensional advective-dispersive equation;

$$\frac{\partial C(x,t)}{\partial t} + \frac{\rho_b}{n}\frac{\partial S(x,t)}{\partial t} = \frac{\partial}{\partial x}\left(D\frac{\partial C(x,t)}{\partial x}\right) - \frac{\partial}{\partial x}\left(UC(x,t)\right) - kC(x,t), \tag{2.16}$$

which can be simplified by assuming dispersion coefficient D and the water velocity U are constant in a steady system to become:

$$\frac{\partial C(x,t)}{\partial t} + \frac{\rho_b}{n}\frac{\partial S(x,t)}{\partial t} = D\frac{\partial^2 C(x,t)}{\partial x^2} - U\frac{\partial C(x,t)}{\partial x} - kC(x,t) \tag{2.17}$$

When considering colloids and conservative solutes such as Br^-, the fifth term, the decay term, in Eqn. 2.17 can be set to zero since the colloids and solutes will not decay within the timescale of the experiments being examined. When considering radioisotopes such as ^{137}Cs and ^{90}Sr, the decay term can be assumed to be zero when the timescale of transport is much less than the half-life of the isotopes. ^{137}Cs has a half life of 30.2 years and ^{90}Sr has a half life of 28.8 years, so the

decay will be negligible for timescales less than a few weeks, which were used for this analysis. Equation 2.17 simplifies to become the familiar zero-decay advective-dispersive equation:

$$\frac{\partial C(x,t)}{\partial t} + \frac{\rho_b}{n}\frac{\partial S(x,t)}{\partial t} = D\frac{\partial^2 C(x,t)}{\partial x^2} - U\frac{\partial C(x,t)}{\partial x} \tag{2.18}$$

1D Transport with Langmuir Kinetic Adsorption to Quartz. By adding the Langmuir kinetic mass transfer equations (Eqns. 2.10 and 2.11) into Equation 2.18, the equation becomes:

$$\begin{aligned}\frac{\partial C(x,t)}{\partial t} &+ k_{as1}'\left(X_{a1} - S_1(x,t)\right)\frac{\rho_b}{n}C(x,t) - \frac{\rho_b}{n}k_{sa1}'C_{Na}S_1(x,t) \\ &+ k_{as2}'\left(X_{a2} - S_2(x,t)\right)\frac{\rho_b}{n}C(x,t) - \frac{\rho_b}{n}k_{sa2}'C_{Na}S_2(x,t) \\ &= D\frac{\partial^2 C(x,t)}{\partial x^2} - U\frac{\partial C(x,t)}{\partial x}\end{aligned} \tag{2.19}$$

This equation assumes the desorption rate is a function of the sodium concentration (C_{Na}) and the adsorption capacity is a function of a constant sorbed sodium concentration. Equation 2.19 represents cation transport through a one-dimensional porous medium with two-site Langmuir sorption to the quartz surface. One-site sorption can be represented by setting the sorption capacity of the second site, $X_{a2,}$ to zero.

Colloid Transport (DLVO Theory). To expand Eqn. 2.19 to account for colloid transport, the nature of colloid transport through a one-dimensional porous media must be understood. Colloid transport has been well-established and characterized and is conceptualized by DLVO theory (Derjaguin and Landau, 1941; Verwey and Overbeek, 1948). DLVO theory represents the potential energy of surface interactions by accounting for double layer repulsion/attraction, London-van der Waals attraction, and short range forces (steric repulsion and hydration). DLVO also accounts for the effect of ionic strength on surface interactions, where van der Waals forces are always important and high ionic strength and double layer repulsion is more important at low

ionic strength. The balance of long range repulsive double layer forces and short range attractive van der Waals forces establishes a potential energy barrier near the quartz surface that must be overcome to result in particle surface sorption (Figure 2.15). There are two minimum energy positions that can result in colloid sorption. The primary minimum is the result of the van der Waals forces near the surface and is represented by an irreversible infinite negative energy potential at the surface.

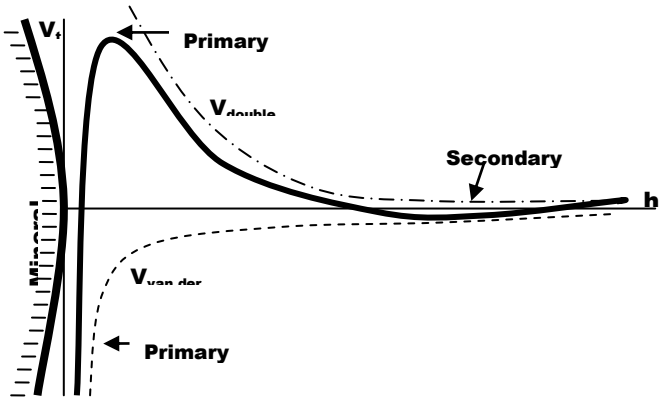

Figure 2.15. Representation of the potential energy profile resulting from the balance of double layer repulsion forces and van der Waals attraction forces of DLVO theory. A negatively charged particle can be stable at either the primary or secondary minimum, however, the secondary minimum provides for continued transport within the secondary minimum. Figure from Turner (2005).

When ionic strength is high, the thickness of the double layer is compressed and the van der Waals forces dominate the system, resulting in an increased attachment rate and decreased detachment rate. When ionic strength is low, the double layer thickness is large, decreasing the attachment rate and increasing the detachment rate.

Colloid Attachment Rate (k_{cs}). Many studies have applied DLVO theory to develop kinetic models that incorporate time-dependent rate functions. The deposition behavior of colloids has been shown to be well-represented by a model developed by (Rajagopalan and Tien, 1976) and modified by (Tufenkji and Elimelech, 2004). The model assumes spherical soil grain surfaces and describes colloid attachment based on hydrodynamic fluid properties and interception, sedimentation, and diffusion of colloid particles (Yao et al., 1971) in terms of collision efficiency α and collision frequency η.

The total collision frequency is the sum of three intermediate collision frequencies:

$$\eta = \eta_I + \eta_{sed} + \eta_{Br} \tag{2.20}$$

where η_I, η_{sed}, and η_{Br} represent collision efficiencies from particle interception, sedimentation, and from Brownian motion.

For particle interception, where a particle flow path grazes the collector surface, the collision frequency is described by the following equations:

$$\eta_I = 0.55 A_s N_R^{1.675} N_A^{0.125} \tag{2.21}$$

$$A_s = \frac{2\left(1-p^5\right)}{2-3p+3p^5-2p^6} \tag{2.22}$$

$$p = \left(1-n\right)^{1/3} \tag{2.23}$$

$$N_R = \frac{d_g}{d_c} \tag{2.24}$$

$$N_A = \frac{A_h}{12\pi\ \mu\ r_c^2 U'} \tag{2.25}$$

where η_I is the collision frequency for intercepted particles, A_s is Happel's model parameter (utilizing p and n), N_R is the aspect ratio, N_A is a dimensionless parameter that combines van der

Waals attraction forces and fluid velocity effects, d_c is the colloidal particle diameter (m), d_g is the spherical collector grain diameter (m), A_h is the Hamaker constant (J), μ is the absolute fluid viscosity (g m^{-1} s^{-1}), r_c is the colloidal particle radius (m), and U' is the Darcy velocity of the fluid (m s^{-1}).

For a particle that deposits on the sand surface (deposition), the collision frequency is represented by the following equations:

$$\eta_{sed} = 0.22 N_R^{-0.24} N_G^{1.11} N_{vdW}^{0.053} \tag{2.26}$$

$$N_G = \frac{\rho_c - \rho_f}{18 \mu U'} g d_c^2 \tag{2.27}$$

$$N_{vdW} = \frac{A_h}{k_b T} \tag{2.28}$$

where η_{sed} is the deposition collision frequency, N_R is the aspect ratio, N_G is the ratio of the Stokes particle settling velocity to the fluid velocity, N_{vdW} is the van der Waals parameter characterizing the ratio of van der Waals interaction energy to the thermal energy of the particle, ρ_c is the colloidal particle density (2.5 kg m^{-3}), ρ_f is the density of the fluid (1.0 kg m^{-3}), g is the gravitational acceleration constant (9.81 m s^{-2}), d_c is the colloidal particle diameter (m), A_h is the Hamaker constant (J), k_b is the Boltzmann constant (1.38×10^{-23} m^2 kg s^{-2} °K^{-1}), and T is the fluid temperature (298 °K).

For a particle that collides with the grain collector due to Brownian motion and diffusion, the collision frequency, η_{Br}, is calculated as:

$$\eta_{Br} = 2.4 A_S^{1/3} N_R^{-0.081} N_{Pe}^{-0.715} N_{vdW}^{0.052} \tag{2.29}$$

$$N_{Pe} = \frac{U' d_c}{D_\infty} \tag{2.30}$$

$$D_{\infty} = \frac{k_b T}{6\pi\ \mu\ r_c} \tag{2.31}$$

where A_s is Happel's model parameter (utilizing p and n), N_R is the aspect ratio, N_{Pe} is the Peclet number (a dimensionless ratio of convective transport to diffusive transport), U' is the Darcy velocity of the fluid (m s^{-1}), d_c is the colloidal particle diameter (m), D_{∞} is the colloidal diffusivity determined by the Stokes-Einstein equation (cm^2 s^{-1}), k_b is the Boltzmann constant (1.38×10^{-23} m^2 kg s^{-2} $°K^{-1}$), and T is the fluid temperature (298 °K), μ is the absolute fluid viscosity (g m^{-1} s^{-1}), and r_c is the colloidal particle radius (m).

Hydrodynamic forces dictate collision frequency (η) and the DLVO theory forces dictate collision efficiency (α). The collision efficiency is defined as the number of successful collisions (attachments) per number of collisions and is related to DLVO theory through the following equation:

$$\alpha = \Gamma \exp\left(-\frac{\phi_{\max}}{k_b T}\right) \tag{2.32}$$

where Γ is the gamma function, ϕ_{max} is the DLVO maximum potential energy, k_b is the Boltzmann constant (1.38×10^{-23} m^2 kg s^{-2} $°K^{-1}$), and T is the fluid temperature (298 °K). Since ϕ_{max} represents the DLVO forces, it is a function of the ionic strength and pH of the fluid.

Saiers et al., (1994b) and others have reported about the difficulty in predicting $\phi_{max,}$ *a priori*, thus the collision efficiency, α, is often determined experimentally by conducting a column breakthrough and using the following equations;

$$\eta_{\exp} = -\frac{4}{3}\frac{r_g}{(1-n)L}\ln\left(\frac{C_c}{C_{co}}\right) \tag{2.33}$$

$$\alpha_{\exp} = \frac{\eta_{\exp}}{\eta} \tag{2.34}$$

where r_g is the collector grain radius (m), n is the porous media porosity, C_c is the influent colloid concentration (g L^{-1}), C_{co} is the effluent colloid concentration once it reaches a stable plateau (g L^{-1}), and L is the column length (m).

The kinetic rate of attachment of colloids to the sand surface can be calculated by using the following equation:

$$k_{cs} = \frac{3}{2}\alpha_{\exp}\eta U\frac{1-n}{d_c} \tag{2.35}$$

where k_{cs} is the rate of colloid attachment, α_{exp} is the experimentally determined collision efficiency, η is the composite collision frequency, U is the Darcy velocity of the fluid (m s^{-1}), n is the porosity, and d_c is the colloidal particle diameter (m).

Colloid Detachment Rate (k_{sc}). The detachment of colloids into the mobile fluid phase can be divided into two parts: (i) colloid detachment from the matrix surface into the boundary layer porewater and, (ii) diffusion of the colloid to the mobile bulk fluid (Ryan and Gschwend, 1994b). The detachment rate has been modeled as a function of the potential energy barrier at the surface that must be overcome by the following equation:

$$k_{\det} \approx A_h \exp\left(\frac{-(\phi_{\max}-\phi_{\min})}{k_b T}\right) \tag{2.36}$$

where A_h is the Hamaker constant (J), ϕ_{max} and ϕ_{min} are the maximum and primary minimum potential energies in the DLVO energy barrier, respectively, and k_b is the Boltzmann constant (1.38×10^{-23} m^2 kg s^{-2} °K^{-1}), and T is the fluid temperature (298 °K). In order to provide a finite value for the minimum energy barrier, either a distance of closest approach for the colloids must be assumed (around 0.4 to 0.5 nm), or the Born repulsion concept can be applied (Feke et al., 1984). Similar to the colloid attachment rate, the detachment rate is difficult to predict *a priori*.

Once the colloid has detached from the matrix, the rate of diffusion through the hydrodynamic boundary layer, δ_{bl}, into the mobile porewater can be estimated by the following equation:

$$\delta_{bl} \sim r_g \left(\frac{D_\infty}{U' r_g} \right)^{1/3} \tag{2.37}$$

where r_g is the collector grain radius (m), D_∞ is the colloidal diffusivity determined by the Stokes-Einstein equation ($cm^2\ s^{-1}$), and U' is the Darcy velocity of the fluid ($m\ s^{-1}$). The boundary layer thickness can then be used to calculate the colloid release rate due to diffusion though the layer using the following equation:

$$k_{dif} = \frac{D_\infty}{\delta_{bl}^2} \tag{2.38}$$

where D_∞ is the colloidal diffusivity determined by the Stokes-Einstein equation ($cm^2\ s^{-1}$) and δ_{bl} is the boundary layer thickness (m).

In systems where the pH is increased or the ionic strength is decreased and particle detachment from the grain surface is favored, the diffusion through the boundary layer into the mobile porewater becomes the rate-limiting step. By combining Equations 2.37 and 2.38 with the Stokes-Einstein equation for particle diffusion, the overall colloid detachment rate can be calculated using the following equation:

$$k_{cs} \approx \left(\frac{k_b T}{6\pi\ \mu\ r_c} \right)^{1/3} \frac{U'^{2/3}}{r_g^{4/3}} \tag{2.39}$$

where k_b is the Boltzmann constant ($1.38 \times 10^{-23}\ m^2\ kg\ s^{-2}\ K^{-1}$), T is the porewater temperature (298 K), U' is the Darcy velocity of the fluid ($m\ s^{-1}$), μ is the absolute fluid viscosity ($g\ m^{-1}\ s^{-1}$), r_g is the collector grain radius (m), and r_c is the colloidal particle radius (m).

Combining equations for the colloidal attachment and detachment rates yields a linear mass transfer rate described by the following equation:

$$\frac{\rho_b}{n}\frac{\partial S_c(x,t)}{\partial t} = k_{sc}C_c(x,t) - \frac{\rho_b}{n}k_{cs}S_c(x,t) \tag{2.40}$$

where $S_c(x,t)$ is the immobile colloid concentration or concentration of colloids attached to quartz grains (g g^{-1}), k_{sc} is the colloid attachment rate (min^{-1}), k_{cs} is the colloid detachment rate (min^{-1}), and C_c is the colloid concentration in solution (g L^{-1}). Saiers et al. (1994b) found that positively charged colloids can exhibit a blocking effect, which reduces the colloid attachment as a function of the concentration of colloids sorbed to the quartz surface. When a blocking function is required, the following equation for a non-linear colloid deposition rate is appropriate:

$$\frac{\rho_b}{n}\frac{\partial S_c(x,t)}{\partial t} = k_{cs}\left(\frac{X_{cs} - S_c(x,t)}{X_{cs}}\right)C_c(x,t) - \frac{\rho_b}{n}k_{sc}S_c(x,t) \tag{2.41}$$

where ρ_b is the porous media bulk density, n is the porosity, X_{cs} is the deposition capacity of immobile colloids attached to the quartz grains (g g^{-1}), $S_c(x,t)$ is the immobile colloid concentration or concentration of colloids attached to quartz grains (g g^{-1}), k_{sc} is the colloid attachment rate (min^{-1}), k_{cs} is the colloid detachment rate (min^{-1}), and C_c is the colloid concentration in solution (g L^{-1}). The nonlinear nature of this equation results from the assumption that there is a finite colloid sorption capacity.

Colloid-Facilitated Transport Governing Equation. The presence of colloids in the influent liquid increases the complexity of the transport system. The addition of the colloidal phase necessitates the addition of more mechanisms into the cation transport equations to account for cations that interact with the mobile and immobile colloids. The advective-dispersive transport equation must be modified to include the mobile and immobile phases and appears as the following:

$$\frac{\partial C(x,t)}{\partial t}+\frac{\rho_b}{n}\frac{\partial S(x,t)}{\partial t}+\frac{\partial\left(C_c(x,t)C_p(x,t)\right)}{\partial t}+\frac{\rho_b}{n}\frac{\partial\left(S_c(x,t)S_p(x,t)\right)}{\partial t}$$
$$=D\frac{\partial^2\left(C(x,t)+C_c(x,t)C_p(x,t)\right)}{\partial x^2}-U\frac{\partial\left(C(x,t)+C_c(x,t)C_p(x,t)\right)}{\partial x} \quad (2.42)$$

where $C_c(x.t)C_p(x,t)$ represents the cation concentration on mobile colloids and $S_c(x,t)S_p(x,t)$ represents the cation concentration on the immobile colloids. The transport of cations sorbed to mobile colloids are also subjected to advection and dispersion of the colloidal phase, which is accounted for in the fifth and sixth terms in Eqn. 2.42. An important assumption in this model is that the dispersivity coefficient (D) of the colloids is the same as the dispersivity coefficient determined for bromide and used for the cations.

Cation/Colloid Kinetic Transport. In order to investigate the effect of desorption kinetic rates on the increased transport of cations, the mass transfer of cations between the mobile and immobile colloids must be accounted for.

A second-order equation describing the exchange of cations with sodium on the mobile and immobile colloids surface takes the form:

$$C_c(x,t)\frac{\partial C_p(x,t)}{\partial t}=k_{ac1}'\left(X_c-C_{p1}(x,t)\right)C_c(x,t)C(x,t)-k_{ca1}'C_{Na}C_{p1}(x,t)C_c(x,t) \quad (2.43)$$

where k_{ac1}' is a second-order rate constant for contaminant cation adsorption to a single site on the illite surface ($\mu M^{-1}\ h^{-1}$), k_{ca1}' is a second-order rate constant for contaminant cation desorption from a single site on the illite surface ($\mu M^{-1}\ h^{-1}$), $C_{p1}(x,t)$ is the sorbed contaminant concentration on a single site of the mobile colloid surface ($\mu mol\ g^{-1}$), X_c is the contaminant sorption capacity to the illite surface ($\mu mol\ g^{-1}$), and $C_c(x,t)$ is the illite colloid concentration (g

L^{-1}). The linear nature of the cation adsorption to the clay colloid surface suggests that the sorbed concentration of cations will be much less than the total capacity ($C_p(x,t) << X_c$), however, this assumption was not made in our analysis, allowing us to test this relationship.

The sorption of contaminants onto immobile colloids has a similar form to the equation above:

$$\frac{\rho_b}{n} S_c(x,t) \frac{\partial S_p(x,t)}{\partial t} = k_{ac1}'\left(X_c - S_{p1}(x,t)\right)\frac{\rho_b}{n} S_c(x,t) C(x,t) - \frac{\rho_b}{n} k_{ca1}' C_{Na} S_{p1}(x,t) S_c(x,t) \tag{2.44}$$

where $S_c(x,t)$ is the immobile colloid concentration (g g^{-1}), $S_p(x,t)$ is the concentration of cations sorbed to the immobile colloids (μmol g^{-1}), C_{Na} is the sodium concentration μM, and k_{ac1}' and k_{ca1}' are the cation adsorption and desorption rates (μM^{-1} h^{-1}) to the immobile colloids, respectively. The adsorption term (second term) is independent of the C_{Na}, but is implicitly included in the illite adsorption capacity X_c.

The above equation can expanded to account for two sorption sites by incorporating the necessary terms into the mass balance equation for cations sorbed to mobile colloids to take the form:

$$\frac{\partial\left(C_c(x,t)C_p(x,t)\right)}{\partial t} = \frac{\partial\left(C_c(x,t)C_{p1}(x,t)\right)}{\partial t} + \frac{\partial\left(C_c(x,t)C_{p2}(x,t)\right)}{\partial t} \tag{2.45}$$

$$X_c = X_{c1} + X_{c2} \tag{2.46}$$

$$\frac{\partial\left(C_c(x,t)C_{p1}(x,t)\right)}{\partial t} = D\frac{\partial^2\left(C_c(x,t)C_{p1}(x,t)\right)}{\partial x^2} - U\frac{\partial\left(C_c(x,t)C_{p1}(x,t)\right)}{\partial x}$$
$$+ k_{ac1}'\left(X_{c1} - C_{p1}(x,t)\right)C_c(x,t)C(x,t) - k_{ca1}'C_{Na}C_{p1}(x,t)C_c(x,t) \qquad (2.47)$$
$$- k_{cs}\left(\frac{X_{cs} - S_c}{X_{cs}}\right)C_c(x,t)C_{p1}(x,t) + \frac{\rho_b}{n}k_{sc}S_{p1}(x,t)S_c(x,t)$$

$$\frac{\partial\left(C_c(x,t)C_{p2}(x,t)\right)}{\partial t} = D\frac{\partial^2\left(C_c(x,t)C_{p2}(x,t)\right)}{\partial x^2} - U\frac{\partial\left(C_c(x,t)C_{p2}(x,t)\right)}{\partial x}$$
$$+ k_{ac2}'\left(X_{c2} - C_{p2}(x,t)\right)C_c(x,t)C(x,t) - k_{ca2}'C_{Na}C_{p2}(x,t)C_c(x,t) \qquad (2.48)$$
$$- k_{cs}\left(\frac{X_{cs} - S_c}{X_{cs}}\right)C_c(x,t)C_{p2}(x,t) + \frac{\rho_b}{n}k_{sc}S_{p2}(x,t)S_c(x,t)$$

where k_{ac2}' is a second-order rate constant for contaminant cation adsorption to the second site on the illite surface ($\mu M^{-1}\ h^{-1}$), k_{ca2}' is a second-order rate constant for contaminant cation desorption from the second site on the illite surface ($\mu M^{-1}\ h^{-1}$), $C_{p2}(x,t)$ is the sorbed contaminant concentration on site 2 of the mobile colloid surface ($\mu mol\ g^{-1}$), $S_{p2}(x,t)$ is the sorbed contaminant concentration on site 2 of the deposited colloid surface ($\mu mol\ g^{-1}$).

The mass balance equation for contaminants sorbed to two different binding sites on the immobile colloids looks similar to Equation 2.45 and takes the form:

$$\frac{\partial\left(S_c(x,t)S_p(x,t)\right)}{\partial t} = \frac{\partial\left(S_c(x,t)S_{p1}(x,t)\right)}{\partial t} + \frac{\partial\left(S_c(x,t)S_{p2}(x,t)\right)}{\partial t} \qquad (2.49)$$

Combining the Equation 2.49 with the sorption and desorption rate equations yield:

$$\frac{\rho_b}{n}\frac{\partial\left(S_c(x,t)S_{p1}(x,t)\right)}{\partial t} = k_{ac1}'\left(X_{c1} - S_{p1}(x,t)\right)\frac{\rho_b}{n}S_c(x,t)C(x,t)$$
$$- \frac{\rho_b}{n}k_{ca1}'C_{Na}S_{p1}(x,t)S_c(x,t) + k_{cs}\left(\frac{X_{cs} - S_c}{X_{cs}}\right)C_c(x,t)C_{p1}(x,t) \qquad (2.50)$$
$$- \frac{\rho_b}{n}k_{sc}S_{p1}(x,t)S_c(x,t)$$

$$\frac{\rho_b}{n}\frac{\partial\left(S_c(x,t)S_{p2}(x,t)\right)}{\partial t} = k_{ac2}'\left(X_{c2}-S_{p2}(x,t)\right)\frac{\rho_b}{n}S_c(x,t)C(x,t)$$
$$-\frac{\rho_b}{n}k_{ca2}'C_{Na}S_{p2}(x,t)S_c(x,t)+k_{cs}\left(\frac{X_{cs}-S_c}{X_{cs}}\right)C_c(x,t)C_{p2}(x,t) \qquad (2.51)$$
$$-\frac{\rho_b}{n}k_{sc}S_{p2}(x,t)S_c(x,t)$$

where the right hand side of Eqn. 2.50 represents the sorption to the "fast" sites on the colloids and the right hand side of equation 2.51 represents the sorption to the "slow" sites of the colloids. These equations only account for sorption and desorption from the mobile colloids and the additional transport due to advection and dispersion of the mobile colloids will be accounted for in the complete transport equation.

Combining Eqns. 2.50 and 2.51 with the colloid-facilitated advective-dispersive transport equation yields the following governing equation for the transport of cations in all 4 phases: aqueous transport, sorption to/from sand binding sites, sorption to/from strong and weak mobile colloid binding sites, and to/from strong and weak binding sites on immobile colloids.

$$\frac{\partial C(x,t)}{\partial t}+k_{as1}'\left(X_{a1}-S_1(x,t)\right)\frac{\rho_b}{n}C(x,t)-\frac{\rho_b}{n}k_{sa1}'C_{Na}S_1(x,t)$$
$$+k_{as2}'\left(X_{a2}-S_2(x,t)\right)\frac{\rho_b}{n}C(x,t)-\frac{\rho_b}{n}k_{sa2}'C_{Na}S_2(x,t)$$
$$+k_{ac1}'\left(X_{c1}-C_{p1}(x,t)\right)C_c(x,t)C(x,t)-k_{ca1}'C_{Na}C_{p1}(x,t)C_c(x,t)$$
$$+k_{ac2}'\left(X_{c2}-C_{p2}(x,t)\right)C_c(x,t)C(x,t)-k_{ca2}'C_{Na}C_{p2}(x,t)C_c(x,t) \qquad (2.52)$$
$$+k_{ac1}'\left(X_{c1}-S_{p1}(x,t)\right)\frac{\rho_b}{n}S_c(x,t)C(x,t)$$
$$-\frac{\rho_b}{n}k_{ca1}'C_{Na}S_{p1}(x,t)S_c(x,t)+k_{ac2}'\left(X_{c2}-S_{p2}(x,t)\right)\frac{\rho_b}{n}S_c(x,t)C(x,t)$$
$$-\frac{\rho_b}{n}k_{ca2}'C_{Na}S_{p2}(x,t)S_c(x,t)=D\frac{\partial^2 C(x,t)}{\partial x^2}-U\frac{\partial C(x,t)}{\partial x}$$

This equation accounts for advective-dispersive colloid-facilitated transport of cations with second-order sorption kinetics from two binding sites on mobile and immobile colloids and two binding sites on the quartz sand. The above equation has nine parameters that need to be either experimentally measured or mathematically fitted using a parameter optimization scheme: $C(x,t)$, $S_1(x,t)$, $S_2(x,t)$, $C_c(x,t)$, $S_c(x,t)$, $C_{p1}(x,t)$, $S_{p1}(x,t)$, $C_{p2}(x,t)$, $S_{p2}(x,t)$. This equation was simplified to the cation advective-dispersive transport equation by setting the colloid concentration (C_c) equal to zero. A more detailed description of the model optimization and a mathematical model to solve the nine equations simultaneously is provided by Turner et al. (2006).

Parameter Estimation. Optimal parameter values were selected by fitting the experimental data with a saturated colloid-facilitated transport model written by Turner et al. (2006). Dissolved cesium and strontium experiments were used to fit model parameters for quartz binding capacities and rate coefficients. Published values for quartz grains and illite colloid binding rate coefficients and capacities in Saiers and Hornberger (1996) and Turner et al. (2006) were used as initial parameter values. Bromide breakthrough experiments were used to calculate the dispersion coefficient (D) used for the solute transport model. Parameter values were manually adjusted to minimize root mean square error and to ensure the fit matched important features of the graph such as maximum concentration values and sharp transition points. Colloid-facilitated transport experiments parameters were determined by manually adjusting the parameters to minimize root mean square error and ensure the fit matched important graph features.

REFERENCES

Abadzic, S., Ryan, J., 2001. Particle release and permeability reduction in a natural zeolite (clinoptilolite) and sand porous medium. Environmental Science & Technology 35, 4502-4508.

Adeleye, S., Clay, P., Oladipo, M., 1994. Sorption of cesium, strontium, and europium ions on clay-minerals. Journal of Materials Science 29, 954-958.

Albarran, N., Missana, T., Garcia-Gutierrez, M., Alonso, U., Mingarro, M., 2011. Strontium migration in a crystalline medium: effects of the presence of bentonite colloids. Journal of Contaminant Hydrology 122, 76-85.

Allen, J.R.L., 1988. Modern-period muddy sediments in the severn estuary (Southwestern UK) - A pollutant-based model for dating and correlation. Sedimentary Geology 58, 1.

Alonso, U., Missana, T., Patelli, A., Rigato, V., Rivas, P., 2003. Study of the contaminant transport into granite microfractures using nuclear ion beam techniques. Journal of Contaminant Hydrology 61, 95-105.

Anderson, J., Bouma, J., 1977a. Water-Movement through pedal soils. 1. Saturated flow. Soil Science Society of America Journal 41, 413-418.

Anderson, J., Bouma, J., 1977b. Water-Movement through pedal soils. 2. Unsaturated flow. Soil Science Society of America Journal 41, 419-423.

Bea, S., Carrera, J., Soler, J., Ayora, C., Saaltink, M., 2004. Simulation of remediation alternatives for a Cs-137 contaminated soil. Radiochimica Acta 92, 827-833.

Bekhit, H., Hassan, A., Harris-Burr, R., Papelis, C., 2006. Experimental and numerical investigations of effects of silica colloids on transport of strontium in saturated sand columns. Environmental Science & Technology 40, 5402-5408.

Benjamin, M., 2002. Water Chemistry. McGraw Hill, New York, p. 668.

Bostick, B., Vairavamurthy, M., Karthikeyan, K., Chorover, J., 2002. Cesium adsorption on clay minerals: An EXAFS spectroscopic investigation. Environmental Science & Technology 36, 2670-2676.

Bouby, M., Geckeis, H., Lutzenkirchen, J., Mihai, S., Schafer, T., 2011. Interaction of bentonite colloids with Cs, Eu, Th and U in presence of humic acid: A flow field-flow fractionation study. Geochimica Et Cosmochimica Acta 75, 3866-3880.

Bouma, J., Anderson, J., 1977. Water and chloride movement through soil columns simulating pedal soils. Soil Science Society of America Journal 41, 766-770.

Bradford, S., Yates, S., Bettahar, M., Simunek, J., 2002. Physical factors affecting the transport and fate of colloids in saturated porous media. Water Resources Research 38.

Bucur, C., Olteanu, C., Pavelescu, M., 2007. Sorption of CESIUM-137 on soil samples. Journal of Environmental Protection and Ecology 8, 649-654.

Bunn, R., Magelky, R., Ryan, J., Elimelech, M., 2002. Mobilization of natural colloids from an iron oxide-coated sand aquifer: Effect of pH and ionic strength. Environmental Science & Technology 36, 314-322.

Cassel, D., Krueger, T., Schroer, F., Norum, E., 1974. Solute movement through disturbed and undisturbed soil cores. Soil Science Society of America Journal 38, 36-40.

Chen, G., Flury, M., Harsh, J., Lichtner, P., 2005. Colloid-facilitated transport of cesium in variably saturated Hanford sediments. Environmental Science & Technology 39, 3435-3442.

Cheng, T., Saiers, J., 2010. Colloid-Facilitated Transport of Cesium in Vadose-Zone Sediments: The Importance of Flow Transients. Environmental Science & Technology 44, 7443-7449.

Comans, R., Hilton, J., Voitsekhovitch, O., Laptev, G., Popov, V., Madruga, M., Bulgakov, A., Smith, J., Movchan, N., Konoplev, A., 1998. A comparative study of radiocesium mobility measurements in soils and sediments from the catchment of a small upland oligotrophic lake (Devoke Water, UK). Water Research 32, 2846-2855.

Comans, R., Hockley, D., 1992. Kinetics of Cesium Sorption on Illite. Geochimica Et Cosmochimica Acta 56, 1157-1164.

Cygan, R., Nagy, K., Brady, P., 1996. Molecular models of metal sorption on kaolinite. Abstracts of Papers of the American Chemical Society 211, 96-GEOC.

Czapar, G., Horton, R., Fawcett, R., 1992. Herbicide and tracer movement in soil columns containing an artificial macropore. Journal of Environmental Quality 21, 110-115.

Czigany, S., Flury, M., Harsh, J., 2005. Colloid stability in vadose zone aggregate. Hanford sediments. Environmental Science & Technology 39, 1506-1512.

Davis, J., Kent, D., 1990. Surface complexation modeling in aqueous geochemistry. Reviews in Mineralogy 23, 177-260.

Dawson, L., Pohl, P., 1997. Modeling and risk assessment of a 30-year-old subsurface radioactive-liquid drain field. Water Resources Research 33, 2535-2545.

de Jonge, L., Kjaergaard, C., Moldrup, P., 2004a. Colloids and colloid-facilitated transport of contaminants in soils: An introduction. Vadose Zone Journal 3, 321-325.

de Jonge, L., Moldrup, P., Rubaek, G., Schelde, K., Djurhuus, J., 2004b. Particle leaching and particle-facilitated transport of phosphorus at field scale. Vadose Zone Journal 3, 462-470.

DeNovio, N., 2004. Particle and Particle-Facilitated Contaminant Transport in the Vadose Zone. University of Colorado-Boulder, Boulder, CO.

DeNovio, N., Saiers, J., Ryan, J., 2004. Colloid movement in unsaturated porous media: Recent advances and future directions. Vadose Zone Journal 3, 338-351.

Derjaguin, B., Landau, L., 1941. Theory of the stability of strongly charged lyophobic soils and of the adhesion of strongly charged particles in solutions of electrolytes. Acta Physicochim URSS 14, 633-662.

Duran, E., Povinec, P., Fowler, S., Airey, P., Hong, G., 2004. Cs-137 and Pu239+240 levels in the Asia-Pacific regional seas. Journal of Environmental Radioactivity 76, 139-160.

Egeberg, P., 2000. The effect of river liming on the accumulation of radiocesium in sediments from a down stream lake. Aquatic Sciences 62, 68-78.

El-Farhan, Y., Denovio, N., Herman, J., Hornberger, G., 2000. Mobilization and transport of soil particles during infiltration experiments in an agricultural field, Shenandoah Valley, Virginia. Environmental Science & Technology 34, 3555-3559.

Fedoroff, M., Lefevre, G., Duc, M., Milonjic, S., Neskovic, C., 2004. Sorption mechanisms and sorption models. Progress in Advanced Materials and Processes 453-454, 305-314.

Feke, D., Prabhu, N., Mann, J., 1984. A formulation of the short-range repulsion between spherical colloidal particles. Journal of Physical Chemistry 88, 5735-5739.

Flury, M., Czigany, S., Chen, G., Harsh, J., 2004. Cesium migration in saturated silica sand and Hanford sediments as impacted by ionic strength. Journal of Contaminant Hydrology 71, 111-126.

Flury, M., Mathison, J., Harsh, J., 2002. In situ mobilization of colloids and transport of cesium in Hanford sediments. Environmental Science & Technology 36, 5335-5341.

Fujikawa, Y., Fukui, M., 1991. Analysis of Radioactive Cesium and Cobalt Adsorption to Rocks Using the 2-Site Kinetic-Model Equations. Journal of Contaminant Hydrology 8, 43-69.

Galambos, M., Kufcakova, J., Rosskopfova, O., Rajec, P., 2010. Adsorption of cesium and strontium on natrified bentonites. Journal of Radioanalytical and Nuclear Chemistry 283, 803-813.

Gao, B., Saiers, J., Ryan, J., 2004. Deposition and mobilization of clay colloids in unsaturated porous media. Water Resources Research 40, -.

Gomez-Suarez, C., Van der Mei, H., Busscher, H., 2000. Air bubble-induced detachment of positively and negatively charged polystyrene particles from collector surfaces in a parallel-plate flow chamber. Journal of Adhesion Science and Technology 14, 1527-1537.

Gomez-Suarez, C., van der Mei, H., Busscher, H., 2001. Air bubble-induced detachment of polystyrene particles with different sizes from collector surfaces in a parallel plate flow chamber. Colloids and Surfaces A-Physicochemical and Engineering Aspects 186, 211-219.

Grolimund, D., Borkovec, M., Barmettler, K., Sticher, H., 1996. Colloid-facilitated transport of strongly sorbing contaminants in natural porous media: A laboratory column study. Environmental Science & Technology 30, 3118-3123.

Hakanson, L., 2004. Modelling the transport of radionuclides from land to water. Journal of Environmental Radioactivity 73, 267-287.

Honeyman, B., 1999. Geochemistry - Colloidal culprits in contamination. Nature 397, 23-24.

Hsu, C.-N., Chang, K.-P., 1994. Sorption and desorption behavior of cesium on soil components. Applied Radiation and Isotopes 45, 433-437.

Hull, L., Schafer, A., 2008. Accelerated transport of Sr-90 following a release of high ionic strength solution in vadose zone sediments. Journal of Contaminant Hydrology 97, 135-157.

Iijima, K., Tomura, T., Shoji, Y., 2010. Reversibility and modeling of adsorption behavior of cesium ions on colloidal montmorillonite particles. Applied Clay Science 49, 262-268.

Ito, T., Otosaka, S., Kawamura, H., 2007. Estimation of total amounts of anthropogenic radionuclides in the Japan sea. Journal of Nuclear Science and Technology 44, 912-922.

IUPAC, 2002. Definition and classification of colloids.

Jackson, R.E., Inch, K.J., 1989. The in-situ adsorption of 90Sr in a sand aquifer at the Chalk River Nuclear Laboratories. Journal of Contaminant Hydrology 4, 27-50.

Jacobsen, O., Moldrup, P., Larsen, C., Konnerup, L., Petersen, L., 1997. Particle transport in macropores of undisturbed soil columns. Journal of Hydrology 196, 185-203.

Jeong, H., Hwang, W., Kim, E., Han, M., 2009. Radiological risk assessment for an urban area: Focusing on a drinking water contamination. Annals of Nuclear Energy 36, 1313-1318.

Johansen, M., Hakonson, T., Whicker, F., Breshears, D., 2003. Pulsed redistribution of a contaminant following forest fire: Cesium-137 in runoff. Journal of Environmental Quality 32, 2150-2157.

Kersting, A., Efurd, D., Finnegan, D., Rokop, D., Smith, D., Thompson, J., 1999. Migration of plutonium in ground water at the Nevada Test Site. Nature 397, 56-59.

Kissel, D., Ritchie, J., Burnett, E., 1973. Chloride movement in undisturbed swelling clay soil. Soil Science Society of America Journal 37, 21-24.

Kluitenberg, G., Horton, R., 1989. Pressurized layer reduces transport through compacted clay liners. Journal of Environmental Quality 18, 228-232.

Kobayashi, T., Otosaka, S., Togawa, O., Hayashi, K., 2007. Development of a non-conservative radionuclides dispersion model in the ocean and its application to, surface cesium-137 dispersion in the Irish Sea. Journal of Nuclear Science and Technology 44, 238-247.

Kowall, S., 2001. The DOE vadose zone science and technology roadmap: A national program to address characterization, monitoring, and simulation of subsurface contaminant fate and transport., WM '01. DOE, Tucson, AZ.

Kretzschmar, R., Borkovec, M., Grolimund, D., Elimelech, M., 1999. Mobile subsurface colloids and their role in contaminant transport. Advances in Agronomy 66, 121-193.

Krosshavn, M., Bjornstad, H., Engh, L., Lien, H., Salbu, B., 1996. Speciation of Cs-137 and Sr-90 in discharges from the pulp industry and the Marine recipient. Journal of Environmental Radioactivity 32, 157-164.

Kumar, S., Tomar, B., Ramanathan, S., Manchanda, V., 2006. Effect of humic acid on cesium sorption on silica colloids. Radiochimica Acta 94, 369-373.

Laegdsmand, M., Villholth, K., Ullum, M., Jensen, K., 1999. Processes of colloid mobilization and transport in macroporous soil monoliths. Geoderma 93, 33-59.

Lafrance, P., Marineau, L., Perreault, L., Villeneuve, J., 1994. Effect of natural dissolved organic-matter found in groundwater on soil adsorption and transport of pentachlorophenol. Environmental Science & Technology 28, 2314-2320.

Laverov, N., Velichkin, V., Malkovsky, V., Tarasov, N., Dikov, Y., 2010. A Comprehensive Study of the Spread of Radioactive Contamination in the Geological Medium Near Lake Karachai, Chelyabinsk oblast. Geology of Ore Deposits 52, 5-13.

Lenhart, J., Saiers, J., 2002. Transport of silica colloids through unsaturated porous media: Experimental results and model comparisons. Environmental Science & Technology 36, 769-777.

Lenhart, J., Saiers, J., 2003. Colloid mobilization in water-saturated porous media under transient chemical conditions. Environmental Science & Technology 37, 2780-2787.

Li, Y., Ghodrati, M., 1997. Preferential transport of solute through soil columns containing constructed macropores. Soil Science Society of America Journal 61, 1308-1317.

Litaor, M.I., Thompson, M.L., Barth, G.R., Molzer, P.C., 1994. Plutonium-239+240 and Am-241 in Soils East of Rocky-Flats, Colorado. Journal of Environmental Quality 23, 1231-1239.

Matsunaga, T., Nagao, S., Ueno, T., Takeda, S., Amano, H., Tkachenko, Y., 2004. Association of dissolved radionuclides released by the Chernobyl accident with colloidal materials in surface water. Applied Geochemistry 19, 1581-1599.

McBride, M., 1994. Environmental chemistry of soils. Oxford University Press, New York.

McCarthy, J., Degueldre, C., 1993. Sampling and characterization of colloids and particles in groundwater for studying their role in contaminant transport. In: Buffle, J., van Leeuwen, H.P. (Eds.), Environmental Particle: Volume 2. Lewis Publishers, Ann Arbor, pp. 247-315.

McCarthy, J., Zachara, J., 1989. Subsurface transport of contaminants- Mobile colloids in the subsurface environment may alter the transport of contaminants. Environmental Science & Technology 23, 496-502.

McDowell-Boyer, L., 1992. Chemical Mobilization of Micron-Sized Particles in Saturated Porous Media Under Steady Flow Conditions. Environmental Science & Technology 26, 586-593.

McDowell-Boyer, L., Hunt, J., Sitar, N., 1986. Particle transport through porous media. Water Resources Research 22, 1901-1921.

McGechan, M., 2002. Transport of particulate and colloid-sorbed contaminants through soil, part 2: Trapping processes and soil pore geometry. Biosystems Engineering 83, 387-395.

McGechan, M., Lewis, D., 2002. Transport of particulate and colloid-sorbed contaminants through soil, part 1: General principles. Biosystems Engineering 83, 255-273.

Missana, T., Garcia-Gutierrez, M., Alonso, U., 2004. Kinetics and irreversibility of cesium and uranium sorption onto bentonite colloids in a deep granitic environment. Applied Clay Science 26, 137-150.

Noell, A., Thompson, J., Corapcioglu, M., Triay, I., 1998. The role of silica colloids on facilitated cesium transport through glass bead columns and modeling. Journal of Contaminant Hydrology 31, 23-56.

NRC, 2000. Research Needs in Subsurface Science. National Academy Press, Washington, DC.

Pace, M., Mayes, M., Jardine, P., McKay, L., Yin, X., Mehlhorn, T., Liu, Q., Gurleyuk, H., 2007. Transport of Sr2+ and SrEDTA(2-) in partially-saturated and heterogeneous sediments. Journal of Contaminant Hydrology 91, 267-287.

Parker, J., 1984. Analysis of solute transport in column tracer studies. Soil Science Society of America Journal 48, 719-724.

Phillips, R., Quisenberry, V., Zeleznik, J., Dunn, G., 1989. Mechanism of water entry into simulated macropores. Soil Science Society of America Journal 53, 1629-1635.

Pilgrim, D., Huff, D., 1983. Suspended sediment in rapid subsurface stormflow on a large field plot. Earth Surface Processes and Landforms 8, 451-463.

Rajagopalan, R., Tien, C., 1976. Trajectory Analysis of Deep-Bed Filtration with Sphere-in-Cell Porous-Media Model. Aiche Journal 22, 523-533.

Robison, W., Conrado, C., Bogen, K., Stoker, A., 2003. The effective and environmental half-life of Cs-137 at Coral Islands at the former US nuclear test site. Journal of Environmental Radioactivity 69, 207-223.

Rod, K., Um, W., Flury, M., 2010. Transport of Strontium and Cesium in Simulated Hanford Tank Waste Leachate through Quartz Sand under Saturated and Unsaturated Flow. Environmental Science & Technology 44, 8089-8094.

Roy, S., Dzombak, D., 1997. Chemical factors influencing colloid-facilitated transport of contaminants in porous media. Environmental Science & Technology 31, 656-664.

Ryan, J., Elimelech, M., 1996. Colloid mobilization and transport in groundwater. Colloids and Surfaces A-Physicochemical and Engineering Aspects 107, 1-56.

Ryan, J., Gschwend, P., 1994a. Effect of solution chemistry on clay colloid release from an iron oxide-coated aquifer sand. Environmental Science & Technology 28, 1717-1726.

Ryan, J., Gschwend, P., 1994b. Effects of ionic-strength and flow-rate on colloid release-Relating kinetics to intersurface potential-energy. Journal of Colloid and Interface Science 164, 21-34.

Ryan, J., Illangasekare, T., Litaor, M., Shannon, R., 1998. Particle and plutonium mobilization in macroporous soils during rainfall simulations. Environmental Science & Technology 32, 476-482.

Saiers, J., Hornberger, G., 1996a. Migration of Cs-137 through quartz sand: Experimental results and modeling approaches. Journal of Contaminant Hydrology 22, 255-270.

Saiers, J., Hornberger, G., 1996b. The role of colloidal kaolinite in the transport of cesium through laboratory sand columns. Water Resources Research 32, 33-41.

Saiers, J., Hornberger, G., 1999. The influence of ionic strength on the facilitated transport of cesium by kaolinite colloids. Water Resources Research 35, 1713-1727.

Saiers, J., Hornberger, G., Gower, D., Herman, J., 2003. The role of moving air-water interfaces in colloid mobilization within the vadose zone. Geophysical Research Letters 30, -.

Saiers, J., Hornberger, G., Harvey, C., 1994a. Colloidal silica transport through structured, heterogeneous porous-media. Journal of Hydrology 163, 271-288.

Saiers, J., Hornberger, G., Liang, L., 1994b. First-order and second-order kinetics approaches for modeling the transport of colloidal particles in porous-media. Water Resources Research 30, 2499-2506.

Saiers, J., Lenhart, J., 2003a. Colloid mobilization and transport within unsaturated porous media under transient-flow conditions. Water Resources Research 39, -.

Saiers, J., Lenhart, J., 2003b. Ionic-strength effects on colloid transport and interfacial reactions in partially saturated porous media. Water Resources Research 39, -.

Satmark, B., Albinsson, Y., Liang, L., 1996. Chemical effects of goethite colloid on the transport of radionuclides through a quartz-packed column. Journal of Contaminant Hydrology, 231-241.

Shevenell, L., McCarthy, J., 2002. Effects of precipitation events on colloids in a karst aquifer. Journal of Hydrology 255, 50-68.

Sims, D., Andrews, W., Wang, X., Creber, K., 2007. Measuring and modeling transport properties of actinide and fission product contaminants in unsaturated prairie soil. Journal of Environmental Engineering and Science 6, 219-229.

Solovitch-Vella, N., Garnier, J., Ciffroy, P., 2006. Influence of the colloid type on the transfer of Co-60 and Sr-85 in silica sand column under varying physicochemical conditions. Chemosphere 65, 324-331.

Spurlock, F., Biggar, J., 1990. Effect of naturally-occuring soluble organic-matter on the adsorption and movement of simazine [2-chloro-4,6-bis(ethylamino)-s-triazine] in hanford sandy loam. Environmental Science & Technology 24, 736-741.

Steefel, C., Carroll, S., Zhao, P., Roberts, S., 2003. Cesium migration in Hanford sediment: a multisite cation exchange model based on laboratory transport experiments. Journal of Contaminant Hydrology 67, 219-246.

Stepanets, O., Ligaev, A., Borisov, A., Travkina, A., Shkinev, V., Danilova, T., Miroshnikov, A., Migunov, V., 2009. Geoecological investigations of the Ob-Irtysh River Basin in the Khanty-Mansi Autonomous region: Yugra in 2006-2007. Geochemistry International 47, 657-671.

Stumm, W., Morgan, J., 1996. Aquatic Chemistry, Chemical Equlibria and Rates in Natural Waters. John Wiley & Sons, Inc., New York, p. 1022.

Sverjensky, D., 2002. Standard states for surface sites and surface species in surface complexation models. Abstracts of Papers of the American Chemical Society 223, U607-U607.

Sverjensky, D., 2006. Prediction of the speciation of alkaline earths adsorbed on mineral surfaces in salt solutions. Geochimica Et Cosmochimica Acta 70, 2427-2453.

Swartz, C., Gschwend, P., 1998. Mechanisms controlling release of colloids to groundwater in a Southeastern Coastal Plain aquifer sand. Environmental Science & Technology 32, 1779-1785.

Szenknect, S., Gaudet, J., Dewiere, L., 2003. Evaluation of distribution coefficients for the prediction of strontium and cesium migration in a natural sand at different water contents. Journal De Physique Iv 107, 1279-1282.

Tang, X., Weisbrod, N., 2010. Dissolved and Colloidal Transport of Cesium in Natural Discrete Fractures. Journal of Environmental Quality 39, 1066-1076.

Tegen, I., Dorr, H., 1996. Mobilization of cesium in organic rich soils: Correlation with production of dissolved organic carbon. Water Air and Soil Pollution 88, 133-144.

Thiessen, K., Thorne, M., Maul, P., Prohl, G., Wheater, H., 1999. Modelling radionuclide distribution and transport in the environment. Environmental Pollution 100, 151-177.

Tipping, E., 1996. Hydrochemical modelling of the retention and transport of metallic radionuclides in the soils of an upland catchment. Environmental Pollution 94, 105-116.

Triay, I., Lu, N., Cotter, C., Kitten, H., 1997. Iron oxide colloid facilitated plutonium transport in groundwater. Americal Chemical Society. American Chemical Society, Las Vegas.

Tufenkji, N., Elimelech, M., 2004. Correlation equation for predicting single-collector efficiency in physicochemical filtration in saturated porous media. Environmental Science & Technology 38, 529-536.

Turner, N., 2005. The effect of desorption kinetics on the colloid-facilitated transport of cesium-137 and strontium-90 in a saturated quartz porous medium. Civil, Environmental, and Architectural Engineering. University of Colorado-Boulder, Boulder, CO, p. 182.

Turner, N., Ryan, J., Saiers, J., 2006a. Effect of desorption kinetics on colloid-facilitated transport of contaminants: Cesium, strontium, and illite colloids. Water Resources Research 42.

Turner, N., Ryan, J., Saiers, J., 2006b. Effect of desorption kinetics on colloid-facilitated transport of contaminants: Cesium, strontium, and illite colloids. Water Resources Research 42, -.

Utsunomiya, S., Kersting, A., Ewing, R., 2009. Groundwater Nanoparticles in the Far-Field at the Nevada Test Site: Mechanism for Radionuclide Transport. Environmental Science & Technology 43, 1293-1298.

van der Perk, M., Slavik, O., 2003. Simulation of event-based and long-term spatial redistribution of Chernobyl-derived radiocaesium within catchments using geographical information system embedded models. Hydrological Processes 17, 943-957.

van Genuchten, M., 1980. A closed-form equation for predicting the hydraulic conductivity of unsaturated soils. Soil Science Society of America Journal 44, 892-898.

Verwey, E., Overbeek, J., 1948. Theory of the stability of lyophobic colloids.

Vilks, P., Baik, M., 2001. Laboratory migration experiments with radionuclides and natural colloids in a granite fracture. Journal of Contaminant Hydrology 47, 197-210.

Vilks, P., Cramer, J., Bachinski, D., Doern, D., Miller, H., 1993. Studies of colloids and suspended particles, Cigar Lake Uranium Deposit, Sasketchewan, Canada. Applied Geochemistry 8, 605-616.

Wan, J., Tokunaga, T., 1997. Film straining of colloids in unsaturated porous media: Conceptual model and experimental testing. Environmental Science & Technology 31, 2413-2420.

Wan, J., Tokunaga, T., 2002. Partitioning of clay colloids at air-water interfaces. Journal of Colloid and Interface Science 247, 54-61.

Wan, J., Wilson, J., 1994a. Colloid transport in unsaturated porous-media. Water Resources Research 30, 857-864.

Wan, J., Wilson, J., 1994b. Visualization of the role of the gas-water interface on the fate and transport of colloids in porous-media. Water Resources Research 30, 11-23.

Weisbrod, N., Dahan, O., Adar, E.M., 2002. Particle transport in unsaturated fractured chalk under arid conditions. Journal of Contaminant Hydrology 56, 117-136.

Yao, K., Habibian, M., Omelia, C., 1971. Water and waste water filtratyion- concepts and applications. Environmental Science & Technology 5, 1105-&.

Zhuang, J., Flury, M., Jin, Y., 2003. Colloid-facilitated Cs transport through water-saturated Hanford sediment and Ottawa sand. Environmental Science & Technology 37, 4905-4911.

Zygmunt, J., Chibowski, S., Klimowicz, Z., 1998. The effect of sorption properties of soil minerals on the vertical migration rate of cesium in soil. Journal of Radioanalytical and Nuclear Chemistry 231, 57-62.

CHAPTER 3

EFFECT OF COLLOID TYPE ON COLLOID-FACILITATED TRANSPORT OF CESIUM AND STRONTIUM

ABSTRACT

The sorption of contaminants to mobile colloids has been shown to increase the transport of contaminants in a process known as colloid-facilitated transport. Colloid surface properties such as mineralogy, size, and surface charge have been found to influence the potential for colloid-facilitated transport in laboratory experiments. We examined the role of colloid type on the potential to enhance transport of cesium and strontium cations through quartz sand in a pH 7.3 and 0.1 mM ionic strength suspension simulating groundwater interacting with mobile colloids at the edge of a contaminant plume. Four colloid types were compared: two varieties of illite (IMt-1 and IMt-2), silica, and clay colloids eluted from saprolite soil cores from Oak Ridge, TN. Analysis of the colloids by energy dispersive x-ray spectroscopy showed distinct differences in Al, Fe, Mg, and K amounts and desorption isotherms showed large differences in equilibrium sorption capacity between colloid type and between cesium and strontium. Illite, silica and Oak Ridge colloids increased the transport of cesium and strontium. IMt-1 increased transport the most, followed by IMt-2, Oak Ridge, and silica colloids. All of the colloids tested also decreased the binding capacity of the quartz sand, presumably due to the double layer of deposited colloids blocking binding sites from cations in solution. Colloid-facilitated transport

was most pronounced with cesium for IMt-1 and silica, and with strontium for the Oak Ridge colloids.

INTRODUCTION

Many laboratory experiments and computer model simulations have shown that enhanced transport can occur when a contaminant strongly associates with mobile colloids and release kinetics are slow relative to the rate of flow (McCarthy and Zachara, 1989; Kretzschmar et al., 1999). Comparing results between sets of experiments has been difficult; however, due to the differences between data sets in parameters such as suspension pH, ionic strength, and dominant ions, and system variables such as flow rate, porous media, and colloid type and preparation. Many radioactive waste sites have problems with high pH solutions (> pH 10) leaking into the vadose zone and these systems have been shown to allow for colloid-facilitated transport. There has been speculation about what happens at the edges of these contaminant plumes where the pH and ionic strength decrease to levels orders of magnitude lower than available experiments were conducted with.

Radionuclides such as cesium-137 and strontium-90 are of particular interest due to their relatively long half-life (30.2 yr and 28.8 yr, respectively) and their abundance in contaminated soils from the 1957 Kyshtym nuclear release near Mayak, Russia, the 1985 Chernobyl nuclear facility explosion in Ukraine, and the 2011 Fukushima Daiichi nuclear facility disaster in Japan. Many Department of Energy (DOE) sites in the United States have contaminated soils from improper storage and disposal of nuclear hazardous waste. Cesium and strontium have been found to exhibit varying sorption kinetics with clay minerals such as kaolinite (Cornell, 1993; Saiers and Hornberger, 1996a) and illite (Comans and Hockley, 1992; Cornell, 1993; Turner et

al., 2006a), which also makes them good surrogates to study the potential mechanisms for the enhanced transport of other strongly-sorbing contaminants.

Colloid-facilitated transport of radionuclides and other strongly sorbing contaminants has been observed in both field and laboratory experiments (Chaper 2). Colloids have a high sorptive capacity resulting from their high surface area to mass ratio, which makes them effective sorbents of low solubility, strongly sorbing contaminants such as radionuclides, metals, and nonpolar organic compounds such as polychlorinated biphenyls. Enhanced transport is favored when release kinetics between the mobile colloid and pore water are slow relative to the pore water velocity. The Damköhler number (D_a) has been used by Bold et al. (2003) and others to estimate the relative importance of equilibrium versus kinetic desorption for cations and can be calculated for fast (D_{a1}) and slow (D_{a2}) binding sites using the following equation,

$$D_{a1} = \frac{k_{ca1} X_c F_{c1} C_c L}{U} \tag{3.1}$$

$$D_{a2} = \frac{k_{ca2} X_c (1 - F_{c1}) C_c L}{U} \tag{3.2}$$

where k_{ca} is the desorption rate coefficient (1 = fast sites and 2 = slow sites), X_c is the cation sorption capacity of the colloids, F_{c1} is the fraction of sites that are fast binding sites, C_c is the concentration of illite, L is the length of the column, and U is the pore water velocity. It has been suggested that systems with $D_a < 100$ are modeled best with a kinetic model and when $D_a < 0.01$ contaminant desorption from the colloids can be completely neglected.

Colloid-facilitated transport in saturated porous media has been studied for many years and has led to an understanding of the dominant mechanisms controlling transport. The traditional advective-dispersive equation works well for modeling conservative tracers and contaminants and also for contaminants that are mobile in the aqueous phase. It has been shown;

however, that the advective-dispersive equation can under-predict the distance a contaminant can move when contaminants are sorbed to mobile colloids (Saiers and Hornberger, 1996a). Three conditions are necessary for colloid-facilitated transport of a contaminant to occur: (1) there must be a source of colloids, (2) contaminants must associate with the colloids and desorb slowly relative to the rate of transport, and (3) the colloids must remain mobile for a relatively long distance.

A mathematical colloid-facilitated transport model has been developed to account for the mechanisms introduced in the conceptual model. These models solve Richards' equation to simulate fluid flow through the porous media, colloid filtration theory (DLVO theory) to simulate colloid transport, attachment, and detachment, and a combination of kinetically fast and slow binding sites to simulate the sorption surfaces on the porous media and colloid surfaces. Saiers and Hornberger (1996b) developed a model for colloid transport with kaolinite and other colloids. Turner et al. (2006) developed a colloid-facilitated transport model to account for illite transport with two-site kinetically-controlled sorption of cesium and strontium. This model was used to simulate the results from saturated sand column breakthrough experiments and found that colloids enhanced cesium transport more than strontium due to the relatively fast desorption kinetics for strontium and slow desorption kinetics for cesium from the frayed edges of illite colloids. Colloid-facilitated transport also increased cesium transport in Hanford sediments (Cheng and Saiers, 2010); however, the complexity of natural sediments prevented making definitive conclusions on the affect that binding strengths and colloid properties played on enhanced transport.

The effect that colloid type plays on the transport of cesium and strontium at the dilution edge of a contaminant plume when pore water pH decreases below pH 10 and the ionic strength

decreases below 1 mM is not well understood. There is no direct comparison available to determine the effect of colloid type on colloid facilitated transport at circumneutral pH and low ionic strength. Our experiments have been designed to provide more insight into linking pore-scale sorption mechanisms to these potential field-scale transport processes.

MATERIALS AND METHODS

Overview. We conducted a series of breakthrough experiments with 7.5×10^{-7} M cesium and 7.5×10^{-6} M strontium at pH 7.3 and 0.1 mM ionic strength. Four colloid types were compared: two varieties of illite (IMt-1 and IMt-2), silica, and clay colloids eluted from saprolite soil cores from Oak Ridge, TN. Analysis of the colloids showed distinct differences in Al, Fe, Mg, and K amounts and desorption isotherms showed large differences in equilibrium sorption capacity and desorption rates between colloid type and between cesium and strontium.

We measured the breakthrough of dissolved and colloid-associated cesium and strontium using a small glass column set-up. Cesium and strontium were selected due to their prevalence on US Department of Energy (DOE) sites and because they exhibit contrasting sorption kinetics with quartz and colloids (divalent strontium holds its water of hydration much stronger than monovalent cesium). We used 5 types of clay for isotherms and 4 types of clay for the breakthrough experiments. The types of clay used were two types of illite (IMt-1 and IMt-2), silica, natural colloids from Oak Ridge, TN, and kaolinite. These clays exhibited varying sorption properties due to their different structures (i.e., edge charge, face charge/ terminal oxygen groups). The clays were imaged by scanning electron microscope and elemental analysis was determined using energy dispersive x-ray spectroscopy (EDS). Desorption isotherms and breakthrough experiments were conducted in a homogeneous quartz sand porous medium and

results were modeled to analyze the complex relationships between fluid transport, particle transport, and desorption kinetics.

Colloid Preparation. Two types of illite and one type of kaolinite were obtained from the Clay Minerals Society Clay Repository at Purdue University: IMt-1, IMt-2 and GBa1. These illite samples were from Silver Hill, Montana and represent different locations of the same geologic deposit. Silica colloids were purchased from Nissan, Inc. (model ZL). Natural colloids were eluted from undisturbed soil cores collected from Oak Ridge National Laboratory in TN, USA in the summer of 2008 (Mohanty et al., 2011). A core was flushed with high-purity water (>18 MΩ cm resistivity) for 6 hours and the effluent liquid was collected and settled for two weeks.

IMt-1, IMt-2, and kaolinite pieces were ground to a powder using a ceramic mortar and pestle. Powder (50 g) was added to 800 mL of high-purity water in a 1.5 L blender (Osterizer, Model 6630) and blended at high speed for 20 minutes. 5 mL of stock Nissan ZL suspension was sonicated in a bath (Fisher Scientific; FS 9H) for 30 minutes and was added to 800 mL of high-purity water. The five colloidal suspensions were subjected to a rinse process to remove calcium, magnesium and other cations and replace them with sodium (Appendix C). This process also neutralized any acid or base neutralizing capacity of the colloids and produced colloids in equilibrium with the final 0.1 mM ionic strength and 7.3 pH experimental solutions.

The colloidal fraction of the clay slurries were separated from larger particles by adding 0.1 mM sodium bicarbonate to make a 1 g L^{-1} suspension and settling for 24 h at room temperature (~22 °C) in HDPE graduated cylinders (1 L). Assuming the particles were spheres, a calculation of the Stokes settling velocity determined the maximum diameter of the particles remaining in the upper 18.5 cm of the column was less than 8.1 µm. The top 18.5 cm of solution was then decanted and reserved for experiments.

The mass concentration of the colloid suspensions was determined gravimetrically. 10 mL aliquots were transferred to glass vials and the water was evaporated by oven drying at 100 °C for 24 hours. The colloid mass concentrations (mg L^{-1}) were calculated as the difference in initial and final mass, divided by 0.01 L.

Solution and Suspension Chemistry. The background solution for experiments was made to simulate the chemistry of rainwater that has just entered the vadose zone. A 1 M stock solution of sodium bicarbonate (Mallinckrodt AR®, analytical reagent grade) was made to enable precision at lower concentrations. Stock sodium bicarbonate was added to high-purity water (> 18 MΩ cm resistivity) to make a 0.1 mM background solution and was allowed 24 hours to equilibrate with the atmosphere (1655 m above sea level). The calculated ionic strength based on carbonate speciation and ion concentration was 0.10 mM and the solution pH was 7.3 (± 0.1).

Cation solutions (7.5×10^{-7} M cesium and 7.5×10^{-6} M strontium) were made by adding stock solutions to 0.1 M sodium bicarbonate. Stock solutions (0.1 M cesium and 0.75 M strontium) were made with cesium chloride ($CsCl \cdot 6H_2O$) or strontium chloride salts ($SrCl_2 \cdot 6H_2O$) from MP Biomedicals (Cat. No. 150589 and 152583, respectively). Cesium was added at a lower concentration than strontium to ensure similar colloid-associated fractions (Turner et al., 2006). The cesium or strontium concentration was measured by spiking the solutions with a small amount (approximately 2.5×10^{-10} M ^{137}Cs or ^{90}Sr) of radioactive $^{137}CsCl$ or $^{90}SrCl$ dissolved in HCl from Eckert and Ziegler Isotope Products (Valencia, CA).

Colloid suspensions were made with the same cation concentrations as dissolved solutions. Stored colloids were sonicated for 30 minutes and added to the 0.1 mM sodium bicarbonate to make the final experimental colloid concentration of 100 ± 5.8 mg L^{-1} for IMt-1, IMt-2, and Oak Ridge and 200 ± 3.2 mg L^{-1} for silica colloids. Although preliminary isotherms

confirmed sorption equilibrium was approached within a few hours, the solutions were allowed to equilibrate for 24 h before each experiment to ensure consistency. Colloid concentration was measured by turbidity (Hach, XR) and correlated to mass concentration from the drying procedure discussed above.

pH and Colloid Concentration Measurements. The dissolved cation solutions, colloid suspensions, and column effluent samples were measured for pH, colloid concentration, and colloid size. pH was measured using a combination electrode (Orion, 9107BN) and pH meter (Orion, 250A+) calibrated with low ionic strength buffer solutions (Orion, Purewater® pH 6.97 and 9.15).

Colloid concentration was correlated to turbidity by first using a turbidimeter (Hach, 2100N) with the factory calibration checked with 0.1, 1, 10, and 100 NTU Formazin gel standards (Hach, Gelex®, 25890-00). Linear calibration was determined using colloid dilutions of 1, 10, 50, 100, and 200 mg L^{-1}. A linear regression produced the relationship between colloid concentration and nephlametric turbidity units (NTU).

Colloid Size Distribution Measurements. The particle size distribution in the illite suspensions was measured by dynamic light scattering (Particle Sizing Systems, NICOMP 380 DLS). The minimum particle size was determined by sequential filtering using 0.45, 0.2, 0.1, and 0.01 µm membrane syringe filters (Millipore Millex® GN, nylon, 13 mm; Whatman, Anotop 10, inorganic membrane, 10 mm). The colloidal suspension was diluted with 0.10 mM sodium bicarbonate solution to reduce the scattering intensity of the instrument between 250 and 350 kHz. The samples were measured using a 30 minute run time and the mean particle diameter and standard deviation were determined for three separate measurements.

Measurement of ^{137}Cs and ^{90}Sr by Liquid Scintillation Counting. The exact activity of the ^{137}Cs or ^{90}Sr solutions was measured by liquid scintillation counting (Packard, Tri Carb 1600TR). The main advantage of measuring the cation concentration by liquid scintillation counting of beta decays was the capability to measure total, dissolved, and sorbed cesium or strontium in samples with clay present without the need to digest the samples. Based on the long half-life of the isotopes used (30.2 y for ^{137}Cs and 28.8 y for ^{90}Sr), radioactive decay was negligible and not accounted for in calculations. A 2 mL aliquot of sample was added to 5 mL of scintillation cocktail (Packard, Ultima Gold) in a 7 mL borosilicate glass liquid scintillation vial.

The detection window was set to 0 to 2,000 keV for ^{137}Cs and 0 to 350 keV for ^{90}Sr to eliminate the detection of secondary decays from ^{90}Y (Lee et al., 2002). The counts were time-averaged for 5 minutes and the resulting count rate (counts per minute, or CPM) was correlated with a linear regression to 0, 10^{-7} 10^{-6}, 10^{-5}, 10^{-4}, 10^{-3} M standards. The quench of the sample (loss of signal due to sample conditions) was measured using the transformed Spectral Index of External Standard (t-SIE), which was calculated using the external ^{133}Ba source inducing a Compton spectrum in the scintillation cocktail.

Total cation concentrations were determined by liquid scintillation counting of the unfiltered samples. Dissolved cation concentration was measured by passing the sample through a 0.2 µm nylon filter (Millipore Millex® GN, nylon, 13 mm diameter) for illite and kaolinite and 0.02 µm filter (Whatman Anatop 10, inorganic membrane, 10 mm) for silica and Oak Ridge colloids and analyzing the effluent by liquid scintillation counting. The colloid-sorbed fraction was calculated by subtracting the dissolved cation concentrations from the total concentration such that,

$$C_{sorb} = C_{tot} - C_{dis} \quad (3.4)$$

where C_{tot} was the total cation concentration (M), C_{dis} was the dissolved cation concentration (M), and C_{sorb} was the concentration (M) of cation sorbed to the colloidal fraction.

Porous Medium. Well-rounded, medium-sphericity Ottawa quartz sand (Accusand 40/60, Unimin Corp.) was used as the porous media in all experiments. Roundness and sphericity were determined comparing microscope images to the Krumbein roundness chart and Riley sphericity index (Krumbein and Sloss, 1963). The sand was comprised of 99.8% SiO_2, less than 0.1% metal oxides (Ti, Fe, Al, K, Mg, Na, and Ca), and less than 0.1% organic compounds based on loss of ignition measurements (Unimin Corp.).

A preliminary rinse was conducted before the sand was sorted to remove fine particles. Batches of sand (2 kg) were stirred with a stainless steel spoon in a polyethylene bucket and rinsed with high purity water until the turbidity of the rinse water was below 10 NTU. The sand was transferred to borosilicate glass pans and oven-dried at 80° C for 16 h. The rinsed and dried sand was sorted through stainless steel sieves using a sieve shaker (W.S. Tyler, RX-29 Ro-Tap) according to ASTM D 422-63[1] (Rowell, 1994). The fraction that passed through a 45 mesh sieve (354 μm) and was retained on a 50 mesh sieve (297 μm) was stored in sealed containers. For this +50/-45 fraction, we assumed that $d_{50} = 325$ μm.

The sieved sand was cleaned using a procedure similar to the procedure used by Lenhart and Saiers (2002). Holes (10, 1.3 cm diameter) were drilled in the bottom of a 19 L polyvinyl chloride (PVC) bucket and covered with 104 μm stainless steel mesh (Spectra Mesh®, 146 439) held in place with silicone sealant. The bucket was ¼ filled with sand and placed inside a second 19 L PVC bucket. A nitric acid solution (10% by volume) was added until it was ponded 3 cm above the sand surface. The sand was stirred with a stainless steel spoon to release any air that

was trapped in the pores and was soaked in the acid for 36 h to dissolve any adsorbed metals. After 36 h, the bucket with the sand was raised to allow the acid to drain through the holes in the bucket and the sand was rinsed with a constant flow of high-purity water for 6-12 h or until the drainage water reached pH 5.7. A base rinse was conducted next to remove any remaining dust and silica colloids. Sand (1 kg) was transferred to 1 L HDPE bottles and 0.002 M NaOH was added to leave 2 cm of headspace in the bottles. The bottles were placed on a shaker table set at 150 oscillations per minute for 2 h. The sand was transferred to the modified PVC bucket and rinsed with high-purity water until the pH of the rinse water approached 5.7 and the turbidity dropped below 0.4 NTU. The sand was oven dried at 80°C for 16 h and sealed in a clean PVC bucket until use in breakthrough experiments.

Analysis of Sand and Clay Composition. The quartz grain surfaces were imaged with a low vacuum scanning electron microscope (LVSEM, JSM-6480LV) to visually inspect the morphology and surface roughness of the grains. Energy dispersive x-ray (EDS) spectroscopy (JEOL, Noram System Six) was used to analyze the sand for elemental composition. Sand grains were mounted on metal studs with double-sided carbon tape and viewed in the LVSEW at a pressure of about 1 Pa, 10-15 kV accelerating voltage, and a spot size near 50 µm. Focus and stigmation were iteratively adjusted and images with magnification of 10,000× were captured and compared to archived pictures to qualitatively estimate sphericity and roundness of the grains (Krumbein and Sloss, 1963).

Desorption Isotherms. Clay samples (45 mL of approximately 100 mg L^{-1}) were equilibrated with 7.5×10^{-7} cesium or 7.5×10^{-6} strontium for 72 hours. At the end of this equilibration time, the samples were measured for total and dissolved cesium or strontium. Samples were centrifuged for 120 minutes at 1650 rfc. The supernatant was poured from the sample and the

volume was recorded. This volume was replaced with pH 7.3, 0.1 mM sodium bicarbonate. The samples were shaken by hand for 30 sec to resuspend all particles from the bottom of the centrifuge tube and the samples were placed in a sonic bath for 15 minutes. The samples were placed on a wrist-action shaker (Burrell, Model 75) and shaken horizontally at a rate of 5 shakes per second for 5 days and samples were periodically removed and measured for cation concentration.

Column Set-up. The column experiments were conducted using a borosilicate glass liquid chromatography column (2.5 cm diameter and 15 cm long; Kontes®) (Figure 3.1). Threaded collars secured Teflon® inserts lined with 100 µm polypropylene mesh in the top and bottom of the column. The column was mounted vertically from a ring stand and the top fitting was

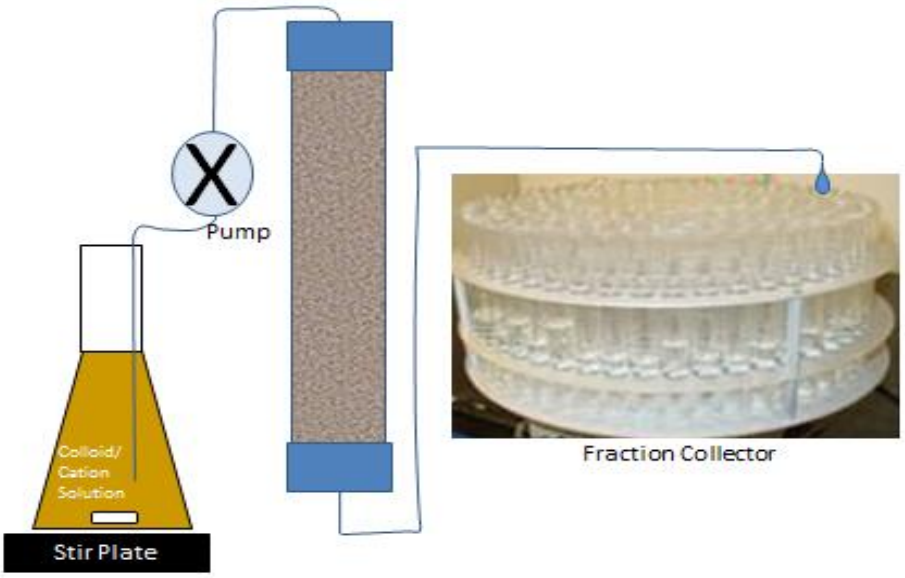

Figure 3.1. Column-set-up. Colloid and cation solutions in equilibrium are placed on a stir plate and pumped through the column from top to bottom. The effluent from the bottom of the column is collected in a fraction collector and measured for total, dissolved, cation concentration by liquid scintillation counting and colloidal concentration by turbidity.

connected to a peristaltic pump (Cole Parmer Masterflex ®, 7553-70 motor; 7014-20 pump head; Stir-pak® 50002-02 controller) with #13 Tygon® tubing. The pump was set to a flow rate of 2.4 mL min^{-1} (±0.2). Tubing was replaced after each experiment to prevent contamination. Another section of #13 tubing carried effluent from the bottom of the column to a fraction collector (Eldex, U-200 Universal) loaded with 20 mL polystyrene test tubes set to advance on 5 minute intervals.

Initial Packing. The column was wet-packed according to the following procedure. Background solution was poured in from the top of the column to a depth of 2 cm. Increments of sand (25 g) were added to the column. After each addition, the column was stirred with a polystyrene rod to minimize layering. After every 1 cm of sand added, the column was tapped on all sides with a rubber mallet to ensure uniform packing and consistent porosity between experiments. The weights of sand and background solution added to the column were recorded and used to confirm the porosity and mass of sand in the columns. After packing, background solution (pH 7.3, I 0.1 mM) was passed through the column for 10 to 15 pore volumes until effluent pH and turbidity stabilized to pH 7.3 ± 0.1 and below 0.3 NTU, respectively.

Tracer Tests. The dispersion coefficient (*D*) of bromide was determined by pumping 4.0 mM sodium bromide (Fisher Scientific, S255-500) solution through the column. Bromide was measured with a bromide-specific electrode (Accumet, Cat. No. 13-620-525) and meter (Orion, 720A) calibrated with 10^{-2}, 10^{-3}, 10^{-4}, 10^{-5}, and 10^{-6} M bromide standards (Fisher Scientific, S255-500).

Column Transport Experiments. Saturated breakthrough experiments were conducted to test the effect of three variables on cation transport: (1) presence of colloids, (2) radioactive cation

(cesium or strontium), and (3) colloid type (IMt-1 and IMt-2 illite, Oak Ridge colloids, and silica). Experiments were run until the normalized effluent concentration (C/C_0) exceeded 0.5, or 50% breakthrough. The influent solution was then switched to the background solution (0.1 mM $NaHCO_3$) and continued for 10-20 additional pore volumes. Ten breakthrough experiments were conducted with cesium and strontium (Table 3.1).

Table 3.1. Outline of experimental conditions to test effect of colloid type on colloid-facilitated transport.

Experiment ID	Cation	Colloid
1	Cs	None
2	Sr	None
3	Cs	IMt-2
4	Sr	IMt-2
5	Cs	Oak Ridge
6	Sr	Oak Ridge
7	Cs	Silica
8	Sr	Silica
9	Cs	IMt-1
10	Sr	IMt-1

Mathematical Model. The colloid-facilitated transport code developed by (Turner et al., 2006a) was used to model the experimental results (see Chapter 2 for a detailed description). The MATLAB® code solves the Richards' equation for water movement and accounts for the presence of cations and colloids. A predictor-corrector scheme was used to solve the nonlinear surface chemistry equations and non-linear, two-site sorption was used to represent the different kinetics exhibited by the strong edge sites and weaker face charges found on some clay surfaces (e.g., illite). The rate coefficients controlling colloid and cation transport were determined by fitting the experimental results for total, dissolved, and colloid-associated cesium or strontium with a sum of least squares parameter optimization code. Model simulations were implemented

within MATLAB® (Version 7.11.0, The Mathworks, Natick, MA). The spatial discretization, Δx, and timestep, Δt, used in the model were adjusted to ensure mathematical stability. The Peclet number, $N_{Pe,,}$ and Courant number, Cr, represent the dimensionless ratios of advection to dispersion and transport distance to spatial discretization, respectively (Clark, 1996; Zheng and Bennett, 2002).

RESULTS

Images and Elemental Analysis. LVSEM images of the colloids and quartz surfaces are shown below (Figure 3.2). The kaolinite (Fig 3.2d) exhibited an expanded "book-like" structure while the IMt-2 illite (Figure 3.2c) showed clear layering of sheets with edges and faces visible.

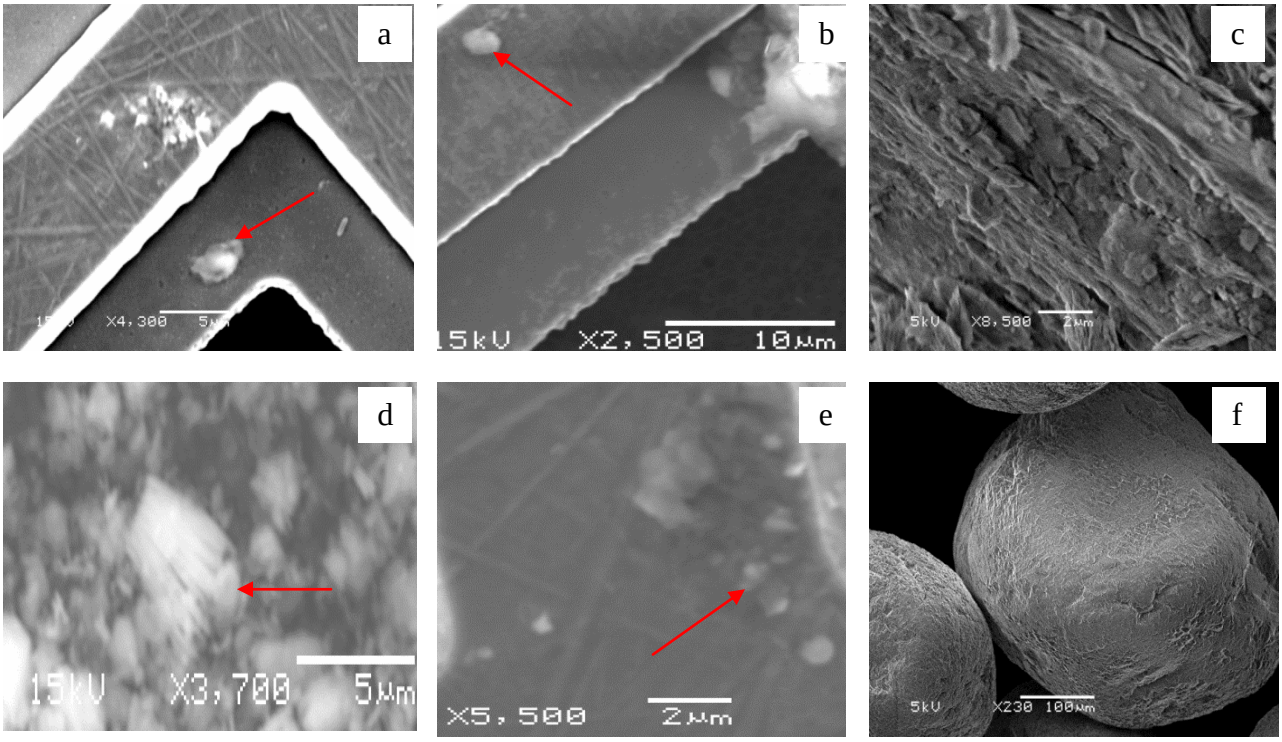

Figure 3.2. LVSEM images of (a) Oak Ridge colloids, (b) silica colloids, (c) aggregated IMt-2 illite, (d) kaolinite colloids, (e) IMt-1 illite colloids, and (f) quartz sand. Arrows point to colloids in respective images.

Particle size (assuming uniform, spherical particles) was measured by dynamic light scattering. The mean diameter was 1518.8 ± 33 µm, 1793.4 ± 77 µm, 1518.8 ± 32 µm, and 262.7 ± 37 µm for IMt-1, IMt-2, Oak Ridge, and silica colloids, respectively (Figure 3.3).

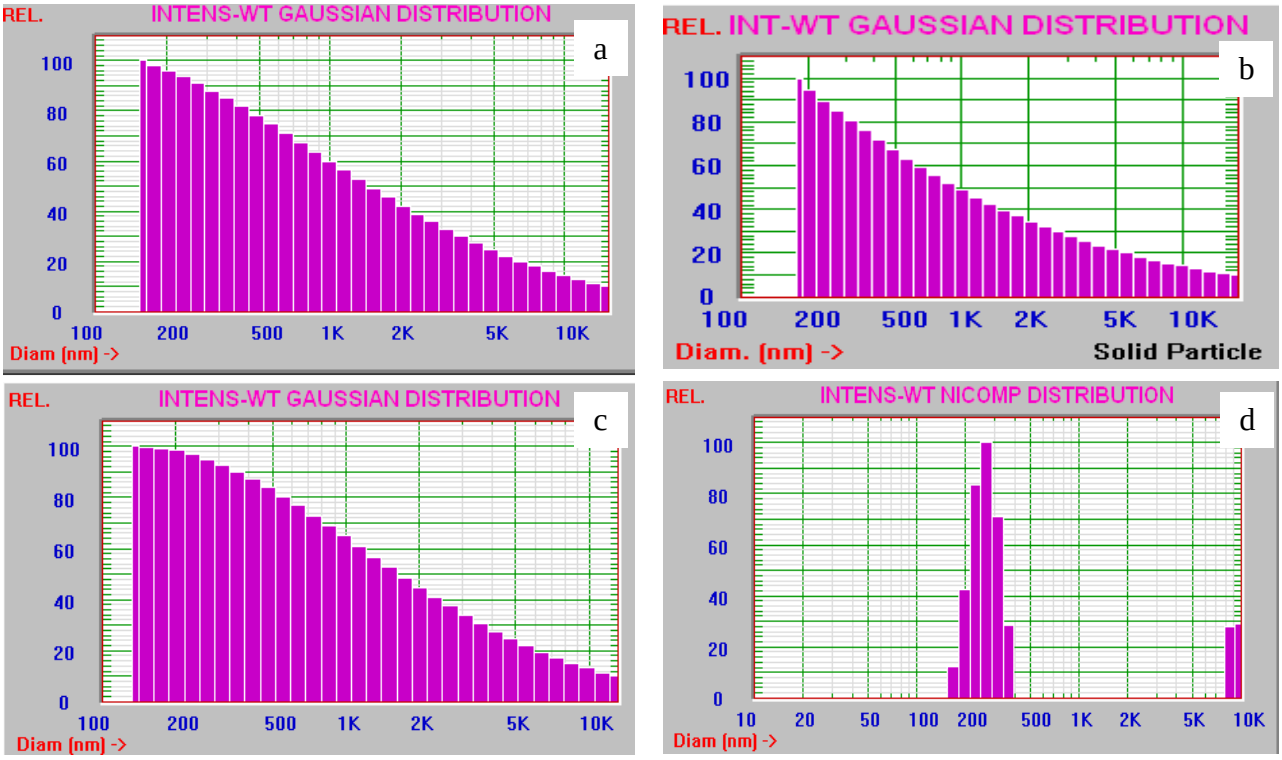

Figure 3.3. Particle size distributions for (a) IMt-1, (b) IMt-2, (c) Oak Ridge, and (d) silica colloids.

EDS analysis (Table 3.2) determined that Oak Ridge, IMt-1 and IMt-2 colloids are composed of O, Mg, Al, Si, K, and Fe. The IMt-1 colloid surface was over 16% Fe, while IMt-2 and Oak Ridge colloids were 2.2 and 2.4% Fe by weight, respectively. The silica colloids were 60% O and 22% Si without a trace of any other elements. Kaolinite was 63% O, 16% Al and 17% Si without any other elements present. The carbon tape used to mount the samples for LVSEM imaging may add the carbon signal. The purity of the quartz sand was confirmed to be 62% O and 38% Si. The quartz grain shape was well-rounded with edges of the crystalline structure visible at 230 times magnification.

Table 3.2. Elemental composition (% by weight) of colloids and quartz sand from EDS analysis.

	Colloids					Sand
Element	*OR*	*Silica*	*Imt-1*	*Imt-2*	*Kaol*	*Quartz*
C	9.12	18	13.8	14.84	3.9	-
O	59.57	60.42	53.55	53.03	62.62	62.13
Mg	1.36	-	1.22	0.81	-	-
Al	8.36	-	6.03	7.91	16.18	-
Si	15.04	21.57	7.74	16.7	17.29	37.87
K	4.07	-	1.34	4.55	-	-
Fe	2.37	-	16.32	2.17	-	-
Total	100	100	100	100	100	100

Desorption Isotherms. The concentration of cations sorbed to the colloid surface after a 72 h equilibration period was used for the initial percent cation sorbed calculation. Subsequent sorbed fractions were calculated as the percent of the original sorbed cations that remained on the colloid surface over time. The desorption isotherm data showed that most of the cesium and strontium desorbed from the colloids within the first 30 min and very little desorbed after 30 minutes (Figure 3.4). For all colloid types, 2-3 times more cesium desorbed from the colloid surfaces than for strontium.

The percent of 7.5×10^{-7} M cesium sorbed after 72 hours varied based on colloid type. IMt-1 sorbed the most cesium with over 70% sorbed. IMt-2 and Oak Ridge colloids sorbed similar amounts. IMt-2 sorbed 40-45% for duplicate results and Oak Ridge colloids sorbed about 48%. Silica colloids sorbed 24% of the cesium and kaolinite colloids sorbed the least amount with only 14% sorbed.

A different sorption order was observed with 7.5×10^{-6} M strontium. Oak Ridge colloids sorbed almost 70% of the strontium from solution. IMt-1 illite sorbed 54% of the strontium,

which was close to the 49-53% sorbed for IMt-2 illite. Kaolinite sorbed almost 45% and silica sorbed the least amount with about 30% sorbed.

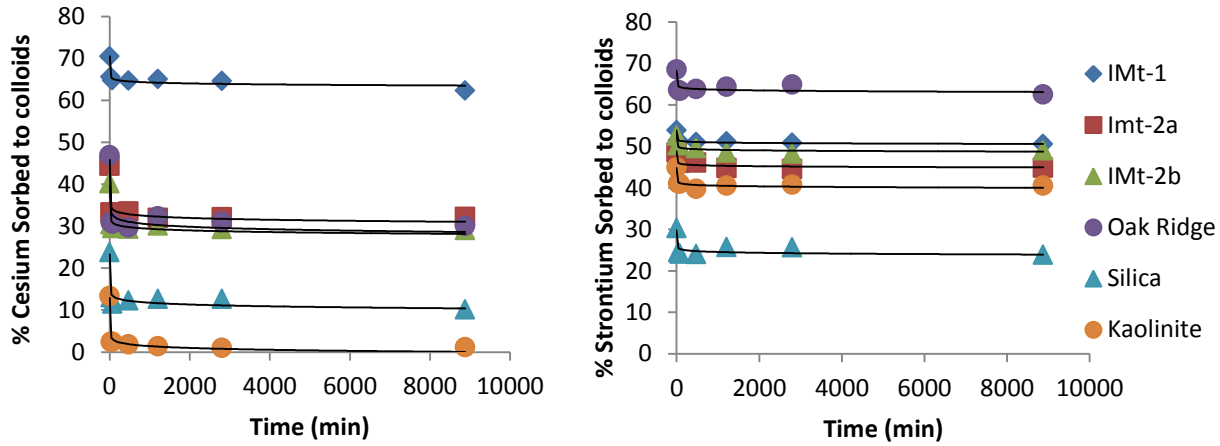

Figure 3.4. Desorption isotherms for cesium (left) and strontium (right) for illite (IMt-1 and IMt-2), Oak Ridge, silica, and kaolinite colloids.

Conservative Tracer Results. The dispersion coefficient (*D*) for the cations and colloids was determined by conducting breakthrough experiments using bromide as a conservative tracer (Figure 3.5). The volume of water that passed through the column until C/C_0 reached 0.50 was 28.5 mL. This was very similar to the volume of water measured when packing the column (28.9 mL) and was used as the measurement of one pore volume for modeling simulations. The porosity (*n*) of the packed columns was calculated as 0.33 ± 0.01 for all breakthrough experiments using Eqn. 3.7.

$$n = \frac{m_{sand} d_p}{V} \qquad (3.7)$$

where m_{sand} is the mass of sand, d_p is the density of quartz (2.65 g cm^{-3}), and V is the column volume (cm^3).

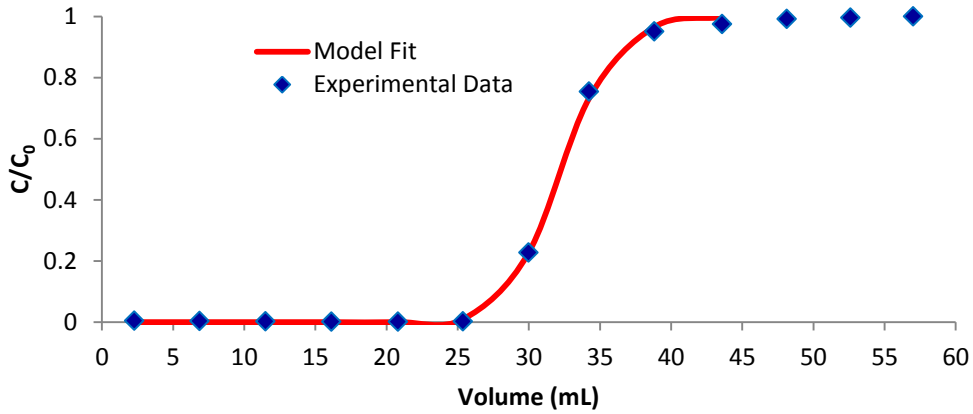

Figure 3.5. Bromide tracer data for 15 cm glass column set-up for column position (top) and cumulative effluent volume (bottom). Concentration is plotted on the y-axis and vertical position of bromide front in meters (m) or volume of water (mL) passed through the column is plotted on the x-axis.

The optimal dispersion coefficient (D) was determined by minimizing the calculated error between the measured C/C_0 and the calculated C/C_0 for the analytical advective-dispersive transport equation (Ogata and Banks, 1961);

$$\frac{C(x,t)}{C_o} = \frac{1}{2}\left[erfc\left(\frac{x-Ut}{\sqrt{4Dt}}\right) + \exp\left(\frac{xU}{D}\right) erfc\left(\frac{x+Ut}{\sqrt{4Dt}}\right)\right] \quad (3.8)$$

where $C(x,t)$ is the bromide concentration in the effluent at the bottom of the column (µM), C_0 is the influent bromide concentration (µM), x is the average distance the solute front has traveled in the column (cm), U is the average linear pore water velocity (cm h^{-1}), t is time (h^{-1}), and D is the hydrodynamic dispersion coefficient (cm^2 h^{-1}). The error between the experimental C/C_0 and calculated C/C_0 was minimized to yield the optimal value of D of 9.27 cm^2 h^{-1}.

Experimental Overview. The results from the dissolved and colloid-facilitated breakthrough experiments were used to determine the sand and colloid sorption parameters by fitting the results with the mathematical model described in Chapter 2. Dissolved transport data was used to determine the quartz sorption parameters for the adsorption rate coefficient k_{as}, desorption rate coefficient k_{sa}, and adsorption capacity X_a for cesium and strontium. The colloid-facilitated transport data was used to determine the adsorption and desorption parameters for the colloids. The adsorption and desorption rate coefficients of the cations to a fast binding site (k_{ac1} and k_{ca1}, respectively), slower binding site (k_{ac2} and k_{ca2}, respectively), cation adsorption capacity of the colloids X_c, and fraction of illite binding sites of the fast type F_{c1} were determined from model fits. The quartz adsorption capacity X_a was also refitted for the colloid-facilitated experiments, with the capacity from the dissolved experiments being used as an initial condition.

Dissolved Cation Breakthrough Results. Column breakthrough experiments were conducted to determine a range for the sand sorption capacity X_a of the model. Cesium breakthrough ($C/C_0 > 0.50$) occurred near 24 pore volumes and aqueous strontium breakthrough occurred near 16 pore volumes (Fig. 3.6). 100% of the cesium was removed from the pore water until a steep breakthrough front was observed near 20 pore volumes; however, strontium exhibited a very small initial plateau near 1% that was not removed by the quartz sand.

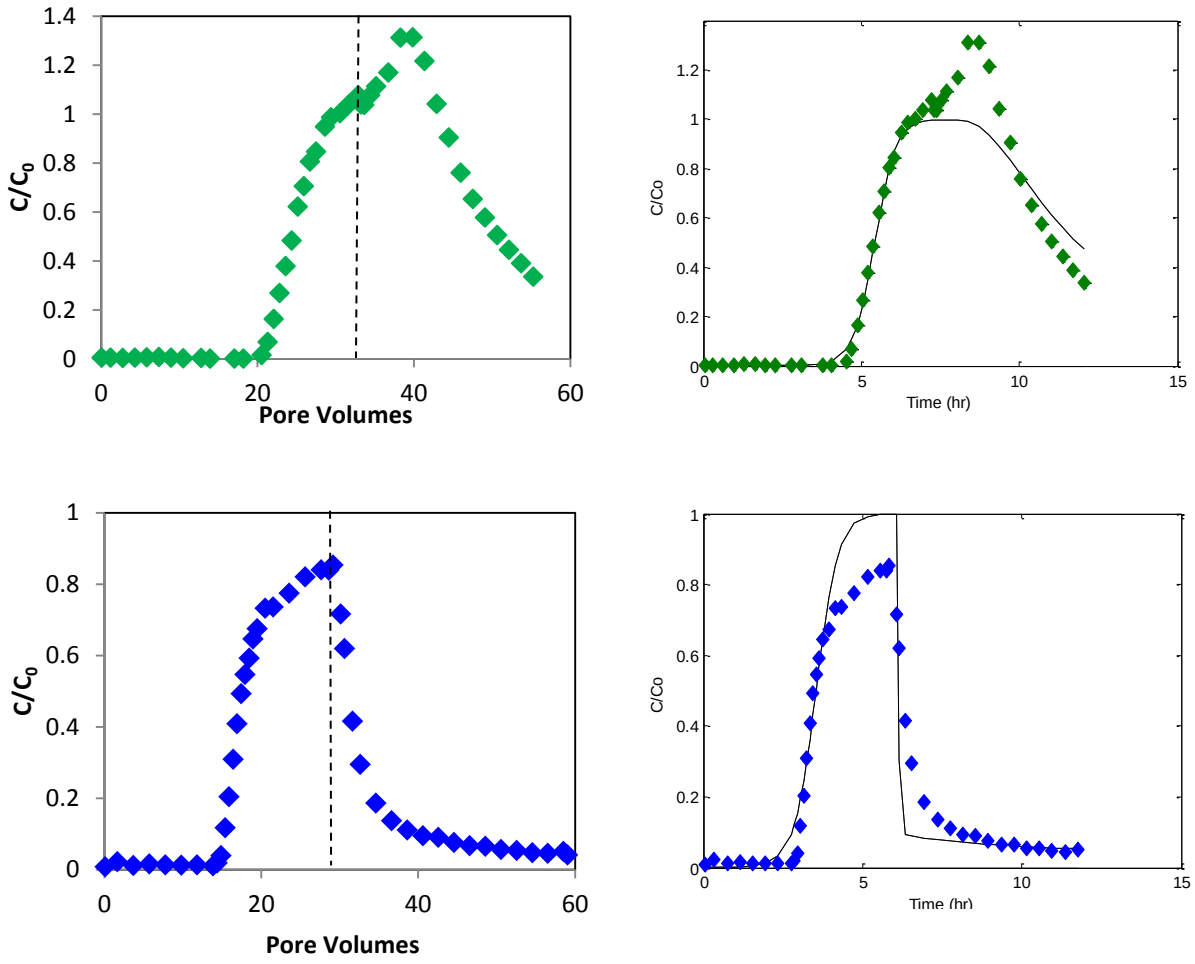

Figure 3.6. Experimental data (left) and model fits (right) for dissolved cesium (top, $R^2 = 0.95$) and strontium (bottom, R^2=0.86).

Dissolved Cation Model Results. The best-fit values for the sand adsorption rate and desorption rate coefficients were 4.9 and 0.036 μM^{-1} h^{-1}, respectively ($R^2 = 0.95$) for cesium with an adsorption capacity of 0.0080 µmol g^{-1} and 0.40 and 0.00028 μM^{-1} h^{-1}, respectively (R^2 = 0.86) for strontium with an adsorption capacity of 0.027 µmol g^{-1}. The model was able to match the cesium experimental data well, with 100% of the cesium being adsorbed to the quartz surface and 0% leaving the column in the effluent for the first 5 h (20 pore volumes). The model also

matched the sharp increase in cesium after 5 h and accurately predicted the time and slope of the cesium breakthrough. After the solution was switched to background solution without cesium, the data shows an increase in cesium concentration above $C/C_0 = 1$, which the model was unable to predict. The model also over-predicted the desorption tail of the experiment with the model predicting more cesium desorption from the sand than was observed in the experimental data.

The model was able to match the strontium data well. The model under-predicted the maximum concentration after 6 h (29 pore volumes). After the solution was switched to the background solution, the model predicted the sharp decrease in effluent concentration observed in the data; however, the model slightly over-predicted the amount of strontium desorbing from the quartz surface back into solution during the first 2 h.

Colloid Transport Results and Modeling. IMt-1 and IMt-2 exhibited similar transport properties in the column (Figures 3.7-3.10). Breakthrough occurred near 1 pore volume and effluent concentration approached a steady maximum plateau near 90% of the influent colloid concentrations. Oak Ridge colloid breakthrough also occurred near 1 pore volume; however, the effluent colloid concentration approached a plateau below 85% of the influent concentration. The silica breakthrough appeared within the first pore volume of effluent and reached 100% before 1 cumulative pore volume passed through the column. The order of colloid attachment in the quartz column from most mobile to least mobile was: silica > IMt-1 = IMt-2 > Oak Ridge.

The model was able to predict the colloid breakthrough behavior well for all colloid types, with the main features being (1) breakthrough within 2 pore volumes, (2) a plateau at a maximum value and (3) very little colloid release after the solution was switched to background solution. For experiments with IMt-1 and IMt-2, the effluent concentration approached a maximum plateau near $C/C_0 = 0.90$. For Oak Ridge colloids and silica colloids, the effluent

concentration approached a maximum value near C/C_0 = 0.85 and 0.99, respectively. 10% of the IMt-1 and IMt-2 colloids were removed from suspension by the quartz, while 15% of the Oak Ridge colloids were removed and 1% of the silica was removed. All colloid types were held nearly irreversibly to the quartz surface (or not available to desorb in the case of silica) and little release occurred when the solution was switched to the background solution.

The three parameters used to fit the model to the experimental data were colloid attachment rate coefficient, k_{cs}, colloid detachment rate coefficient, k_{sc}, and the colloid attachment capacity, X_c (Table 3.3). The optimal values for k_{cs} for IMt-1, IMt-2, Oak Ridge, and silica were 0.63 h^{-1} ± 0.040, 0.58 h^{-1} ± 0.18, 0.79 h^{-1} ± 0.12, and 0.050 h^{-1} ± 0.0, respectively. These values match the general trends observed in the experimental data with silica having the least attachment, Oak Ridge colloids having the most attachment, and IMt-1 and IMt-2 colloids having exhibiting similar attachment.

The optimal values for k_{sc} for IMt-1, IMt-2, Oak Ridge, and silica were 0.0050 h^{-1} ± 0.0, 0.0090 h^{-1} ± 0.0020, 0.0050 h^{-1} ± 0.0, and 0.0050 h^{-1} ± 0.0, respectively. As was discussed earlier, there was very little detachment of colloids from the quartz surface after the suspension was switched to background solution. The small colloid detachment rates corresponded to a very small amount of colloid detachment from the quartz surface.

The optimal values for X_c for IMt-1, IMt-2, Oak Ridge, and silica were 0.00010 μmol g^{-1}, 0.000080 μmol g^{-1}, 0.0010 μmol g^{-1}, and 0.0001 μmol g^{-1}, respectively. The highest attachment capacity was found for Oak Ridge colloids and was nearly 10 times higher than for silica, IMt-1, and IMt-2 colloids.

Colloid-Facilitated Transport Results and Modeling. Figures 3.7-3.10 show the breakthroughs of dissolved, colloidal, and total fractions of cesium and strontium with IMt-1,

IMt-2, Oak Ridge, and silica colloids, respectively. Table 3.3 contains parameter values used for the model fits. The model was able to adequately fit the experimental data for all of the colloids tested. The quartz adsorption and desorption rate coefficients determined in the aqueous cation breakthrough experiment were held constant for the colloid-facilitated transport modeling. The quartz adsorption capacity; however, was reduced from 0.0080 μmol g^{-1} for aqueous cesium transport to 0.00070, 0.0015, 0.0060, and 0.0060 μmol g^{-1} for experiments with IMt-1, IMt-2, Oak Ridge, and silica colloids, respectively. These are reductions of a factor of 11.4, 5.3, 1.3, and 1.3 or an average reduction of a factor of 4.9 ± 4.8. The quartz strontium adsorption capacity was reduced from 0.027 μmol g^{-1} to 0.0070, 0.010, 0.026 μmol g^{-1}, for experiments with IMt-1, IMt-2 and Oak Ridge colloids, respectively, and increased to 0.031 μmol g^{-1} for silica colloids.

For IMt-1 (Figure 3.7), both cesium and strontium breakthrough was increased by the presence of colloids. Breakthrough occurred after 2 pore volumes for cesium and 3.7 pore volumes for strontium, which were 12.3 times and 4.4 times faster than dissolved breakthrough. The quartz was able to remove little of the cesium or strontium from the IMt-1 clay. After the solution was switched to the background solution, more cesium desorbed from the quartz sand sorbed colloids than strontium. Due to the very small amount of colloid mobilization, less than 1% of the cesium or strontium was associated with re-mobilized colloids.

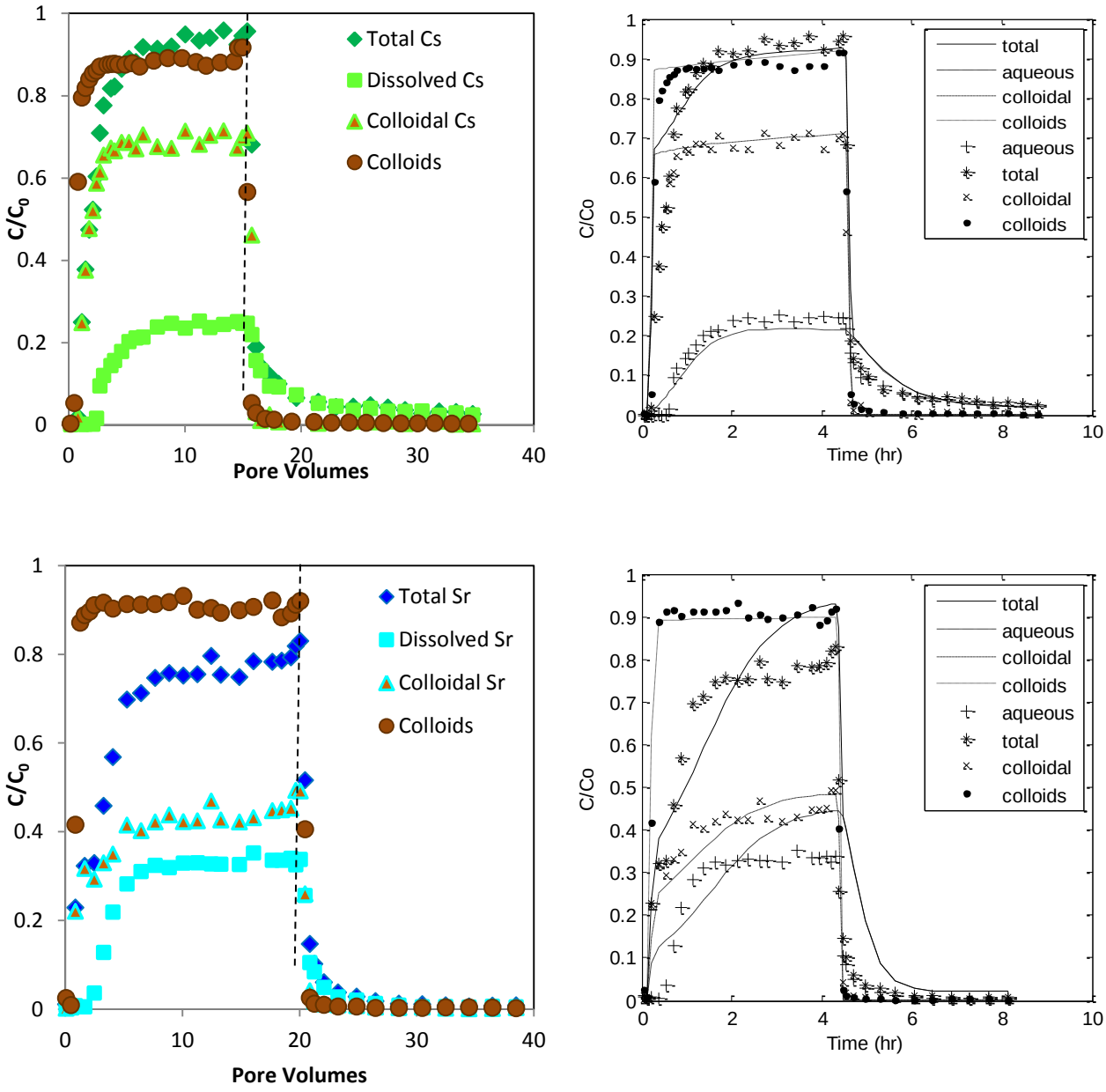

Figure 3.7. Breakthrough data (left) and model fits (right) for IMt-1 colloids and cesium (top, R^2=0.93) and strontium (bottom, R^2=0.90).). Filled circles represent colloids, diamonds (or *) denote total concentration, filled triangles (or ×) denote colloid-sorbed concentration, and squares (or +) denote dissolved cation concentration.

The model was able to predict the transport behavior with IMt-1 illite fairly well (Fig. 3.7) with R^2 = 0.93 and 0.90 for cesium and strontium, respectively. For total cesium, the model

simulation over predicted the time to breakthrough by a small amount, but reached a maximum value near 95%. The early breakthrough was caused by colloid-associated cesium, which was also over predicted in the first pore volume. The magnitude of colloidal cesium concentration was accurately predicted near a 65 and 70%. Dissolved cesium breakthrough was well predicted with the same general shape as the experimental data. After the solution was switched to background solution at 4.6 h, the model over-predicted the amount of dissolved and total cesium in the effluent by less than 5% and accurately predicted the quick drop and steady minimum concentration near C/C_0 = 0.03 after 6.5 h. The colloidal cesium concentration was accurately predicted to be neat zero due to the lack of IMt-1 in the effluent.

For strontium, the model correctly simulated the early increase in total strontium up to C/C_0 = 0.30, but does not match the steep increase to 75-80% total strontium breakthrough before reaching a near stable maximum (Fig. 3.7). The model matches the colloidal strontium breakthrough well, with a nearly stable plateau is reached near C/C_0 = 0.40. The dissolved strontium breakthrough was poorly matched and the model under-predicted the first appearance of strontium in the effluent and then over-predicted the concentration after 2 h. After switching to background solution, the model over-predicted the total and dissolved strontium concentration for the first hour and by ~3% for the final 2 h.

The optimal IMt-1 adsorption and desorption rate coefficients for the fast and slow sites (k_{ac1}, k_{ca1} and k_{ac2}, k_{ca2}; respectively) were the same values as those reported by Turner et al. (2006) for IMt-2 with 1.5 and 0.15 μM^{-1} h^{-1} for k_{ac1} and k_{ca1}, respectively and 0.90 and 0.00060 μM^{-1} h^{-1} for k_{ac2} and k_{ca2}, respectively, for cesium and 1.5 and 0.15 μM^{-1} h^{-1} for k_{ac1} and k_{ca1}, respectively, and 1.1 and 0.090 μM^{-1} h^{-1} for k_{ac2} and k_{ca2}, respectively, for strontium. The fraction of fast to slow binding sites on IMt-1 colloids, F_{c1}, for cesium was optimal at 0.0010,

which means almost all of the binding sites were strong sites. For strontium, F_{c1} was found to be optimal at 0.55. Colloid cation adsorption capacities were found to be 11 and 150 μmol g^{-1} for cesium and strontium, respectively.

For IMt-2 (Figure 3.8), cesium and strontium breakthrough was increased less than for IMt-1 but was still very significant. Breakthrough occurred after 4.8 pore volumes for cesium and 6.0 pore volumes for strontium, which was 5.1 and 2.7 times faster than dissolved breakthrough, respectively. After 1 pore volume of suspension passed through the column, an intermediate plateau near 10% of the influent solution concentration was observed for both cesium and strontium. This plateau increased very slightly over the next 3-4 pore volumes until a sharp increase in concentration. After switching to background solution, more cesium than strontium desorbed from the quartz and attached colloids with less than 1% of the cations associated with remobilized colloids.

The model was able to predict the total cation transport behavior with IMt-2 illite present fairly well (Figure 3.8) with R^2 = 0.91 and 0.79 for cesium and strontium, respectively. For cesium, the model simulation over-predicted the initial appearance of total and colloidal cesium concentration in the first pore volume (0.2 h) near 20%. After 1 h (~5 pore volumes), the model accurately predicted the total concentrations of cesium and the aqueous and colloid-associated fractions near 60 and 30%, respectively. After the switch to background solution, the model accurately predicted the concentration of colloidal cesium near zero, but over-predicted the total and dissolved cesium concentrations in the first 2 h and then under-predicted the total and dissolved cesium concentrations after that.

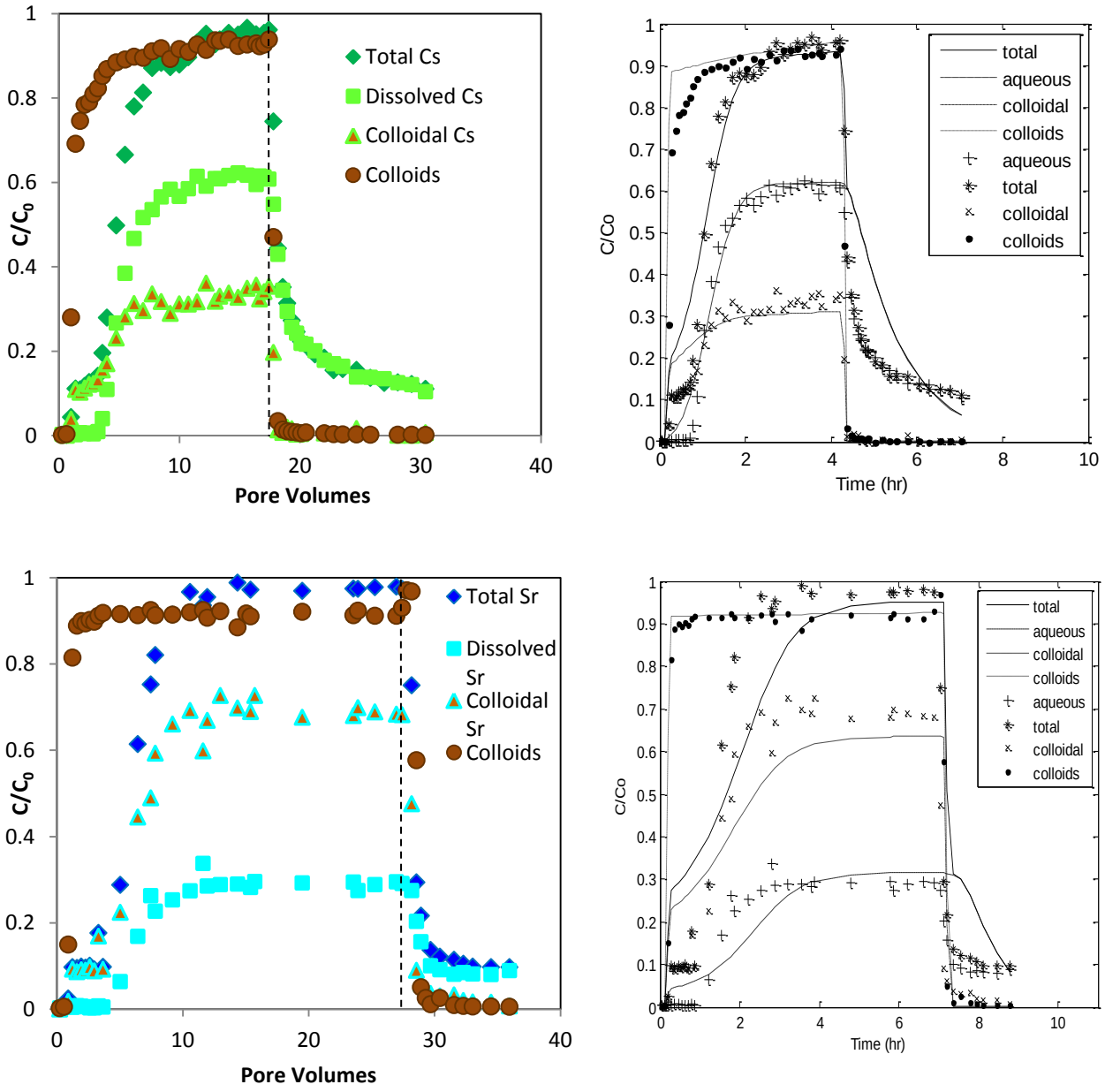

Figure 3.8. Breakthrough data (left) and model fits (right) for IMt-2 colloids and cesium (top, R^2=0.91) and strontium (bottom, R^2=0.79). Filled circles represent colloids, diamonds (or *) denote total concentration, filled triangles (or ×) denote colloid-sorbed concentration, and squares (or +) denote aqueous cation concentration.

For strontium and IMt-2, the model simulation over-predicted the initial appearance of total and colloidal strontium concentration in the first pore volume (0.2 h) near 25%, while the data only reached a concentration near 10%. After 1 h (5 pore volumes), the increase in

concentration was less steep than the experimental result. After 3 h, the model matched the total, dissolved, and colloidal strontium concentrations within 5%. After the switch to background solution, the model over-predicted the amount of total and dissolved strontium in the effluent for the first 1.5 h, but correctly predicted a concentration near zero for the colloidal strontium in the effluent.

The optimal values found for IMt-2 adsorption and desorption rate coefficients for cesium with fast and slow sites (k_{ac1}, k_{ca1} and k_{ac2}, k_{ca2}; respectively) were 1.5 and 0.15 μM^{-1} h^{-1} for k_{ac1} and k_{ca1}, respectively and 0.90 and 0.00060 μM^{-1} h^{-1} for k_{ac2} and k_{ca2}, respectively. For strontium, the optimal values were 1.5 and 0.15 μM^{-1} h^{-1} for k_{ac1} and k_{ca1}, respectively, and 1.1 and 0.090 μM^{-1} h^{-1} for k_{ac2} and k_{ca2}, respectively. The fraction of fast to slow binding sites on IMt-2 colloids, F_{c1}, for optimal at 0.50 for cesium and 0.55 for strontium. Colloid cation adsorption capacities were found to be 20 and 250 $\mu mol\ g^{-1}$ for cesium and strontium, respectively.

For Oak Ridge colloids (Figure 3.9), 50% breakthrough occurred after 11.5 pore volumes for cesium and 7.0 pore volumes for strontium, which were 2.1 times and 2.3 times faster than dissolved breakthrough. After 1 pore volume of suspension passed through the column, an intermediate plateau between 11-16% cesium concentration and 26-32% strontium concentration was observed until a sharp increase in effluent concentration after 8 pore volumes and 5.5 pore volumes, respectively. After the cation/colloid suspension was switched to background solution, more cesium than strontium desorbed from the quartz and colloid surfaces, with less than 1% of

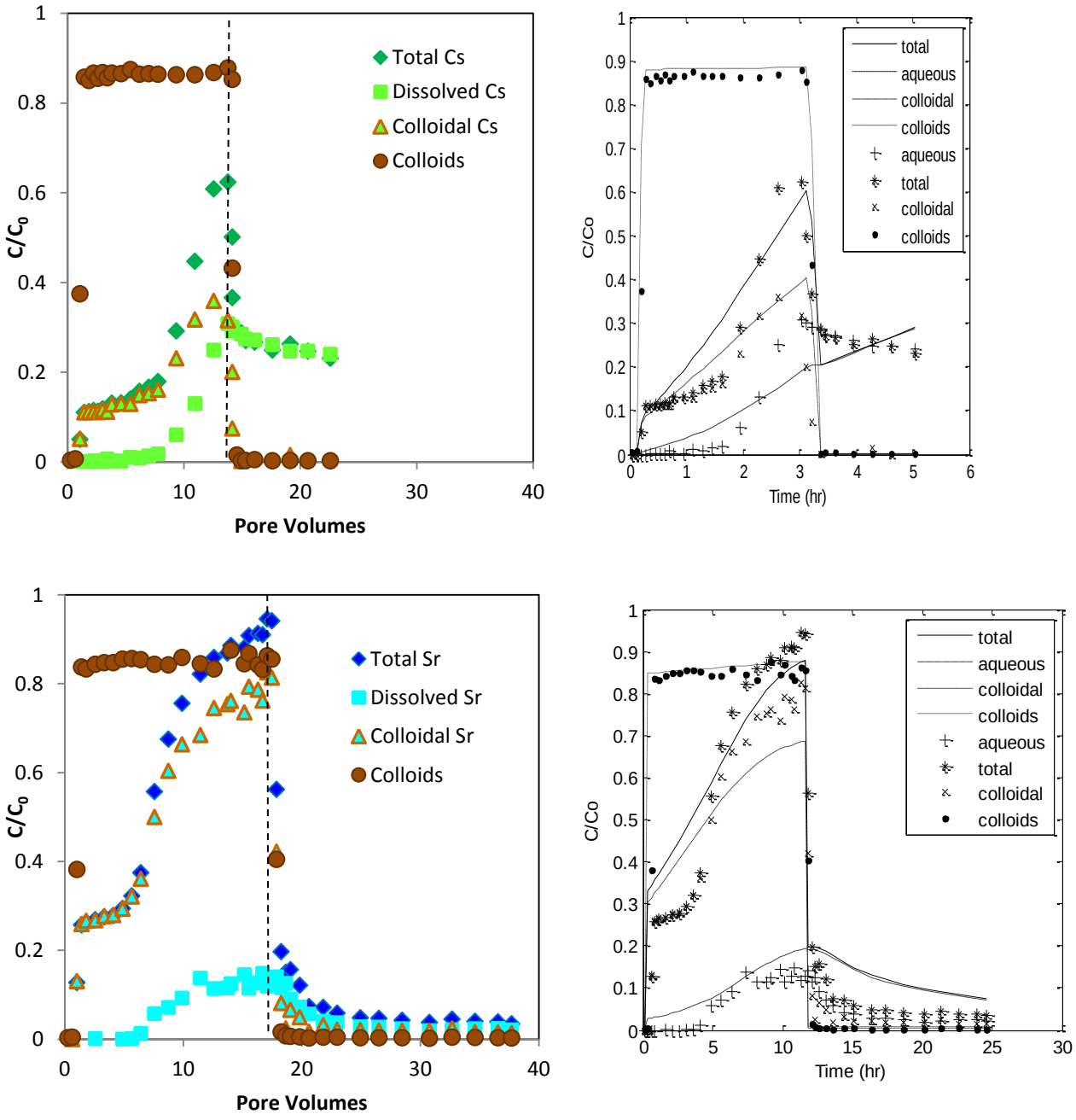

Figure 3.9. Breakthrough data (left) and model fits (right) for Oak Ridge colloids and cesium (top, R^2=0.91) and strontium (bottom, R^2=0.80). Filled circles represent colloids, diamonds (or *) denote total concentration, filled triangles (or ×) denote colloid-sorbed concentration, and squares (or +) denote aqueous cation concentration.

the cations on remobilized colloid surfaces due to the strong attachment of the colloids to the quartz surface. The model predicted the total cation transport behavior with Oak Ridge colloids

well (Figure 3.9) with R^2 = 0.91 and 0.80 for cesium and strontium, respectively. For cesium, the model simulation accurately predicted an initial appearance of total and colloidal cesium concentration in the first pore volume (0.2 h) near 10%. The model predicted a linear increase in the total and colloidal cesium; however, the experimental data exhibited a slowly increasing plateau in the total and colloidal cesium from 10%-20% and a sharp increase after 1.5 h. The model also over-predicted the concentration of dissolved cesium in the effluent before 2 h and under-predicted the concentration after 2 h. After the switch to background solution, the model predicted an increase in the total and dissolved cesium concentrations from 20% to 30%, whereas, the experimental data resulted in a decrease transitioning to a steady minimum near 25%.

For strontium, the model simulation under-predicted the initial appearance of total and colloidal strontium concentration in the first pore volume (0.2 h) near 33% (near 26% for the data). The model predicted a linear increase in the total and colloidal cesium concentration; however, the experimental data exhibited a slowly increasing plateau for total and colloidal strontium from 25%-30% and a sharp increase after 4 h. The model accurately predicted that most of the total transport of strontium was in the colloidal phase. The model predicted that 3-4% of the total effluent cesium was in the dissolved phase after the first 0.2 h; however, a concentration near zero was measured in the experiments until after 4 h. After the switch to background solution, the model over-predicted the amount of total and dissolved strontium in the effluent for the first 1.5 h, but correctly predicted a concentration near zero for the colloidal strontium in the effluent.

The optimal values found for Oak Ridge colloid adsorption and desorption rate coefficients for cesium with fast and slow sites (k_{ac1}, k_{ca1} and k_{ac2}, k_{ca2}; respectively) were 1.5 and

0.20 μM^{-1} h^{-1} for k_{ac1} and k_{ca1}, respectively and 1.4 and 0.010 μM^{-1} h^{-1} for k_{ac2} and k_{ca2}, respectively. For strontium, the optimal values were 1.1 and 0.33 μM^{-1} h^{-1} for k_{ac1} and k_{ca1}, respectively, and 2.0 and 0.024 μM^{-1} h^{-1} for k_{ac2} and k_{ca2}, respectively. The fraction of fast to slow binding sites on IMt-2 colloids, F_{c1}, was 0.20 for cesium and 0.53 for strontium. Colloid cation adsorption capacities were found to be 47 and 150 $\mu mol\ g^{-1}$ for cesium and strontium, respectively.

For silica colloids (Figure 3.10), breakthrough occurred after 18.2 pore volumes for cesium and 23 pore volumes for strontium, which was an increase of 1.3 times for cesium but a decrease of 1.4 times for strontium. Most of the cations were removed from the pore water for the first 13-15 pore volumes, with less than 3% of the cesium or strontium leaving the column without being desorbed from the silica colloids. After the suspension was switched to background solution, both cesium and strontium were more readily desorbed from the quartz than with other colloids, with more cesium being released than strontium.

The model predicted the total cation transport behavior with silica colloids very well (Figure 3.10) with $R^2 = 0.96$ and 0.94 for cesium and strontium, respectively. For cesium, the model simulation predicted an initial appearance of total and colloidal cesium concentration in the first pore volume (0.2 h) near 4%, but did not maintain a steady value as was observed in the experimental data. The model also over-predicted the dissolved cesium concentration over the first 3 h. After 4 h, the model accurately predicted a steep linear increase in the total cesium concentration approaching a value above 90%; however, the dissolved concentration was over-predicted by nearly 10%. After 4 h, the data exhibited a colloidal cesium

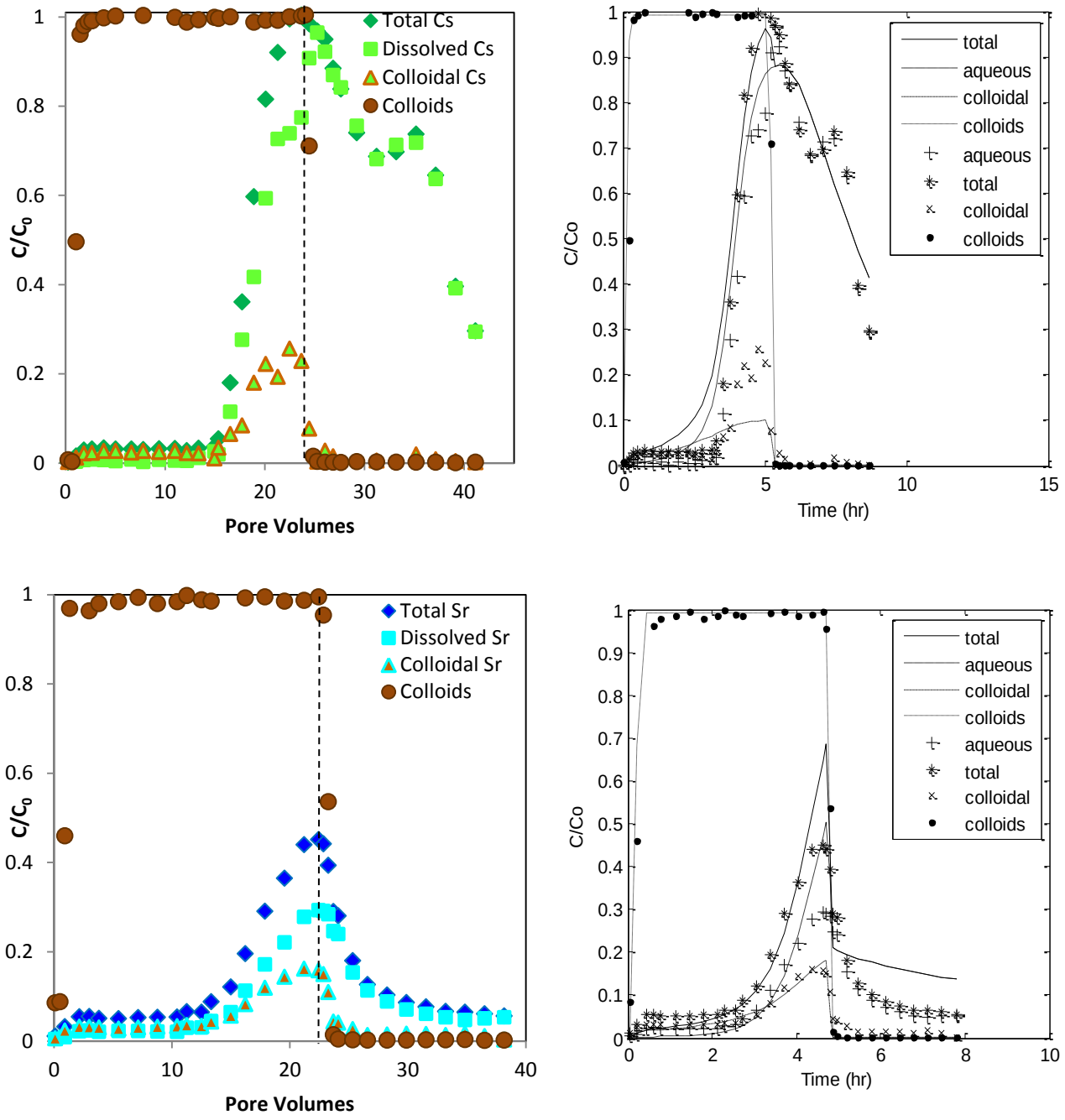

Figure 3.10. Breakthrough data (left) and model fits (right) for silica colloids and cesium (top, R^2=0.96) and strontium (bottom, R^2=0.94). Filled circles represent colloids, diamonds (or *) denote total concentration, filled triangles (or ×) denote colloid-sorbed concentration, and squares (or +) denote aqueous cation concentration.

concentration near 20%; however, the model predicted a value near 10%. After the switch to background solution, the model accurately predicted a steady decrease in total and dissolved concentration while the colloidal concentration was nearly zero.

For strontium and silica, the model simulation under-predicted an initial appearance of total and colloidal strontium concentration in the first pore volume (0.2 h) but accurately simulated the steep increase in total and dissolved strontium after 2.5 h. The model also accurately simulated the colloidal strontium concentration after 3 h. After the switch to background solution, the model accurately predicted the rapid decrease in dissolved and total strontium concentrations to less than 25% in the first 0.25 h; however, the model over-predicted the strontium desorption from the sand by almost 50% within 0.5 h. The model correctly predicted a concentration near zero for the colloidal strontium in the effluent.

The optimal modeled values for silica colloid adsorption and desorption rate coefficients for cesium with fast and slow sites (k_{ac1}, k_{ca1} and k_{ac2}, k_{ca2}; respectively) were 1.5 and 0.15 μM^{-1} h^{-1} for k_{ac1} and k_{ca1}, respectively and 0.90 and 0.0006 μM^{-1} h^{-1} for k_{ac2} and k_{ca2}, respectively. For strontium, the optimal values were 1.5 and 1.0 μM^{-1} h^{-1} for k_{ac1} and k_{ca1}, respectively, and 1.1 and 0.09 μM^{-1} h^{-1} for k_{ac2} and k_{ca2}, respectively. The fraction of fast to slow binding sites on silica colloids, F_{c1}, was 0.99 for cesium and 0.90 for strontium. Colloid cation adsorption capacities were found to be 5.5 and 75 $\mu mol\ g^{-1}$ for cesium and strontium, respectively.

Model values are summarized in Table 3.3. For cesium and strontium breakthrough with colloids, IMt-1 had the shortest cumulative pore volumes until 50 % breakthrough ($C/C_0 > 0.50$) and silica had the longest breakthrough times. For silica and strontium, the breakthrough times were similar to the breakthrough times with no colloids present.

Table 3.3. Experimental conditions and modeling parameters that provided best fits for dissolved and colloid-facilitated cesium and strontium transport experiments.

Experimental Conditions						Modeling Parameters													
							Sand Sorption			Colloid Transport			Colloid Sorption						
Experiment ID	Colloid Type	$[Cs^+]$ (M)	$[Sr^{2+}]$ (M)	C_c (mg L^{-1})	U (cm h^{-1})	D (cm^2 h^{-1})	k_{ras} (μM^{-1} h^{-1})	k_{sra} (μM^{-1} h^{-1})	X_a (μmol g^{-1})	k_{cs} (h^{-1})	k_{sc} (h^{-1})	X_c (g g^{-1})	k_{cac1} (μM^{-1} h^{-1})	k_{cac1} (μM^{-1} h^{-1})	k_{cac2} (μM^{-1} h^{-1})	k_{cac2} (μM^{-1} h^{-1})	X_c (μmol g^{-1})	F_{c1}	R^2
1	None	7.5×10^{-7}	0	0	81.5	9.3	4.87	0.036	0.0080	0	0	0	0	0	0	0	0	0	0.95
2	None	0	7.5×10^{-6}	0	79.2	9.3	0.40	0.0028	0.027	0	0	0	0	0	0	0	0	0	0.86
3	IMt-1	7.5×10^{-7}	0	100	70.4	9.3	4.85	0.036	0.00070	0.65	0.0050	0.0010	1.5	0.15	0.90	0.00060	11	0.001	0.93
4	IMt-1	0	7.5×10^{-6}	100	78.5	9.3	0.40	0.0028	0.0070	0.60	0.0050	0.0010	1.5	0.15	1.1	0.090	150	0.55	0.90
5	IMt-2	7.5×10^{-7}	0	100	83.4	9.3	4.85	0.036	0.0015	0.70	0.0070	0.0010	1.5	0.15	0.90	0.00060	20	0.50	0.91
6	IMt-2	0	7.5×10^{-6}	100	78.5	9.3	0.40	0.0028	0.0090	0.45	0.0050	0.00080	1.5	0.15	1.1	0.090	250	0.55	0.79
7	Oak Ridge	7.5×10^{-7}	0	100	81.5	9.3	4.85	0.036	0.0060	0.7	0.0050	0.0010	1.5	0.20	1.4	0.010	47	0.20	0.91
8	Oak Ridge	0	7.5×10^{-6}	100	78.5	9.3	0.40	0.0028	0.026	0.87	0.0050	0.0010	1.1	0.33	2.0	0.024	150	0.53	0.80
9	Silica	7.5×10^{-7}	0	200	86.7	9.3	4.85	0.036	0.0060	0.05	0.0050	0.0010	1.5	0.15	0.90	0.00060	5.5	0.99	0.96
10	Silica	0	7.5×10^{-6}	200	78.5	9.3	0.40	0.0028	0.031	0.05	0.0050	0.0010	1.5	1.0	1.1	0.090	75	0.90	0.94

The order of breakthrough for colloids increasing the breakthrough time was IMt-1 >IMt-2> Oak Ridge > silica.

DISCUSSION

Dissolved Cation Sorption to Quartz. Saiers and Hornberger (1996a) found that a two-site Langmuir sorption model for cesium sorption to quartz was needed at high ionic strengths; however, with ionic strength of 0.002 M, the kinetic Langmuir model used for our model captured most of the variability (R^2 = 0.94 versus 0.99). Dissolved cation transport was well quantified (R^2 = 0.95) with the kinetic Langmuir model values of the cation adsorption rate coefficient, $k_{as1,}$ (μM^{-1} h^{-1}), desorption rate coefficient k_{sa1} (μM^{-1} h^{-1}), and adsorption capacity of the quartz for cesium X_a (μmol g^{-1}) of 4.85, 0.36, and 0.0080, respectively. Turner et al. (2006) successfully modeled breakthrough results with a one-site kinetic model for cesium. For strontium transport with quartz, Li et al. (2011) found that Langmuir sorption predicted breakthrough and release well, and our one-site model confirms this with good correlation to the data (R^2 = 0.86). Sverjensky (2006) found that strontium sorbed to crystalline quartz in a tetra nucleic fashion.

The adsorption rate coefficients determined by the model for cation breakthrough with saturated quartz sand were different for cesium and strontium. For cesium, the adsorption (k_{as}) and desorption rate (k_{sa}) coefficients were found to be 3.3 and 0.014 μM^{-1} h^{-1}, respectively; which match well to the values found by Saiers and Hornberger (1996) and Turner et al. (2006). Adsorption and desorption rate coefficients for strontium and quartz were 0.40 and 0.00028 μM^{-1} h^{-1}, respectively. The adsorption rate coefficient was larger than the 0.14 value reported by Turner et al., (2006); but may be due to flow that was nearly 5 times faster in our experiments.

The strontium adsorption rate coefficient was very insensitive to changes based on the sensitivity analysis of Turner et al. (2006). Turner et al. (2006) suggested that the difference in strontium adsorption rate compared to cesium was a result of the larger hydration sphere of strontium inhibited by either less electrostatic interaction or the larger hydration sphere. The very slow desorption; however, suggests inner sphere binding to the quartz is possible. Sverjensky (2006) reported that strontium forms a tetranuclear bond with quartz binding sites and potentially could exhibit inner sphere binding.

The quartz binding capacity (X_a) for cesium and strontium determined the location of the breakthrough curve and match well with those published by Turner et al. (2006). Because cesium is a large monovalent cation, it is more easily dehydrated than the small, divalent strontium and can more strongly associate to quartz binding sites (Kitamura et al., 1999). The strontium breakthrough appears first in our experiments due to the 10 times higher concentration of strontium over cesium; however, the strontium breakthrough occurs at only 2 times as fast, meaning strontium uses 5 times more binding sites than cesium on the quartz surface. This is consistent with strontium and cesium forming outer sphere complexes with the quartz surface and the ion exchange capacity being much larger for divalent strontium ions, even with the larger hydration sphere.

The model fits showed that cesium adsorbed to the quartz surface more rapidly that strontium, but also desorbed more rapidly. Although dehydrated cesium has been suggested to be able to bind to quartz in an inner sphere manner (Kim et al., 1996a; Kim et al., 1996b; Kim and Kirkpatrick, 1997; Parkman et al., 1998; Chen and Hayes, 1999; Chen et al., 2006), the rapid desorption observed in these experiments suggests it was still binding in a more easily reversible,

outer sphere manner. Bostick et al. (2002) used EXAFS to determine that it is possible for cesium to form inner sphere complexes with siloxane functional groups.

Colloid Transport. Breakthrough of all of the colloids tested (IMt-1, IMt-2, silica, and Oak Ridge colloids) occurred within one pore volume. The order of retention of colloids in the column was Oak Ridge > IMt-1 ≥ IMt-2 > silica and was controlled by the attachment rate coefficient (k_{cs}). The negative zeta potential of the silica colloids repelled them from the surface of the quartz, as expected. The solution pH (7.3) was above the pH_{pzc} for silica and near the pH_{pzc} for illite, resulting in some deposition. The Oak Ridge colloids have been reported as consisting mostly illite (Mohanty et al., 2011), and their retention in the column was similar to the retention of illite. The detachment of all colloids was minimal and all colloids had a detachment rate coefficient near 0.0050 h^{-1}. Minimal colloid detachment has been observed by Saiers et al. (1994b) with anatase and boehmite and Turner et al. (2006) with IMt-2 illite. Second-order colloid attachment with a colloid deposition capacity allowed the model to fit the slowly increasing values of for illite and Oak Ridge colloids.

Colloid-Facilitated Transport. The presence of colloids decreased the number of pore volumes to breakthrough for all colloids with cesium and all colloids except silica for strontium (Figure 3.11). IMt-1 and IMt-2 illite have been reported as having the same properties (Clay Mineral Repository); however, our results suggest differences in mineralogy. When compared to IMt-2, IMt-1 decreased the pore volumes to breakthrough by over two times for cesium and nearly two times for strontium. The colloid order for the fraction of cesium sorbed (Figure 3.4) for different colloids matched the order of increased transport with IMt-1 > IMt-2 > Oak Ridge > silica.

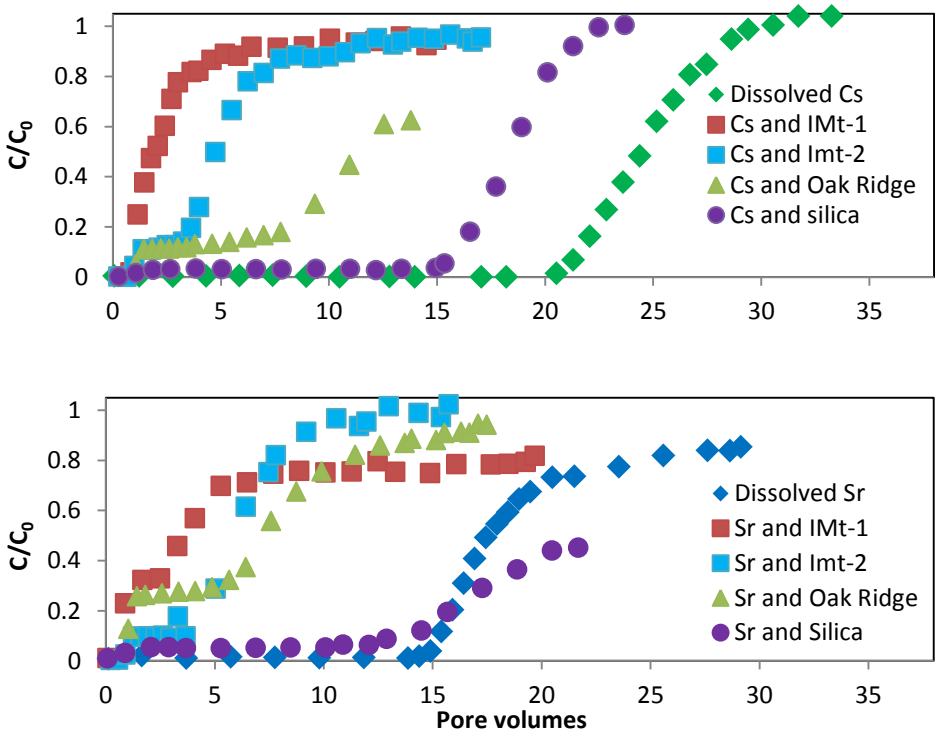

Figure 3.11. Comparison of cesium (top) and strontium (bottom) breakthrough with no colloids and IMt-1, Oak Ridge, and silica colloids present.

The order of increased transport for strontium with colloids was IMt-1 > IMt-2 > IMt-2 > silica. IMt-1 colloids had more capacity for cesium than strontium; however, both cations were held strongly during transport experiments. Oak Ridge colloids have been reported to be a mix of illite and other clays (Mohanty et al., 2011) and the desorption isotherms and transport experiments suggest they have a fraction of kaolinite, silica, or other colloids that reversibly sorb cations. For silica, transport of cesium was slightly decreased; however, transport of strontium appeared to slightly increase. Silica colloids retarding transport of strontium has been observed in column experiments by Bekhit et al. (2006) and Albarran et al. (2011) observed bentonite colloids retarding strontium transport through a fractured granite column; however, these we a result of strontium adsorbed to deposited colloids.

On average, strontium desorbed more readily from the clay binding sites than cesium and is consistent with a majority of strontium binding through outer sphere binding and and cesium binding through more stronger inner sphere complexation.

Model results showed that cesium and strontium had equivalent adsorption rates to the strong binding sites for illite and Oak Ridge colloids; however, cesium had significantly slower desorption rates. Strontium desorption may have been faster due to faster exchange rates with sodium, effects of the diffuse double layer surrounding the illite, or the larger hydration sphere inhibiting complexation to the illite surface and remaining in the outer layer. In order to form inner sphere complexation with the colloid surface, the adsorbed water molecules must be released from the cation (Bostick et al., 2002; Sverjensky, 2002). This occurs more easily for cesium than strontium due to less energy needed to release the water molecules. Strontium was able to occupy fifteen to twenty five times more binding sites on the colloids than cesium, which was likely due to the ten times higher concentration of divalent strontium replacing more sodium from the colloid binding sites.

Hypothesis Validation and Environmental Implications. The experimental results and corresponding modeling fits support our hypothesis that the type of colloids present affects the potential for colloid-facilitated transport of cesium and strontium. For cesium, the presence of IMt-1, IMt-2, Oak Ridge colloids, and silica colloids decreased the number of pore volumes before breakthrough by a factor of 12, 5.1, 2.1 and 1.3, repectively (Figure 3.12). For strontium, the presence of IMt-1, IMt-2, and Oak Ridge colloids decreased the number of pore volumes before breakthrough by a factor of 4.4, 2.7, and 2.3 while silica colloids increased transport by a factor of 1.2, respectively (Figure 3.12). Colloid desorption rate coefficients determined the

amount of increased transport and sorbed cesium or strontium was carried through the column attached to mobile colloids.

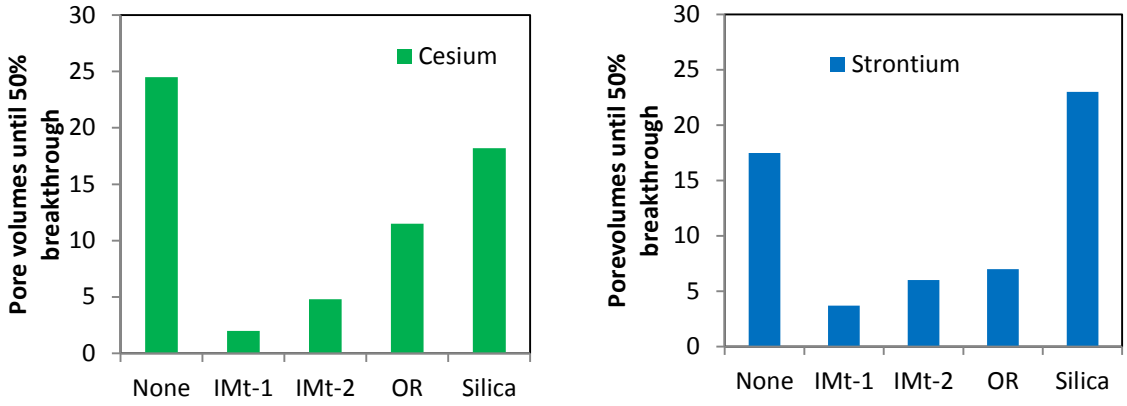

Figure 3.12. Effect of colloid type on number of pore volumes until breakthrough for cesium (left) and strontium (right).

The key parameters were the quartz and colloid cation binding capacities and their respective adsorption and desorption rate coefficients. Slow desorption kinetics are expected to be important when extending these conclusions when considering cesium and strontium transport with natural soil colloids. The type of colloids present in a particular environmental scenario will have a large effect on the likelihood that colloid-facilitated transport will occur and need to be accounted for in risk assessment and contaminant transport modeling. The most important factors were the contaminant desorption rate coefficient of the colloids and the colloid and quartz sorption capacities of the cation.

REFERENCES

Albarran, N., Missana, T., Garcia-Gutierrez, M., Alonso, U., Mingarro, M., 2011. Strontium migration in a crystalline medium: effects of the presence of bentonite colloids. Journal of Contaminant Hydrology 122, 76-85.

Bekhit, H., Hassan, A., Harris-Burr, R., Papelis, C., 2006. Experimental and numerical investigations of effects of silica colloids on transport of strontium in saturated sand columns. Environmental Science & Technology 40, 5402-5408.

Bold, S., Kraft, S., Grathwohl, P., Liedl, R., 2003. Sorption/desorption kinetics of contaminants on mobile particles: Modeling and experimental evidence. Water Resources Research 39, SBH 3-1:8.

Bostick, B., Vairavamurthy, M., Karthikeyan, K., Chorover, J., 2002. Cesium adsorption on clay minerals: An EXAFS spectroscopic investigation. Environmental Science & Technology 36, 2670-2676.

Chen, C., Coleman, M., Katz, L., 2006. Bridging the gap between macroscopic and spectroscopic studies of metal ion sorption at the oxide/water interface: Sr(II), Co(II), and Pb(II) sorption to quartz. Environmental Science & Technology 40, 142-148.

Chen, C., Hayes, K., 1999. X-ray absorption spectroscopy investigation of aqueous Co(II) and Sr(II) sorption at clay-water interfaces. Geochimica Et Cosmochimica Acta 63, 3205-3215.

Cheng, T., Saiers, J., 2010. Colloid-Facilitated Transport of Cesium in Vadose-Zone Sediments: The Importance of Flow Transients. Environmental Science & Technology 44, 7443-7449.

Clark, M., 1996. Transport Modeling for Environmental Engineers and Scientists. Wiley, New York.

Comans, R., Hockley, D., 1992. Kinetics of Cesium Sorption on Illite. Geochimica Et Cosmochimica Acta 56, 1157-1164.

Cornell, R., 1993. Adsorption of cesium on minerals- a review. Journal of Radioanalytical and Nuclear Chemistry-Articles 171, 483-500.

Kim, Y., Cygan, R., Kirkpatrick, R., 1996a. Cs-133 NMR and XPS investigation of cesium adsorbed on clay minerals and related phases. Geochimica Et Cosmochimica Acta 60, 1041-1052.

Kim, Y., Kirkpatrick, R., 1997. Na-23 and Cs-133 NMR study of cation adsorption on mineral surfaces: Local environments, dynamics, and effects of mixed cations. Geochimica Et Cosmochimica Acta 61, 5199-5208.

Kim, Y., Kirkpatrick, R., Cygan, R., 1996b. Cs-133 NMR study of cesium on the surfaces of kaolinite and illite. Geochimica Et Cosmochimica Acta 60, 4059-4074.

Kitamura, A., Fujiwara, K., Yamamoto, T., Nishikawa, S., Moriyama, H., 1999. Analysis of adsorption behavior of cations onto quartz surface by electrical double-layer model. Journal of Nuclear Science and Technology 36, 1167-1175.

Kretzschmar, R., Borkovec, M., Grolimund, D., Elimelech, M., 1999. Mobile subsurface colloids and their role in contaminant transport. Advances in Agronomy 66, 121-193.

Krumbein, W., Sloss, L., 1963. Stratigraphy and Sedimentation. Freeman, San Francisco.

Lee, M., Chung, K., Choi, G., Lee, C., 2002. Measurement of Sr-90 in aqueous samples using liquid scintillation counting with full spectrum DPM method. Applied Radiation and Isotopes 57, 257-263.

Lenhart, J., Saiers, J., 2002. Transport of silica colloids through unsaturated porous media: Experimental results and model comparisons. Environmental Science & Technology 36, 769-777.

Li, Y., Tian, S., Qian, T., 2011. Transport and retention of strontium in surface-modified quartz sand with different wettability. Journal of Radioanalytical and Nuclear Chemistry 289, 337-343.

McCarthy, J., Zachara, J., 1989. Subsurface transport of contaminants- Mobile colloids in the subsurface environment may alter the transport of contaminants. Environmental Science & Technology 23, 496-502.

Mohanty, S., Ryan, J., Saiers, J., 2011. Mobilization of cesium and strontium in a vadose zone by cation exchange, organic matter, and colloids: A laboratory and field study. Abstracts of Papers of the American Chemical Society 242.

Ogata, A., Banks, R.B., 1961. A solution of the differential equation of longitudinal dispersion in porous media, Professional Paper 411-A. U.S. Geological Survey, Washington, D.C.

Parkman, R., Charnock, J., Livens, F., Vaughan, D., 1998. A study of the interaction of strontium ions in aqueous solution with the surfaces of calcite and kaolinite. Geochimica Et Cosmochimica Acta 62, 1481-1492.

Rowell, D., 1994. Soil Science: methods and applications. Longman Scientific & Technical, University of Michigan.

Saiers, J., Hornberger, G., 1996. Migration of Cs-137 through quartz sand: Experimental results and modeling approaches. Journal of Contaminant Hydrology 22, 255-270.

Saiers, J., Hornberger, G., Liang, L., 1994. First-order and second-order kinetics approaches for modeling the transport of colloidal particles in porous-media. Water Resources Research 30, 2499-2506.

Sverjensky, D., 2002. Standard states for surface sites and surface species in surface complexation models. Abstracts of Papers of the American Chemical Society 223, U607-U607.

Sverjensky, D., 2006. Prediction of the speciation of alkaline earths adsorbed on mineral surfaces in salt solutions. Geochimica Et Cosmochimica Acta 70, 2427-2453.

Turner, N., Ryan, J., Saiers, J., 2006. Effect of desorption kinetics on colloid-facilitated transport of contaminants: Cesium, strontium, and illite colloids. Water Resources Research 42.

Zheng, C., Bennett, G., 2002. Applied Contaminant Transport Modeling. Wiley-Interscience, New York.

CHAPTER 4

THE EFFECT OF DESORPTION KINETICS AND UNSATURATED CONDITIONS IN THE COLLOID-FACILITATED TRANSPORT OF CESIUM AND STRONTIUM

ABSTRACT

The sorption of contaminants to mobile colloids has been shown to increase the transport of contaminants. Laboratory experiments and model simulations have shown that enhanced transport can occur; however, a limited number of studies have left uncertainty in understanding the potential for enhanced transport in unsaturated porous media. A series of breakthrough experiments were conducted to determine the potential for illite colloids to enhance cesium and strontium transport through a homogeneous quartz sand porous medium with relative saturation (S_{eff}) values of 1.0, 0.80, and 0.21. Model simulations were used to evaluate the effects of desorption kinetics on colloid-facilitated transport. Pore volumes until breakthrough was the same for all values of S_{eff} without colloids. The presence of illite colloids decreased pore volumes until breakthrough for both cesium and strontium. Illite colloids enhanced the transport of cesium to a greater extent than for strontium, a result we attribute to the strong adsorption of cesium to the frayed edge sites. We were able to predict cesium and strontium breakthrough with and without illite colloids at all values of S_{eff} using a kinetic sorption model with one quartz binding site and two kinds of colloid binding sites– (1) fast sites that represented planar surfaces and (2) slower sites that represented adsorption to the frayed edges. Unsaturated conditions with

colloids increased the transport of cesium and strontium relative to saturated conditions due to slow desorption kinetics from the illite clay and the decreased residence time.

INTRODUCTION

The presence of colloids has been shown to increase the transport rate of cesium and strontium in saturated porous media (Saiers and Hornberger, 1996b; Noell et al., 1998; Flury et al., 2002; Solovitch-Vella et al., 2006; Turner et al., 2006a), unsaturated porous media (Szenknect (Szenknect et al., 2003; Chen et al., 2005; Pace et al., 2007; Cheng and Saiers, 2010), and fractured media (Vilks and Baik, 2001; Albarran et al., 2011). Three conditions are necessary for colloid-facilitated transport of a contaminant to occur: (1) there must be a source of colloids, (2) contaminants must associate with the colloids and desorb slowly relative to the rate of transport, and (3) the colloids must remain mobile for a relatively long distance.

Previous review papers have documented the origin, size distribution, abundance, and chemical make-up of colloids in natural and perturbed subsurface systems (Ryan and Elimelech, 1996; McGechan and Lewis, 2002; de Jonge et al., 2004a; DeNovio et al., 2004). Concentrations of mobile colloids in excess of 1 g L^{-1} have been reported for both simulated and natural rainfall events (Allen, 1988; Ryan et al., 1998; DeNovio et al., 2004). Physical perturbations and chemical perturbations (decrease in ionic strength, increase in pH, or a change in dominant cation composition) drive colloid mobilization (Saiers and Lenhart, 2003b; Gao et al., 2004).

The mobilization of colloids through porous media has no effect on contaminant transport rates if (1) the contaminant doesn't associate with the colloids, (2) the dissolved contaminant travels faster than the colloids, or (3) the contaminant desorbs quickly from the colloids.

Transport rates of contaminants that do not significantly sorb to colloids are unaffected by the presence of colloids (Spurlock and Biggar, 1990; Lafrance et al., 1994). Colloids (especially clays, metal oxides, and carbonates) can readily adsorb a variety of contaminants through ion exchange and surface complexation reactions (Sverjensky, 2002, 2006).

Once mobilized, colloids travel through porous media by advection and dispersion until they are removed from flow by a variety of deposition mechanisms. In saturated soils, colloids can be removed from flow by (i) straining and (ii) attachment to mineral grain surfaces. Straining is a physical mechanism and takes place when the size of a colloid moving through flow is larger than the size of the pore opening, resulting in the colloid getting "stuck" (McDowell-Boyer et al., 1986). Attachment to the mineral grain surface is a physicochemical mechanism that depends on the rate of colloid transport from the bulk fluid to the grain surface and the probability that a colloid-grain collision will result in attachment (Ryan and Elimelech, 1996) Most mineral colloids have a negative charge which leads to increased mobility within a negatively charged porous media such as sand or a mineral soil due to electrical repulsion and attachment is not favored when collisions occur.

Slow desorption kinetics allow for a contaminant to remain associated with a colloid even when there is very little contaminant remaining in the dissolved phase. Field observations have suggested that slow radionuclide desorption kinetics from colloids can increase the transport of plutionium (Triay et al., 1997; Honeyman, 1999; Kersting et al., 1999), uranium (Vilks et al., 1993), europium (Kersting et al., 1999; Bouby et al., 2011), thorium (Bouby et al., 2011) and cesium (Kersting et al., 1999). Laboratory experiments by Roy and Dzombak (1997) demonstrated the importance of desorption rates on contaminant transport.

Much of the previous research has focused on saturated flow conditions; however, some experiments with unsaturated conditions have shown the potential for colloids to enhance transport at lower moisture contents due to increased flow velocities and decreased reactive surface area. Radionuclides such as cesium and strontium are of particular interest due to their abundance in contaminated vadose zone soils at Department of Energy (DOE) sites in the United States and because they exhibit varying desorption kinetics with clay minerals such as illite. Modeling results suggest that colloid-facilitated transport of cesium and strontium in saturated porous media is represented best with kinetic models for kaolinite (Saiers and Hornberger, 1999), illite (Turner et al., 2006a), and combinations of natural clay colloids (Flury et al., 2002; Steefel et al., 2003; Zhuang et al., 2003; Flury et al., 2004).

Purpose of Research. The purpose of these experiments was to isolate the main variables controlling colloid-facilitated transport in unsaturated porous media systems: colloid transport, aqueous contaminant transport, cation adsorption to the porous medium, and colloid-associated contaminant transport. The transport of colloids has been well-studied in recent years; however, data that provides for testing models under unsaturated conditions is limited in the literature. Previous laboratory experiments and model simulations have shown that enhanced transport can occur when cesium or strontium strongly associates with mobile colloids and release kinetics are slow relative to the rate of flow (Saiers (Saiers and Hornberger, 1996b; Flury et al., 2002; Steefel et al., 2003; Zhuang et al., 2003; Turner et al., 2006a; Cheng and Saiers, 2010).

Our experiments were designed to investigate the effect of unsaturated conditions on the enhanced transport of cesium and strontium. Recent work has found colloid-facilitated transport increased cesium transport in unsaturated Hanford sediments (Cheng and Saiers, 2010); however, the complexity of natural sediments prevented the analysis to make conclusions about

the effect that cation binding strength and cation/colloid desorption kinetics played on enhanced transport.

Once colloids with sorbed contaminants are mobilized, there is little experimental data to determine how desorption rates will affect the fate of the adsorbed contaminant. It has also been difficult to provide reliable mechanism-based parameters for field-scale and risk assessment decisions. This research produced experimental breakthrough curves to provide data for modeling the potential for illite colloids to enhance the transport of cesium and strontium through a sand column under both saturated and unsaturated conditions. A colloid-facilitated transport model was used to provide insight into which mechanisms drive the colloid-facilitated transport of cesium and strontium.

MATERIALS AND METHODS

Overview. Breakthrough experiments were performed to help understand dissolved and colloid-associated cesium and strontium transport during steady saturated and unsaturated conditions. The results were then fitted with a colloid-facilitated transport model developed by Turner et al. (2006) and modified to account for unsaturated conditions. Cesium and strontium were selected due to their prevalence on US Department of Energy (DOE) sites and because they exhibit contrasting sorption rates with quartz and colloid surfaces (divalent strontium has a higher affinity for water that cesium and has a larger, more tightly held hydration shell). We used illite clay particles as colloids because they can be represented as having two physically different binding sites– (1) fast sites that represented ion exchange to planar surfaces and (2) slower sites that represented sorption to the frayed edges. The use of a homogeneous quartz porous medium

allowed us to model the complex relationships between fluid transport, particle transport, and sorption kinetics.

Solution Chemistry. The background solution for experiments was made to simulate the chemistry of rainwater that has just entered the vadose zone. A 1 M stock solution of sodium bicarbonate (Mallinckrodt AR®, analytical reagent grade) was made to enable precision at lower concentrations. Stock sodium bicarbonate was added to high-purity water (> 18 MΩ cm resistivity) to make a 0.1 mM background solution and was allowed 24 hours to equilibrate with the atmosphere (1655 m above sea level). The calculated ionic strength based on carbonate speciation and ion concentration was 0.10 mM and the solution pH was 7.3 (± 0.1).

Cation solutions (7.5×10^{-7} M cesium and 7.5×10^{-6} M strontium) were made by adding stock solutions to 0.1 M sodium bicarbonate. Stock solutions (0.1 M cesium and 0.75 M strontium) were made with cesium chloride ($CsCl \bullet 6H_2O$) or strontium chloride salts ($SrCl_2 \bullet 6H_2O$) from MP Biomedicals (Cat. No. 150589 and 152583, respectively). Cesium was added at a lower concentration than strontium to ensure similar colloid-associated fractions (Turner *et al.*, 2006). The cesium or strontium concentration was measured by spiking the solutions with a small amount (approximately 2.5×10^{-10} M ^{137}Cs or ^{90}Sr) of radioactive $^{137}CsCl$ or $^{90}SrCl$ dissolved in HCl from Eckert and Ziegler Isotope Products (Valencia, CA).

Colloid Preparation. Illite particles for the experiments were processed from IMt-2 illite obtained from the Source Minerals Society Clay Repository at Purdue University. The illite pieces were ground to a powder using a ceramic mortar and pestle. A rinse process was conducted to remove calcium, magnesium, and other cations from the illite and replace them with sodium. Illite powder (50 g) was added to 800 mL of high-purity water in a 1.5 L blender (Osterizer, Model 6630) and blended at high speed for 20 min. The slurry was transferred to a 1

L borosilicate glass flask and sonicated for 30 min in an ultrasonic bath (Fisher Scientific, Model FS9H). The slurry was then transferred into polypropylene centrifuge tubes (50 mL) and centrifuged (Thermo IEC, Centra MP4) at 1650 rcf for 30 min. The almost-clear supernatant solution was decanted and replaced with high-purity water. The centrifuge tubes were vigorously shaken by hand for 30 sec to resuspend the aggregated colloids stuck to the bottom, sonicated, and centrifuged again. This process was repeated at least four more times until the specific conductance of the supernatant was < 10 μS cm^{-1} with a conductivity meter (Orion 105) and conductivity cell (Thermo Scientific 011050). The process was repeated once more with 0.1 mM sodium bicarbonate (pH 7.3 ± 0.1) to prepare the colloids for settling and to equilibrate the colloids with 0.1 mM sodium. After the final rinse, most binding sites on the illite particles were assumed to be occupied with sodium.

The colloidal fraction of the illite slurry was separated from larger particles by using a high density polyethylene (HDPE) tub (50 L volume) as a large sedimentation column. The tub was filled with 30 L of 0.1 mM sodium bicarbonate and rinsed illite slurry was added to make a final concentration of 0.8 g L^{-1}. The suspension was allowed to settle for 24 h at room temperature (~22 °C ± 2). Based on a calculation of the Stokes settling velocity and assuming the particles were spheres, the maximum diameter of the particles remaining in the upper 18.5 cm of the column was less than 8.1 μm in diameter.

A peristaltic pump (Cole Parmer, 7014-20) was used to transfer the top 18.5 cm of solution to a HDPE container (20 L volume) for storage until use in the experiments. A float was attached to the influent tube to ensure liquid was removed from the top of the settling column and a slow flow rate (100 mL per minute) was used to minimize disturbances to the water column that may have resuspended larger particles from the bottom of the tub. Each batch

produced about 18 L of illite suspension of about 130 mg L^{-1} concentration. The exact concentration was measured and diluted to 100 mg L^{-1} ± 5 with 0.1 mM sodium bicarbonate.

pH and Colloid Concentration Measurements. The colloid suspension was measured for pH and colloid concentration before use in experiments. Suspension and sample pH was measured using a combination electrode (Orion, 9107BN) and meter (Orion, 250A+) calibrated with low ionic strength pH standard solutions (Orion, Purewater®). Ionic strength adjuster (5 M $NaNO_3$) was added (0.1 mL per 10 mL sample) to mitigate the effects of ionic strength on pH measurements.

Colloid concentration was correlated to turbidity using a turbidimeter (Hach, 2100N). The factory calibration checked with 0.1, 1, 10, and 100 NTU Formazin gel standards (Hach, Gelex®, 25890-00). Linear calibration for illite was determined using colloid concentrations of 1, 10, 50, 100, and 200 mg L^{-1} made as dilutions from the settled IMt-2 illite. The mass concentration of the colloid suspensions was determined gravimetrically. Four 0.1 µm filters (MilliPore®, 25 mm diameter) were weighed and 25 mL of the colloid suspension was passed through each filter. The filters were dried at 80 °C for 24 h and re-weighed. The difference in mass was divided by the suspension volume to give the colloid concentration. A linear regression resulted in the relationship between colloid concentration, C_c, (mg L^{-1}) and turbidity, T, in nephelometric turbidity units (NTU):

$$C_c = 0.824 \times T + 0.277 \qquad (R^2 = 0.97) \tag{4.1}$$

Colloid Size Distribution Measurements. The particle size distribution in the illite suspensions was measured by dynamic light scattering (DLS) (Particle Sizing Systems, NICOMP 380 ZLS). The size distribution was confirmed by sequential filtering using 3.0, 0.8, 0.45, 0.2, 0.1, and 0.02

μm syringe filters (Millipore Millex® GN, nylon, 13 mm diameter; Whatman Anotop 10, inorganic membrane, 10 mm diameter). The colloidal suspension was diluted with 0.1 mM sodium bicarbonate solution to reduce the scattering intensity of the colloidal suspension (about 0.2 mg L^{-1}) to between 250 and 350 kHz. The samples were measured using a 30 min run time. The mean particle diameter and standard deviation were determined for six separate measurements. Both Gaussian and NICOMP fitting parameters were recorded. The Gaussian fit was calculated with a two parameter least-squares optimization and the NICOMP fit used a four-parameter inverse LaPlace transform optimization routine (Particle Sizing Systems, 2006). The best fit was determined by minimizing the χ^2 error.

Measurement of ^{137}Cs and ^{90}Sr by Liquid Scintillation Counting. The exact activity of the ^{137}Cs or ^{90}Sr solutions was measured by liquid scintillation counting (Packard, Tri Carb 1600TR). The main advantage of measuring the cation concentration by liquid scintillation counting of beta decays was the capability to measure total, dissolved, and sorbed cesium or strontium in samples with clay present without the need to digest the samples. Based on the long half-life of the isotopes used (30.2 y for ^{137}Cs and 28.8 y for ^{90}Sr), radioactive decay was negligible and not accounted for in calculations. A 2 mL aliquot of sample was added to 5 mL of scintillation cocktail (Packard, Ultima Gold) in a 7 mL borosilicate glass liquid scintillation vial.

The detection window was set to 0 to 2,000 keV for ^{137}Cs and 0 to 350 keV for ^{90}Sr to eliminate the detection of secondary decays from ^{90}Y (Lee et al., 2002). The counts were time-averaged for 5 minutes and the resulting count rate (counts per minute, or CPM) was correlated with a linear regression to 0, 10^{-7} 10^{-6}, 10^{-5}, 10^{-4}, 10^{-3} M standards. The quench of the sample (loss of signal due to sample conditions) was measured using the transformed Spectral Index of

External Standard (t-SIE), which was calculated using the external ^{133}Ba source inducing a Compton spectrum in the scintillation cocktail.

Total cation concentrations were determined by liquid scintillation counting of the unfiltered samples. Dissolved cation concentrations were measured by passing the sample through a 0.2 µm filter (Millipore Millex® GN, nylon, 13 mm diameter) and analyzing the filtrate concentration. The difference between the total and dissolved cation concentration was calculated to be the colloid-associated cation concentration.

Colloid Suspensions. Colloid suspensions were prepared by adding illite colloids to atmosphere-equilibrated background solution to make a final colloid concentration of 100 mg L^{-1}. Stock cation solution was added to the colloid suspension. Preliminary adsorption experiments showed that equilibrium was approached within a few hours; however, the colloids were equilibrated with the cations for 24 h before each experiment to ensure that adsorption equilibrium was reached.

Porous Medium. Well-rounded, medium-sphericity Ottawa quartz sand (Accusand 40/60, Unimin Corp.) was used as the porous media in all experiments. Roundness and sphericity were determined comparing microscope images to the Krumbein roundness chart and Riley sphericity index (Krumbein and Sloss, 1963). The sand was comprised of 99.8% SiO_2, less than 0.1% metal oxides (Ti, Fe, Al, K, Mg, Na, and Ca), and less than 0.1% organic compounds based on loss of ignition measurements (Unimin Corp.).

A preliminary rinse was conducted before the sand was sorted to remove fine particles. Batches of sand (2 kg) were stirred with a stainless steel spoon in a polyethylene bucket and rinsed with high purity water until the turbidity of the rinse water was below 10 NTU. The sand was transferred to borosilicate glass pans and oven-dried at 80° C for 16 h. The rinsed and dried

sand was sorted through stainless steel sieves using a sieve shaker (W.S. Tyler, RX-29 Ro-Tap) according to ASTM D 422-63[1] (Rowell, 1994). The fraction that passed through a 45 mesh sieve (354 μm) and was retained on a 50 mesh sieve (297 μm) was stored in sealed containers. For this +50/-45 fraction, we assumed that d_{50} = 325 μm.

The sieved sand was cleaned using a procedure similar to the procedure used by Lenhart and Saiers (2002). Holes (10, 1.3 cm diameter) were drilled in the bottom of a 19 L polyvinyl chloride (PVC) bucket and covered with 104 μm stainless steel mesh (Spectra Mesh®, 146 439) held in place with silicone sealant. The bucket was ¼ filled with sand and placed inside a second 19 L PVC bucket. A nitric acid solution (10% by volume) was added until it was ponded 3 cm above the sand surface. The sand was stirred with a stainless steel spoon to release any air that was trapped in the pores and was soaked in the acid for 36 h to dissolve any adsorbed metals. After 36 h, the bucket with the sand was raised to allow the acid to drain through the holes in the bucket and the sand was rinsed with a constant flow of high-purity water for 6-12 h or until the drainage water reached pH 5.7. A base rinse was conducted next to remove any remaining dust and silica colloids. Sand (1 kg) was transferred to 1 L HDPE bottles and 0.002 M NaOH was added to leave 2 cm of headspace in the bottles. The bottles were placed on a shaker table set at 150 oscillations per minute for 2 h. The sand was transferred to the modified PVC bucket and rinsed with high-purity water until the pH of the rinse water approached 5.7 and the turbidity dropped below 0.4 NTU. The sand was oven dried at 80°C for 16 h and sealed in a clean PVC bucket until use in breakthrough experiments.

Analysis of Sand Composition. The quartz grain surfaces were imaged with a low vacuum scanning electron microscope (LVSEM, JSM-6480LV) to visually inspect the morphology and surface roughness of the grains. Energy dispersive x-ray (EDS) spectroscopy (JEOL, Noram

System Six) was used to analyze the sand for elemental composition. Sand grains were mounted on metal studs with double-sided carbon tape and viewed in the LVSEW at a pressure of about 1 Pa, 10-15 kV accelerating voltage, and a spot size near 50 μm. Focus and stigmation were iteratively adjusted and images with magnification of 10,000× were captured and compared to archived pictures to qualitatively estimate sphericity and roundness of the grains (Krumbein and Sloss, 1951).

Column Set-up. A 1.3 cm (½") thick cast acrylic tube (12.7 cm diameter, 32.8 cm length) was used as the column. The tube was suspended from a PVC ring screwed to the middle of the column and supported by a wooden frame in the containment tank (Figure 4.1). A 45° bevel on the top edge of the column shed excess rainfall away from the center of the column. Experimental solutions were applied to the top of the column with a rainfall simulator. The rainfall simulator was made from two 13.7 diameter disks and a ring of 1.3 cm acrylic plastic with a threaded barb fitting installed in the top and attached to the influent pump tubing. Holes (38) were drilled in the bottom disk of the rainfall simulator with 1.25 cm spacing to accept Luer-Lok® fittings. Stainless steel hypodermic needles (BD PrecisionGlide, 25-guage, 305456) were then screwed into the Luer-Lok® fittings. The rainfall simulator was suspended 1 cm above the top of the sand surface to minimize potential disturbances to the sand surface due to the erosive force of the falling drops. The sand in the column was supported by an acrylic plastic disk with a pattern of holes (38) covered with 104 μm mesh size stainless steel screen (Spectra/Mesh®). This prevented sand from entering the tubing while still allowing the clay colloids to pass through without clogging. Luer-Lok® fittings were inserted in holes in the bottom disk and connected with tubing to an acrylic plastic manifold. All mating surfaces between the column and bucket were sealed with silicone adhesive.

Three peristaltic pumps and controllers regulated the fluid flow in the experiments. One pump transferred solution from the influent tank to the rainfall simulator. Column effluent from the manifold was split with a y-connector. A small amount (0.5 mL min^{-1}) was pumped to a fraction collector (U-200 Universal, Eldex) filled with filled with polystyrene test tubes (15 cm length × 1 cm diameter) and the rest of the effluent (about 29 mL min^{-1}) was pumped (Cole Parmer, Masterflex®,7553-20 pump motor, Easy Load II LS pump head) to a waste container.

Excess rainfall from experiments with S_{eff} values of 1.0 and 0.80 was allowed to flow over the edge of the column into a PVC collector and was pumped to the waste collector. The column experiments were conducted inside a large (1.2 m length, 0.9 m depth, and 0.6 m width) containment tank made of 1.3 cm acrylic plastic to shield emission of beta radiation and to contain any potential spills.

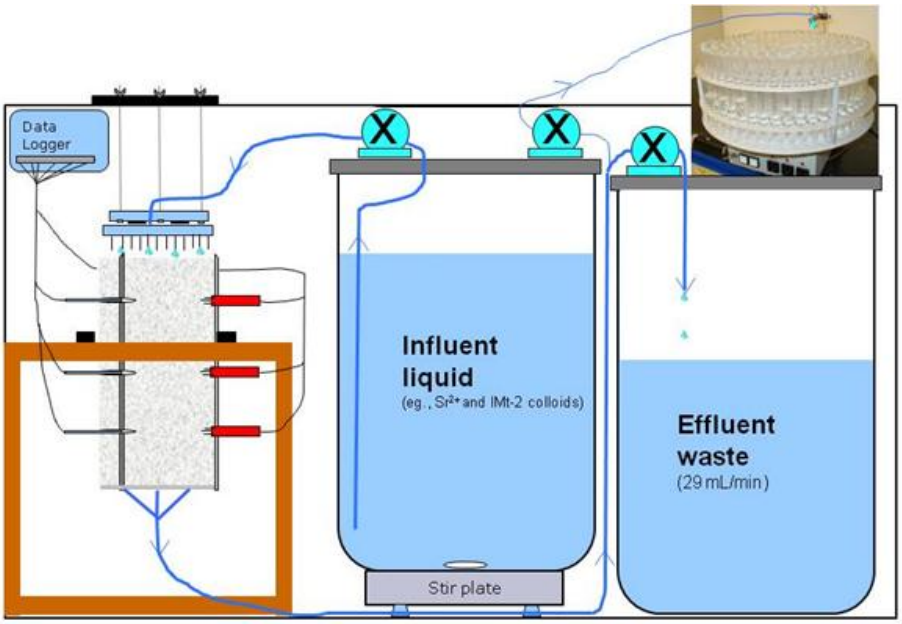

Figure 4.1. Experimental set-up used for breakthrough experiments. A peristaltic pump transferred influent solutions and colloid suspensions to the rainfall simulator at the top of the column. Two other peristaltic pumps removed effluent from the bottom of the column and separated the flow into a sample stream that went to a fraction collector and a waste stream.

Measurement of Porous Medium Moisture Content and Tension. The column was instrumented with three moisture sensors (Delta-T Devices Ltd., ML2x ThetaProbe) located 7.7, 16.4, and 25.1 cm from the top of the column and two tensiometers located 7.7 and 16.4 cm from the top. The moisture sensors measured the apparent dielectric constant, k_a, of the air-water-sand system, which is the unitless ratio of the electrical permittivity, ε, to the permittivity of a vacuum, ε_0. k_a was correlated to volumetric moisture content ($m^3\ m^{-3}$). The tensiometers measured the change in resistance of a silica wafer/wheatstone bridge system, which was correlated to porous medium tension (cm H_20) though calibration at various porous medium suction values (0 to 80 cm).

The tensiometers were constructed according to a design of Eching and Hopmans (1993) with high-flow ceramic cups (Soil Moisture Corp., 2100-200CR-B1M3) and differential pressure transducers (Honeywell/Microswitch, 26PCAFA6D). Tensiometers were calibrated to suction head by fabricating a vacuum chamber with three fittings (Swage-Lok®) securely holding three tensiometers vertically with the tips enclosed in the chamber. The pressure in the chamber was adjusted with a valve connected to the building's vacuum system. The suction inside the chamber was incrementally increased and the suction pressure was measured by the height of water lifted in a tube hanging below the chamber. Data from the tensiometers and moisture probes was monitored using a data logger (Delta-T Devices, Ltd., DL2e) to ensure uniform conditions along the depth of the column and steady conditions during the duration of breakthrough experiments.

Initial Column Packing. The column was wet-packed according to the following procedure. Background solution was poured in from the top of the column to a depth of 2 cm. Increments of sand (50 g) were added to the column. The column was stirred after each addition with a

polystyrene rod to minimize layering from different shaped sand grains settling at slightly different velocities. After every 2-3 cm of sand added, the column was tapped on all sides with a rubber mallet to ensure uniform packing and consistent porosity. The weight of sand and background solution added to the column were recorded and used to confirm the porosity measured by the moisture sensors.

Establishing Steady Flow Conditions. After packing, background solution (pH 7.3, I 0.1 mM) was passed through the column for 10 to 15 pore volumes until effluent pH and turbidity stabilized to pH 7.3 ± 0.1 and below 0.4 NTU (± 0.1), respectively.

Experiments were conducted using three relative saturation values (S_{eff}). The relative saturation (0-1) was defined as the amount of pore space that is filled with water in relation to the residual water content,

$$S_{eff} = \frac{\theta - \theta_r}{\theta_S - \theta_r} \quad (4.2)$$

where S_{eff} is the effective saturation, θ is the experimental moisture content ($m^3\ m^{-3}$), θ_r is the residual moisture content ($m^3\ m^{-3}$), and θ_S is the moisture content at saturation ($m^3\ m^{-3}$) .

For unsaturated experiments, the column was drained to the residual moisture content θ_r (θ_r = 0.05) and then re-wetted to the desired S_{eff} with background solution. For S_{eff} = 1.0 and 0.80, solution was allowed to pond above the sand surface approximately 0.5 cm. For S_{eff} = 0.21, the rainfall simulator was used to apply the simulated groundwater to the top of the column and the effluent pump was set to a slightly higher rate than the influent pump to maintain consistent unsaturated conditions for the duration of the experiment. Effluent was pumped from the bottom of the column at a rate of 24.1 to 30.0 mL min^{-1} for all experiments and the flow rate was periodically checked and recorded.

Measuring Porous Medium Hydraulic Properties. Hydraulic properties of the sand were determined by bromide tracer tests for S_{eff} = 1.0, 0.80, and 0.21 using 4.0 mM NaBr solution. Bromide was measured using a bromide-specific electrode (Accumet, Cat. No. 13-620-525) and meter (Orion, 720A) calibrated with 10^{-2}, 10^{-3}, 10^{-4}, 10^{-5}, and10^{-6} M bromide solutions (Fisher Scientific, S255-500).

Experimental Conditions. Column experiments were conducted to test the effect of three variables on cation transport: (1) colloid concentration (0 or 100 mg L^{-1}), (2) radioactive cation (cesium or strontium), and (3) relative saturation (S_{eff} = 1.0, 0.80, or 0.21).

Colloid concentration (100 mg L^{-1} ± 5.2), ionic strength (0.1 mM), and pH (7.3 ± 0.1) were all within ranges expected to be found in contaminated natural soil systems. The flow rate was maintained between 24 and 31 mL min^{-1} for all experiments, resulting in average linear porewater velocities that increased as the relative saturation decreased (Table 4.1).

Once steady moisture conditions were established, the background solution was switched to the desired experimental solution (Table 4.1). A colloid concentration of 100 mg L^{-1} was selected to test a representative colloid concentration found in natural environments and in arid DOE sites such as the Hanford Tank Farm, WA (Flury et al., 2002). Cesium and strontium were selected as the radioactive cations due to their different adsorption characteristics with illite clay and their prevalence at contaminated U.S. Department of Energy sites. Relative saturation values of 1.0, 0.80, and 0.21 were selected to provide insight into transport across the range of S_{eff} found in natural soils.

Table 4.1. Experimental conditions for 12 breakthrough experiments with cesium and strontium as contaminants, illite colloids, and S_{eff} values of 1.0, 0.80, and 0.21. *Cc* is colloid concentration, *U* is average pore water velocity, and *D* is the dispersion coefficient.

Exp. #	Relative Saturation (S_{eff})	$[Cs^+]$ (M)	$[Sr^{2+}]$ (M)	C_c (mg L^{-1})	U (cm h^{-1})	D (cm^2 h^{-1})
1	1.0	7.5×10^{-7}	0	0	17.3	4.1
2	1.0	0	7.5×10^{-6}	0	41.8	4.1
3	1.0	7.5×10^{-7}	0	100	34.6	4.1
4	1.0	0	7.5×10^{-6}	100	34.6	4.1
5	0.80	7.5×10^{-7}	0	0	55.1	4.8
6	0.80	0	7.5×10^{-6}	0	43.2	4.8
7	0.80	7.5×10^{-7}	0	100	53.8	4.8
8	0.80	0	7.5×10^{-6}	100	53.1	4.8
9	0.21	7.5×10^{-7}	0	0	206	308
10	0.21	0	7.5×10^{-6}	0	208	308
11	0.21	7.5×10^{-7}	0	100	194	308
12	0.21	0	7.5×10^{-6}	100	151	308

Illite colloid suspensions (100 mg L^{-1}) were equilibrated with the cation solution (7.5×10^{-7} M Cs^+ or 7.5×10^{-6} M Sr^{2+}) for 24 h before being applied to the column. During equilibration, the suspensions were stirred with a 5 cm Teflon® stir bar in a large HDPE tub. Effluent samples were collected at intervals of 25 min. Experiments were run until the normalized effluent concentration (C/C_0) exceeded 0.90. The influent solution was then

switched to the background solution (0.1 mM $NaHCO_3$) and continued for 20-40 additional pore volumes.

Mathematical Model. A modified version of the colloid-facilitated transport code written by Turner et al. (2006) was used to model the experimental results (see Chapter 3 for a detailed description). The MATLAB® code solves the Richards' equation for water movement and accounts for the presence of cations and colloids. A two-site model was used to represent colloid transport and a non-linear, two-site model was used to represent the different sorption kinetics exhibited by the strong edge sites and weaker planar sites found on the illite surface. The rate coefficients controlling colloid and cation transport were determined by fitting the experimental results to the colloid-facilitated transport model output by using a least-squares parameter optimization code. Model simulations were implemented within MATLAB® (Version 7.11.0, The Mathworks, Natick, MA) by running a script written for each experimental result with the function file adapted from Turner et al. (2006).

Dissolved cation experiments was used to determine the quartz sorption parameters for the adsorption rate coefficient (k_{as}), desorption rate coefficient (k_{sa}), and adsorption capacity (X_a) for cesium and strontium. The colloid-facilitated transport data was then used to determine the adsorption and desorption parameters for the colloids which were the adsorption and desorption rate coefficients of the cations to a potentially fast illite binding site (k_{ac1} and k_{ca1}, respectively), adsorption and desorption rate coefficients of the cations to a potentially slower illite binding site (k_{ac2} and k_{ca2}, respectively), the illite adsorption capacity of the cations (X_c), and the fraction of illite binding sites of the fast type (F_{c1}). The quartz adsorption capacity (X_a) was also refitted for the colloid-facilitated experiments, with the capacity from the dissolved experiments being used as an initial condition. A series of over 200 simulations was used to isolate the optimal

parameter values that predicted the experimental results for S_{eff} = 1.0, 0.80, and 0.21, with emphasis on maintaining the same values for all three relative saturation values.

After isolating the optimal values for the set of parameters, a sensitivity analysis was conducted by systematically varying each parameter value above and below the optimal value and graphing the data in relation to the calculated R^2 value for each subsequent model fit.

The spatial discretization, Δx, and time-step, Δt, used in the model were adjusted to ensure mathematical stability. The Peclet number, $N_{Pe,}$ is the dimensionless ratio used to determine the relative importance of advection and dispersion. The system was assumed to be dominated by advection when N_{Pe} was less than 2 (Clark, 1996; Zheng and Bennett, 2002) using the following equation,

$$N_{Pe} = \frac{U\Delta x}{D} \leq 2 \tag{4.3}$$

where U is the average linear porewater velocity (cm h^{-1}), Δx is the model spatial discretization (cm), and D is the dispersion coefficient (cm h^{-1}).

Another number used to ensure mathematical stability of the model is the Courant number (Cr), the ratio of the transport distance to the spatial discretization. The Courant number is required to be less than 1 to ensure mathematical stability. This can be interpreted as ensuring the cations and colloid travel through less than one spatial discretization per timestep (Clark, 1996; Zheng and Bennett, 2002) and was calculated as;

$$Cr = \frac{U\Delta t}{\Delta x} \leq 1 \tag{4.4}$$

where U is the average linear porewater velocity (cm h^{-1}), Δt is the length of a timestep in the model (h^{-1}), and Δx is the model spatial discretization (cm). Due to the delayed breakthough of

the cations in the experiments, *Cr* and N_{Pe} can be much larger than the recommended values for stability without resulting in mathematical instability (Turner, 2005).

RESULTS

Illite Characterization. Based on the Stokes settling velocity of the illite particles in the rinsed suspension, the maximum size of the illite colloids was calculated to be 8.1 µm after 24 h of settling. Sequential filtration showed that 79.5% (± 0.1) of the illite colloids were between 3.0 µm and 0.80 µm in diameter for three samples (Figure 4.2).

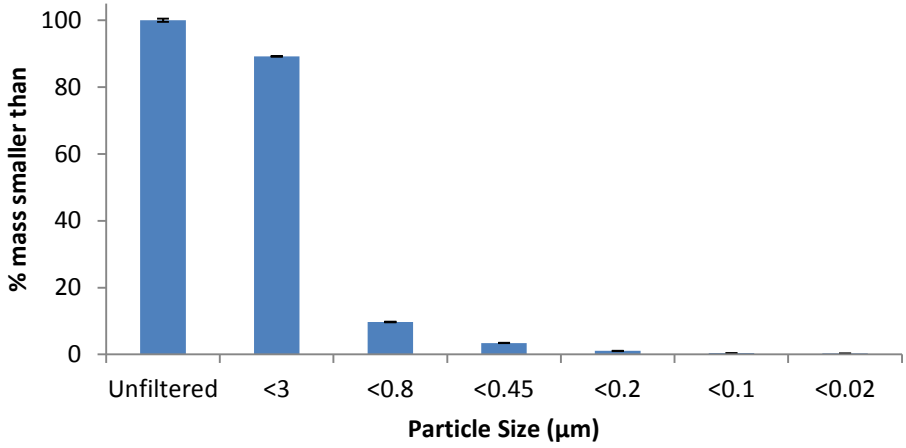

Figure 4.2. Result of sequential filtering with percent of mass from a 100 mg L-1 sample passing through the filter on the y-axis and the corresponding filter size on the x-axis.

Particle size (assuming uniform, spherical particles) was measured by dynamic light scattering. The mean diameter was 1790.0 ± 77 µm for the Gaussian distribution and 1508.9 ± 168.7 µm for the NICOMP method (Figure 4.3). Because the measure of correlation, χ^2, was near 0.20 (less than 3.0 selection criteria for using NICOMP analysis), the Gaussian distribution was determined to be the more appropriate result.

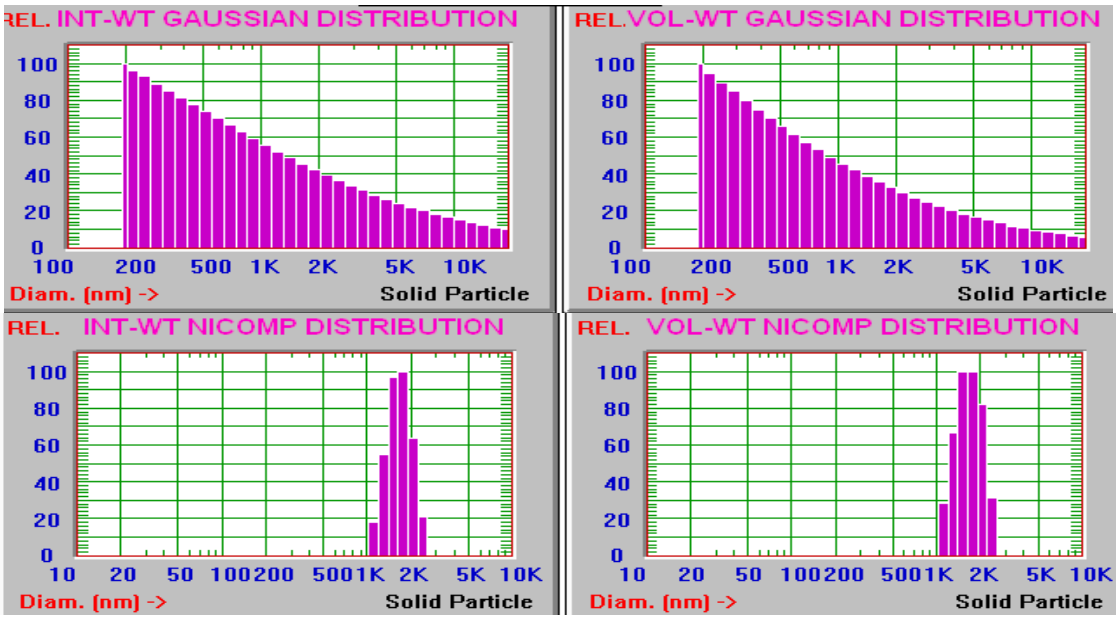

Figure 4.3. Particle size results for Gaussian distribution (top) and NICOMP distribution (bottom). Graph on left are for intensity weighting and right are volume weighting.

The layered nature of the illite can be observed in the LVSEM image below. The edges of these layers form the frayed edge binding sites that justify the two-site sorption model for the illite colloids (Figure 4.4).

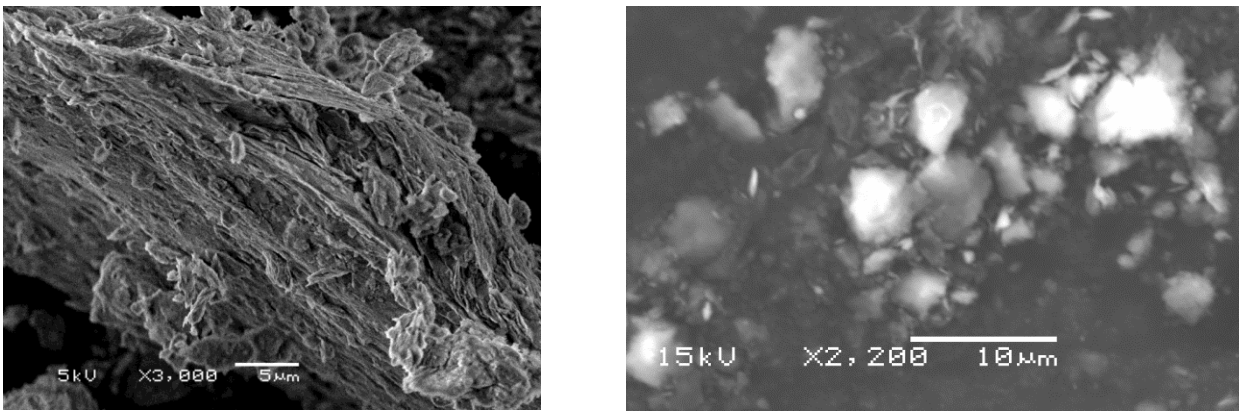

Figure 4.4 LVSEM image of IMt-2 illite from Silver Mountain, Montana, USA. Magnification was 3000×; accelerating voltage was 5 kV.

Sand Characterization. LVSEM images confirm the well-rounded, medium sphericity nature of the quartz grains (Fig. 4.5).

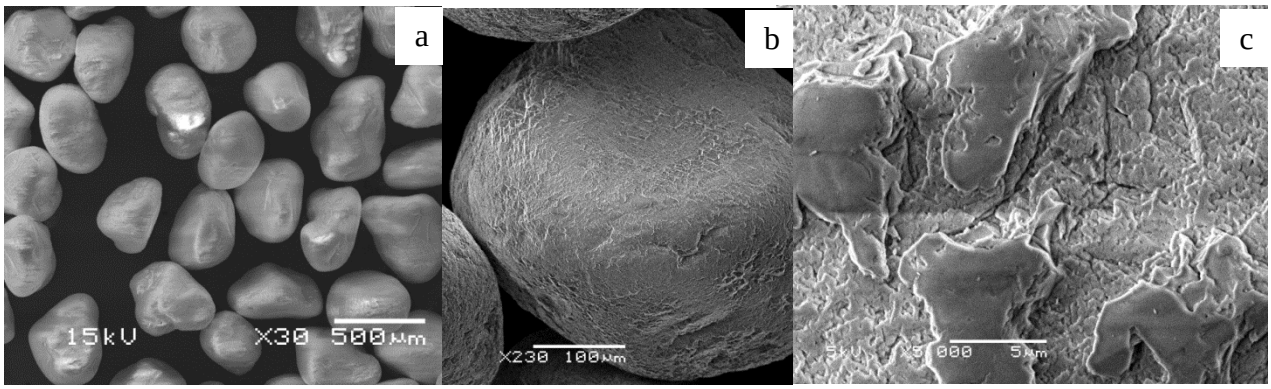

Figure 4.5. LVSEM images of quartz surface at under magnification of 30× (a), 230× (b), and 5000× (c).

The edges of the quartz crystalline structure can be observed at 5000× magnification, provided surface roughness for colloid deposition. The tensiometer and moisture sensors (top and middle) were used together during column drainage and imbibition to measure the relationship between soil tension (cm H_2O) and moisture content (cm^3 cm^{-3}). About 20 cm H_2O suction was required to drain the largest pores and the experimental residual moisture content (θ_r) was about 0.05 (Figure 4.6).

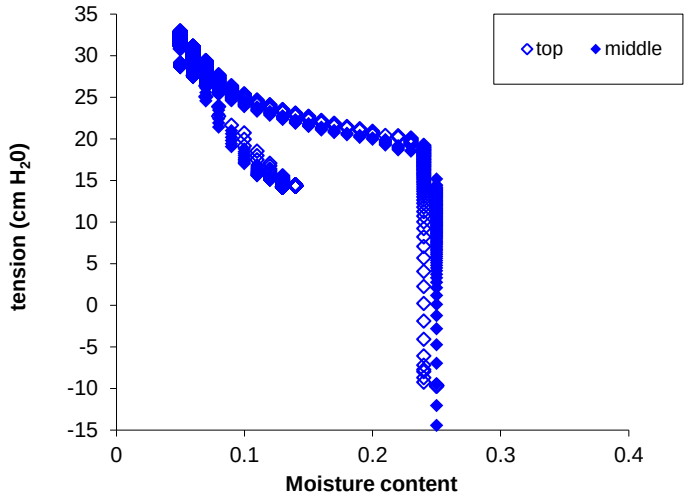

Figure 4.6. Characteristic curve for the 7.7 cm (top) and16.4 cm (middle) below the sand surface.. The starting moisture content was 0.12 (S_{eff} = 0.21), then the column was drained to MC = 0.05 (S_{eff} = 0) and re-wetted to MC = 0.26 (S_{eff} = 0.80).

Effect of S_{eff} on Conservative Tracer Transport. Cation and colloid transport parameters were determined for breakthrough experiments using bromide as a conservative tracer. Bromide breakthrough experiments were performed for S_{eff} = 1.0, 0.80, and 0.21 (Fig. 4.7). The cumulative volume of water that passed through the column until C/C_0 reached 0.50 was 1,537 ± 2 mL for two replicates conducted at S_{eff} = 1.0. This volume of water is similar to volume of water measured when packing the column (1,511 ± 10 mL) for the same experiments, which was used as the total pore volume all experimental results.

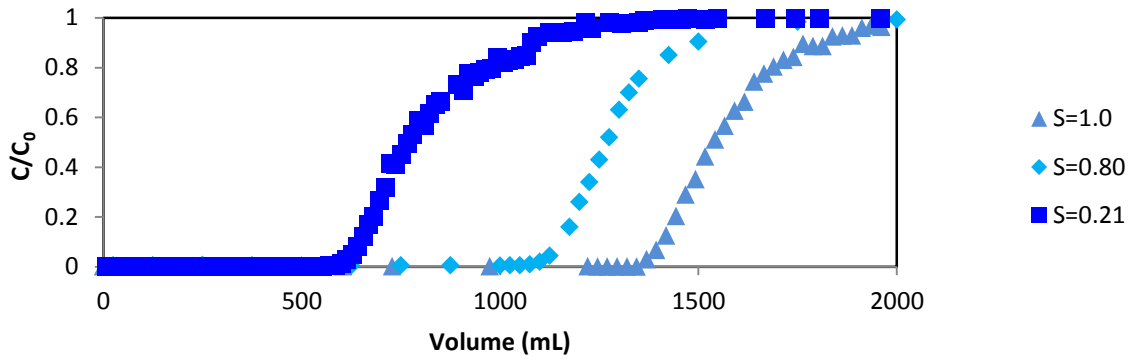

Figure 4.7. Bromide tracer data for relative saturation (S_{eff}) equal to 1.0, 0.80an d 0.21. Volume of water (mL) passed through the column is plotted on the x-axis and relative concentration of bromide (C/C_0) is on the y-axis.

The optimal hydrodynamic dispersion coefficient (D) was determined by minimizing the calculated error between the measured C/C_0 and the calculated C/C_0 for the analytical advective-dispersive transport equation (Ogata & Banks 1961);

$$\frac{C(x,t)}{C_o} = \frac{1}{2}\left[erfc\left(\frac{x-Ut}{\sqrt{4Dt}}\right) + \exp\left(\frac{xU}{D}\right) erfc\left(\frac{x+Ut}{\sqrt{4Dt}}\right)\right] \qquad (4.3)$$

where $C(x,t)$ is the bromide concentration in the effluent at the bottom of the column (µM), C_0 is the influent bromide concentration (µM), x is the average distance the solute front has traveled in the column (cm), U is the average linear porewater velocity (cm h^{-1}), t is time (h^{-1}), and D is the hydrodynamic dispersion coefficient (cm^2 h^{-1}). The error between the experimental C/C_0 and calculated C/C_0 was minimized to yield the optimal value of D for each value of S_{eff}.

The optimized values of D were found to be 4.1, 4.8, and 308 cm^2 h^{-1} for S_{eff} = 1.0, 0.80, and 0.21, respectively (Figure 4.8). These values were used in the transport model for cations and colloids. Although the colloids are much larger than the hydrated ions, this value was

assumed to be the same for cesium, strontium, and the colloids due to the small Peclet numbers (<1) proving the system was dominated by advection and diffusion was minimal.

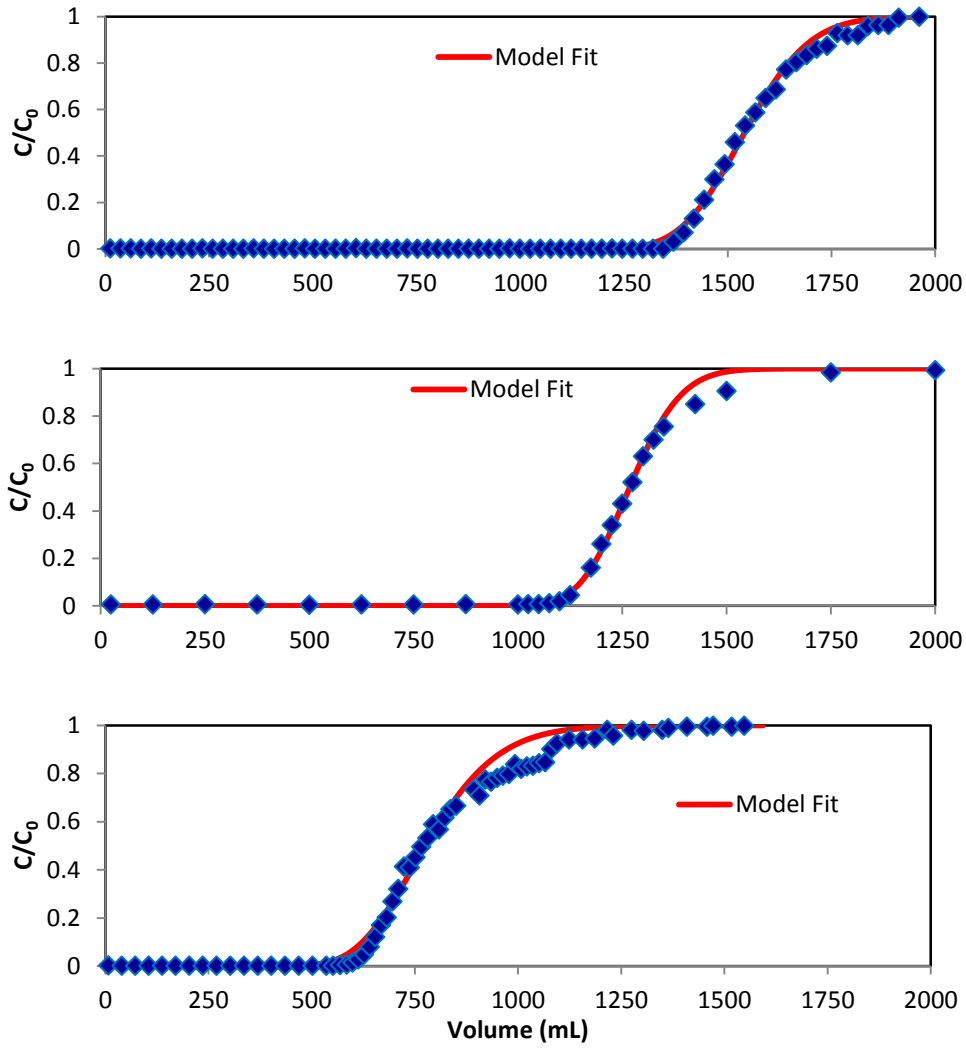

Figure 4.8. Modeled tracer data showing the volume of tracer passed through the column on the x-axis and the relative concentration (C/C_0) on the y-axis. The data points are the measured bromide concentrations from the breakthrough experiments and the lines are the modeled fit with the optimized dispersivity (D). The top graph is S_{eff} = 1.0 (D = 4.1), middle graph is S_{eff} = 0.80 (D = 4.8), and the bottom graph is for S_{eff} = 0.21 (D = 308).

Effect of S_{eff} on Dissolved Cesium Transport. Dissolved cesium breakthrough experiments were conducted for S_{eff} values of 1.0, 0.80, and 0.21 (Figure 4.9). Breakthrough occurred after 40, 44, and 42 pore volumes for S_{eff} = 1.0, 0.80, and 0.21, respectively. The quartz adsorbed 100% of the cesium for the first 36 pore volumes (39 h, 30 h, and 28 h for S_{eff} = 1.0, 0.80, and 0.21, respectively). Once the concentration was above the cesium-137 detection limit for liquid scintillation counting, the concentration increased linearly until C/C_0 approached a value of 1.0. The number of pore volumes at which breakthrough occurred was independent of S_{eff}.

After switching to background solution, there was an initial increase in the effluent concentration above C/C_0 =1.0 for S_{eff} = 1.0 that was not observed at lower S_{eff} values. For all values of S_{eff}, the first 10 pore volumes of background solution remained at a concentration near (or above) C/C_0 = 1.0 before slowly decreasing. About 30 pore volumes of background solution passed through the column before C/C_0 dropped below 0.5. The desorption tail had a gradual decline in slope.

The model was able to match the experimental data well (Figure 4.9). Best-fit model simulations determined that the rate coefficients for cesium adsorption to and desorption from quartz were 3.3 and 0.018 $\mu M^{-1}\ h^{-1}$ for all values of S_{eff}. The best-fit quartz adsorption capacity was 0.012 $\mu mol\ g^{-1}$ for all S_{eff}, suggesting all of the binding sites were available for cesium binding even when 80% of the pore space was filled with air. For S_{eff} = 1.0, the model didn't predict the increase in C/C_0 above 1.0 that was observed in the data. The model slightly under-predicted the amount of cesium desorption for the first 25 h of background solution, then slightly over-predicted the cesium concentration after 25 h. The sensitivity analysis showed that all three fitting parameters (k_{as1}, k_{sa1}, and X_a) were very sensitive to changes (Figure 4.16), with X_a being

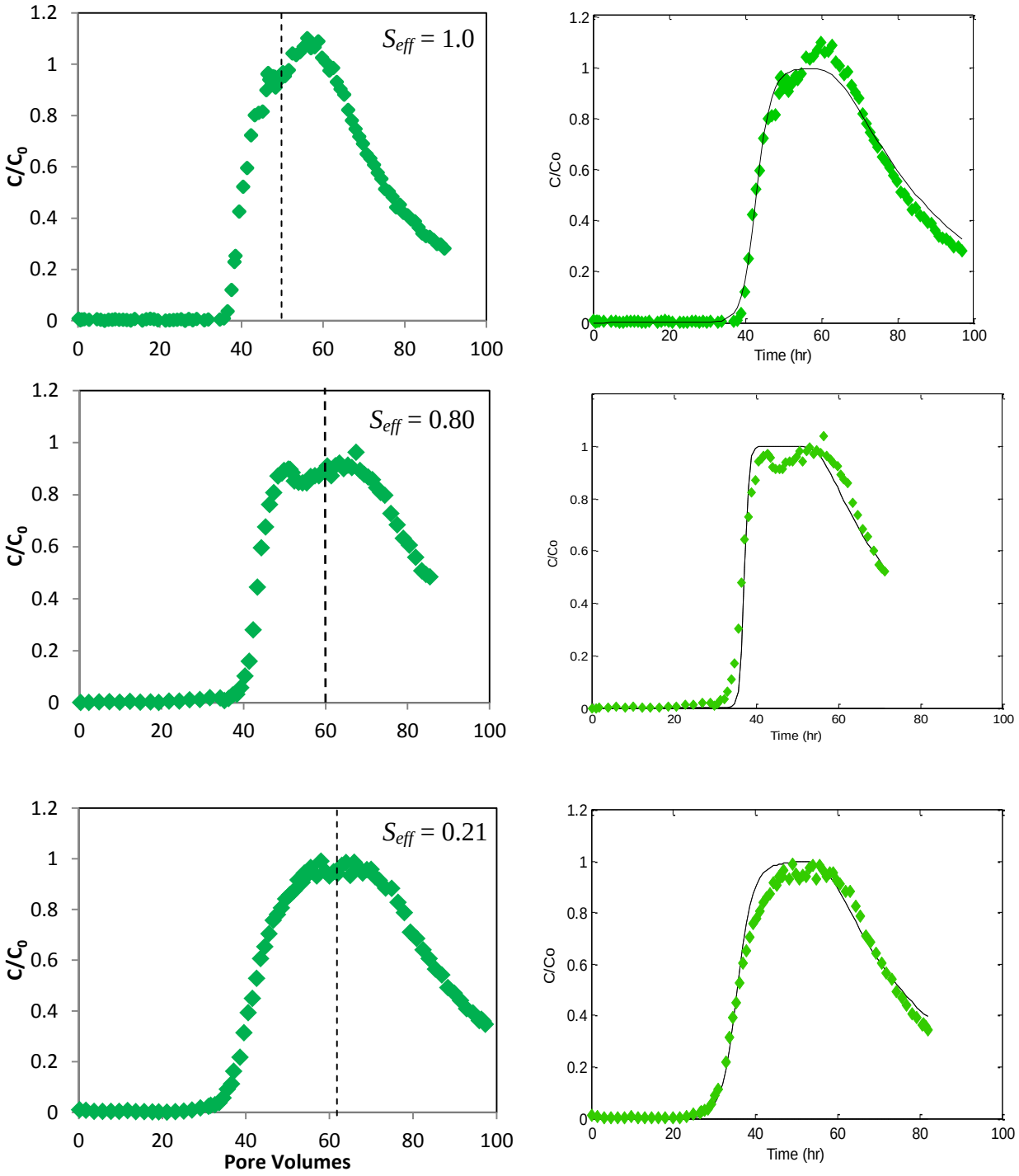

Figure 4.9. Dissolved cesium breakthrough data (left) and model fits (right) for S_{eff} = 1.0 (top, R^2 =0.98), 0.80 (middle, R^2 = 0.97), and 0.21 (bottom, R^2 = 0.98). The y-axis is the dimensionless unit (C/C_0). The x-axis is cumulative pore volumes for data and time (h) for model fits. One pore volume was equal to a residence time of 0.88 h ± 0.12. Vertical dashed lines denote when solution was switched to background solution.

the most sensitive and k_{as1} being the least sensitive. A summary of dissolved cesium transport results is provided in Table 4.2.

Effect of S_{eff} on Dissolved Strontium Transport. Breakthrough experiments for dissolved strontium were conducted at relative saturation (S_{eff}) values of 1.0, 0.80, and 0.21 (Figure 4.10) with porewater velocities of 41.8, 43.2, and 208 cm h^{-1}, respectively. The quartz adsorbed 100% of the strontium for the first 15 pore volumes (10-15 h) for all S_{eff} values. Once the concentration was above the strontium-90 detection limit for liquid scintillation counting, the concentration increased linearly until C/C_0 approached a value near 1.0. The 50% breakthrough occurred at 20, 21, and 20 pore volumes for S_{eff} = 1.0, 0.80, and 0.21, respectively (Table 4.2). The number of pore volumes until breakthrough was independent of S_{eff}.

After switching to background solution, the strontium in the effluent decreased below C/C_0 = 0.50 within 3 pore volumes. Desorption tails exhibit a steep decline in slope until the effluent concentration decreases below C/C_0 = 0.2, then decreased more slowly for the remainder of the experiment. A summary of dissolved strontium transport results is provided in Table 4.3.

The model accurately predicted the sharp increase in strontium concentration after 10 h; however, the model over-predicted the slope of the breakthrough front. The model also over-predicted strontium desorption in the first 10 h (~12 pore volumes), but matched desorption tails very closely after 10 h. The optimal values for k_{as1}, k_{sa1}, and X_a were found to be 0.40 μM^{-1} h^{-1}, 0.00028 μM^{-1} h^{-1}, and 0.029 µmol g^{-1} for S_{eff} = 1.0. The same values for k_{as1} and k_{sa1} were used for S_{eff} = 0.80 and 0.21; however, the quartz adsorption capacity X_a was increased to 0.031 and 0.034 μM^{-1} h^{-1} for S_{eff} = 0.80 and 0.21, respectively.

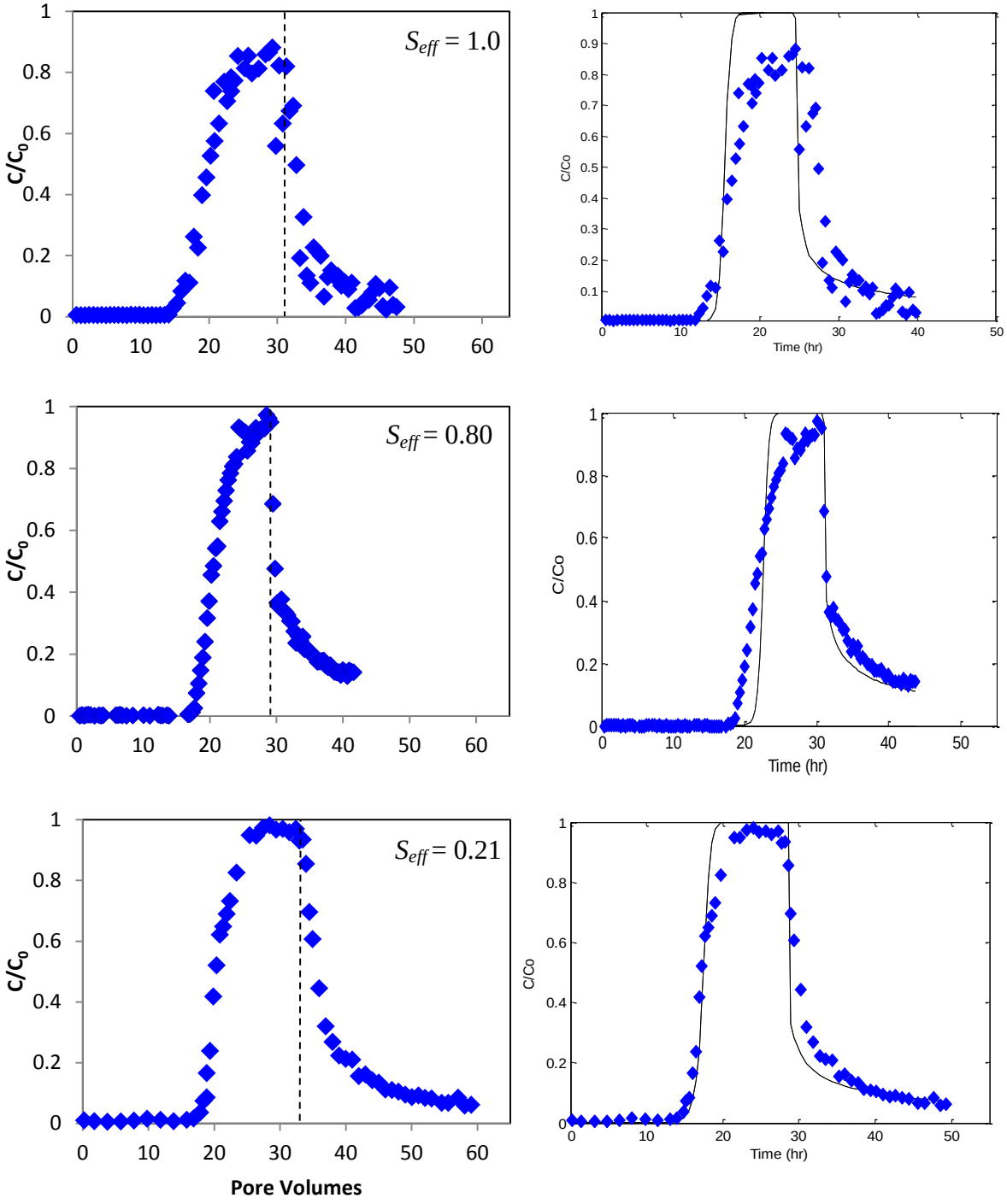

Figure 4.10. Dissolved strontium breakthrough data (left) and model fits (right) for S_{eff} = 1.0 (top, R^2 =0.79), 0.80 (middle, R^2 = 0.91), and 0.21 (bottom, R^2 = 0.92). The y-axis is the dimensionless unit (C/C_0). The x-axis is cumulative pore volumes for data and time (h) for model fits. One pore volume was equal to a residence time of 0.88 h ± 0.12. Vertical dashed lines denote when solution was switched to background solution.

Table 4.2. Experimental conditions for dissolved cation breakthrough and release experiments with average pore water velocity (U) and cumulative pore volumes of solution passed through the column (PVs, 1511 mL = 1 PV). PVs until $C/C_0 > 0.5$ represents breakthrough and PVs until $C/C_0 < 0.5$ represents the number of pore volumes required for cesium concentration to drop below $C/C_0 = 0.5$ after switching to background solution.

Cation		S_{eff}	U (cm h^{-1})	PVs until $C/C_0 > 0.5$	PVs until $C/C_0 < 0.5$
$[Cs^+]$ (M)	$[Sr^{2+}]$ (M)				
7.5×10^{-7}	0	1.0	17.3	40	30
0	7.5×10^{-6}	1.0	41.8	20	1
7.5×10^{-7}	0	0.80	55.1	44	27
0	7.5×10^{-6}	0.80	43.2	21	1
7.5×10^{-7}	0	0.21	206	42	33
0	7.5×10^{-6}	0.21	208	20	2.5

Effect of S_{eff} on Colloid Transport. Colloid breakthrough experiments were conducted with S_{eff} values of 1.0, 0.80, and 0.21 with a colloid concentration of 100 (± 5.2) mg L^{-1} for all experiments. For a relative saturation of 1.0, 0.80, and 0.21, the porewater velocities were 41.8, 53.2, and 153 cm h^{-1}, respectively. The colloids appeared in the column effluent within one pore volume (Figure 4.11 and 4.12). The effluent colloid concentration approached a steady maximum value between $C/C_0 = 0.85$ and 0.90 with 10-15% of colloids attached to the quartz surface and removed from suspension. Reducing S_{eff} from 1.0 to 0.21 resulted in increased colloid retention in the column.

The model was able to fit the colloid transport well, with R^2 values greater than 0.95. As S_{eff} was decreased from 1.0 to 0.80 and 0.21, the colloid attachment rate coefficient k_{cs} increased from 0.20 ± 0.07 h^{-1} to 0.25 ± 0.07 h^{-1} and 1.7 ± 0.50 h^{-1}, respectively. The colloid detachment rate k_{sc} and colloid attachment capacity of quartz X_{cs} remained constant for all values of S_{eff} at 0.0020 ± 0.0000 h^{-1} and 0.00010 ± 0.0000 g g^{-1}, respectively.

Effect of S_{eff} on Colloid-Facilitated Transport of Cesium. Colloid-facilitated transport breakthrough experiments were conducted with cesium for S_{eff} values of 1.0, 0.80, and 0.21 with pore water velocities of 34.6, 53.8, and 194 cm h^{-1}, respectively.

The addition of illite to the influent solution decreased the total capacity of the sand to remove cesium from solution (Figure 4.11). The number of pore volumes to breakthrough decreased as S_{eff} decreased – the 50% breakthrough of total cesium occurred at 7.8, 5.7, and 3.4 pore volumes for S_{eff} values of 1.0, 0.80, and 0.21, respectively (Table 4.3). For S_{eff} = 1.0, 1-2% of the cesium appeared in the effluent until a steep increase after 6 pore volumes. For S_{eff} = 0.80, nearly 20% of the total cesium was measured in the effluent before the second pore volume. The total cesium concentration remained constant after 2 pore volumes until the dissolved and total cesium concentration increased after 5 pore volumes. For S_{eff} = 0.21, 20% of the total cesium was measured in the effluent within the first pore volume.

After switching to background solution, colloid-associated cesium concentration dropped below C/C_0 = 0.01 within one pore volume for all S_{eff}; however, dissolved cesium desorbed readily for the quartz for S_{eff} = 1 and very little for S_{eff} = 0.80 and 0.21.

Results for model fits of cesium colloid-facilitated transport experiments for S_{eff} = 1.0, 0.80, and 0.21 confirm that the presence of colloids increased the transport of cesium (Figure 4.11). Table 4.4 shows the parameters used for the model fits. The model fits were best for S_{eff} = 1.0 (R^2 = 0.96. The model was able to adequately fit the experimental data for S_{eff} = 0.80 (R^2 = 0.86) and 0.21 (R^2 = 0.78). The quartz adsorption and desorption rate coefficients were the same as dissolved cesium breakthrough experiments. In order to fit the model results to the experimental data, the quartz adsorption capacity was reduced from 0.012 μM^{-1} h^{-1} for to 0.0018, 0.0012, and 0.0011 μM^{-1} h^{-1} for S_{eff} = 1.0, 0.80, and 0.21, respectively. These are reductions of a

factor of 6.7, 10.0, and 10.9 or an average reduction of a factor of 9.2 ± 2.2. The fraction of fast binding sites (F_{c1}) on the colloids ranged between 0.45 and 0.32, which may be attributed to differences in the batches of source clay used. These values were determined based on the fraction of cesium or strontium adsorbed to the clay at equilibrium.

The optimal values for the rate coefficients for cesium adsorption to and desorption from the illite colloids for the fast and slow sites (k_{ac1}, k_{ca1} and k_{ac2}, k_{ca2}; respectively) were the same as those reported by Turner et al. (2006) with 1.5 and 0.15 μM^{-1} h^{-1} for k_{ac1} and k_{ca1}, respectively and 0.9 and 0.0006 μM^{-1} h^{-1} for k_{ac2} and k_{ca2}, respectively.

For S_{eff} = 1.0, the model over-predicted the total and dissolved cesium for the first 7 h (8 pore volumes) before accurately predicting the stable value near C/C_0 = 0.80 and 0.25, respectively. After switching to background solution, the model predicted a small increase in total and aqueous cesium before accurately predicting the slope of the decrease in total and aqueous concentration.

For S_{eff} =0.80, the model accurately predicted the early plateau in total and colloid-associated cesium near C/C_0 = 0.25 from 1 to 3 h (1 to about 4 pore volumes) followed by an increase to a second stable value near C/C_0 = 0.40 for aqueous cesium and C/C_0 = 0.90 for total cesium. After the switch to background solution, the model predicted a small increase in the total and dissolved cesium concentration before decreasing and accurately predicted the rapid decrease in colloid-associated cesium below C/C_0 = 0.20.

For S_{eff} = 0.21, the model accurately predicted the total cesium concentration between 2 and 7 h, but over-predicted the concentration before 2 h and under-predicted the concentration after 7 h. The colloid-associated cesium was over-predicted for the first 2 h and under-predicted from 2 h to 9 h. The aqueous cesium concentration was over-predicted for the first 7 h; however,

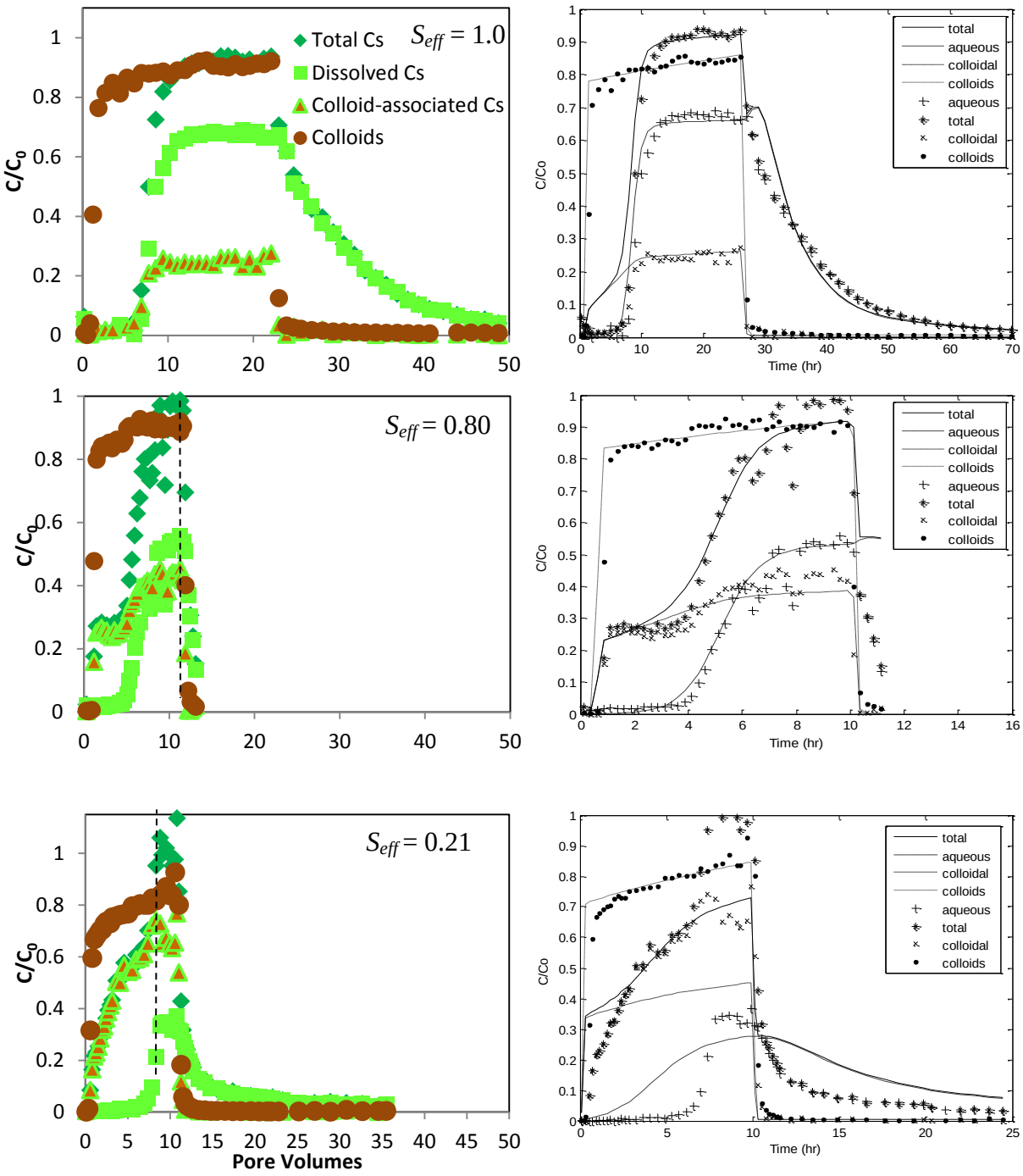

Figure 4.11. Breakthrough results (left) and model fits (right) of 7.5×10^{-7} M cesium equilibrated with 100 ± 5.2 mg L^{-1} illite for S_{eff} values of 1.0 (top, $R^2 = 0.96$), 0.80 (middle, $R^2 = 0.86$), and 0.21 (bottom, $R^2 = 0.80$). Model fits for colloid-facilitated transport of cesium with S_{eff} = 1.0 (top), 0.80 (middle) and 0.21(bottom). Model fits are represented by solid and dashed lines and symbols denote experimental data: • denotes colloid concentration, * denotes total cesium concentration, × denotes colloid-sorbed cesium concentration, and + denotes dissolved cesium concentration.

the maximum value was near the experimental data. After the switch to background solution, the model under-predicted the decrease in total and aqueous cesium, but accurately predicted the rapid decrease in colloid-associated cesium.

Effect of S_{eff} on Colloid-Facilitated Transport of Strontium. Colloid-facilitated transport breakthrough experiments were conducted with 7.5×10^{-6} M strontium in equilibrium with 100 mg L^{-1} illite. For S_{eff} values of 1.0, 0.80, and 0.21, average pore water velocities were 34.6, 53.1, and 205 cm h^{-1}, respectively. Breakthrough of total strontium occurred at 5.6, 6.3, and 3.1 pore volumes for S_{eff} values of 1.0, 0.80, and 0.21, respectively (Figure 4.12 and Table 4.3).

The addition of colloids to the influent solution decreased the total capacity of the sand to remove strontium from solution. For $S_{eff} = 1.0$, there was a very small amount of strontium in the effluent after 1 pore volume ($C/C_0 < 0.05$). After about 5 pore volumes, the amount of strontium in the effluent increased rapidly, but approached a maximum value that was less than $C/C_0 = 1.0$. For $S_{eff} = 0.80$, nearly 10% of the total strontium was measured in the effluent before the second pore volume. The total strontium concentration remained constant near $C/C_0 = 0.10$ until increasing sharply after 4 pore volumes. For $S_{eff} = 0.21$, total strontium concentration increased near 10% within one pore volume and increased sharply until C/C_0 near 1.0 after 5 pore volumes. For all S_{eff} values, strontium in the effluent dropped below $C/C_0 = 0.5$ within 2 pore volumes of switching to background solution.

Results for model fits of strontium colloid-facilitated transport experiments for $S_{eff} = 1.0$, 0.80, and 0.21 confirm that the presence of colloids increased the transport of strontium (Figure 4.12). Table 4.4 details the parameters used for the model fits.

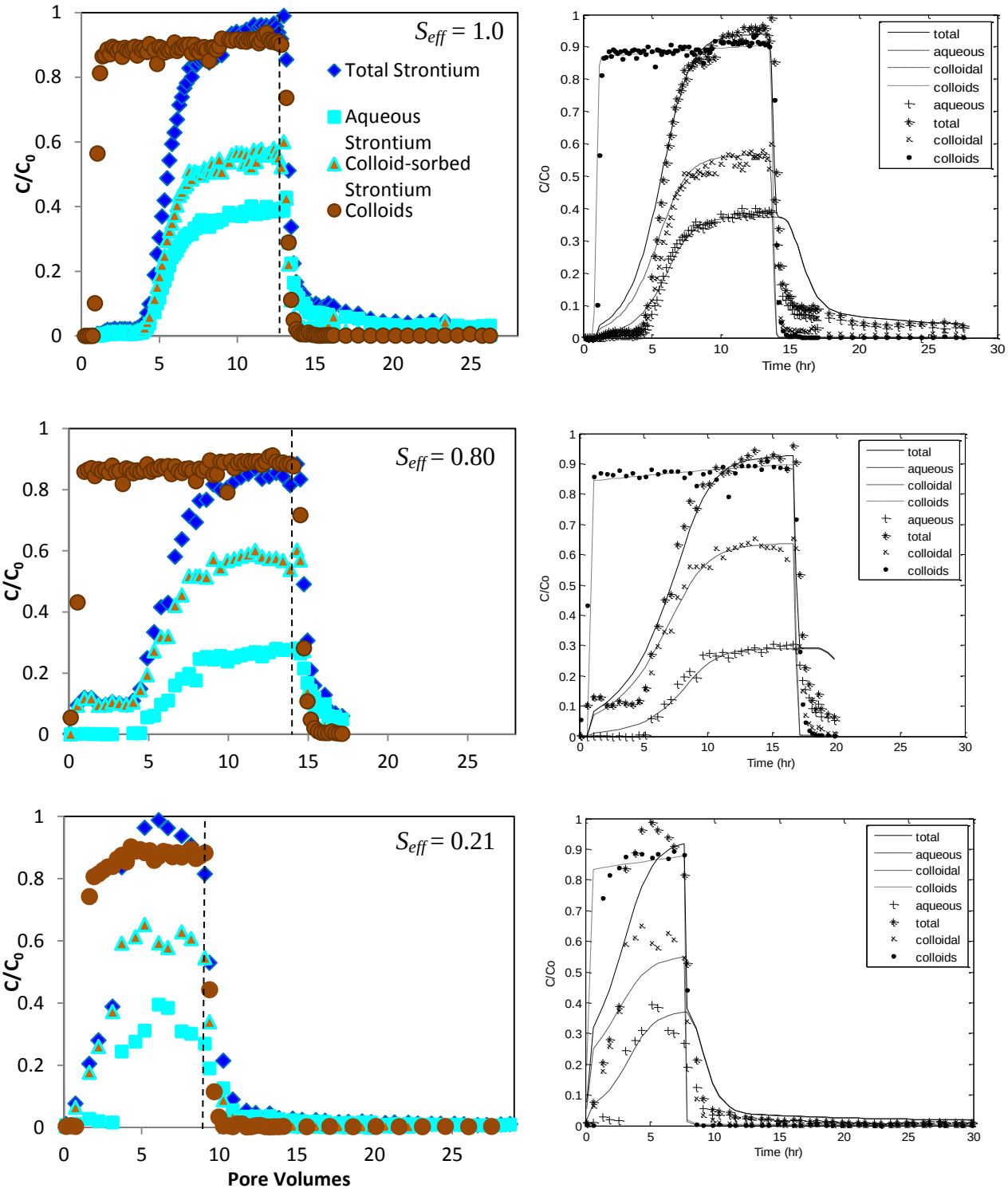

Figure 4.12. Breakthrough results for 7.5×10^{-6} M strontium equilibrated with 100 ± 5.2 mg L^{-1} illite for S_{eff} values of 1.0 (top, $R^2 = 0.95$), 0.80 (middle, $R^2 = 0.80$), and 0.21 (bottom, $R^2 = 0.69$). Model fits for colloid-facilitated transport of cesium with S_{eff} = 1.0 (top), 0.80 (middle) and 0.21(bottom). Model fits are represented by solid and dashed lines and symbols denote experimental data: • denotes colloid concentration, * denotes total strontium concentration, × denotes colloid-sorbed strontium concentration, and + denotes dissolved strontium concentration.

The model fits were best for S_{eff} = 1.0 (R^2 = 0.95) and S_{eff} = 0.80 (R^2 = 0.89), and marginal for S_{eff} = 0.21 (R^2 = 0.69). The quartz adsorption and desorption rate coefficients were the same as were determined in the dissolved strontium breakthrough experiment for S_{eff} =1.0. In order to fit the model results to the experimental data, the quartz adsorption capacity was reduced from 0.031 μM^{-1} h^{-1} for dissolved cesium transport to 0.0069, 0.0060, and 0.0050 μM^{-1} h^{-1} for S_{eff} = 1.0, 0.80, 0.21, respectively, or a reduction by a factor of 5.3 ± 0.9 . The fraction of fast binding sites (F_{c1}) on the colloids was found to be 0.55 for all S_{eff} values.

The optimal values for the colloid adsorption and desorption rate coefficients for the fast and slow sites (k_{ac1}, k_{ca1} and k_{ac2}, k_{ca2}; respectively) were the same as those reported by Turner et al. (2006) with 1.5 and 0.15 μM^{-1} h^{-1} for k_{ac1} and k_{ca1}, respectively, and 1.1 and 0.090 μM^{-1} h^{-1} for k_{ac2} and k_{ca2}, respectively.

For S_{eff} = 1.0, the model was able to predict the total, colloid-associated, and dissolved strontium concentration well. The model slightly over-predicted the concentrations in the first 5 h (6 pore volumes); however, the model accurately predicted the sharp increases in concentration after 5 h and values for C/C_0 = 0.95, 0.55, and 0.4 for total, colloid, associated, and dissolved strontium, respectively. For the first 5 h after the switch to background solution, the model over-predicted the concentration of total and aqueous strontium desorbing from the quartz.

For S_{eff} = 0.80, the model matched the early increase in total and colloid-associated strontium to C/C_0 = 0.10 from 1 h to 5 h well. After 5 h, the model also predicted the increase in total, colloid-associated, and dissolved strontium to C/C_0 = 0.90, 0.60, and 0.30, respectively. After the switch to background solution, the model accurately predicted the rapid decrease in colloid-associated strontium; however, the decrease in dissolved and total strontium was over-predicted.

For S_{eff} = 0.21, the model over-predicted the total, colloid-associated, and dissolved strontium for the first 2 h and over-predicted the concentrations from 2 h to 8 h, although the maximum values approached the experimental values after 8 h. After the switch to background solution, the model over-predicted the total and colloid-associated concentrations for the first 5 h before approaching the experimental values near C/C_0 = 0.1. The model accurately predicted the rapid decrease in colloid-associated strontium due to the absence of colloids in the effluent.

Table 4.3. Experimental conditions for colloid-facilitated breakthrough and release experiments with cesium and strontium, average pore water velocity (U), and cumulative pore volumes of suspensions passed through the column (PVs, 1511 mL = 1 PV). PVs until $C/C_0 > 0.5$ represents breakthrough and PVs until $C/C_0 < 0.5$ represents the number of pore volumes required for cesium concentration to drop below C/C_0 = 0.5 after switching to background solution.

Cation		S_{eff}	U (cm h^{-1})	**PVs until** $C/C_0 > 0.5$	**PVs of 0 M until** $C/C_0 < 0.5$
[Cs^+]	**[Sr^{2+}]**				
7.5×10^{-7}	0	1.0	34.6	7.8	3.5
0	7.5×10^{-6}	1.0	34.6	5.5	0.3
7.5×10^{-7}	0	0.80	53.8	5.7	0.5
0	7.5×10^{-6}	0.80	53.1	5.9	0.3
7.5×10^{-7}	0	0.21	194	3.6	0.5
0	7.5×10^{-6}	0.21	205	3.4	0.3

Table 4.4. Experimental conditions and modeling parameters that provided best fits for dissolved and colloid-facilitated transport experiments with cesium and strontium for S_{eff} = 1.0, 0.80, and 0.21.

Experimental Conditions						Modeling Parameters													
							Sand Sorption			Colloid Transport			Colloid Sorption						
Experiment ID	S_{eff}	[Cs^{+}] (M)	[Sr^{2+}] (M)	IMt-2 (mg L^{-1})	U (cm h^{-1})	D (cm^2 h^{-1})	k_{sa1} (μM^{-1} h^{-1})	k_{sa1} (μM^{-1} h^{-1})	X_a (μmol g^{-1})	k_{cs} (h^{-1})	k_{sc} (h^{-1})	X_{cs} (g g^{-1})	k_{ca1} (μM^{-1} h^{-1})	k_{ca1} (μM^{-1} h^{-1})	k_{ca2} (μM^{-1} h^{-1})	k_{ca2} (μM^{-1} h^{-1})	X_c (μmol g^{-1})	F_{c1}	R^2
1	1.0	7.5×10^{-7}	0	0	17.3	4.1	3.3	0.018	0.012	0	0	0	0	0	0	0	0	0	0.98
2	1.0	0	7.5×10^{-6}	0	41.8	4.1	0.40	0.00028	0.029	0	0	0	0	0	0	0	0	0	0.79
3	1.0	7.5×10^{-7}	0	100	34.6	4.1	3.3	0.018	0.0018	0.20	0.0020	0.00010	1.5	0.15	0.90	0.00060	7.4	0.45	0.96
4	1.0	0	7.5×10^{-6}	100	34.6	4.1	0.40	0.00028	0.0060	0.15	0.0020	0.00010	1.5	0.15	1.1	0.09	200	0.55	0.95
5	0.80	7.5×10^{-7}	0	0	55.1	4.8	3.3	0.018	0.012	0	0	0	0	0	0	0	0	0	0.97
6	0.80	0	7.5×10^{-6}	0	43.2	4.8	0.40	0.00028	0.031	0	0	0	0	0	0	0	0	0	0.91
7	0.80	7.5×10^{-7}	0	100	53.8	4.8	3.3	0.018	0.0012	0.30	0.0020	0.00010	1.5	0.15	0.90	0.00060	12.7	0.40	0.86
8	0.80	0	7.5×10^{-6}	100	53.1	4.8	0.40	0.00028	0.0068	0.20	0.0020	0.00010	1.5	0.15	1.1	0.04	200	0.55	0.89
9	0.21	7.5×10^{-7}	0	0	206	308	3.3	0.018	0.012	0	0	0	0	0	0	0	0	0	0.98
10	0.21	0	7.5×10^{-6}	0	208	308	0.40	0.00028	0.033	0	0	0	0	0	0	0	0	0	0.92
11	0.21	7.5×10^{-7}	0	100	194	308	3.3	0.018	0.0011	2.1	0.002	0.00010	1.5	0.15	0.90	0.00060	19.5	0.32	0.80
12	0.21	0	7.5×10^{-6}	100	205	308	0.40	0.00028	0.0040	1.2	0.002	0.00010	1.5	0.15	1.1	0.09	200	0.55	0.89

DISCUSSION

Overview. The focus of this section is to analyze the results of the modeling fits and resulting quartz and colloid adsorption and desorption rate coefficients. This analysis can help elucidate the processes controlling the transport of cesium and strontium and extend them to more general environmental conditions. The first section addresses the mechanisms responsible for the breakthrough curves at different relative saturation values with respect to the presence of cations (cesium and strontium) and colloids (no illite and illite). The second section addresses the ability of the mathematical model to fit the data including goodness-of-fit, sensitivity, and challenges in fitting the data. The third section addresses the hypothesis that the desorption kinetics of the contaminant from the colloids is the main factor controlling the potential for colloid-facilitated transport, and the difference between colloid-facilitated transport of cesium and strontium. The final section addresses the environmental implications for colloid-facilitated transport based on the results from this study.

Model Parameter Fits and Sensitivity. The model was able to fit the experimental data relatively well for cesium and strontium with and without colloids present at S_{eff} = 1.0, 0.80, and 0.21. The fits of highest correlation coefficients were achieved with no colloids present and colloid-facilitated experiments with S_{eff} = 1.0. The model had some difficulty in predicting the desorption tail for cesium and strontium experiments, especially within the first few hours after switching to background solution.

The model fits were found to depend largely on the sensitivity of the variables. The model was not very sensitive to the fraction of binding sites designated as “fast” type-1 or “slow” type-2 for the dissolved cation transport; therefore, only fast type-1 sites were used for the sand surface. Sensitivity analysis of the cesium and strontium fitting parameters showed that the most

important variable for matching the location of the steep breakthrough front was the cation adsorption capacity of the quartz, X_a. Increasing the value of X_a changed the location of the breakthrough front; however, there was little change in the overall shape (Figure 4.13).

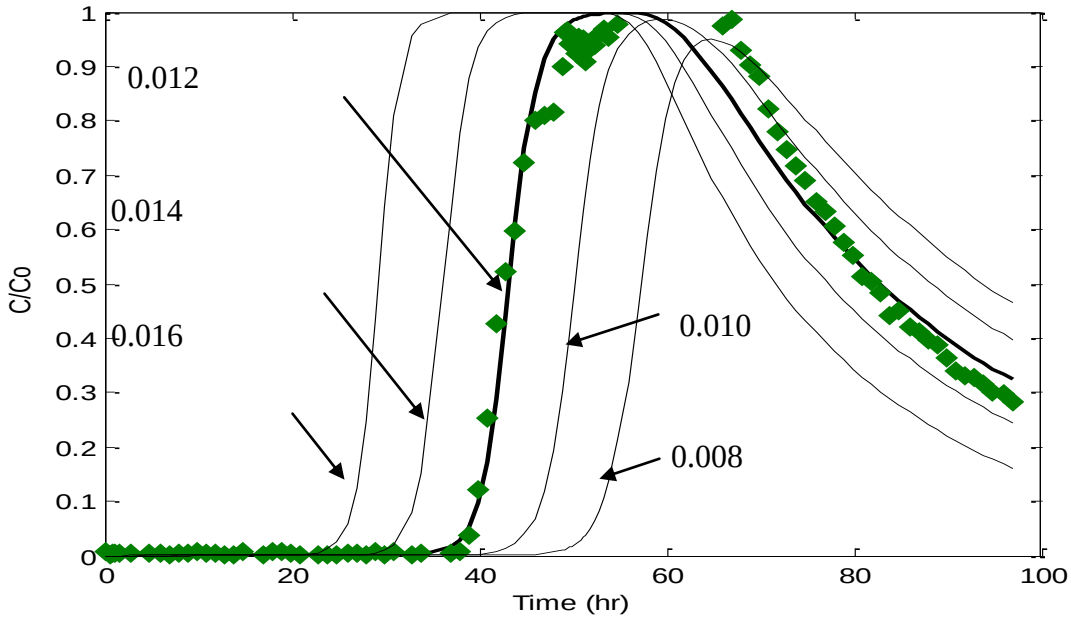

Figure 4.13. Sensitivity of simulated breakthrough curves to changes in X_a for dissolved cesium with S_{eff} = 1.0. Numbers on graph are values of X_a used for the simulation.

Increasing X_a moved the breakthrough front to the left (under-estimated time to breakthrough) and decreasing X_a moved the breakthrough to the right (over-estimated time to breakthrough). The effect of changing X_a had the same effect on the location of the strontium breakthrough. The best model fit was achieved using a sand capacity of 0.012 µM g^{-1} for cesium and 0.028 µM g^{-1} for strontium (Table 4.5). The quartz had a 2.3 times greater capacity for strontium than cesium, likely due to a higher affinity due to inner sphere binding.

Turner at al. (2006) also found that strontium was able to adsorb to more quartz binding sites that cesium. This result is consistent with ion exchange behavior representing outer-sphere binding of cesium and strontium to the sand surface by exchanging with sodium ions in the diffuse double layer. Compared to monovalent cesium, the divalent strontium has a greater ability to compete with other ions in the diffuse double layer of the quartz (sodium in this case).

The rate coefficients for cation adsorption to and desorption from for quartz determined by the model were 24 and 500 times larger for cesium than for strontium, respectively (Figure 4.14). This suggests that cesium adsorbed to quartz more readily than strontium and adsorption was more reversible for cesium than strontium.

For colloid-facilitated transport experiments, the goodness-of-fit depended largely on the fraction of fast and slow binding sites on the illite colloids (F_{c1}) and the magnitude of the slow binding site desorption rate coefficients (k_{sa2} and k_{sa2}) . Cesium showed a large sensitivity to both F_{c1} and k_{sa2}, which indicates that cesium transport was dependent on the number of slow sites and the desorption rate coefficient from the slow sites (Figure 4.15). In contrast, strontium showed no sensitivity to the fraction of fast and slow sites. This reflects the similarity in the optimal adsorption and desorption rate coefficients for strontium and illite (Figure 4.16).

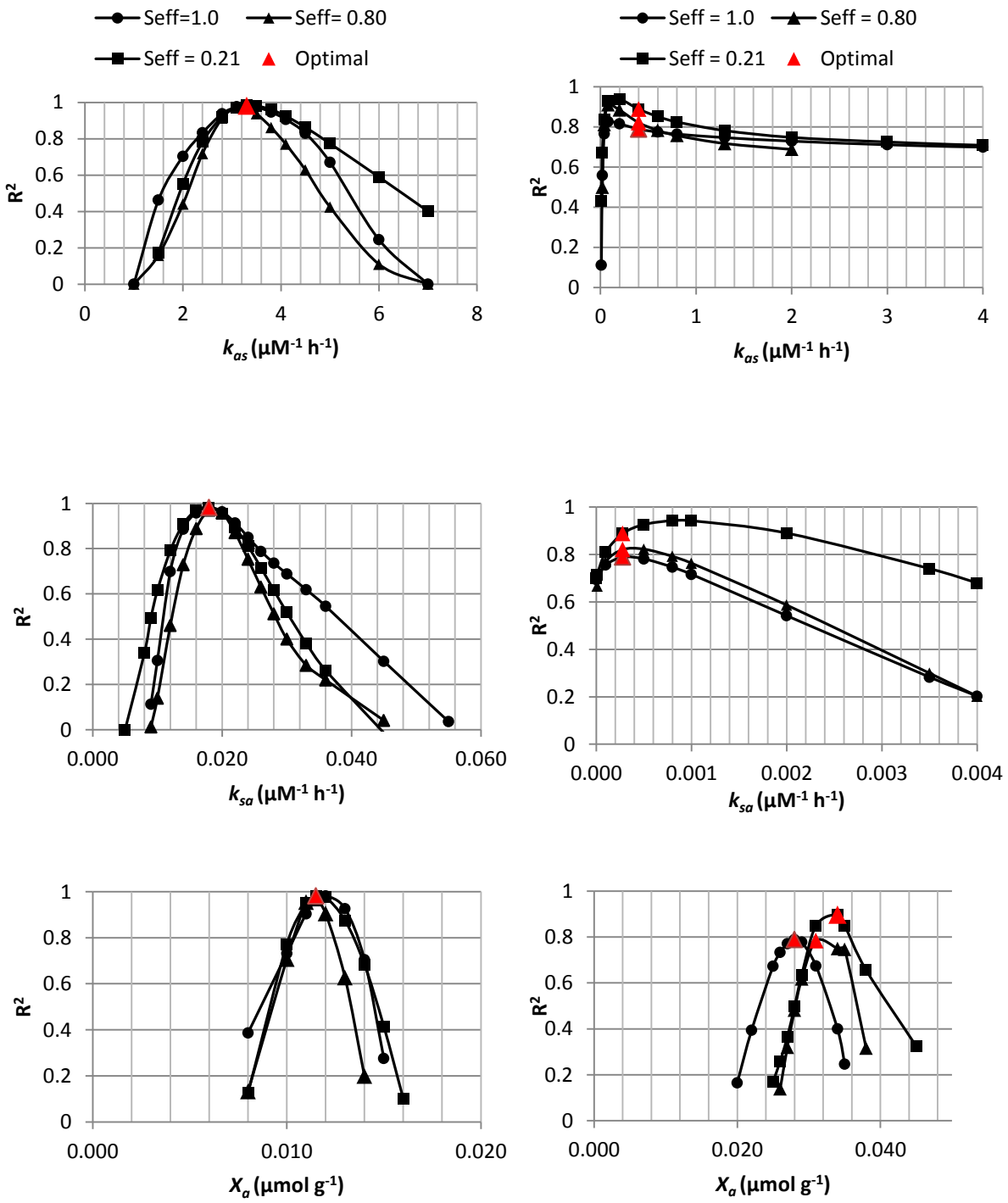

Figure 4.14. Sensitivity analysis of k_{as1} (top), k_{sa1} (middle), and X_a (bottom) for dissolved cesium (left) and strontium (right). S_{eff} =1.0, 0.80, and 0.21 are represented by filled circles, triangles, and squares, respectively. Red triangles represent the values used in the model best-fit results from Figure 4.10.

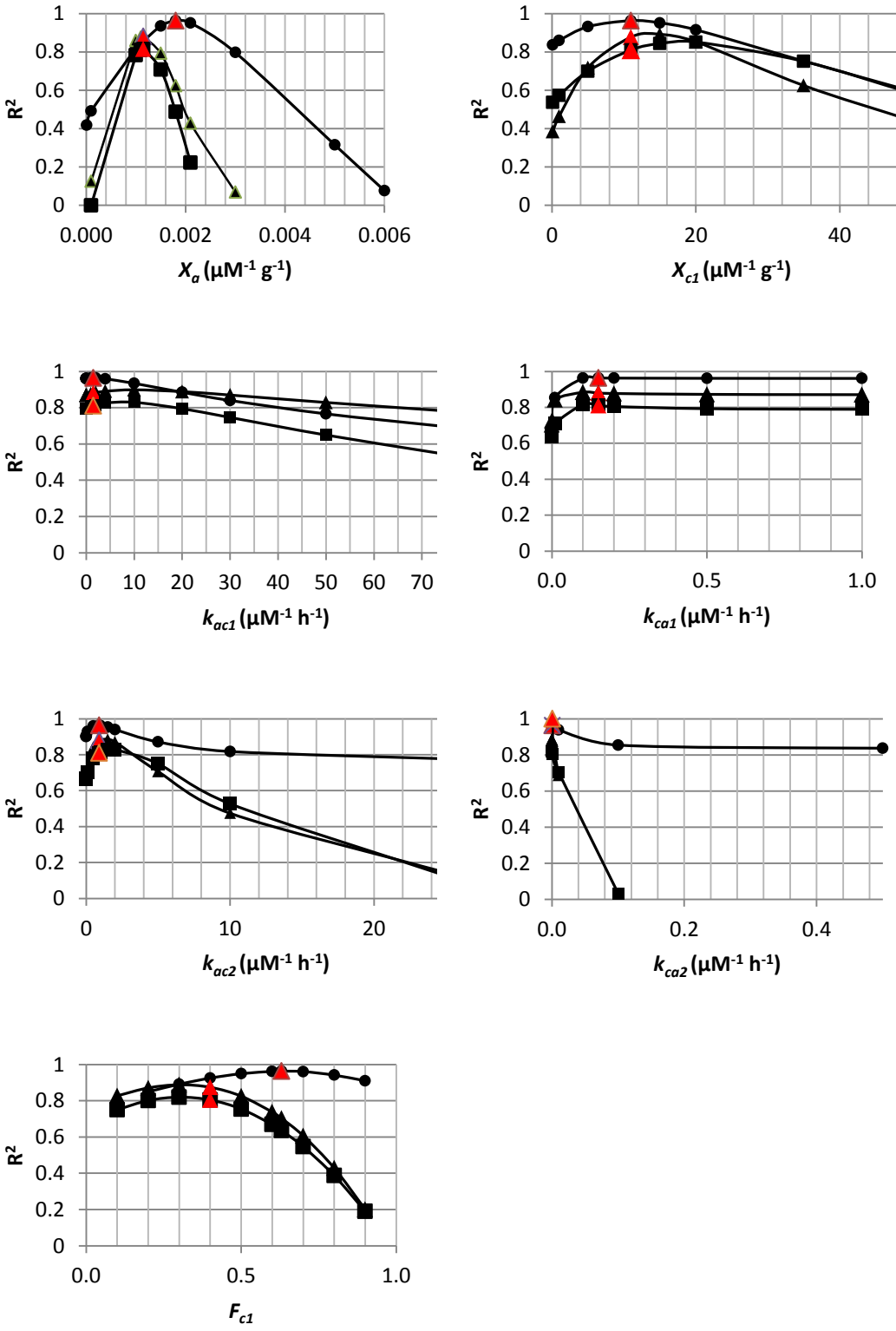

Figure 4.15. Sensitivity analysis on seven parameters used to fit the model to results from colloid-facilitated transport experiments with cesium for S_{eff} = 1.0 (circles), 0.80 (triangles), and 0.21 (squares). Red triangles denote the values used for the best fit results.

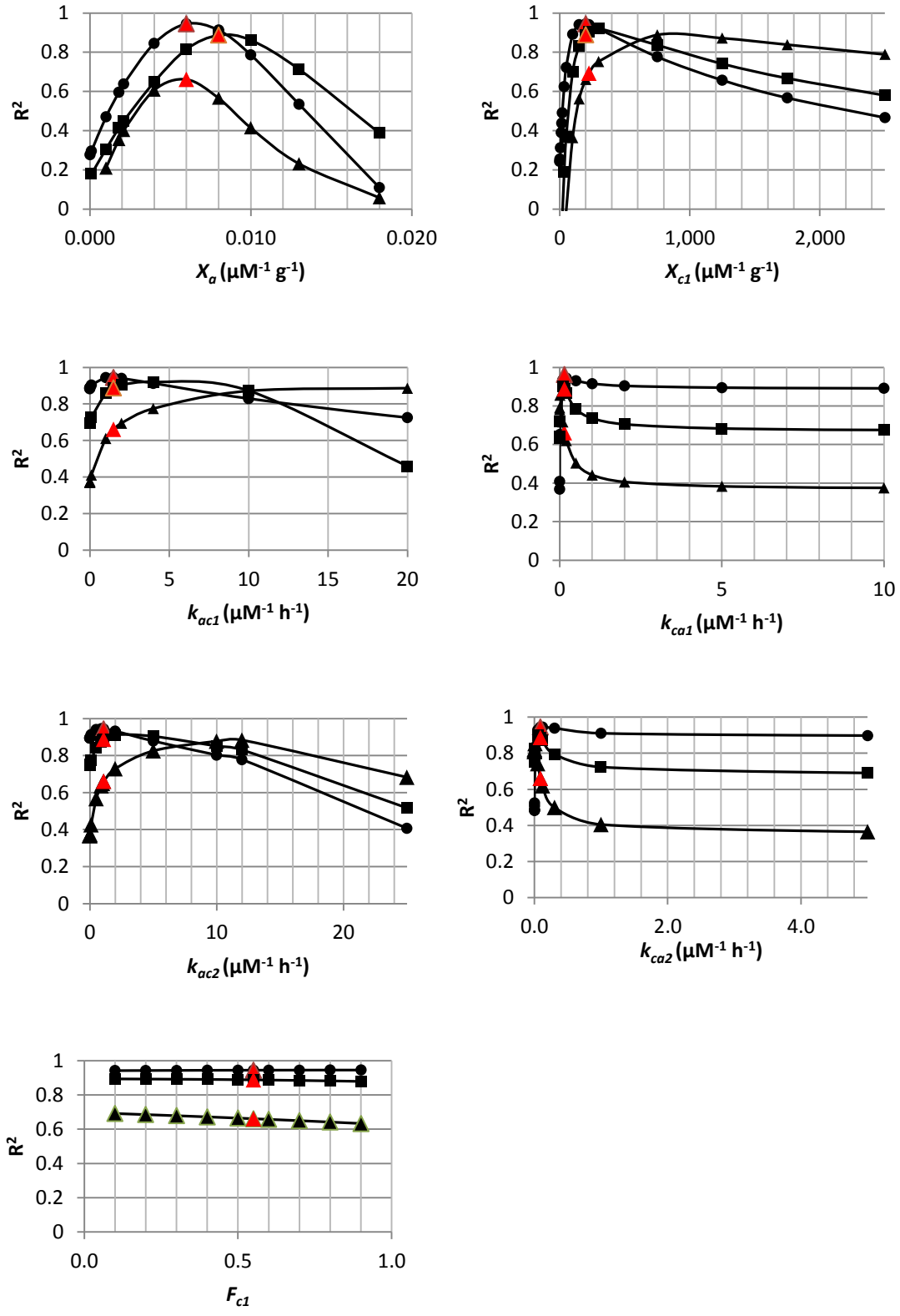

Figure 4.16. Sensitivity analysis on seven parameters used to fit the model to results from colloid-facilitated transport experiments with strontium for S_{eff} = 1.0 (circles), 0.80 (triangles), and 0.21 (squares). Red triangles denote the values used for the best fit results.

Mechanisms Responsible for Dissolved Transport. The model was able to accurately predict the transport of dissolved cesium and strontium with one-site, second-order sorption kinetics. The transport of dissolved cations was controlled by the combined effects of the adsorption rate coefficient k_{as1} (μM^{-1} h^{-1}), desorption rate coefficient k_{sa1} (μM^{-1} h^{-1}), and adsorption capacity of the quartz for cesium or strontium X_a (μmol g^{-1}). The experimental results show that the quartz initially removed all of the cesium and strontium from the pore water before a steep increase in the effluent concentration approached C/C_0 =1.0 (Figure 4.17).

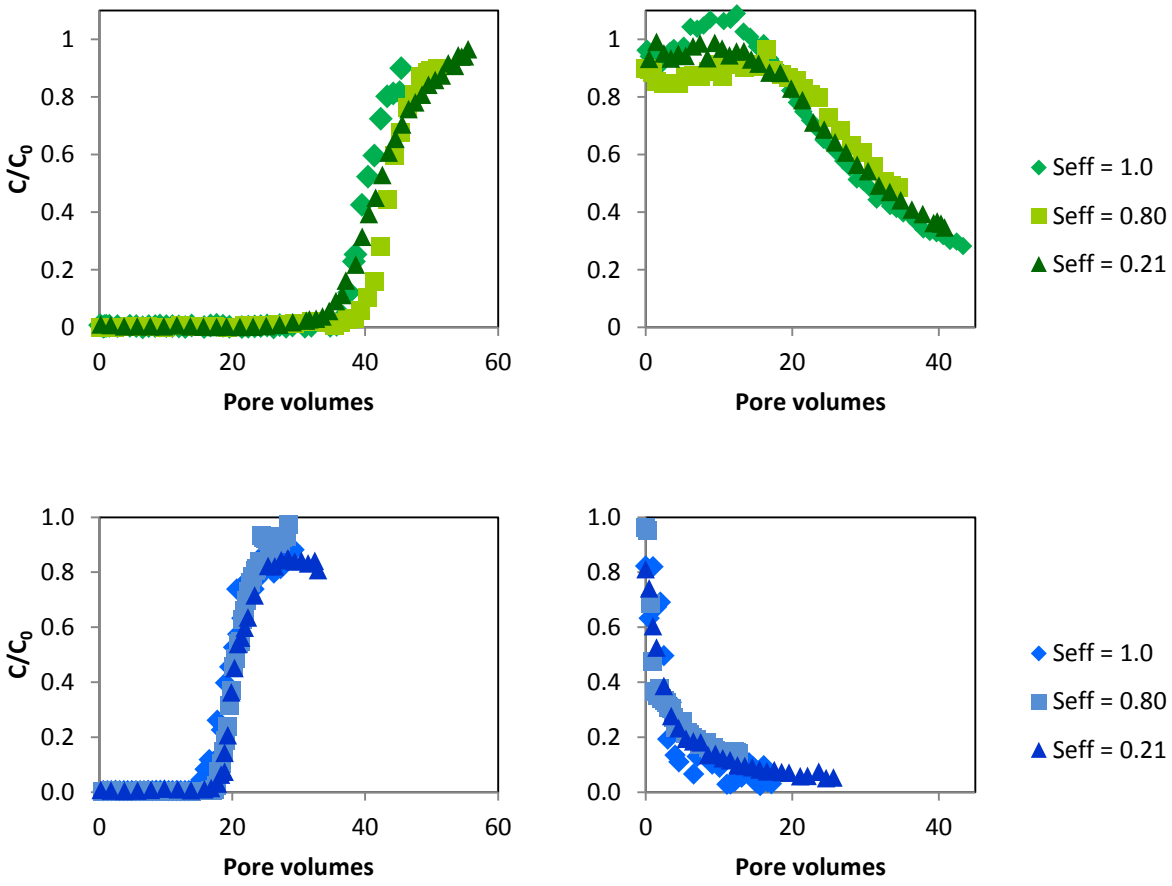

Figure 4.17. Results for dissolved cesium breakthrough (top left) and release (top right) and dissolved strontium breakthrough (bottom left) and release (bottom right) for S_{eff} = 1.0, 0.80, and 0.21.

The rate coefficients determined by the model for cation sorption with quartz sand are different for cesium and strontium. For cesium, the adsorption and desorption rate coefficients were found to be 3.3 and 0.014 $\mu M^{-1}\ h^{-1}$, respectively. For strontium, the adsorption and desorption rates were found to be 0.40 and 0.00028 $\mu M^{-1}\ h^{-1}$, respectively. Svarjensky (2006) reported that strontium can form strong inner-sphere complexes with the quartz surface. The magnitude of X_a determined the location of the breakthrough curve and the ratio of k_{sa1} to k_{as1}. The parameters X_a, k_{sa1}, and k_{as1} for cesium and strontium did not change with decreasing values of S_{eff}. This is evidence that all of the sand binding sites were readily accessible to dissolved cesium or strontium even when nearly 80% of the pore space was filled with air. When S_{eff} = 0.80 and 0.21, the mobile pore water will be in smaller pores; but since these pores have the same surface characteristics as the larger pores, no change in k_{as1} and k_{sa1} should be detected. Chen et al. (2005) reported finding a decrease in the quartz desorption rate as S_{eff} was decreased; however, they did not suggest a physical mechanism that may have been responsible for the decrease.

For the dissolved cation transport experiments, the model fits were sensitive to all three fitting parameters (X_a, k_{as1}, and k_{sa1}). The values found for X_a for cesium and strontium match well with those determined by Turner et al. (2006). Because cesium is a large monovalent cation, it is more easily dehydrated than the smaller, divalent strontium and can more strongly adsorb to quartz binding sites (Kitamura et al., 1999). The model fits showed that both cesium and strontium adsorbed to the quartz surface rapidly. Cesium desorbed more rapidly than strontium. Although dehydrated cesium has been suggested to be able to bind to quartz by an inner-sphere mechanism (Kim et al., 1996a; Kim et al., 1996b; Kim and Kirkpatrick, 1997; Parkman et al., 1998; Chen and Hayes, 1999; Chen et al., 2006), the rapid desorption observed in

these experiments and the desorption rate coefficients from the model suggest this was not the case in our experiments, and my be attributed to the low cesium concentration used.

Turner at al. (2006) conducted experiments with two ionic strengths and noted that cesium desorbed faster than strontium at low ionic strength (I = 0.1 mM, same as our experiments) but slower than strontium at a higher ionic strength (I= 2.0). These results suggest that cesium desorption rates are related to the rate that sodium is exchanged with cesium, while strontium desorption rates are largely independent of sodium concentration.

Mechanisms Responsible for Colloid Transport. For all values of S_{eff}, the colloids appeared in the column effluent near the first pore volume, which confirms that the colloids moved at the rate of the pore water and had a similar value for the dispersion coefficient D as the bromide tracer. As S_{eff} was decreased from 1.0 to 0.21, the average linear pore water velocity increased by a factor of 4. The average colloid deposition rate coefficients increased from 0.20± 0.07 h^{-1} to 0.25± 0.07 h^{-1} and 1.7± 0.51 h^{-1} for S_{eff} values of 1.0, 0.80, and 0.21, respectively. The increase in colloid deposition rate coefficients with decreasing S_{eff} likely resulted from an increase in the colloid collision frequency (η) due to the decrease in the cross-sectional area of the flow paths from the addition of the air phase and the increase in the flow velocity. The negative surface potential of the illite colloids should not make them attracted to the negative air-water interfaces present in the experiments for S_{eff} = 0.80 and 0.21 (Saiers et al, 1996b). The cation present – cesium or strontium – had no effect on the colloid breakthrough.

The colloid detachment rate, k_{sc}, and colloid attachment capacity of quartz, X_{cs}, remained constant for all values of S_{eff}. Very little colloid release was observed after the colloid suspension was switched to the background solution. The modeled detachment rates are similar to other values found in the literature and represent very little colloid detachment, which

suggests the illite grains were deposited in the primary energy minimum of the sand surface based on DLVO theory (Derjaguin and Landau, 1941; Verwey and Overbeek, 1948).

Mechanisms Responsible for Colloid-Facilitated Transport. The model simulations for the experiments shown above produced cation desorption rate coefficients from illite that were substantially different between cesium and strontium (Table 4.6). Cesium and strontium desorption rate coefficients were found to be consistent for all S_{eff} values. Cation desorption from the fast sites on illite was 250 times faster and 1.7 times faster than desorption from the slow sites for cesium and strontium, respectively.

The dimensionless Damköhler number (D_a) was used by Bold et al. (2003) and others to estimate the relative importance of equilibrium versus kinetic desorption for colloid-facilitated transport of contaminants. D_a can be calculated for fast (D_{a1}) and slow (D_{a2}) binding sites as

$$D_{a1} = \frac{k_{ca1} X_c F_{c1} [Colloid] L}{U} \tag{4.4}$$

$$D_{a2} = \frac{k_{ca2} X_c (1 - F_{c1}) [Colloid] L}{U} \tag{4.5}$$

where k_{ca} is the desorption rate coefficient (1 = fast sites and 2 = slow sites), X_c is the cation sorption capacity of the colloids, F_{c1} is the fraction of sites that are fast binding sites, [Colloid] is the concentration of illite (0.1 g L^{-1}), L is the length of the column (33.5 cm), and U is the pore water velocity. It has been suggested that systems with $D_a < 100$ are modeled best with a kinetic model and when $D_a < 0.01$ contaminant desorption from the colloids can be completely neglected. D_a for the cesium desorption from fast sites were 0.048, 0.047, 0.016 and from slow sites were 0.00024, 0.00028, and 0.00014 for S_{eff} values of 1.0, 0.80, and 0.21, respectively (Table 4.5). D_a for the strontium desorption from fast sites were 1.6, 1.0, 0.27 and for slow sites were 0.78, 0.51, and 0.13 for S_{eff} values of 1.0, 0.80, and 0.21, respectively (Table

4.5). The D_a values for cesium confirm that the kinetic two-site model is appropriate for modeling cesium and strontium colloid-facilitated transport in the experimental system we used. The values of D_{a2} for cesium were almost 40 times smaller than for strontium and support the idea that cesium is more susceptible to colloid-facilitated transport than strontium. As S_{eff} was reduced, the pore water velocity was increased and retention time in the column was reduced. This resulted in less time for the contaminant cations to desorb from the slow, frayed edge sites on the illite clay and increased the transport of the cesium more than for strontium.

Table 4.5. Calculations of Damköhler numbers for cation desorption from illite colloids.

		Desorption Rate Coefficient k_{ca} (μM^{-1} h^{-1})		Cation adsorption capacity	Fraction of fast sites	Velocity U	Damköhler Number	
Cation	S_{eff}	fast (n =1)	slow (n=2)	X_c, µmol g^{-1}	F_{c1}	(cm h^{-1})	D_{a1} fast	D_{a2} slow
	1.0	0.15	0.00060	7.4	0.45	34.6	0.048	0.00024
Cs	0.80	0.15	0.00060	12.7	0.40	53.8	0.047	0.00028
	0.21	0.15	0.00060	19.5	0.32	194	0.016	0.00014
	1.0	0.15	0.090	200	0.55	34.6	1.60	0.784
Sr	0.80	0.15	0.090	200	0.55	53.1	1.04	0.511
	0.21	0.15	0.090	200	0.55	205	0.27	0.132

The model fits for the colloid-facilitated breakthrough data were relatively good for cesium transport at S_{eff} values of 1.0, 0.80 and, 0.21 with the presence of 100 mg L^{-1} illite. For all values of S_{eff}, the quartz adsorption capacity for cesium (X_a) was reduced from 0.010 to 0.0012 µM g^{-1}. The presence of colloids decreased the number of pore volumes required for breakthrough to occur at all values of S_{eff} (Figure 4.18) and for both cesium and strontium. When S_{eff} = 1.0, the addition of 100 mg L^{-1} illite colloids decreased the number of pore volumes

to breakthrough from 39 to 7.5 for cesium and from 20.5 to 4.5 for strontium. The decrease is attributed a reduction in the quartz adsorption capacity X_a by the attached colloids for cesium and strontium by factors of 5 and 7, respectively. Turner et al. (2006) suggested that attached colloids may have blocked cations from having access to quartz binding sites nearby. A small ($C/C_0 < 2\%$) amount of both cesium and strontium bound to the colloids appeared in the effluent after one pore volume. The quartz was able to strip most of the adsorbed cesium or strontium from the colloids for the first 7 pore volumes for cesium and 4 pore volumes for strontium. Reducing S_{eff} from 1.0 to 0.80 with colloids present did not decrease the number of pore volumes to total cation breakthrough; however, it did increase the concentration of the colloid-associated cesium and strontium appearing as early plateaus in the column effluent after one pore volume (Figure 4.18).

For cesium, the magnitude of the early plateau increases from near 1% to almost 27% when S_{eff} is reduced from 1.0 to 0.80. These plateaus represent the amount of cesium that can be desorbed into the pore water and adsorbed to the quartz surface during the time it takes the pore water to flow through the column. As S_{eff} is reduced, the transport velocity is increased and there is less time for the colloid-sorbed cesium or strontium to desorb from the colloids and adsorb to quartz binding sites.

The main reason for this increased transport after one pore volume is the slow desorption kinetics of the cations from the colloids. Kinetic models have demonstrated the importance of the relationship between the desorption rate coefficients and fluid flow velocity on the colloid-facilitated transport of contaminants in saturated systems (Bold et al., 2003; Cvetkovic et al., 2004; Bekhit et al., 2006; Turner et al., 2006a). Modeling experimental results of colloid-facilitated transport of cesium with silica (Noell et al., 1998) and kaolinite (Saiers and

Hornberger, 1996b, 1999) were found to be best with a kinetic approach. Two-site models for cesium sorption to illite have also been used by many researchers (Comans and Hockley, 1992; Zachara et al., 2002).

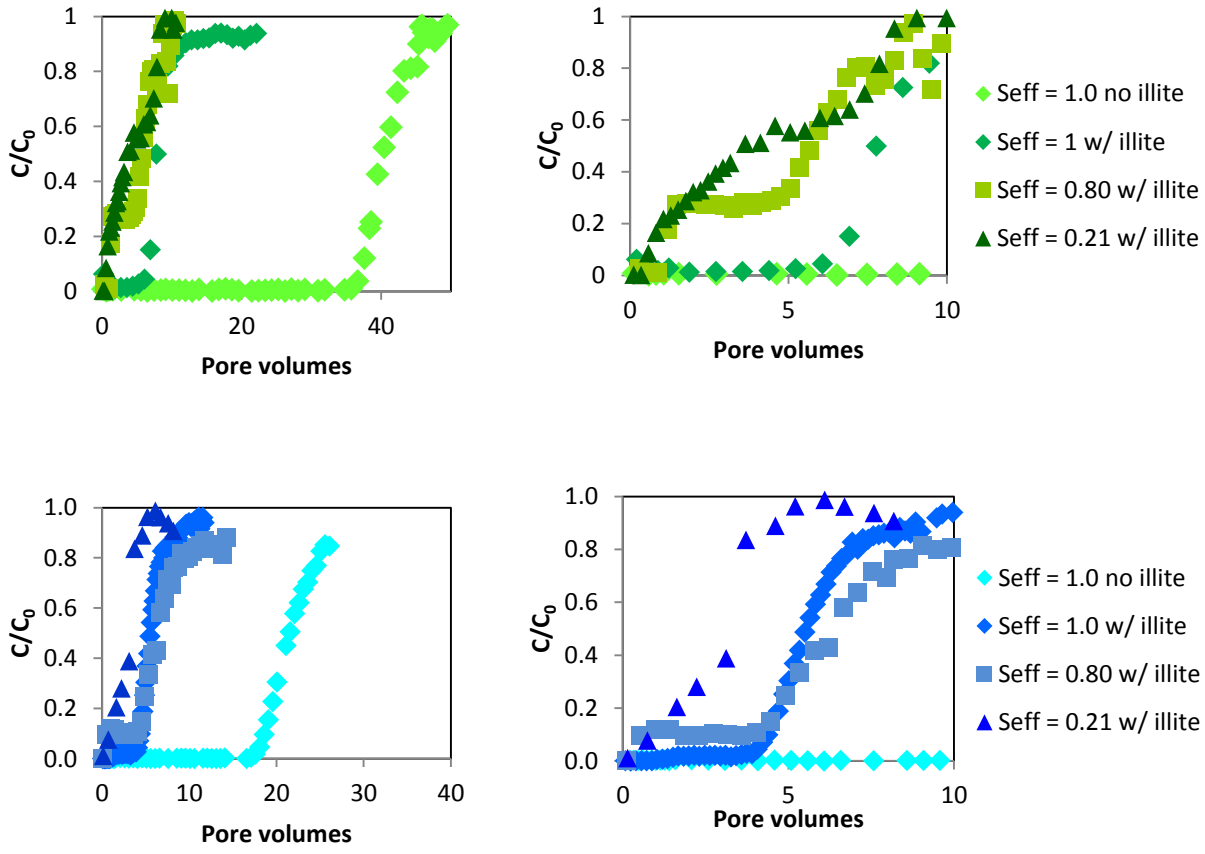

Figure 4.18. Effect of relative saturation on total cesium (top) and strontium (bottom) breakthrough in the presence of illite clay colloids for S_{eff} = 1.0, 0.80, and 0.21.

Adding colloids to the cation solution decreased the number of pore volumes until C/C_0 > 0.5 from about 41 to less than 7, with even more reduction as S_{eff} was reduced from 1.0 to 0.21 (Figure 4.18). After switching to background solution, experiments with colloids also reduced

the number of pore volumes until $C/C_0 < 0.5$ from near 30 to less than 4, with further reduction occurring at lower values of S_{eff} (Figure 4.18). This is evidence that the cesium is readily desorbed from the quartz and not from the illite clay.

The differences were not as large for strontium, but were still very significant. Adding colloids to the cation solution decreased the number of pore volumes until $C/C_0 > 0.5$ from about 20 to less than 6, with even more reduction as S_{eff} was reduced from 1.0 to 0.21 (Figure 4.19). After switching to background solution, experiments with colloids had little effect on number of pore volumes until $C/C_0 < 0.5$, all of which were less than 1 pore volume, (Figure 4.19). This is evidence that the strontium is tightly bound to the quartz surface.

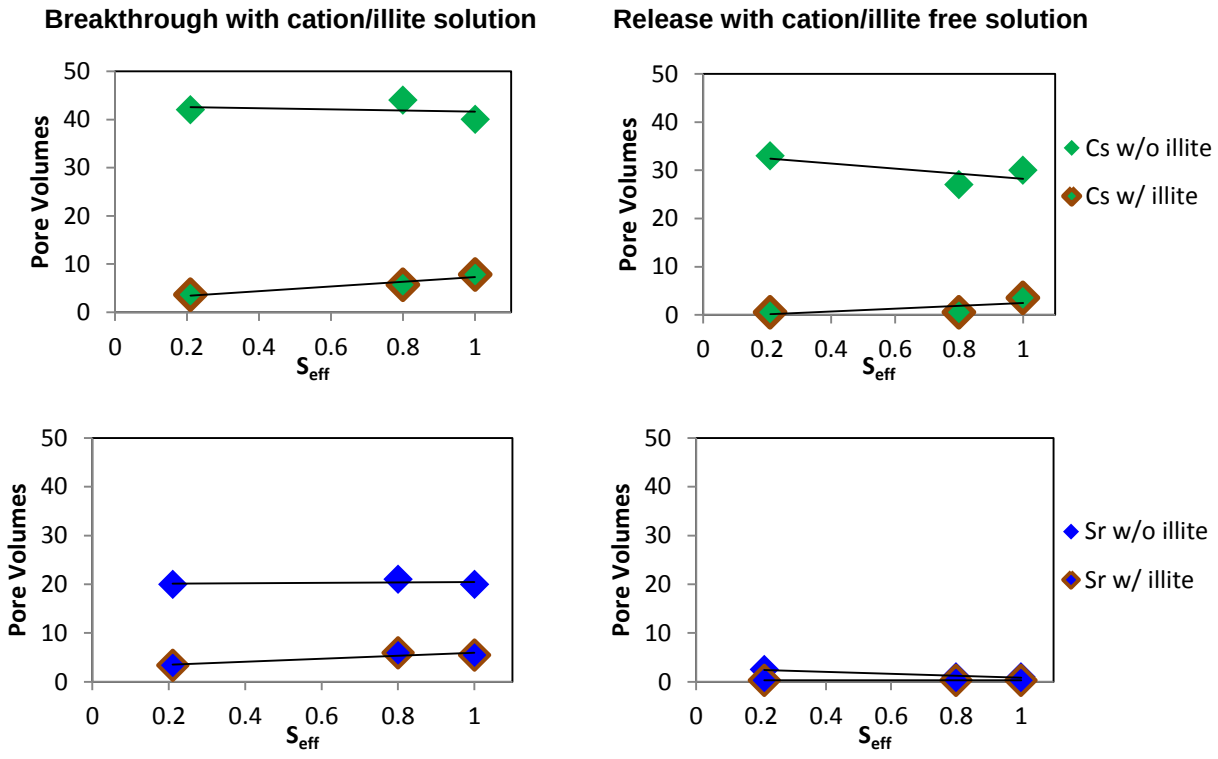

Figure 4.19. Effect of relative saturation and colloids on the number of pore volumes until $C/C_0 > 0.5$ for breakthrough (left graphs) and $C/C_0 < 0.5$ for release (right graphs) for cesium (top graphs) and strontium (bottom graphs).

A similar effect was observed with strontium, for which the quartz binding capacity was reduced from 0.025 to 0.012 μM g^{-1}. The presence of the illite colloids reduced the quartz capacity for cesium adsorption by a factor of 8.3 and for strontium adsorption by a factor of 2.1. Illite had a larger effect on reducing the total quartz binding capacity for cesium than for strontium, possibly due to the higher affinity of strontium for the quartz binding sites.

Hypothesis Validation and Governing Parameters. The results of the experiments and model simulations suggest that slow desorption of the cations from the illite colloids can increase the role of colloid-facilitated transport in contaminant transport under unsaturated conditions. Cesium and strontium colloid-facilitated transport was effectively modeled with two binding sites on the illite surface representing fast, planar sites and slow, frayed edge sites with second-order sorption kinetics. When S_{eff} was reduced to 0.80 and 0.21, the increased flow velocities decreased the residence time in the column and increased the importance of the slow desorption rate coefficients of the colloids. For the first five pore volumes, slower desorption of cesium from the frayed edge sites of the colloids resulted in more cesium moving through the column sorbed to colloids than for strontium.

At S_{eff} = 1.0, the addition of colloids increased the transport of cesium more than strontium; however, both increases were largely due to a decrease in the capacity of quartz to adsorb cations in the presence of colloids. Contrary to our hypothesis, the experimental and modeling results showed that reducing S_{eff} did not result in faster cesium and strontium transport. This was likely because cesium and strontium readily adsorb to the quartz surface. For S_{eff} = 0.21, the water seems to remain mobile through all of the pore space allowing all of the quartz binding sites to remain available.

It was expected that reducing S_{eff} would cause an increase in colloid deposition and would result in less colloid-facilitated transport when $S_{eff} = 0.21$. However, the negative surface charge of the illite colloids and the high pore water velocities resulted in very little affinity between the illite and the negatively charged air-water interfaces found in the unsaturated quartz sand porous medium, which caused colloid transport to only be slightly reduced by reductions in S_{eff}. This was also suggested by the model simulations.

Environmental Implications. These experimental and modeling results have important implications for extending our understanding of how colloid-facilitated transport can lead to increased contaminant transport in the environment and at contaminated U.S. Department of Energy sites. The differences between the colloid-facilitated transport of cesium and strontium underscore the importance of accounting for desorption kinetics of contaminants from colloids when assessing the potential for colloid-facilitated transport. Unsaturated conditions increase the potential for colloid-facilitated transport due to the increased flow velocities and decreased residence time, which increases the importance of desorption kinetics

The contrasting cesium and strontium desorption kinetics also offer insight into more complicated natural systems. Contaminants like cesium that can bind by an inner-sphere mechanism to the frayed edge sites of illite and have a much higher potential for increased transport through colloid-facilitated transport. Strontium, which exhibited higher desorption rate coefficients and showed desorption from both the fast, planar sites and slow, frayed edge sites, would be less susceptible to colloid-facilitated transport because more of its transport would occur in the dissolved phase.

The results from these experiments show the importance of characterizing the colloids present and determining the potential for slow contaminant desorption. Slower contaminant

desorption caused by frayed-edge sites increases the potential for colloid-facilitated transport. Unsaturated conditions increase the potential for colloid-facilitated transport by decreasing travel times and also available surface area for adsorption to occur. Slower flow would lead to increased time for the contaminants to desorb from the colloids, and would lead to longer breakthrough times. Adding to the complexity, flow through natural soils is intermittent and subject to drying and wetting cycles. At lower values of S_{eff}, the increased flow velocities and decreased contact times make the desorption kinetic rate coefficients increasingly important.

REFERENCES

Albarran, N., Missana, T., Garcia-Gutierrez, M., Alonso, U., Mingarro, M., 2011. Strontium migration in a crystalline medium: effects of the presence of bentonite colloids. Journal of Contaminant Hydrology 122, 76-85.

Allen, J.R.L., 1988. Modern-period muddy sediments in the severn estuary (Southwestern UK) - A pollutant-based model for dating and correlation. Sedimentary Geology 58, 1.

Bekhit, H., Hassan, A., Harris-Burr, R., Papelis, C., 2006. Experimental and numerical investigations of effects of silica colloids on transport of strontium in saturated sand columns. Environmental Science & Technology 40, 5402-5408.

Bold, S., Kraft, S., Grathwohl, P., Liedl, R., 2003. Sorption/desorption kinetics of contaminants on mobile particles: Modeling and experimental evidence. Water Resources Research 39, SBH 3-1:8.

Bouby, M., Geckeis, H., Lutzenkirchen, J., Mihai, S., Schafer, T., 2011. Interaction of bentonite colloids with Cs, Eu, Th and U in presence of humic acid: A flow field-flow fractionation study. Geochimica Et Cosmochimica Acta 75, 3866-3880.

Chen, C., Coleman, M., Katz, L., 2006. Bridging the gap between macroscopic and spectroscopic studies of metal ion sorption at the oxide/water interface: Sr(II), Co(II), and Pb(II) sorption to quartz. Environmental Science & Technology 40, 142-148.

Chen, C., Hayes, K., 1999. X-ray absorption spectroscopy investigation of aqueous Co(II) and Sr(II) sorption at clay-water interfaces. Geochimica Et Cosmochimica Acta 63, 3205-3215.

Chen, G., Flury, M., Harsh, J., Lichtner, P., 2005. Colloid-facilitated transport of cesium in variably saturated Hanford sediments. Environmental Science & Technology 39, 3435-3442.

Cheng, T., Saiers, J., 2010. Colloid-Facilitated Transport of Cesium in Vadose-Zone Sediments: The Importance of Flow Transients. Environmental Science & Technology 44, 7443-7449.

Clark, M., 1996. Transport Modeling for Environmental Engineers and Scientists. Wiley, New York.

Comans, R., Hockley, D., 1992. Kinetics of Cesium Sorption on Illite. Geochimica Et Cosmochimica Acta 56, 1157-1164.

Cvetkovic, V., Painter, S., Turner, D., Pickett, D., Bertetti, P., 2004. Parameter and model sensitivities for colloid-facilitated radionuclide transport on the field scale. Water Resources Research 40.

de Jonge, L., Kjaergaard, C., Moldrup, P., 2004. Colloids and colloid-facilitated transport of contaminants in soils: An introduction. Vadose Zone Journal 3, 321-325.

DeNovio, N., Saiers, J., Ryan, J., 2004. Colloid movement in unsaturated porous media: Recent advances and future directions. Vadose Zone Journal 3, 338-351.

Eching, S., Hopmans, J., 1993. Optimization of hydraulic functions from transient outflow and soil-water pressure data. Soil Science Society of America Journal 57, 1167-1175.

Flury, M., Czigany, S., Chen, G., Harsh, J., 2004. Cesium migration in saturated silica sand and Hanford sediments as impacted by ionic strength. Journal of Contaminant Hydrology 71, 111-126.

Flury, M., Mathison, J., Harsh, J., 2002. In situ mobilization of colloids and transport of cesium in Hanford sediments. Environmental Science & Technology 36, 5335-5341.

Gao, B., Saiers, J., Ryan, J., 2004. Deposition and mobilization of clay colloids in unsaturated porous media. Water Resources Research 40, -.

Honeyman, B., 1999. Geochemistry - Colloidal culprits in contamination. Nature 397, 23-24.

Kersting, A., Efurd, D., Finnegan, D., Rokop, D., Smith, D., Thompson, J., 1999. Migration of plutonium in ground water at the Nevada Test Site. Nature 397, 56-59.

Kim, Y., Cygan, R., Kirkpatrick, R., 1996a. Cs-133 NMR and XPS investigation of cesium adsorbed on clay minerals and related phases. Geochimica Et Cosmochimica Acta 60, 1041-1052.

Kim, Y., Kirkpatrick, R., 1997. Na-23 and Cs-133 NMR study of cation adsorption on mineral surfaces: Local environments, dynamics, and effects of mixed cations. Geochimica Et Cosmochimica Acta 61, 5199-5208.

Kim, Y., Kirkpatrick, R., Cygan, R., 1996b. Cs-133 NMR study of cesium on the surfaces of kaolinite and illite. Geochimica Et Cosmochimica Acta 60, 4059-4074.

Kitamura, A., Fujiwara, K., Yamamoto, T., Nishikawa, S., Moriyama, H., 1999. Analysis of adsorption behavior of cations onto quartz surface by electrical double-layer model. Journal of Nuclear Science and Technology 36, 1167-1175.

Krumbein, W., Sloss, L., 1963. Stratigraphy and Sedimentation. Freeman, San Francisco.

Lafrance, P., Marineau, L., Perreault, L., Villeneuve, J., 1994. Effect of natural dissolved organic-matter found in groundwater on soil adsorption and transport of pentachlorophenol. Environmental Science & Technology 28, 2314-2320.

Lenhart, J., Saiers, J., 2002. Transport of silica colloids through unsaturated porous media: Experimental results and model comparisons. Environmental Science & Technology 36, 769-777.

McDowell-Boyer, L., Hunt, J., Sitar, N., 1986. Particle transport through porous media. Water Resources Research 22, 1901-1921.

McGechan, M., Lewis, D., 2002. Transport of particulate and colloid-sorbed contaminants through soil, part 1: General principles. Biosystems Engineering 83, 255-273.

Noell, A., Thompson, J., Corapcioglu, M., Triay, I., 1998. The role of silica colloids on facilitated cesium transport through glass bead columns and modeling. Journal of Contaminant Hydrology 31, 23-56.

Pace, M., Mayes, M., Jardine, P., McKay, L., Yin, X., Mehlhorn, T., Liu, Q., Gurleyuk, H., 2007. Transport of Sr2+ and SrEDTA(2-) in partially-saturated and heterogeneous sediments. Journal of Contaminant Hydrology 91, 267-287.

Parkman, R., Charnock, J., Livens, F., Vaughan, D., 1998. A study of the interaction of strontium ions in aqueous solution with the surfaces of calcite and kaolinite. Geochimica Et Cosmochimica Acta 62, 1481-1492.

Rowell, D., 1994. Soil Science: methods and applications. Longman Scientific & Technical, University of Michigan.

Roy, S., Dzombak, D., 1997. Chemical factors influencing colloid-facilitated transport of contaminants in porous media. Environmental Science & Technology 31, 656-664.

Ryan, J., Elimelech, M., 1996. Colloid mobilization and transport in groundwater. Colloid Surface A 107, 1-56.

Ryan, J., Illangasekare, T., Litaor, M., Shannon, R., 1998. Particle and plutonium mobilization in macroporous soils during rainfall simulations. Environmental Science & Technology 32, 476-482.

Saiers, J., Hornberger, G., 1996. The role of colloidal kaolinite in the transport of cesium through laboratory sand columns. Water Resources Research 32, 33-41.

Saiers, J., Hornberger, G., 1999. The influence of ionic strength on the facilitated transport of cesium by kaolinite colloids. Water Resources Research 35, 1713-1727.

Saiers, J., Lenhart, J., 2003b. Ionic-strength effects on colloid transport and interfacial reactions in partially saturated porous media. Water Resources Research 39, -.

Solovitch-Vella, N., Garnier, J., Ciffroy, P., 2006. Influence of the colloid type on the transfer of Co-60 and Sr-85 in silica sand column under varying physicochemical conditions. Chemosphere 65, 324-331.

Spurlock, F., Biggar, J., 1990. Effect of naturally-occuring soluble organic-matter on the adsorption and movement of simazine [2-chloro-4,6-bis(ethylamino)-s-triazine] in hanford sandy loam. Environmental Science & Technology 24, 736-741.

Steefel, C., Carroll, S., Zhao, P., Roberts, S., 2003. Cesium migration in Hanford sediment: a multisite cation exchange model based on laboratory transport experiments. Journal of Contaminant Hydrology 67, 219-246.

Sverjensky, D., 2002. Standard states for surface sites and surface species in surface complexation models. Abstracts of Papers of the American Chemical Society 223, U607-U607.

Sverjensky, D., 2006. Prediction of the speciation of alkaline earths adsorbed on mineral surfaces in salt solutions. Geochimica Et Cosmochimica Acta 70, 2427-2453.

Szenknect, S., Gaudet, J., Dewiere, L., 2003. Evaluation of distribution coefficients for the prediction of strontium and cesium migration in a natural sand at different water contents. Journal De Physique Iv 107, 1279-1282.

Triay, I., Lu, N., Cotter, C., Kitten, H., 1997. Iron oxide colloid facilitated plutonium transport in groundwater. Americal Chemical Society. American Chemical Society, Las Vegas.

Turner, N., 2005. The effect of desorption kinetics on the colloid-facilitated transport of cesium-137 and strontium-90 in a saturated quartz porous medium. Civil, Environmental, and Architectural Engineering. University of Colorado-Boulder, Boulder, CO, p. 182.

Turner, N., Ryan, J., Saiers, J., 2006. Effect of desorption kinetics on colloid-facilitated transport of contaminants: Cesium, strontium, and illite colloids. Water Resources Research 42.

Vilks, P., Baik, M., 2001. Laboratory migration experiments with radionuclides and natural colloids in a granite fracture. Journal of Contaminant Hydrology 47, 197-210.

Vilks, P., Cramer, J., Bachinski, D., Doern, D., Miller, H., 1993. Studies of colloids and suspended particles, Cigar Lake Uranium Deposit, Sasketchewan, Canada. Applied Geochemistry 8, 605-616.

Zachara, J., Flury, M., Harsh, J., 2002. Colloid facilitated migration of radioelements - Mechanisms, significance, and needed conditions. Geochimica Et Cosmochimica Acta 66, A867-A867.

Zheng, C., Bennett, G., 2002. Applied Contaminant Transport Modeling. Wiley-Interscience, New York.

Zhuang, J., Flury, M., Jin, Y., 2003. Colloid-facilitated Cs transport through water-saturated Hanford sediment and Ottawa sand. Environmental Science & Technology 37, 4905-4911.

CHAPTER 5

EFFECT OF PHYSICAL HETEROGENEITY ON COLLOID-FACILITATED TRANSPORT OF CESIUM

ABSTRACT

The objective of this work was to investigate and quantify the effect of physical heterogeneity and unsaturated conditions on colloid-facilitated transport of cesium through quartz sand. A filled earthworm burrow macropore was simulated by adding a 2.5 cm diameter vertical cylinder of large quartz sand (d_{50} = 1.57 mm) to the center of a 33.5 cm long and 12.3 cm diameter fine quartz sand (d_{50} = 0.325 mm) column. Breakthrough experiments were conducted at effective matrix sand saturation (S_{eff}) values of 1.0, 0.80, and 0.21 with and without 100 mg L^{-1} illite colloids present. Bromide breakthrough experiments were used to determine that 32%, 43% and 1% of the total flow was conducted through the macropore for S_{eff} = 1.0, 0.80 and 0.21, respectively. Without illite colloids, the addition of the macropore increased the transport of cesium at S_{eff} = 1.0 and 0.80, but did not increase transport for S_{eff} = 0.21. With illite colloids present, the addition of the macropore increased the transport of cesium for S_{eff} = 1.0 and 0.80. This was due to the macropore conducting water at higher S_{eff} values but not for S_{eff} = 0.21. A model developed for colloid-facilitated transport in homogeneous sand columns was able to simulate the colloid-facilitated transport of cesium with the macropore by separately calculating the transport through the macropore and matrix sand and adding the results.

INTRODUCTION

The presence of colloids in vadose zone and shallow groundwater systems has been shown to increase the transport rate of contaminants in saturated porous media (McCarthy and Zachara, 1989; Honeyman, 1999; Kretzschmar et al., 1999; McGechan, 2002; McGechan and Lewis, 2002; de Jonge et al., 2004a), unsaturated porous media (de Jonge et al., 2004a; DeNovio et al., 2004) and fractured media (Vilks and Baik, 2001). Colloid-facilitated transport occurs when contaminants associate with mobile colloids, which decreases the adsorption rate of the contaminants to the porous medium matrix and has been shown to increase the transport of cesium under saturated conditions with kaolinite (Saiers and Hornberger, 1996b), silica (Noell et al., 1998), and illite (Turner et al., 2006a) and Hanford colloids (Flury et al., 2002; Zhuang et al., 2003) and under unsaturated conditions with natural Hanford colloids (Chen et al., 2005; Cheng and Saiers, 2010).

The presence of macropores and preferential flow paths found in most natural soils has been shown to increase the effect that colloids have on enhancing transport of sorbed contaminants such as atrazine (Seta and Karathanasis, 1997; Sprague et al., 2000), metalochlor (Seta and Karathanasis, 1996), prochloraz (de Jonge et al., 1998), glyphosate (de Jonge et al., 2000), lead (Karathanasis et al., 2005), copper and zinc (Karathanasis, 1999; Karathanasis et al., 2005), phosphorus (McGechan, 2002; de Jonge et al., 2004b; Makris et al., 2006), plutonium (Ryan et al., 1998), and cesium and strontium (Mohanty et al., 2011). Most of the previous research with macropores has either used undisturbed soil monoliths or field conditions, which are both difficult to characterize. In addition, the solutes investigated were usually herbicides or pesticides. No research has been conducted to examine the effects of colloid-facilitated transport of cesium in a well-defined quartz system.

Radionuclides such as cesium are of particular interest due to their abundance in contaminated vadose zone soils at Department of Energy (DOE) sites in the United States and because they exhibit varying sorption kinetics with clay minerals such as illite. Cesium also remains as a surface contaminant in much of eastern Europe from the Chernobyl disaster and around the Fukushima Daiichi Nuclear Power facility in Japan. More precise experiments are necessary to better understand the risk associated with cesium transport from soils with macropores, especially in the presence of colloids and under variable saturation. Our research will utilize a well-characterized quartz system to investigate the main variables controlling colloid-facilitated transport in unsaturated porous media systems with a macropore present. In addition, this simplified system allowed for strict control of initial and boundary conditions to provide data for future modeling applications. The explanation of the transport parameters and mechanisms will be organized by following the conceptual model presented in the next section.

Conceptual Model. A conceptual model (Figure 5.1) shows the interactions between the porewater (with cesium and colloids) in the matrix and macropore sand. At matrix S_{eff} = 1.0, the matrix sand and macropore are both saturated and the higher hydraulic conductivity of the macropore leads to fast flow through the macropore. At matrix S_{eff} = 0.80, the macropore is still saturated and conducts even more porewater than for S_{eff} = 1.0 due to the 20% trapped air in the matrix pores resisting flow. At matrix S_{eff} = 0.21, the suction in the matrix is below the air entry pressure of the macropore resulting in almost all of the flow traveling through the matrix sand.

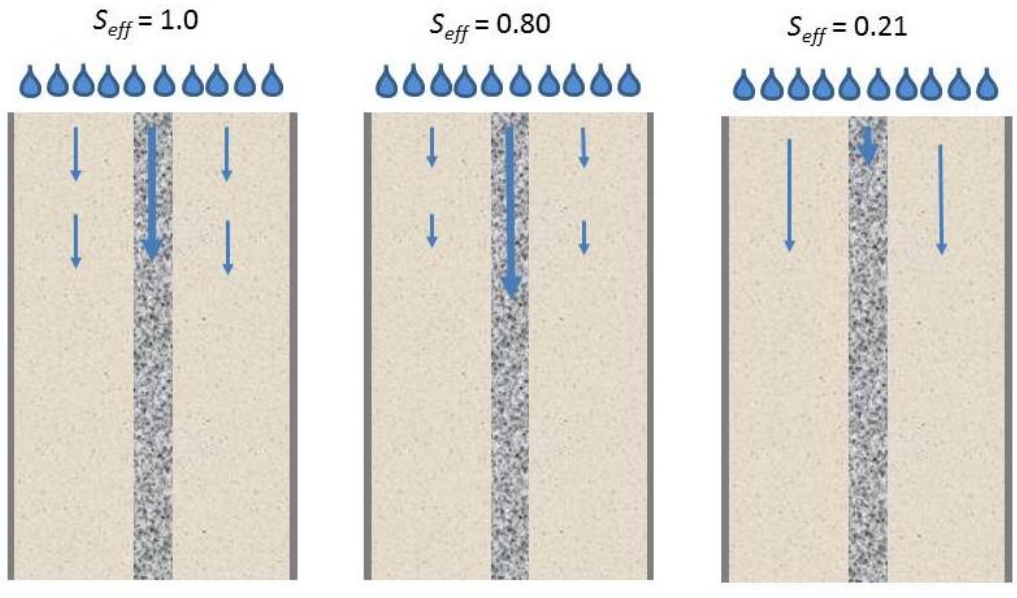

Figure 5.1. Conceptual model for unsaturated colloid-facilitated transport mechanisms. Thick blue arrows represent slow water moving through the matrix sand and thick blue arrows represent faster water moving through the macropore. The length of the arrows represents the amount of water moving through the matrix or macropores. For S_{eff} = 1.0, water will move through the matrix and macropore sand. For S_{eff} = 0.80, more water will move through the macropore due to the 20% air trapped in the matrix sand, which will restrict the flow through the matrix. For S_{eff} = 0.80, most of the water was transported through the matrix sand.

Purpose of Research. The transport of colloids has been well-studied in recent years; however, there are very few examples of experiments studying the effect of a macropore on unsaturated colloid-facilitated transport through a well-characterized quartz sand system. Our experiments are designed to investigate the combined effect of macropore flow and unsaturated conditions on the enhanced transport of cesium. Most colloid-facilitated experiments are conducted using either homogeneous sand or columns packed with dried and sieved soils which overlook the effect that a macropore can have on determining where flow occur will occur. Recent work has found colloid-facilitated transport increased cesium transport in Hanford sediments (Cheng and Saiers, 2010); however, the complexity of natural sediments prevented the analysis to make conclusions about the effect that binding strength and kinetic rates played on enhanced transport.

Since most natural soils have some sort of physical heterogeneity (worm or filled animal burrow, cracks, decayed root channels, or some other preferential flow paths), these experiments will provide a better insight into how colloid-facilitated transport increases the transport of cesium based on desorption kinetics and binding capacities of the colloids and porous medium.

MATERIALS AND METHODS

Overview. Breakthrough experiments were performed to help understand dissolved and colloid-associated cesium transport during steady saturated and unsaturated conditions with and without a macropore. Cesium was selected due to its prevalence on US Department of Energy (DOE) sites and because of its desoption kinetics with illite. Illite clay particles have been shown to have two physically distinct binding sites (weak, kinetically fast binding sites on the planar faces and strong, kinetically slow binding sites on the frayed edges). The use of a well-characterized sand system allowed us to interpret the complex relationships between particle transport, sorption kinetics, and fluid transport in two distinct zones (matrix and macropore).

Column experiments were conducted to test the effect of three variables on cesium transport: (1) colloid concentration (0 or 100 mg L^{-1}), (2) presence of a macropore, and (3) relative saturation (S_{eff} = 1.0, 0.80, or 0.21).

Experiments were conducted with relative saturation values (S_{eff}) in the matrix sand of 1.0, 0.81, and 0.21, where S_{eff} is the normalized amount of pore space that is filled with water in relation to the residual water content,

$$S_{eff} = \frac{\theta - \theta_r}{\theta_S - \theta_r} \tag{5.1}$$

where θ is the experimental moisture content ($m^3\ m^{-3}$), θ_S is the moisture content at saturation ($m^3\ m^{-3}$), and θ_r is the residual moisture content ($m^3\ m^{-3}$). The flow rate was maintained within 5% of 30 mL min^{-1} for all experiments, resulting in average linear porewater velocities that increased as S_{eff} decreased.

Colloid concentration (100 mg L^{-1} ± 5.2), ionic strength (0.1 mM), and pH (7.3 ± 0.1) were all within ranges expected to be found in contaminated natural soil systems. Once steady moisture conditions were established, the background solution was switched to the desired experimental solution. Effluent samples were collected at 25 min intervals. Experiments were run until the normalized effluent concentration (C/C_0) exceeded 0.90. The influent solution was then switched to the background solution (0.1 mM $NaHCO_3$) and continued for 20-40 additional pore volumes. The conditions of the breakthrough experiments are summarized in Table 5.1.

Table 5.1. Experimental conditions for 10 breakthrough experiments with cesium and illite colloids with a macropore. S_{eff} was the relative saturation, and *Cc* was the colloid concentration.

Exp. #	Relative Saturation (S_{eff})	C_c (mg L^{-1})	Macropore
1	1.0	0	N
2	1.0	0	Y
3	1.0	100	N
4	1.0	100	Y
5	0.80	0	N
6	0.80	0	Y
7	0.80	100	N
8	0.80	100	Y
9	0.21	0	N
10	0.21	0	Y
11	0.21	100	N
12	0.21	100	Y

Colloid Preparation. Illite were purchased from the Clay Minerals Society Source Clays Repository (Purdue University). The illite pieces (IMt-2) were ground to a powder using a ceramic mortar and pestle and blended (Osterizer, Model 6630) into a slurry for 20 minutes with high purity water (> 18 MΩ resistivity). The slurry was rinsed repeatedly with 0.1 mM sodium bicarbonate (Mallinckrodt AR®, analytical reagent) to replace any sorbed cations (calcium, magnesium, etc.) with sodium. This procedure is described in detail in Chapter 3 and 4. The colloidal fraction of the illite slurry was separated from larger particles by settling with 0.1 mM sodium bicarbonate in a large tub for 24 hours at room temperature (~22 °C ± 2). The top 18.5 cm was carefully removed and stored. Particle size analysis was determined for each sample.

pH and Colloid Concentration Measurements. pH of suspensions and samples was measured using a pH probe (Orion, 9107BN) and pH meter (Orion, 250A+) calibrated with low ionic strength buffer solutions (Orion, Purewater®). Ionic strength adjuster (5 M $NaNO_3$) was added (0.1 mL per 10 mL sample) to mitigate the effects of ionic strength on pH measurements.

Colloid concentration was correlated to turbidity using a turbidimeter (Hach, 2100N). The factory calibration checked with 0.1, 1, 10, and 100 NTU Formazin gel standards (Hach, Gelex®, 25890-00). Linear calibration for illite was determined using colloid concentrations of 1, 10, 50, 100, and 200 mg L^{-1} made as dilutions from the settled IMt-2 illite. The mass concentration of the colloid suspensions was determined gravimetrically. Four 0.1 µm filters (MilliPore®, 25 mm diameter) were weighed and 25 mL of the colloid suspension was passed through each filter. The filters were dried at 80 °C for 24 h and re-weighed. The difference in mass was divided by the suspension volume to give the colloid concentration. A linear regression resulted in the relationship between colloid concentration, C_c, (mg L^{-1}) and turbidity, T, in nephelometric turbidity units (NTU):

$$C_c = 0.824 \times T + 0.277 \qquad (R^2 = 0.97) \qquad (5.2)$$

Colloid Size Distribution Measurements. The particle size distribution in the illite suspensions was measured by dynamic light scattering (Particle Sizing Systems, NICOMP 380 ZLS). The colloidal suspension was diluted to 0.2 mg L^{-1} with 0.1 mM sodium bicarbonate solution to reduce the scattering intensity of the instrument to between 250 and 350 kHz. A 30 minute run time was used and the mean particle diameter and standard deviation were determined for a Gaussian distribution (Particle Sizing Systems, 2006).

Solution Chemistry. The background solution was made to simulate the chemistry of rainwater that had just entered the vadose zone. A 0.05 M stock solution of sodium bicarbonate was prepared with high-purity water and 2 mL stock per 1 L water and was allowed 24 hours to equilibrate with the atmosphere (1655 m above sea level). The pH was measured to be 7.3 (±0.1).

7.5×10^{-7} M cesium was made by adding stock solutions to 0.1 M sodium bicarbonate. The stock solutions were made with cesium chloride ($CsCl \bullet 6H_2O$) salt (MP Biomedicals, Cat. No. 150589). A small amount of ^{137}Cs (approximately 2.5×10^{-10} M) in the form of $^{137}CsCl$ dissolved in HCl (Eckert and Ziegler Isotope Products,Valencia, CA) was added as a tracer to the cesium solution.

Measurement of ^{137}Cs and ^{90}Sr by Liquid Scintillation Counting. The exact activity of the ^{137}Cs was measured by liquid scintillation counting (Packard, Tri Carb 1600TR). The main advantage of measuring cesium concentration by liquid scintillation counting of beta decays was the capability to measure total, dissolved, and sorbed cesium in clay suspensions without the need to digest the samples. Based on the long half-life of ^{137}Cs (30.2 y), radioactive decay was

negligible and not accounted for in calculations. A 2 mL aliquot of sample was added to 5 mL of scintillation cocktail (Packard, Ultima Gold) in a 7 mL borosilicate glass liquid scintillation vial.

A 0 to 2,000 keV detection window was used. The counts were time-averaged for 5 minutes and the resulting count rate (counts per minute, or CPM) was correlated with a linear regression to 0, 10^{-7} 10^{-6}, 10^{-5}, 10^{-4}, 10^{-3} M standards. The quench of the sample (loss of signal due to sample conditions) was measured using the transformed Spectral Index of External Standard (t-SIE), which was calculated using the external ^{133}Ba source inducing a Compton spectrum in the scintillation cocktail.

Total cation concentrations were determined by liquid scintillation counting of the unfiltered samples. Dissolved cation concentrations were measured by passing samples through a 0.2 μm filter (Millipore Millex® GN, nylon, 13 mm diameter) and analyzing the filtrate concentration. The difference between the total and dissolved cation concentration was calculated to be the colloid-associated cation concentration.

Colloid Suspensions. Before use, the stored illite colloids were sonicated for 30 min in 1 L batches and added to atmosphere-equilibrated background solution to make a final concentration of 100 (± 5.2) mg L^{-1}. Stock 0.1 M cesium solution and a small amount of ^{137}Cs (30 μL/L) were added to make 7.5×10^{-7} M cesium. Preliminary adsorption experiments showed that equilibrium was approached within a few hours; however, the colloids were equilibrated with the cations for 24 h before each experiment to ensure consistency with other published results.

Porous Media. Sand used for the matrix and macropore were purchased separately and processed in the same manner as described in previous chapters. Well-rounded, medium sphericity Ottawa quartz sand (Accusand 40/60, Unimin Corp.) was used as the matrix porous

media and well-rounded, medium sphericity Ottawa quartz sand (Accusand 12/18, Unimin Corp.) was used as the macropore porous media. Roundness and sphericity were determined comparing microscope images to the Krumbein roundness chart and Riley sphericity index (Krumbein and Sloss, 1963). The sand was comprised of 99.8% SiO_2, less than 0.1% metal oxides (Ti, Fe, Al, K, Mg, Na, and Ca), and less than 0.1% organic compounds based on loss of ignition measurements (Unimin Corp.).

The sand was rinsed with high-purity water and dried before it was sorted through stainless steel sieves using a sieve shaker (W.S. Tyler, RX-29 Ro-Tap) according to ASTM D 422-63[1] (Rowell, 1994). The fraction of Accusand 40/60 that passed through a 45 mesh sieve (354 μm) and was retained on a 50 mesh sieve (297 μm) was assumed to be $d_{50} = 325$ μm. The fraction of Accusand 12/18 that passed through a 12 mesh sieve (1.40 mm) and was retained on a 14 mesh sieve (1.68 mm) was assumed to be $d_{50} = 1.57$ mm.

The sieved sand was cleaned using a procedure similar to the procedure used by Lenhart and Saiers (2002). The sand was soaked in a nitric acid solution (10% by volume) for 36 h to dissolve any adsorbed metals and then rinsed with high-purity water until water passing through reached pH 5.7. The sand was then transferred to 1 L HDPE bottles and placed on a shaker table (150 oscillations per minute) for 2 h to remove dust and silica particles. The sand was then rinsed with high-purity water until the pH of the rinse water reached 5.7 and turbidity measurements were below 0.4 NTU. The sand was oven dried at 80°C for 16 h and sealed in a clean PVC bucket until use in breakthrough experiments.

Analysis of Sand Composition. The quartz grain surfaces were imaged with a low vacuum scanning electron microscope (LVSEM, JSM-6480LV) to visually inspect the morphology and surface roughness of the grains. Energy dispersive x-ray (EDS) spectroscopy (JEOL, Noram

System Six) was used to analyze the sand for elemental composition. Sand grains were mounted on metal studs with double-sided carbon tape and viewed in the LVSEW at a pressure of about 1 Pa, 10-15 kV accelerating voltage, and a spot size near 50 μm. Focus and stigmation were iteratively adjusted and images with magnification of 10,000× were captured and compared to archived pictures to qualitatively estimate sphericity and roundness of the grains (Krumbein (Krumbein and Sloss, 1963).

Column Set-up. A 1.3 cm (½") thick cast acrylic tube (12.7 cm diameter, 32.8 cm length) was used as the column. The tube was suspended from a PVC ring screwed to the middle of the column and supported by a wooden frame in the containment tank (Figure 5.2). A 45° bevel on the top edge of the column shed excess rainfall away from the center of the column. Experimental solutions were applied to the top of the column with a rainfall simulator. The rainfall simulator was made from two 13.7 diameter disks and a ring of 1.3 cm acrylic plastic with a threaded barb fitting installed in the top and attached to the influent pump tubing. Holes (38) were drilled in the bottom disk of the rainfall simulator with 1.25 cm spacing to accept Luer-Lok® fittings. Stainless steel hypodermic needles (BD PrecisionGlide, 25-guage, 305456) were then screwed into the Luer-Lok® fittings. The rainfall simulator was suspended 1 cm above the top of the sand surface to minimize potential disturbances to the sand surface due to the erosive force of the falling drops. The sand in the column was supported by an acrylic plastic disk with a pattern of holes (38) covered with 104 μm mesh size stainless steel screen (Spectra/Mesh®). This prevented sand from entering the tubing while still allowing the clay colloids to pass through without clogging. Luer-Lok® fittings were inserted in holes in the bottom disk and connected with tubing to an acrylic plastic manifold. All mating surfaces between the column and bucket were sealed with silicone adhesive.

Three peristaltic pumps and controllers regulated the fluid flow in the experiments. One pump transferred solution from the influent tank to the rainfall simulator. Column effluent from the manifold was split with a y-connector. A small amount (0.5 mL min^{-1}) was pumped to a fraction collector (U-200 Universal, Eldex) filled with filled with polystyrene test tubes (15 cm length × 1 cm diameter) and the rest of the effluent (about 29 mL min^{-1}) was pumped (Cole Parmer, Masterflex®,7553-20 pump motor, Easy Load II LS pump head) to a waste container.

Excess rainfall from experiments with S_{eff} values of 1.0 and 0.80 was allowed to flow over the edge of the column into a PVC collector and was pumped to the waste collector. The column experiments were conducted inside a large (1.2 m length, 0.9 m depth, and 0.6 m width) containment tank made of 1.3 cm acrylic plastic to shield emission of beta radiation and to contain any potential spills.

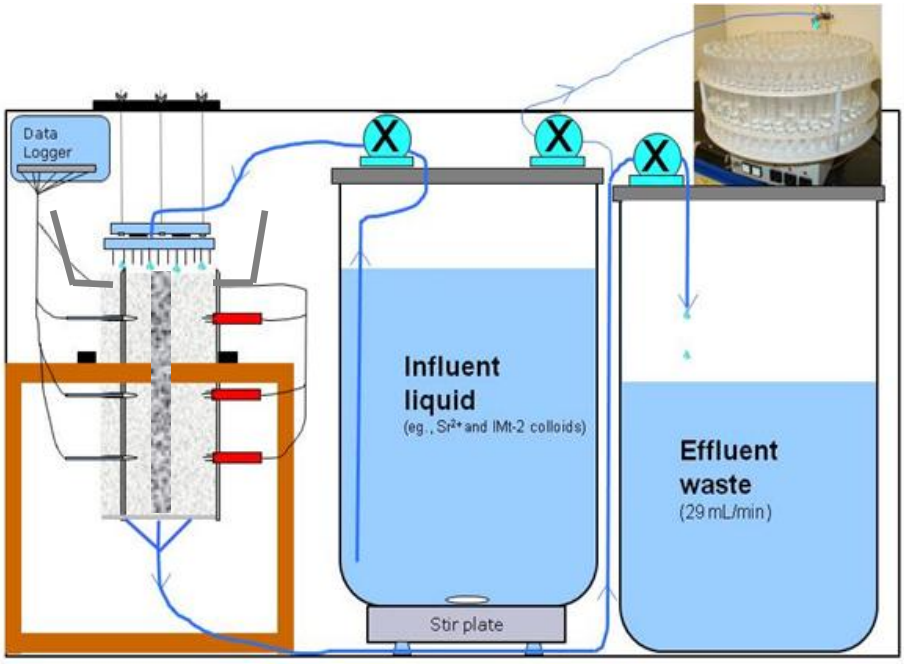

Figure 5.2. Experimental set-up used for breakthrough experiments. A peristaltic pump transferred influent solutions and colloid suspensions to the rainfall simulator at the top of the column. Two other peristaltic pumps removed effluent from the bottom of the column and separated the flow into a sample stream that went to a fraction collector and a waste stream.

The macropore sand properties were also tested using a borosilicate glass liquid chromatography column (2.5 cm diameter and 15 cm long; Kontes®) (details in Chapter 3). Bromide breakthrough, dissolved cesium transport, and colloid-facilitated transport of cesium were tested to provide parameters for the mathematical model (quartz sorption rate coefficients and sorption capacity).

Initial Column Packing. The small column was wet packed according to the procedure in Chapter 3. The large column was wet-packed according to the following procedure. A 2 cm diameter thin-walled brass pipe was positioned vertically in the center of the column. Background solution was poured in from the top of the column to a depth of 2 cm. Increments of d_{50} = 0.325 mm sand (50 g) were added to the column outside of the pipe and increments of d_{50} = 1.57 mm sand (7 g) were added to the inside of the pipe. After each addition, the matrix sand was stirred with a polystyrene rod to minimize layering. After every 2-3 cm of sand added, the column and pipe were tapped on all sides with a rubber mallet to ensure uniform packing and consistent porosity between experiments. The weights of matrix and macropore sand and background solution added to the column were recorded and used to confirm the porosity. The pipe was removed by tapping the side at a high frequency (about 5× per second) to liquefy the sand and allow for the tube to be pulled out while the macropore and matrix sand remained in place. Background solution was then passed through the column for 5 to 10 pore volumes until effluent pH and turbidity stabilized to pH 7.3 ± 0.1 and below 0.3 ± 0.1 NTU, respectively.

Measurement of Porous Medium Moisture Content and Tension. The column was instrumented with three moisture sensors (Delta-T Devices Ltd., ML2x ThetaProbe) located 7.7, 16.4, and 25.1 cm from the top of the column and two tensiometers located 7.7 and 16.4 cm from the top. All sensors measure the matrix porous medium properties. The moisture sensors

measured the apparent dielectric constant, k_a, of the air-water-sand system, which was correlated to volumetric moisture content ($m^3\ m^{-3}$). The tensiometers measured the change in resistance of a silica wafer/wheatstone bridge system connecting to a ceramic tip contacting the porous medium and were correlated to porous medium tension (cm H_20) though calibration at various suction values (0 to 80 cm).

The tensiometers were constructed according to a design of Eching and Hopmans (1993) with high-flow ceramic cups (Soil Moisture Corp., 2100-200CR-B1M3) and differential pressure transducers (Honeywell/Microswitch, 26PCAFA6D). Data from the tensiometers and moisture probes was monitored using a data logger (Delta-T Devices, Ltd., DL2e) to ensure uniform conditions along the depth of the column and steady conditions during the duration of breakthrough experiments.

Establishing Steady Flow Conditions. For unsaturated experiments, the column was drained to the residual moisture content θ_r ($\theta_r = 0.05$) and then re-wetted to the desired S_{eff} with background solution. For $S_{eff} = 1.0$ and 0.80, solution was allowed to pond above the sand surface approximately 0.5 cm. For $S_{eff} = 0.21$, the rainfall simulator was used to apply the simulated groundwater to the top of the column and the effluent pump was set to a slightly higher rate than the influent pump to maintain consistent unsaturated conditions for the duration of the experiment. Effluent was pumped from the bottom of the column at a rate of 28.0 to 32.0 mL min^{-1} for all experiments and the flow rate was periodically measured and recorded.

Measuring Porous Medium Hydraulic Properties. Hydraulic properties of the sand were determined by bromide tracer tests for $S_{eff} = 1.0$, 0.80, and 0.21 using 4.0 mM NaBr solution. Bromide was measured using a bromide-specific electrode (Accumet, Cat. No. 13-620-525) and

meter (Orion, 720A) calibrated with 10^{-2}, 10^{-3}, 10^{-4}, 10^{-5}, and10^{-6} M bromide solutions (Fisher Scientific, S255-500).

Computer Model. The colloid-facilitated transport code developed by (Turner et al., 2006a) was modified to model the experimental results with a macropore present (see Chapter 2 for a detailed description). A MATLAB® code solves the Richards' equation for water movement and accounts for the presence of cations and colloids. Velocities used in the 1D transport model for matrix and macropore zones were calculated as:

$$V_{zone} = \frac{Q f_{zone}}{A_{zone} n S_{eff}} \tag{5.2}$$

where V_{zone} is the velocity in the respective zones (cm h^{-1}), Q is the influent flow rate (mL $h^{-1)}$, f_{zone} is the fraction of flow through the respective zones, A_{zone} is the aerial surface area (121.77 cm^2 for matrix and 4.91 cm^2 for macropore), n is the sand porosity, and S_{eff} is the effective saturation. Results from the bromide breakthrough experiments were used to determine the fraction of flow through the matrix and macropore zones, f_{zone}.

The model was used to analyze each zone separately and the results were added together for analysis. Minimal interaction between the interfaces of the matrix and macropore sand was assumed. A predictor-corrector scheme was used to solve the nonlinear surface chemistry equations and non-linear, two-site sorption was used to represent the different kinetics exhibited by the strong edge sites and weaker face charges found on the illite surface. The rate coefficients controlling colloid and cation transport were determined by fitting the experimental results with a least-squares parameter optimization code. Model simulations were implemented within MATLAB® (Version 7.11.0, The Mathworks, Natick, MA). The special discretization, Δx, and timestep, Δt, used in the model were adjusted to ensure mathematical stability. The Peclet

number, $N_{Pe_{,,}}$ and Courant number, *Cr*, represent the dimensionless ration of advection to dispersion and transport distance to special discretization, respectively (See Appendix H) (Clark, 1996; Zheng and Bennett, 2002).

RESULTS

Illite and Sand Characterization. Sequential filtering using 3.0, 0.8, 0.45, 0.2, 0.1, and 0.02 µm syringe filters (Millipore Millex® GN, nylon, 13 mm diameter; Whatman Anotop 10, inorganic membrane, 10 mm diameter) method showed that 79.5% (± 0.1) of the illite colloids were between 3.0 µm and 0.80 µm in diameter for three samples (Figure 5.3). The exact particle size (assuming uniform, spherical particles) was measured by dynamic light scattering (NICOMP, PS-380). The intensity-weighted mean diameter of illite colloids the suspension was measured to be 1793.4 µm (± 76.7) for a Gaussian distribution. SEM images show the well-rounded nature of the matrix and macropore sand (Figure 5.4).

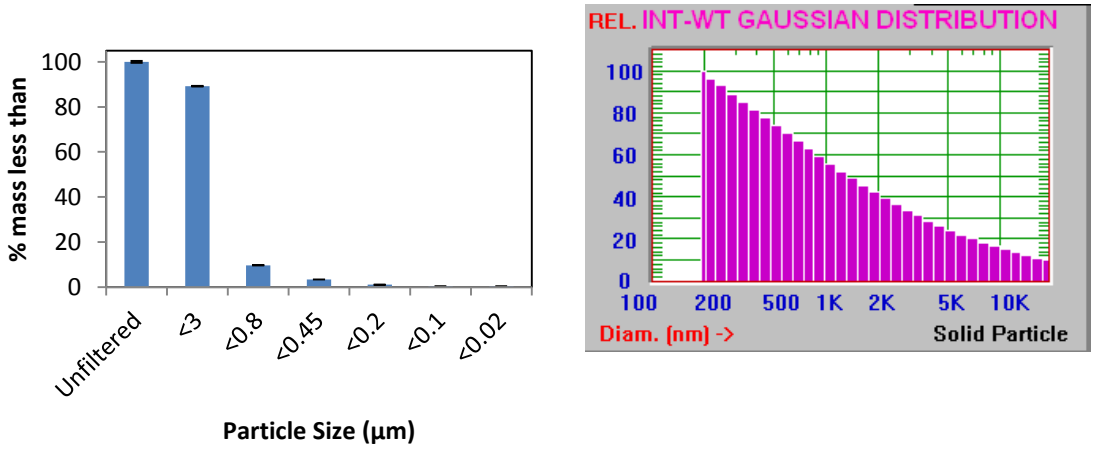

Figure 5.3. Result of sequential filtering (left) with the percent of mass from a 100 mg L^{-1} sample passing through the filter on the y-axis and the corresponding filter size on the x-axis. The intensity weighted Gaussian distribution (right) shows particle size on the x-axis and the percent of particles that are smaller than the size range on the y-axis.

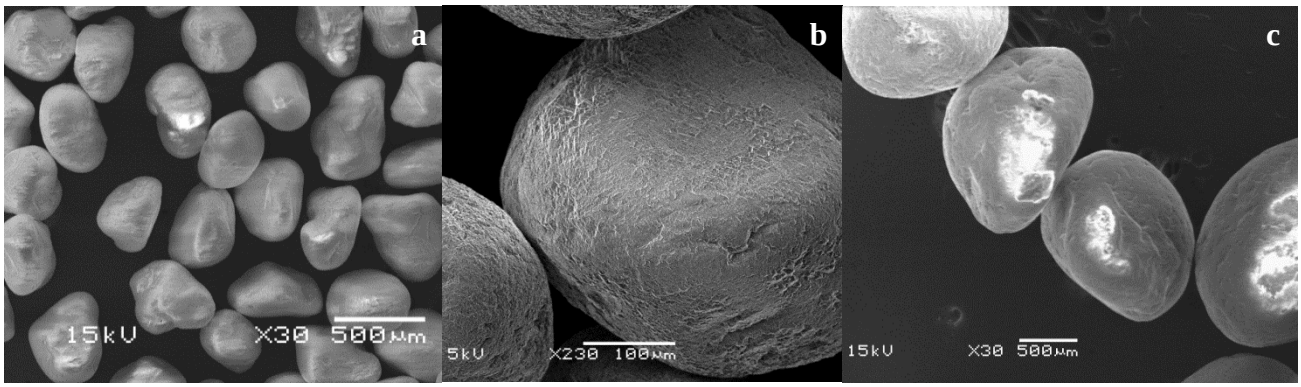

Figure 5.4. LVSEM images of matrix quartz grains under magnification of 30× (a), 230× (b), and macropore quartz grains under magnification of 30× (c).

Effect of S_{eff} and Macropore on Conservative Tracer Transport. Bromide breakthrough with homogeneous sand occurred after 1535 mL, 1265 mL, 767 mL for S_{eff} = 1.0, 0.80, and 0.21, respectively (Figure 5.5). With a macropore, bromide breakthrough occurred after 1945 mL, 1780 mL, and 725 mL for S_{eff} = 1.0, 0.80, and 0.21, respectively (Figure 5.5). For macropore experiments with S_{eff} = 1.0 and 0.80, a primary maximum plateau was observed near C/C_0 = 0.32 and 0.43, respectively, followed by a secondary maximum when C/C_0 approached 1.0. For S_{eff} = 1.0, a very small primary plateau of about 1.5% was observed and breakthrough occurred less than 5% sooner than without a macropore.

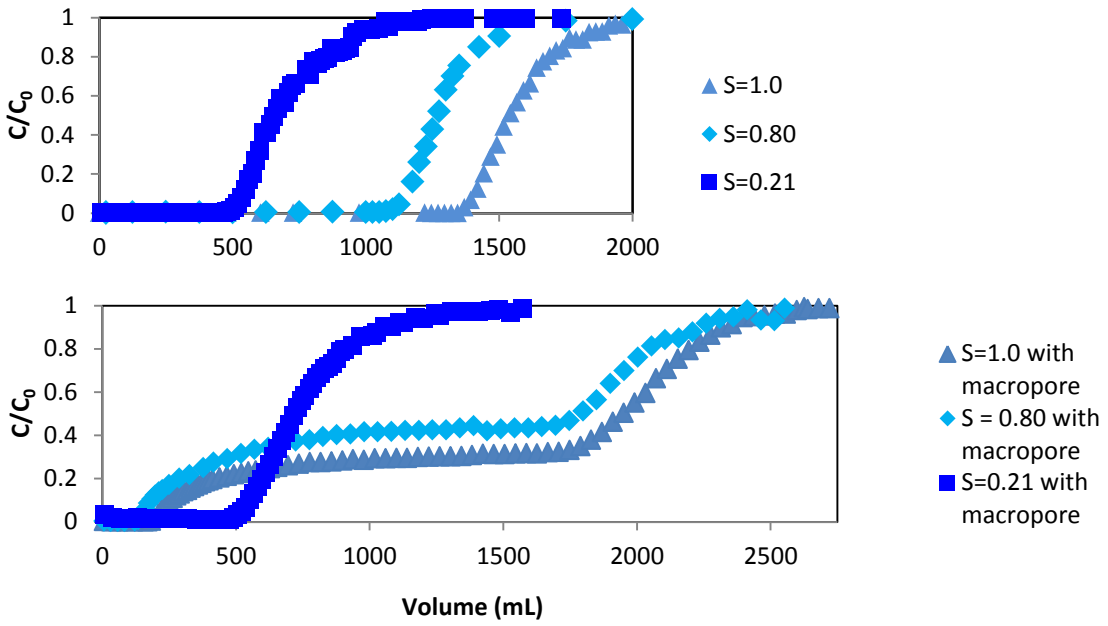

Figure 5.5. Bromide tracer data for relative saturation (S_{eff}) equal to 1.0 (light blue triangles), 0.80 (cyan diamonds), and 0.21 (blue squares) without and with a macropore (top and bottom graph, respectively). Volume of water (mL) passed through the column is plotted on the x-axis and relative concentration (C/C_0) is on the y-axis.

Effect of S_{eff} and Macropore on Dissolved Cesium Transport. Without a macropore present, 50% breakthrough occurred after 40, 44, and 42 pore volumes for S_{eff} = 1.0, 0.80, and 1.0, respectively (Figure 5.6). All of the cesium for the first 30 pore volumes was adsorbed to the sand surface and removed from solution. After cesium was measured in the effluent, the concentration increased linearly until the effluent concentration was 100% of the influent concentration. The location of C/C_0 = 0.5 did not change with different values of S_{eff}. After switching to background solution, the first 10 pore volumes of background solution remained at a concentration near C/C_0=1 before slowly decreasing until the end of the experiment (Figure 5.6). $C/C_0 < 0.5$ occurred after 30 pore volumes for all S_{eff}.

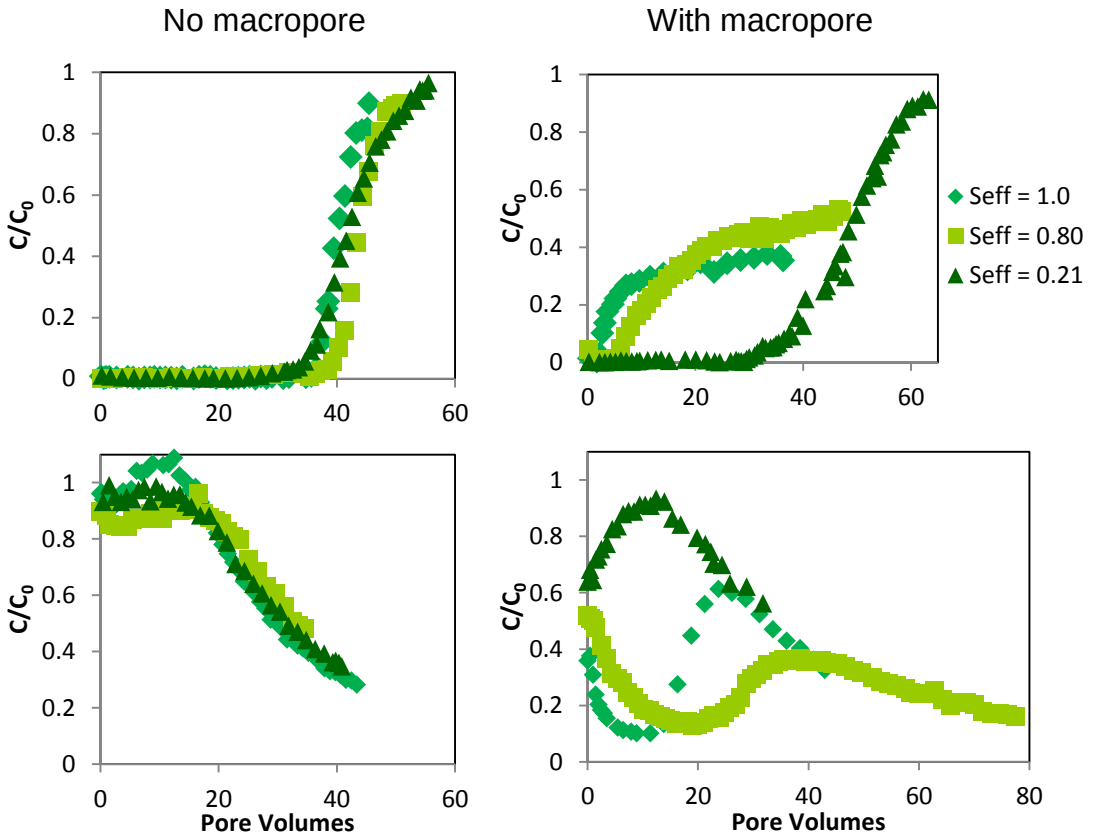

Figure 5.6. Dissolved cesium breakthrough without macropore (top left) and with macropore (top right) compared with aqueous cesium breakthrough without macropore (bottom left) and with macropore (bottom right) for S_{eff} =1.0 (diamonds), 0.80 (squares), and 0.21 (triangles).

With a macropore and for S_{eff} = 1.0 and 0.80, cesium appeared in the effluent after 2 and 5 pore volumes, respectively (Figure 5.6). The concentration quickly increased until C/C_0 approached 0.25 and 0.36 for S_{eff} = 1.0 and 0.80, respectively, then slowly increased after that. 50% breakthrough ($C/C_0 > 0.5$) occurred near 65 pore volumes (extrapolated from a linear projection), 45 pore volumes, and 49 pore volumes for S_{eff} = 1.0, 0.80, and 0.21, respectively. For S_{eff} = 0.21, cesium breakthrough was similar to experiments without a macropore. No cesium was measured in the effluent until after 30 pore volumes. Cesium concentration then increased linearly until approaching C/C_0 = 1.0. After switching to background solution, the effluent

concentration with S_{eff} = 0.21 decreased slowly with the same behavior as without the macropore (Figure 5.6). Concentration for S_{eff} = 1.0 decreased rapidly to a minimum near C/C_0 = 0.10 after 11 pore volumes before rapidly increasing back to C/C_0 = 0.61 within 10 pore volumes. Similarly, the experiment with S_{eff} = 0.80 showed a rapid decrease to C/C_0 = 0.13 after 15 pore volumes, then an increase back to C/C_0 = 0.35 before decreasing again. A summary of the dissolved cesium transport results is provided in Table 5.3.

Table 5.3. Experimental conditions for dissolved cesium breakthrough experiments with average pore water velocity (U) and cumulative pore volumes of solution passed through the column (PVs, 1511 mL = 1 PV). PVs until $C/C_0 > 0.5$ represents breakthrough.

Cation		S_{eff}	Q (mL min^{-1})	PVs until 50%
[Cs^+]	Macropore			
7.5×10^{-7}	No	1.0	24	40
7.5×10^{-7}	Yes	1.0	30	65*
7.5×10^{-7}	No	0.80	30	44
7.5×10^{-7}	Yes	0.80	29	45
7.5×10^{-7}	No	0.21	30	42
7.5×10^{-7}	Yes	0.21	30	49

*Linear extrapolation from experiment that ended prior to 50% breakthrough

The model was able to simulate the dissolved cesium breakthrough behavior relatively well with and without a macropore present. Based on the bromide breakthrough results, 32%, 43% and 1% of the total flow was assumed to be attributed to macropore flow for S_{eff} = 1.0, 0.80, and 0.21, respectively (Figure 5.7). By using these values for f_{zone}, the model was able to predict the primary plateau for S_{eff} = 1.0 and 0.80, as well as the delayed secondary maxima after switching to background solution. For S_{eff} = 0.21, the breakthrough with a macropore was very similar to the homogeneous experiment presented in the previous chapter.

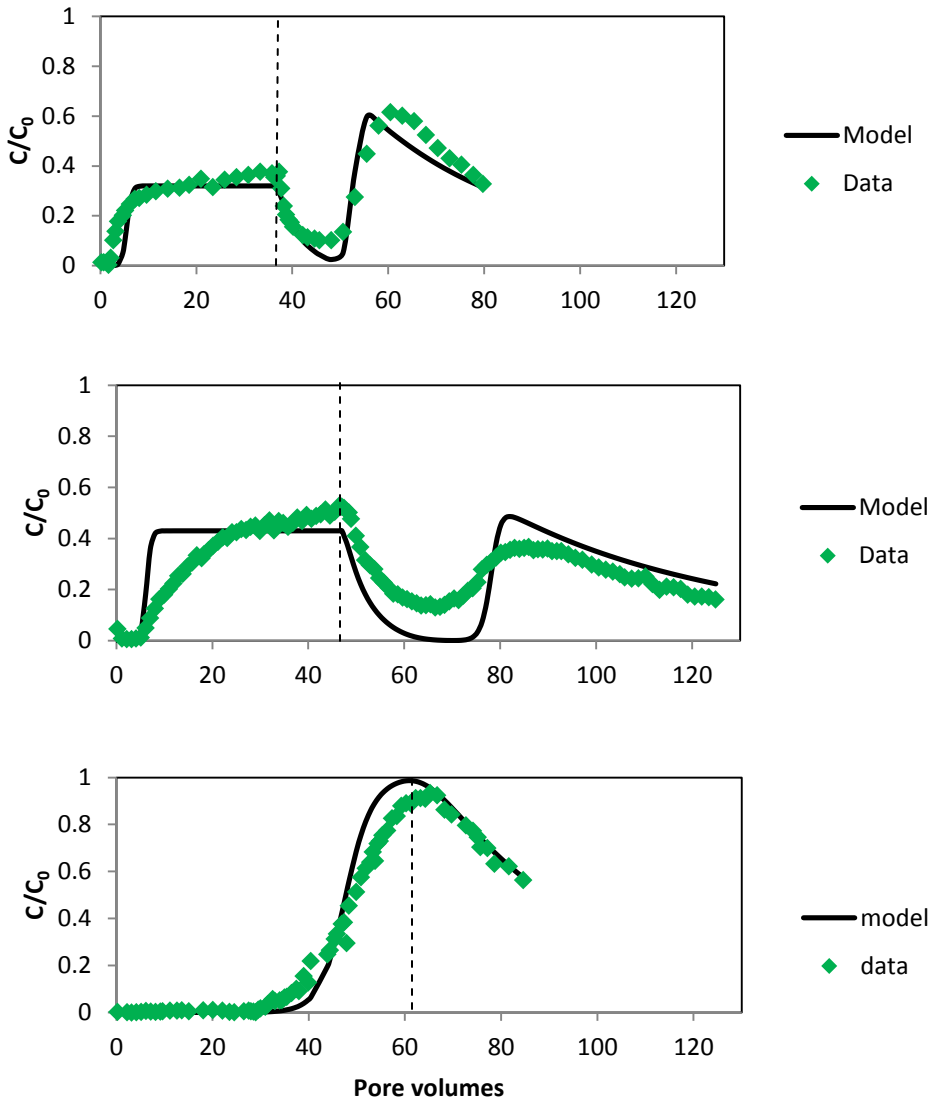

Figure 5.7. Dissolved cesium breakthrough for macropore experiments for S_{eff} = 1.0 (top), 0.80 (middle), and 0.21 (bottom). Diamonds denote cesium breakthrough data and lines show model fits. Dashed line denotes when solution was swiched to background solution.

Effect of S_{eff} and Macropore on Colloid Transport. Colloids appeared within one pore volume for all S_{eff} with and without a macropore (Figure 5.8). Breakthrough was very similar for S_{eff} = 1.0 and 0.80, with a rapid increase to C/C_0 = 0.80 and then a slow linear increase reaching C/C_0 = 0.92 after 10 pore volumes. For S_{eff} = 0.21, colloid concentration increased rapidly to

C/C_0 = 0.70, then increased linearly to C/C_0 = 0.89 after 10 pore volumes. After switching to background solution, colloid concentration for all S_{eff} decreased to less than 0.01 within 5 pore volumes. Model simulations reproduced the colloid breakthrough well (Figure 5.9).

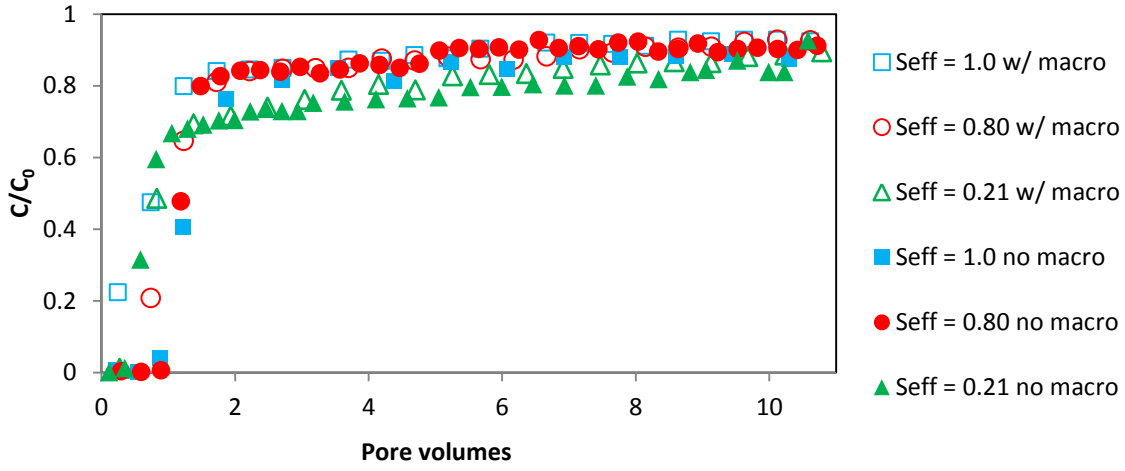

Figure 5.8. Colloid breakthrough with a macropore (open symbols) and without a macropore (closed symbols) for matrix S_{eff} = 1.0 (blue squares), 0.80 (red circles), and 0.21 (green triangles).

Effect of S_{eff} and Macropore on Colloid-Facilitated Transport. Adding 100 mg L^{-1} illite decreased the quartz binding capacity for cesium for all S_{eff}. Breakthrough of total cesium occurred at 7.3, 6.3, and 7.5 pore volumes for S_{eff} values of 1.0, 0.80, and 0.21, respectively (Figure 5.9). The number of pore volumes to breakthrough reflected the assumption that 32%, 43% and 1% of the flow was through the macropore for S_{eff} = 1.0, 0.80, and 0.21, respectively. For S_{eff} = 1.0, the model predicted the total, dissolved, and colloid-associated cesium well. For S_{eff} = 0.80, the model predicted total, dissolved, and colloid-associated cesium

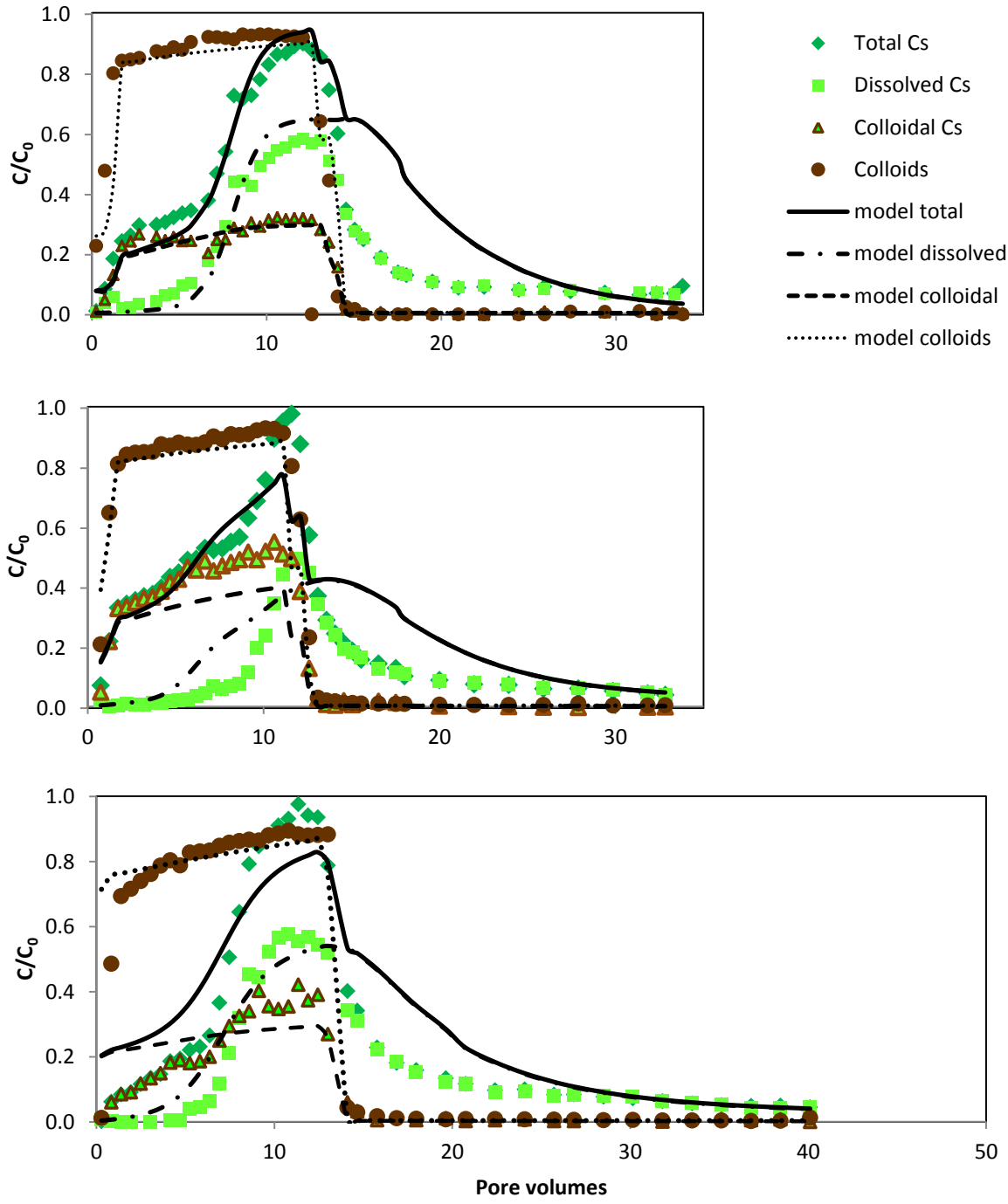

Figure 5.9. Experimental data (symbols) and model results (lines) for breakthrough experiments with a macropore for S_{eff} = 1.0 (top), 0.80 (middle) and 0.21 (bottom).

well for the first 5 pore volumes before over predicting dissolved cesium and under predicting total and colloid-associated cesium. For S_{eff} = 0.21, the model over predicted total and colloid-associated cesium for the first 5 pore volumes, but predicted dissolved cesium well. After switching to background solution, the model over predicted total and dissolved cesium for the first 15 pore volume, then asymptotically approached C/C_0 = 0.05 for all S_{eff}.

DISCUSSION

Mechanisms Responsible for Dissolved Cesium Transport. The presence of a macropore increased bromide transport through the column for S_{eff} = 1.0 and 0.80; however, had little effect on transport for S_{eff} = 0.21 (Fig. 5.10). For S_{eff} = 1.0, the macropore decreased the volume of pore water until bromide was detected (C/C_0 > 0.01) from about 1350 to 182 mL. The primary maximum near C/C_0 = 0.32 suggests that about 32% of the flow was through the macropore and 68% was through the matrix sand. This also corresponded with the 32% increase in volume until complete breakthrough (C/C_0 > 0.99) was achieved (1936 to 2558 mL).

For S_{eff} = 0.80, the macropore decreased the pore volumes until bromide detection from 1070 to 125 mL. The primary maximum near C/C_0 = 0.43 suggests that 43% of the flow was through the macropore and 57% of the flow was though the matrix sand. This also corresponded with the 42% increase in volume until complete breakthrough was achieved (1850 to 2630 mL).

For S_{eff} = 0.21, the macropore had almost no effect on the first detection of bromide (480 to 492 mL) or the volume until complete break through (1248 to 1306 mL), suggesting that at S_{eff} = 0.21, the macropore was almost dry and conducted less than 1% of the pore water. The model simulations for dissolved cesium transport using macropore flow of 32%, 43%, and 1% validate this assumption (Figure 5.7).

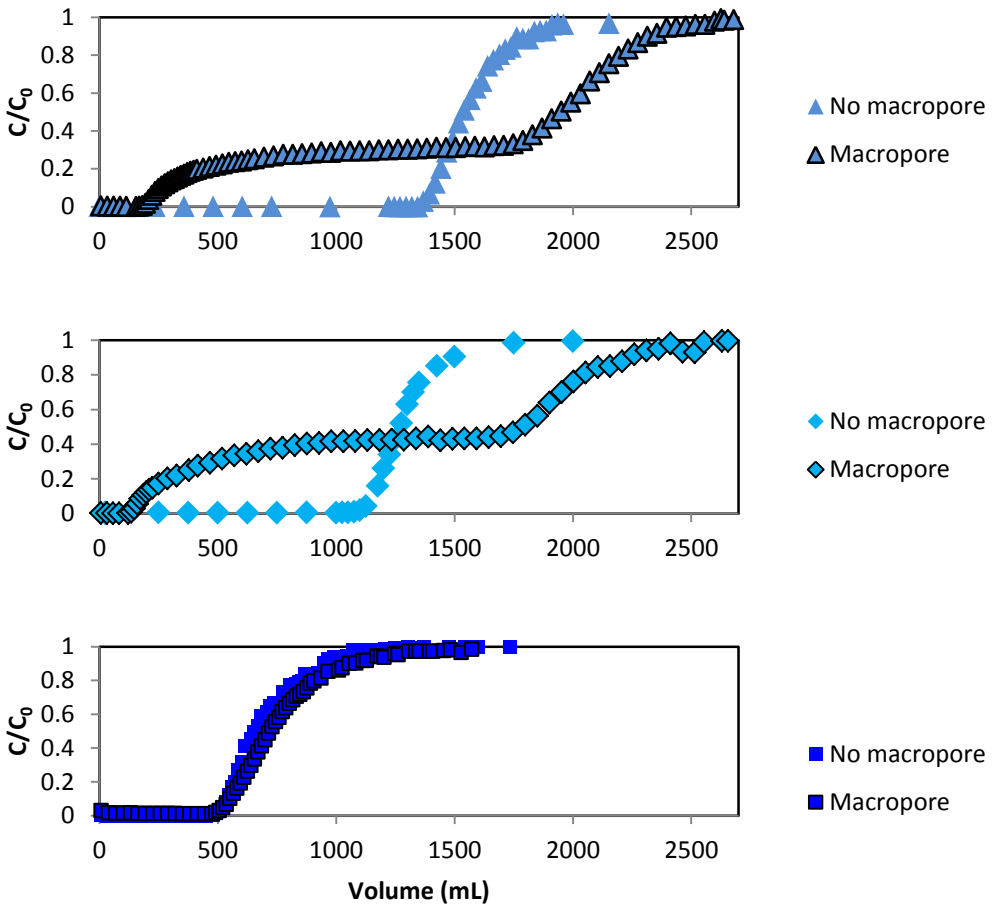

Figure 5.10. Bromide breakthrough curves comparing results with and without a macropore for matrix sand S_{eff} = 1.0 (top), 0.80 (middle), and 0.21 (bottom). Symbols without a border are for homogeneous experiments and symbols with black border are for macropore experiments.

The model parameters for sand adsorption capacity and adsorption and desorption rate coefficients were used directly from homogeneous sand experiments for the matrix and macropore sand without any fitting or optimization required. The slope in the experimental data for S_{eff} = 1.0 and 0.80 is attributed to dispersion and interaction between the interface of the matrix and macropore, and appears to be more significant for S_{eff} = 0.80. Comparison of the

breakthrough data also demonstrates the role of the macropore in increasing transport (Fig. 5.6). Without the macropore, decreasing S_{eff} does not increase the number of pore volumes to breakthrough and also has no effect on the number of porevolumes until $C/C_0 < 0.50$ after switching to background solution.

The macropore decreased the number of pore volumes until dissolved cesium was detected in the column for $S_{eff} = 1.0$ and 0.80 but had almost no effect for $S_{eff} = 0.21$ (Figure 5.7). For $S_{eff} = 1.0$, 32% of the flow was transported through the macropore and within 7 pore volumes the cesium binding sites were mostly occupied and 95% of the cesium in the macropore was measured in the effluent. Once the binding capacity of the macropore sand was occupied, 32% of the influent solution was transported though the column unretarded.

For $S_{eff} = 0.80$, 20% of the matrix sand pore space was filled with trapped air, restricting flow through the matrix sand. This led to more pore water being transported through the macropore (43% based on the bromide breakthrough data) and less traveling thought the matrix (57%) and resulted in a higher primary maximum of cesium in the effluent after 15 pore volumes (Figure 5.7).

For $S_{eff} = 0.21$, the suction in matrix sand pores drained the pores in the macropore sand and less than 2% of the flow was attributed to the macropore. This led to breakthrough behavior that matched $S_{eff} = 0.21$ without the macropore present.

After switching to background solution, the rapid decrease to $C/C_0 = 0.10$ for $S_{eff} = 1.0$ was a result of 32% of the flow moving quickly though the macropore. Since the capacity of the macropore sand was much less than the matrix sand, the macropore sand released most of the adsorbed cesium and then conducted mostly cesium-free background solution. After 11 pore volumes, the pore water traveling slowly through the matrix sand appeared in the effluent. The

secondary maximum in the cesium concentration was a result of the high concentration of cesium in the pore water slowly desorbing from the matrix sand.

The same phenomenon occurred with S_{eff} = 0.80, where the cesium from the macropore sand was readily desorbed within the first 20 pore volumes, then the effluent concentration increased as the pore water moving through the matrix sand mixed with the lower concentration background solution moving through the macropore. A secondary maximum was observed and the total concentration decreased again after 35 pore volumes.

For S_{eff} = 0.21, the release was very similar to the release with no macropore present because the tension in the matrix sand prevented flow through the macropore.

Mechanisms Responsible for Colloid-Facilitated Transport. Macropore flow in the colloid-facilitated transport experiments showed similar results to the bromide and dissolved cesium experiments (Figure 5.11). For S_{eff} = 1.0, the macropore increased the total cesium transported through the column, with over 20% of the total cesium measured before the second pore volume. This was a result of the reduced residence time of the colloids traveling through the macropore, which didn't have enough time to release adsorbed cesium to the pore water. For S_{eff} = 0.80, the same early breakthrough of cesium was observed with a slightly higher maximum. The breakthrough with and without the macropore was similar, suggesting that the effect of adding the colloids is similar to that of adding a macropore. For S_{eff} = 0.21, cesium was detected in the effluent after one pore volume; however, the pore volumes to breakthrough was less.

After the switch to background solution, the desorption tails with S_{eff} = 1.0, 0.80, and 0.21 with a macropore were very similar to each other and almost the same as for S_{eff} = 1.0 and 0.80 without the macropore. This was caused by the decreased residence time from macropore flow.

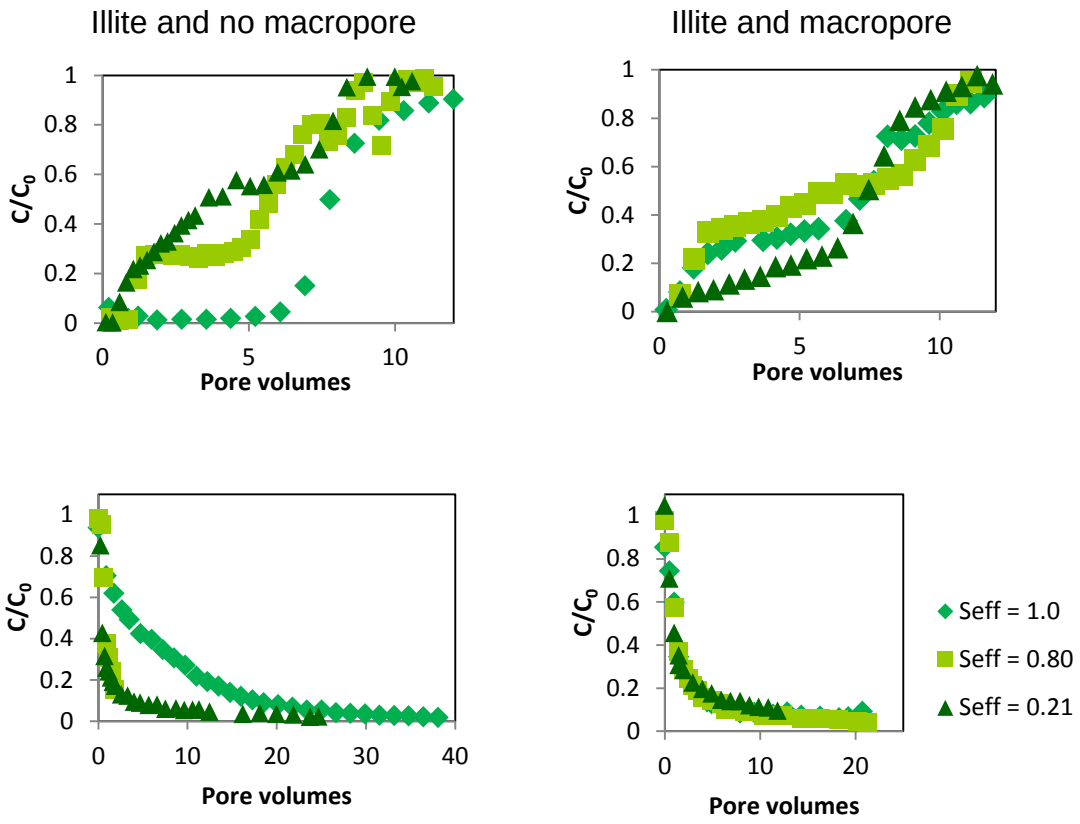

Figure 5.11. Colloid-facilitated transport of cesium without macropore (top left) and with macropore (top right) compared with cesium release without macropore (bottom left) and with macropore (bottom right). Symbols represent total cesium for S_{eff} =1.0 (diamonds), 0.80 (squares), and 0.21 (triangles).

Hypothesis Validation. Experiment and modeling results validated our main hypothesis that the addition of a macropore would increase the transport of cesium at high values of S_{eff} due to reduced residence time in the column with and without colloids present. This was observed with the decreased time until cesium was detected in the effluent with and without colloids for S_{eff} = 1.0 and 0.80. For S_{eff} = 0.21, the tension in the matrix sand was below the air entry pressure of the macropore sand and resulted in very little flow in the macropore and; therefore, no increased transport. The appearance of secondary maxima in the desorption tails for S_{eff} = 1.0 and 0.80

when colloids weren't present was not anticipated, but was simulated by the model. Slow flow through the matrix sand and mixing with mostly cesium-free water from the macropore led to the secondary maxima phenomenon.

Environmental Implications. The conclusion that macropores can greatly increase cesium transport with and without colloids present is important for natural soils, where macropores are ubiquitous. During and immediately after storm events when soils are saturated, the transport of both dissolved and colloid-associated cesium is expected to be a significant source of cesium migration down into the soil profile. As the soil dries out; however, the macropores are expected to cease conducting flow and most of the remaining water will flow slowly through pores small enough to remain filled with pore water. Natural macropores are also more dynamic than the vertical macropore tested in our experiments, and mobile water can be expected to be transported rapidly in the vertical sections of a macropore; however, this water will likely re-enter the matrix pores as S_{eff} decreases or where macropores may change orientation and becomes more horizontal.

Faster flow velocities also have important implications for transport. Dissolved cesium will be readily adsorbed to the soil particles on the macropore surfaces; however, these binding sites will become occupied with cesium, just as the macropore sand binding sites were quickly occupied in our experiments.

REFERENCES

Chen, G., Flury, M., Harsh, J., Lichtner, P., 2005. Colloid-facilitated transport of cesium in variably saturated Hanford sediments. Environmental Science & Technology 39, 3435-3442.

Cheng, T., Saiers, J., 2010. Colloid-Facilitated Transport of Cesium in Vadose-Zone Sediments: The Importance of Flow Transients. Environmental Science & Technology 44, 7443-7449.

Clark, M., 1996. Transport Modeling for Environmental Engineers and Scientists. Wiley, New York.

de Jonge, H., de Jonge, L., Jacobsen, O., 2000. [C-14]glyphosate transport in undisturbed topsoil columns. Pest Management Science 56, 909-915.

de Jonge, H., Jacobsen, O., de Jonge, L., Moldrup, P., 1998. Particle-facilitated transport of prochloraz in undisturbed sandy loam soil columns. Journal of Environmental Quality 27, 1495-1503.

de Jonge, L., Kjaergaard, C., Moldrup, P., 2004a. Colloids and colloid-facilitated transport of contaminants in soils: An introduction. Vadose Zone Journal 3, 321-325.

de Jonge, L., Moldrup, P., Rubaek, G., Schelde, K., Djurhuus, J., 2004b. Particle leaching and particle-facilitated transport of phosphorus at field scale. Vadose Zone Journal 3, 462-470.

DeNovio, N., Saiers, J., Ryan, J., 2004. Colloid movement in unsaturated porous media: Recent advances and future directions. Vadose Zone Journal 3, 338-351.

Flury, M., Mathison, J., Harsh, J., 2002. In situ mobilization of colloids and transport of cesium in Hanford sediments. Environmental Science & Technology 36, 5335-5341.

Honeyman, B., 1999. Geochemistry - Colloidal culprits in contamination. Nature 397, 23-24.

Karathanasis, A., 1999. Subsurface migration of copper and zinc mediated by soil colloids. Soil Science Society of America Journal 63, 830-838.

Karathanasis, A., Johnson, D., Matocha, C., 2005. Biosolid colloid-mediated transport of copper, zinc, and lead in waste-amended soils. Journal of Environmental Quality 34, 1153-1164.

Kretzschmar, R., Borkovec, M., Grolimund, D., Elimelech, M., 1999. Mobile subsurface colloids and their role in contaminant transport. Advances in Agronomy 66, 121-193.

Krumbein, W., Sloss, L., 1963. Stratigraphy and Sedimentation. Freeman, San Francisco.

Lenhart, J., Saiers, J., 2002. Transport of silica colloids through unsaturated porous media: Experimental results and model comparisons. Environmental Science & Technology 36, 769-777.

Makris, K., Grove, J., Matocha, C., 2006. Colloid-mediated vertical phosphorus transport in a waste-amended soil. Geoderma 136, 174-183.

McCarthy, J., Zachara, J., 1989. Subsurface transport of contaminants- Mobile colloids in the subsurface environment may alter the transport of contaminants. Environmental Science & Technology 23, 496-502.

McGechan, M., 2002. Transport of particulate and colloid-sorbed contaminants through soil, part 2: Trapping processes and soil pore geometry. Biosystems Engineering 83, 387-395.

McGechan, M., Lewis, D., 2002. Transport of particulate and colloid-sorbed contaminants through soil, part 1: General principles. Biosystems Engineering 83, 255-273.

Mohanty, S., Ryan, J., Saiers, J., 2011. Mobilization of cesium and strontium in a vadose zone by cation exchange, organic matter, and colloids: A laboratory and field study. Abstracts of Papers of the American Chemical Society 242.

Noell, A., Thompson, J., Corapcioglu, M., Triay, I., 1998. The role of silica colloids on facilitated cesium transport through glass bead columns and modeling. Journal of Contaminant Hydrology 31, 23-56.

Rowell, D., 1994. Soil Science: methods and applications. Longman Scientific & Technical, University of Michigan.

Ryan, J., Illangasekare, T., Litaor, M., Shannon, R., 1998. Particle and plutonium mobilization in macroporous soils during rainfall simulations. Environmental Science & Technology 32, 476-482.

Saiers, J., Hornberger, G., 1996. The role of colloidal kaolinite in the transport of cesium through laboratory sand columns. Water Resources Research 32, 33-41.

Seta, A., Karathanasis, A., 1996. Colloid-facilitated transport of metolachlor through intact soil columns. Journal of Environmental Science and Health Part B-Pesticides Food Contaminants and Agricultural Wastes 31, 949-968.

Seta, A., Karathanasis, A., 1997. Atrazine adsorption by soil colloids and Co-transport through subsurface environments. Soil Science Society of America Journal 61, 612-617.

Sprague, L., Herman, J., Hornberger, G., Mills, A., 2000. Atrazine adsorption and colloid-facilitated transport through the unsaturated zone. Journal of Environmental Quality 29, 1632-1641.

Turner, N., Ryan, J., Saiers, J., 2006. Effect of desorption kinetics on colloid-facilitated transport of contaminants: Cesium, strontium, and illite colloids. Water Resources Research 42.

Vilks, P., Baik, M., 2001. Laboratory migration experiments with radionuclides and natural colloids in a granite fracture. Journal of Contaminant Hydrology 47, 197-210.

Zheng, C., Bennett, G., 2002. Applied Contaminant Transport Modeling. Wiley-Interscience, New York.

Zhuang, J., Flury, M., Jin, Y., 2003. Colloid-facilitated Cs transport through water-saturated Hanford sediment and Ottawa sand. Environmental Science & Technology 37, 4905-4911.

CHAPTER 6

CONCLUSIONS

Colloid-facilitated transport of cesium and strontium in a quartz column was studied by conducting breakthrough experiments and interpreting model results. A model for nonlinear two-site adsorption to colloid surfaces was able to simulate the results for all of the colloid-facilitated transport experiments conducted.

The type of colloid used in saturated experiments, and the resulting desorption rate coefficients calculated from model fits, was important in determining the extent of colloid-facilitated transport. Two types of illite and natural Oak Ridge, TN colloids increased both cesium and strontium transport; however, silica colloids had little effect on transport. Modeling results suggested that the rate coefficients for cation desorption from the slow binding sites on the colloids controlled transport.

Decreasing the effective saturation (S_{eff}) from 1.0 to 0.80 and 0.21 increased the colloid-facilitated transport of cesium and strontium due to decreased residence time. Dahmköhler numbers calculated from the desorption rate coefficients for these experiments suggested that slow desorption kinetics from the frayed edge sites on illite were more important for cesium than strontium.

The addition of a macropore to the quartz sand column with illite and cesium further decreased transport times and higher S_{eff} values and also suggested that slow desorption rate coefficients for cesium control whether or not colloid-facilitated transport will occur. The transport through the macropore and matrix sand were modeled separately and added together to accurately predict transport with and without colloids present. For S_{eff} = 1.0 and 0.80, macropore

flow dominated; however, almost all of the flow was through the matrix sand for $S_{eff} = 0.21$. For dissolved cesium breakthrough experiments with a macropore, delayed maximum values of effluent cesium were observed and modeled after the cesium solution was switched to cesium-free background solution. This feature demonstrates the important role macropores play in variably-saturated porous media transport.

CHAPTER 7

BIBLIOGRAPHY

Abadzic, S., Ryan, J., 2001. Particle release and permeability reduction in a natural zeolite (clinoptilolite) and sand porous medium. Environmental Science & Technology 35, 4502-4508.

Albarran, N., Missana, T., Garcia-Gutierrez, M., Alonso, U., Mingarro, M., 2011. Strontium migration in a crystalline medium: effects of the presence of bentonite colloids. Journal of Contaminant Hydrology 122, 76-85.

Allen, J.R.L., 1988. Modern-period muddy sediments in the severn estuary (Southwestern UK) - A pollutant-based model for dating and correlation. Sedimentary Geology 58, 1.

Anderson, J., Bouma, J., 1977a. Water-Movement through pedal soils. 1. Saturated flow. Soil Science Society of America Journal 41, 413-418.

Anderson, J., Bouma, J., 1977b. Water-Movement through pedal soils. 2. Unsaturated flow. Soil Science Society of America Journal 41, 419-423.

Bekhit, H., Hassan, A., Harris-Burr, R., Papelis, C., 2006. Experimental and numerical investigations of effects of silica colloids on transport of strontium in saturated sand columns. Environmental Science & Technology 40, 5402-5408.

Benjamin, M., 2002. Water Chemistry. McGraw Hill, New York, p. 668.

Bold, S., Kraft, S., Grathwohl, P., Liedl, R., 2003. Sorption/desorption kinetics of contaminants on mobile particles: Modeling and experimental evidence. Water Resources Research 39, SBH 3-1:8.

Bostick, B., Vairavamurthy, M., Karthikeyan, K., Chorover, J., 2002. Cesium adsorption on clay minerals: An EXAFS spectroscopic investigation. Environmental Science & Technology 36, 2670-2676.

Bouby, M., Geckeis, H., Lutzenkirchen, J., Mihai, S., Schafer, T., 2011. Interaction of bentonite colloids with Cs, Eu, Th and U in presence of humic acid: A flow field-flow fractionation study. Geochimica Et Cosmochimica Acta 75, 3866-3880.

Bouma, J., Anderson, J., 1977. Water and chloride movement through soil columns simulating pedal soils. Soil Science Society of America Journal 41, 766-770.

Bradford, S., Yates, S., Bettahar, M., Simunek, J., 2002. Physical factors affecting the transport and fate of colloids in saturated porous media. Water Resources Research 38, 1327-1340.

Bunn, R., Magelky, R., Ryan, J., Elimelech, M., 2002. Mobilization of natural colloids from an iron oxide-coated sand aquifer: Effect of pH and ionic strength. Environmental Science & Technology 36, 314-322.

Cassel, D., Krueger, T., Schroer, F., Norum, E., 1974. Solute movement through disturbed and undisturbed soil cores. Soil Science Society of America Journal 38, 36-40.

Chen, C., Coleman, M., Katz, L., 2006. Bridging the gap between macroscopic and spectroscopic studies of metal ion sorption at the oxide/water interface: Sr(II), Co(II), and Pb(II) sorption to quartz. Environmental Science & Technology 40, 142-148.

Chen, C., Hayes, K., 1999. X-ray absorption spectroscopy investigation of aqueous Co(II) and Sr(II) sorption at clay-water interfaces. Geochimica Et Cosmochimica Acta 63, 3205-3215.

Chen, G., Flury, M., Harsh, J., Lichtner, P., 2005. Colloid-facilitated transport of cesium in variably saturated Hanford sediments. Environmental Science & Technology 39, 3435-3442.

Cheng, T., Saiers, J., 2010. Colloid-Facilitated Transport of Cesium in Vadose-Zone Sediments: The Importance of Flow Transients. Environmental Science & Technology 44, 7443-7449.

Clark, M., 1996. Transport Modeling for Environmental Engineers and Scientists. Wiley, New York.

Comans, R., Hockley, D., 1992. Kinetics of Cesium Sorption on Illite. Geochimica Et Cosmochimica Acta 56, 1157-1164.

Cornell, R., 1993. Adsorption of cesium on minerals- a review. Journal of Radioanalytical and Nuclear Chemistry-Articles 171, 483-500.

Cvetkovic, V., Painter, S., Turner, D., Pickett, D., Bertetti, P., 2004. Parameter and model sensitivities for colloid-facilitated radionuclide transport on the field scale. Water Resources Research 40.

Cygan, R., Nagy, K., Brady, P., 1996. Molecular models of metal sorption on kaolinite. Abstracts of Papers of the American Chemical Society 211, 96-GEOC.

Czapar, G., Horton, R., Fawcett, R., 1992. Herbicide and tracer movement in soil columns containing an artificial macropore. Journal of Environmental Quality 21, 110-115.

Czigany, S., Flury, M., Harsh, J., 2005. Colloid stability in vadose zone aggregate. Hanford sediments. Environmental Science & Technology 39, 1506-1512.

Davis, J., Kent, D., 1990. Surface complexation modeling in aqueous geochemistry. Reviews in Mineralogy 23, 177-260.

de Jonge, H., de Jonge, L., Jacobsen, O., 2000. [C-14]glyphosate transport in undisturbed topsoil columns. Pest Management Science 56, 909-915.

de Jonge, H., Jacobsen, O., de Jonge, L., Moldrup, P., 1998. Particle-facilitated transport of prochloraz in undisturbed sandy loam soil columns. Journal of Environmental Quality 27, 1495-1503.

de Jonge, L., Kjaergaard, C., Moldrup, P., 2004a. Colloids and colloid-facilitated transport of contaminants in soils: An introduction. VADOSE ZONE J 3, 321-325.

de Jonge, L., Moldrup, P., Rubaek, G., Schelde, K., Djurhuus, J., 2004b. Particle leaching and particle-facilitated transport of phosphorus at field scale. Vadose Zone Journal 3, 462-470.

DeNovio, N., 2004. Particle and Particle-Facilitated Contaminant Transport in the Vadose Zone. University of Colorado-Boulder, Boulder, CO.

DeNovio, N., Saiers, J., Ryan, J., 2004. Colloid movement in unsaturated porous media: Recent advances and future directions. Vadose Zone Journal 3, 338-351.

Derjaguin, B., Landau, L., 1941. Theory of the stability of strongly charged lyophobic soils and of the adhesion of strongly charged particles in solutions of electrolytes. Acta Physicochim URSS 14, 633-662.

Eching, S., Hopmans, J., 1993. Optimization of hydraulic functions from transient outflow and soil-water pressure data. Soil Science Society of America Journal 57, 1167-1175.

El-Farhan, Y., Denovio, N., Herman, J., Hornberger, G., 2000. Mobilization and transport of soil particles during infiltration experiments in an agricultural field, Shenandoah Valley, Virginia. Environmental Science & Technology 34, 3555-3559.

Fedoroff, M., Lefevre, G., Duc, M., Milonjic, S., Neskovic, C., 2004. Sorption mechanisms and sorption models. Progress in Advanced Materials and Processes 453-454, 305-314.

Feke, D., Prabhu, N., Mann, J., 1984. A formulation of the short-range repulsion between spherical colloidal particles. Journal of Physical Chemistry 88, 5735-5739.

Flury, M., Czigany, S., Chen, G., Harsh, J., 2004. Cesium migration in saturated silica sand and Hanford sediments as impacted by ionic strength. Journal of Contaminant Hydrology 71, 111-126.

Flury, M., Mathison, J., Harsh, J., 2002. In situ mobilization of colloids and transport of cesium in Hanford sediments. Environmental Science & Technology 36, 5335-5341.

Gao, B., Saiers, J., Ryan, J., 2004. Deposition and mobilization of clay colloids in unsaturated porous media. Water Resources Research 40, W08602.

Gomez-Suarez, C., Van der Mei, H., Busscher, H., 2000. Air bubble-induced detachment of positively and negatively charged polystyrene particles from collector surfaces in a parallel-plate flow chamber. Journal of Adhesion Science and Technology 14, 1527-1537.

Gomez-Suarez, C., van der Mei, H., Busscher, H., 2001. Air bubble-induced detachment of polystyrene particles with different sizes from collector surfaces in a parallel plate flow chamber. Colloids and Surfaces A-Physicochemical and Engineering Aspects 186, 211-219.

Grolimund, D., Borkovec, M., Barmettler, K., Sticher, H., 1996. Colloid-facilitated transport of strongly sorbing contaminants in natural porous media: A laboratory column study. Environmental Science & Technology 30, 3118-3123.

Honeyman, B., 1999. Geochemistry - Colloidal culprits in contamination. Nature 397, 23-24.

IUPAC, 2002. Definition and classification of colloids.

Jacobsen, O., Moldrup, P., Larsen, C., Konnerup, L., Petersen, L., 1997. Particle transport in macropores of undisturbed soil columns. Journal of Hydrology 196, 185-203.

Karathanasis, A., 1999. Subsurface migration of copper and zinc mediated by soil colloids. Soil Science Society of America Journal 63, 830-838.

Karathanasis, A., Johnson, D., Matocha, C., 2005. Biosolid colloid-mediated transport of copper, zinc, and lead in waste-amended soils. Journal of Environmental Quality 34, 1153-1164.

Kersting, A., Efurd, D., Finnegan, D., Rokop, D., Smith, D., Thompson, J., 1999. Migration of plutonium in ground water at the Nevada Test Site. Nature 397, 56-59.

Kim, Y., Cygan, R., Kirkpatrick, R., 1996a. Cs-133 NMR and XPS investigation of cesium adsorbed on clay minerals and related phases. Geochimica Et Cosmochimica Acta 60, 1041-1052.

Kim, Y., Kirkpatrick, R., 1997. Na-23 and Cs-133 NMR study of cation adsorption on mineral surfaces: Local environments, dynamics, and effects of mixed cations. Geochimica Et Cosmochimica Acta 61, 5199-5208.

Kim, Y., Kirkpatrick, R., Cygan, R., 1996b. Cs-133 NMR study of cesium on the surfaces of kaolinite and illite. Geochimica Et Cosmochimica Acta 60, 4059-4074.

Kissel, D., Ritchie, J., Burnett, E., 1973. Chloride movement in undisturbed swelling clay soil. Soil Science Society of America Journal 37, 21-24.

Kitamura, A., Fujiwara, K., Yamamoto, T., Nishikawa, S., Moriyama, H., 1999. Analysis of adsorption behavior of cations onto quartz surface by electrical double-layer model. Journal of Nuclear Science and Technology 36, 1167-1175.

Kluitenberg, G., Horton, R., 1989. Pressurized layer reduces transport through compacted clay liners. Journal of Environmental Quality 18, 228-232.

Kowall, S., 2001. The DOE vadose zone science and technology roadmap: A national program to address characterization, monitoring, and simulation of subsurface contaminant fate and transport., WM '01. DOE, Tucson, AZ.

Kretzschmar, R., Borkovec, M., Grolimund, D., Elimelech, M., 1999. Mobile subsurface colloids and their role in contaminant transport. Advances in Agronomy 66, 121-193.

Krumbein, W., Sloss, L., 1963. Stratigraphy and Sedimentation. Freeman, San Francisco.

Laegdsmand, M., Villholth, K., Ullum, M., Jensen, K., 1999. Processes of colloid mobilization and transport in macroporous soil monoliths. Geoderma 93, 33-59.

Lafrance, P., Marineau, L., Perreault, L., Villeneuve, J., 1994. Effect of natural dissolved organic-matter found in groundwater on soil adsorption and transport of pentachlorophenol. Environmental Science & Technology 28, 2314-2320.

Lee, M., Chung, K., Choi, G., Lee, C., 2002. Measurement of Sr-90 in aqueous samples using liquid scintillation counting with full spectrum DPM method. Applied Radiation and Isotopes 57, 257-263.

Lenhart, J., Saiers, J., 2002. Transport of silica colloids through unsaturated porous media: Experimental results and model comparisons. Environmental Science & Technology 36, 769-777.

Lenhart, J., Saiers, J., 2003. Colloid mobilization in water-saturated porous media under transient chemical conditions. Environmental Science & Technology 37, 2780-2787.

Li, Y., Ghodrati, M., 1997. Preferential transport of solute through soil columns containing constructed macropores. Soil Science Society of America Journal 61, 1308-1317.

Li, Y., Tian, S., Qian, T., 2011. Transport and retention of strontium in surface-modified quartz sand with different wettability. Journal of Radioanalytical and Nuclear Chemistry 289, 337-343.

Litaor, M.I., Thompson, M.L., Barth, G.R., Molzer, P.C., 1994. Plutonium-239+240 and Am-241 in Soils East of Rocky-Flats, Colorado. Journal of Environmental Quality 23, 1231-1239.

Makris, K., Grove, J., Matocha, C., 2006. Colloid-mediated vertical phosphorus transport in a waste-amended soil. Geoderma 136, 174-183.

McBride, M., 1994. Environmental chemistry of soils. Oxford University Press, New York.

McCarthy, J., Degueldre, C., 1993. Sampling and characterization of colloids and particles in groundwater for studying their role in contaminant transport. In: Buffle, J., van Leeuwen,

H.P. (Eds.), Environmental Particle: Volume 2. Lewis Publishers, Ann Arbor, pp. 247-315.

McCarthy, J., Zachara, J., 1989. Subsurface transport of contaminants- Mobile colloids in the subsurface environment may alter the transport of contaminants. Environmental Science & Technology 23, 496-502.

McDowell-Boyer, L., 1992. Chemical Mobilization of Micron-Sized Particles in Saturated Porous Media Under Steady Flow Conditions. Environmental Science & Technology 26, 586-593.

McDowell-Boyer, L., Hunt, J., Sitar, N., 1986. Particle transport through porous media. Water Resources Research 22, 1901-1921.

McGechan, M., 2002. Transport of particulate and colloid-sorbed contaminants through soil, part 2: Trapping processes and soil pore geometry. Biosystems Engineering 83, 387-395.

McGechan, M., Lewis, D., 2002. Transport of particulate and colloid-sorbed contaminants through soil, part 1: General principles. Biosystems Engineering 83, 255-273.

Mohanty, S., Ryan, J., Saiers, J., 2011. Mobilization of cesium and strontium in a vadose zone by cation exchange, organic matter, and colloids: A laboratory and field study. Abstracts of Papers of the American Chemical Society 242.

Noell, A., Thompson, J., Corapcioglu, M., Triay, I., 1998. The role of silica colloids on facilitated cesium transport through glass bead columns and modeling. Journal of Contaminant Hydrology 31, 23-56.

NRC, 2000. Research Needs in Subsurface Science. National Academy Press, Washington, DC.

Ogata, A., Banks, R.B., 1961. A solution of the differential equation of longitudinal dispersion in porous media, Professional Paper 411-A. U.S. Geological Survey, Washington, D.C.

Pace, M., Mayes, M., Jardine, P., McKay, L., Yin, X., Mehlhorn, T., Liu, Q., Gurleyuk, H., 2007. Transport of Sr2+ and SrEDTA(2-) in partially-saturated and heterogeneous sediments. Journal of Contaminant Hydrology 91, 267-287.

Parker, J., 1984. Analysis of solute transport in column tracer studies. Soil Science Society of America Journal 48, 719-724.

Parkman, R., Charnock, J., Livens, F., Vaughan, D., 1998. A study of the interaction of strontium ions in aqueous solution with the surfaces of calcite and kaolinite. Geochimica Et Cosmochimica Acta 62, 1481-1492.

Phillips, R., Quisenberry, V., Zeleznik, J., Dunn, G., 1989. Mechanism of water entry into simulated macropores. Soil Science Society of America Journal 53, 1629-1635.

Pilgrim, D., Huff, D., 1983. Suspended sediment in rapid subsurface stormflow on a large field plot. Earth Surface Processes and Landforms 8, 451-463.

Rajagopalan, R., Tien, C., 1976. Trajectory Analysis of Deep-Bed Filtration with Sphere-in-Cell Porous-Media Model. Aiche Journal 22, 523-533.

Rod, K., Um, W., Flury, M., 2010. Transport of Strontium and Cesium in Simulated Hanford Tank Waste Leachate through Quartz Sand under Saturated and Unsaturated Flow. Environmental Science & Technology 44, 8089-8094.

Rowell, D., 1994. Soil Science: methods and applications. Longman Scientific & Technical, University of Michigan.

Roy, S., Dzombak, D., 1997. Chemical factors influencing colloid-facilitated transport of contaminants in porous media. Environmental Science & Technology 31, 656-664.

Ryan, J., Elimelech, M., 1996. Colloid mobilization and transport in groundwater. Colloids and Surfaces A-Physicochemical and Engineering Aspects 107, 1-56.

Ryan, J., Gschwend, P., 1994a. Effect of solution chemistry on clay colloid release from an iron oxide-coated aquifer sand. Environmental Science & Technology 28, 1717-1726.

Ryan, J., Gschwend, P., 1994b. Effects of ionic-strength and flow-rate on colloid release-Relating kinetics to intersurface potential-energy. Journal of Colloid and Interface Science 164, 21-34.

Ryan, J., Illangasekare, T., Litaor, M., Shannon, R., 1998. Particle and plutonium mobilization in macroporous soils during rainfall simulations. Environmental Science & Technology 32, 476-482.

Saiers, J., Hornberger, G., 1996a. Migration of Cs-137 through quartz sand: Experimental results and modeling approaches. Journal of Contaminant Hydrology 22, 255-270.

Saiers, J., Hornberger, G., 1996b. The role of colloidal kaolinite in the transport of cesium through laboratory sand columns. Water Resources Research 32, 33-41.

Saiers, J., Hornberger, G., 1999. The influence of ionic strength on the facilitated transport of cesium by kaolinite colloids. Water Resources Research 35, 1713-1727.

Saiers, J., Hornberger, G., Gower, D., Herman, J., 2003. The role of moving air-water interfaces in colloid mobilization within the vadose zone. Geophysical Research Letters 30.

Saiers, J., Hornberger, G., Harvey, C., 1994a. Colloidal silica transport through structured, heterogeneous porous-media. Journal of Hydrology 163, 271-288.

Saiers, J., Hornberger, G., Liang, L., 1994b. First-order and second-order kinetics approaches for modeling the transport of colloidal particles in porous-media. Water Resources Research 30, 2499-2506.

Saiers, J., Lenhart, J., 2003a. Colloid mobilization and transport within unsaturated porous media under transient-flow conditions. Water Resources Research 39.

Saiers, J., Lenhart, J., 2003b. Ionic-strength effects on colloid transport and interfacial reactions in partially saturated porous media. Water Resources Research 39.

Satmark, B., Albinsson, Y., Liang, L., 1996. Chemical effects of goethite colloid on the transport of radionuclides through a quartz-packed column. Journal of Contaminant Hydrology, 231-241.

Seta, A., Karathanasis, A., 1996. Colloid-facilitated transport of metolachlor through intact soil columns. Journal of Environmental Science and Health Part B-Pesticides Food Contaminants and Agricultural Wastes 31, 949-968.

Seta, A., Karathanasis, A., 1997. Atrazine adsorption by soil colloids and Co-transport through subsurface environments. Soil Science Society of America Journal 61, 612-617.

Shevenell, L., McCarthy, J., 2002. Effects of precipitation events on colloids in a karst aquifer. Journal of Hydrology 255, 50-68.

Solovitch-Vella, N., Garnier, J., Ciffroy, P., 2006. Influence of the colloid type on the transfer of Co-60 and Sr-85 in silica sand column under varying physicochemical conditions. Chemosphere 65, 324-331.

Sprague, L., Herman, J., Hornberger, G., Mills, A., 2000. Atrazine adsorption and colloid-facilitated transport through the unsaturated zone. Journal of Environmental Quality 29, 1632-1641.

Spurlock, F., Biggar, J., 1990. Effect of naturally-occuring soluble organic-matter on the adsorption and movement of simazine [2-chloro-4,6-bis(ethylamino)-s-triazine] in hanford sandy loam. Environmental Science & Technology 24, 736-741.

Steefel, C., Carroll, S., Zhao, P., Roberts, S., 2003. Cesium migration in Hanford sediment: a multisite cation exchange model based on laboratory transport experiments. Journal of Contaminant Hydrology 67, 219-246.

Stumm, W., Morgan, J., 1996. Aquatic Chemistry, Chemical Equlibria and Rates in Natural Waters. John Wiley & Sons, Inc., New York, p. 1022.

Sverjensky, D., 2002. Standard states for surface sites and surface species in surface complexation models. Abstracts of Papers of the American Chemical Society 223, U607-U607.

Sverjensky, D., 2006. Prediction of the speciation of alkaline earths adsorbed on mineral surfaces in salt solutions. Geochimica Et Cosmochimica Acta 70, 2427-2453.

Swartz, C., Gschwend, P., 1998. Mechanisms controlling release of colloids to groundwater in a Southeastern Coastal Plain aquifer sand. Environmental Science & Technology 32, 1779-1785.

Szenknect, S., Gaudet, J., Dewiere, L., 2003. Evaluation of distribution coefficients for the prediction of strontium and cesium migration in a natural sand at different water contents. Journal De Physique Iv 107, 1279-1282.

Thiessen, K., Thorne, M., Maul, P., Prohl, G., Wheater, H., 1999. Modelling radionuclide distribution and transport in the environment. Environmental Pollution 100, 151-177.

Triay, I., Lu, N., Cotter, C., Kitten, H., 1997. Iron oxide colloid facilitated plutonium transport in groundwater. Americal Chemical Society. American Chemical Society, Las Vegas.

Tufenkji, N., Elimelech, M., 2004. Correlation equation for predicting single-collector efficiency in physicochemical filtration in saturated porous media. Environmental Science & Technology 38, 529-536.

Turner, N., 2005. The effect of desorption kinetics on the colloid-facilitated transport of cesium-137 and strontium-90 in a saturated quartz porous medium. Civil, Environmental, and Architectural Engineering. University of Colorado-Boulder, Boulder, CO, p. 182.

Turner, N., Ryan, J., Saiers, J., 2006. Effect of desorption kinetics on colloid-facilitated transport of contaminants: Cesium, strontium, and illite colloids. Water Resources Research 42.

van Genuchten, M., 1980. A closed-form equation for predicting the hydraulic conductivity of unsaturated soils. Soil Science Society of America Journal 44, 892-898.

Verwey, E., Overbeek, J., 1948. Theory of the stability of lyophobic colloids.

Vilks, P., Baik, M., 2001. Laboratory migration experiments with radionuclides and natural colloids in a granite fracture. Journal of Contaminant Hydrology 47, 197-210.

Vilks, P., Cramer, J., Bachinski, D., Doern, D., Miller, H., 1993. Studies of colloids and suspended particles, Cigar Lake Uranium Deposit, Sasketchewan, Canada. Applied Geochemistry 8, 605-616.

Wan, J., Tokunaga, T., 1997. Film straining of colloids in unsaturated porous media: Conceptual model and experimental testing. Environmental Science & Technology 31, 2413-2420.

Wan, J., Tokunaga, T., 2002. Partitioning of clay colloids at air-water interfaces. Journal of Colloid and Interface Science 247, 54-61.

Wan, J., Wilson, J., 1994a. Colloid transport in unsaturated porous-media. Water Resources Research 30, 857-864.

Wan, J., Wilson, J., 1994b. Visualization of the role of the gas-water interface on the fate and transport of colloids in porous-media. Water Resources Research 30, 11-23.

Weisbrod, N., Dahan, O., Adar, E.M., 2002. Particle transport in unsaturated fractured chalk under arid conditions. Journal of Contaminant Hydrology 56, 117-136.

Yao, K., Habibian, M., Omelia, C., 1971. Water and waste water filtratyion- concepts and applications. Environmental Science & Technology 5, 1105.

Zachara, J., Flury, M., Harsh, J., 2002. Colloid facilitated migration of radioelements - Mechanisms, significance, and needed conditions. Geochimica Et Cosmochimica Acta 66, A867-A867.

Zheng, C., Bennett, G., 2002. Applied Contaminant Transport Modeling. Wiley-Interscience, New York.

Zhuang, J., Flury, M., Jin, Y., 2003. Colloid-facilitated Cs transport through water-saturated Hanford sediment and Ottawa sand. Environmental Science & Technology 37, 4905-4911.